Parametric modelling of integral bridge soil spring reactions

Nicholas Rudyard Featherston

Thesis presented in partial fulfilment of the requirements for the degree of Master of Engineering (Research) in the Faculty of Civil Engineering at Stellenbosch University

Supervisor: Prof. Celeste Viljoen

Department of Civil Engineering

April 2022

Declaration

By submitting this thesis electronically, I declare that the entirety of the work contained therein is my own, original work, that I am the sole author thereof (save to the extent explicitly otherwise stated), that reproduction and publication thereof by Stellenbosch University will not infringe any third party rights and that I have not previously in its entirety or in part submitted it for obtaining any qualification.

N. R. Featherston

Date: April 2022

Abstract

The integral bridge is a bridge structure in which the deck, piers and abutments are all made integral without the use of expansion joints. The joints would normally allow the expansion and contraction of the bridge deck, however now the flexibility inherent in the piers and abutments is utilized. The main design issue in an integral bridge is the effect of the temperature fluctuations and the corresponding movements in the bridge deck.

By its nature, the integral bridge has ends that interact with the embankment soil, as the bridge is subjected to cycles of movement that result in changes in soil pressure from the active to the passive pressure state. Forces inherent in conventional bridge systems also act longitudinally against the backfill soil, however the magnitude of the soil-structure interaction is negligible since the cyclic forces that are created are minor in comparison with those acting on integral bridges. This makes the integral bridge design both a structural and a geotechnical problem of interest.

The interaction between the bridge structure and the surrounding soil is a relatively intricate, three-dimensional scenario that is simplified in analysis modelling. Engineers are interested in two different (but related) issues. The first is the deformation of the soil as load is applied to it by the structural system, the second is the load carrying capacity of the soil. These two phenomena can be described as soil stiffness and soil strength. Clearly, a greater soil stiffness should lead to larger axial forces and bending moments in the deck due to the longitudinal expansion or contraction of the bridge.

Finite Element (FE) approaches to Soil-structure interaction (SSI) usually fall into approaches that characterize the soil using continuum elements and those that represent the soil through springs. In the spring method of analysis, the resistance of the soil lying adjacent to the piles and to the abutment is represented by springs which can be linear, compression only or non-linear in character. The theories used for the calculation of the spring stiffnesses are quite different between the abutments and the piles.

In this thesis, the influence on SSI reactions of pertinent bridge geometry and load parameters was investigated. To this end, a series of parametrically varied 2D and 3D bridge models with soil springs were created and subsequently analysed. The parameters of span length, abutment height and soil condition for different percentages of live load and thermal expansion/contraction/gradient were investigated and their influence on SSI reactions were revealed through the series of parametric model testing.

Pile lateral loading vs deflection relationships tend to be non-linear, however the spring reaction relationship for increasing span and load (once a pile is incorporated into an integral bridge system) was unknown prior to the analysis work captured in this thesis. The basic hypothesis for the thesis is that 3D models with realistic properties assigned to the springs will be required to capture the true behaviour of the integral bridge springs (which are suspected to be non-linear in nature), and that simplified 2D models can nonetheless provide some basic understanding of their behaviour and characteristics, but will not be able to completely model the bridge spring reaction behaviour.

The model test results showed that the maximum spring reactions (for abutments, piles and footings) followed either a linear relationship with increasing span or tended towards more non-linear relationships. The results showed distinct and significant differences between the spring reaction vs span relationships for the abutments and the piles (for the same bridge types). Further interpretation of the test results also showed that as spans increase (irrespective of the abutment height), the maximum spring reaction ratio (abutment/pile reaction ratio) tends towards unity under live loading.

In summary, the spring reaction results clearly demonstrated the influence of soil conditions, the bridge geometry and the applied loads on the spring reactions. It was also noted that significant increases or changes in spring reaction often occurred after the span length of 20m was exceeded.

It is hoped that the model testing and analysis has added valuable knowledge to the study of integral bridges. Further model testing is recommended to determine the characteristics of the spring reactions for much longer lengths of span, typically found in multi-span bridges.

Opsomming

'n Integrale se brugdek, kolomme en landhoofde vorm 'n geheel sonder die gebruik van uitsettingsvoë wat gewoonlik uitsetting en inkrimping van 'n brugdek toelaat. 'n Integrale brug struktuur benut die inherente buigsaamheid van die kolomme en landhoofde. Die hoof ontwerpskwessie in 'n integrale brug, is die effek van temperatuur skommelinge en ooreenstemmende bewegings in die brugdek.

Die integrale brug se eindpunte is in wisselwerking met die grondwalle wanneer die brug onderwerp word aan die bewegingssiklusse wat gronddruk veranderinge vanaf die aktiewe na die passiewe druk toestand, teweeg bring. Kragte inherent aan die konvensionele brug sisteme, werk ook longitudinaal teen die hervul grond. Die omvang van die grondstruktuur interaksie, is egter weglaatbaar aangesien die sikliese kragte wat gekep word, gering is in vergelyking met die kragte wat op die integrale brug inwerk. Dit maak die integrale brug ontwerp beide 'n strukturele en geotegniese probleem van belang.

Die interaksie tussen die brugstruktuur en die omliggende grond is 'n relatiewe ingewikkelde, drie-dimensionele scenario wat vereenvoudig kan word deur analise-modellering. Ingenieurs stel belang in twee verskillende (maar verwante) verskynsels. Een aspek is die vervorming van die grond soos wat lading en druk van die struktuur daarop toegepas word. 'n Tweede aspek is die ladingskapasiteit van die grond. Hierdie twee aspekte kan as grondstyfheid en grondsterkte beskryf word. 'n Hoër grondstyfheid behoort duidelik tot groter aksiale kragte en buigmomente in die brugdek te lei, as gevolg van die longitudinale-uitsetting of -inkrimping van die brug.

Finite Element (FE) benaderings tot Grondstruktuur Interaksie (SSI), verwys gewoonlik na die benutting van grondelemente en die gebruik van veerstelsels. Met die veermetode van analise, verteenwoordig vere (lineêr of nie- lineêr van aard, of bied slegs kompressie) die weerstand van die grond aangrensend tot die heipale en landhoofde. Die teorieë wat gebruik word vir die berekening van die veerstyfheid, verskil vir die landhoofde en die heipale.

In hierdie proefskrif is n reeks parametriese 2D en 3D brugmodelle vir grondvere geskep. Die parameters vir spanlengte, landhoofhoogte en grondtoestand vir verskillende persentasies van die lewendige lading, asook termiese uitsetting/inkrimping/gradiënt, is ondersoek, en die veergedrag is waargeneem en ontleed deur 'n reeks van parametriese model toetsings.

Die veerreaksies vir enkelportaal (enkelspan) integrale brûe is oorweeg, met 'n hipotese dat vir 2D modelle, lineêre gedrag waargeneem sal word as gevolg van die vereenvoudigde model aannames. Met die 3D modelle vir heipale, sal dan 'n nie-lineêre gedrag waargeneem word as gevolg van die nie-lineêre laterale heipaal gedrag karakteristieke, en die gebruik van nie-lineêre vere.

Model toetsresultate het getoon dat die maksimum veerreaksies (vir landhoofde en heipale) óf 'n reguit (lineêre) lyn volg, óf na 'n meer paraboliese kurwe vorm neig en beduidende verskille tussen die veerreaksie kurwes van die landhoofde en heipale (vir dieselfde tipe brug). Verdere interpretasie van die toetsresultate het ook getoon dat, namate die spanlengte toeneem (ongeag landhoof hoogte), die maksimum veerreaksie verhouding (landhoof/heipaal reaksie verhouding) neig na eenheid.

Ter samevatting, die veerreaksie resultate het duidelik die invloed van die grondtoestande, bruggeometrie en toegepaste ladings op die veerreaksies, gedemonstreer. Ook is opgemerk dat beduidende toenames of veranderinge in die veerreaksies dikwels voorgekom het vir spanlengtes van meer as 20m.

Hopelik sal die modeltoetsing en -ontleding waardevolle kennis bydra tot die bestudering van integrale brûe. Verdere modeltoetsing word aanbeveel om die karakteristieke van die veerreaksies vir heelwat langer spanlengtes, asook vir brûe met veelvuldige spanlengtes vas te stel.

Acknowledgements

This dissertation was submitted in partial fulfilment for the Degree of Master of Engineering, in Civil Engineering, at Stellenbosch University. This research was made possible through the continuous support of many people, of whom it is important to acknowledge and thank.

Thank you to my supervisor, Prof Celeste Viljoen, who provided valuable technical support, funding and guidance throughout the period of this thesis, for which I am extremely grateful. I also recognize and appreciate your boundless enthusiasm, energy and positive attitude, without which this thesis would not have been possible.

Thank you to Anuj Asati, Ashish Loya and Ayan Srivastava of Midas for their assistance with queries and licensing during this period.

Thank you to my friends, my partner Julia (Clementine) and my family for your unconditional love and support throughout this period of research, which made the task all the more easier to bear and get through.

Finally, I would like to dedicate my thesis to the memory of my late father who supported me always in whatever career I chose to pursue.

Notation

A	Foundational area
A_y, A_s, A_m, A_v, A_t	Non-dimensional coefficients relating an applied lateral force to deflection, slope, moment, shear, and soil reaction, respectively
B_y, B_s, B_v, B_t	Non-dimensional coefficients relating an applied moment to deflection, slope, moment, shear, and soil reaction, respectively
C_y	Non-dimensional coefficient giving the deflection of a pile, depending on the degree of fixity
cc_s	Spring division along length of pile
D	Pile diameter
DL	Dead load
d	Thermal movement of the bridge deck end
d’	Deflection of an integral bridge abutment at a depth H/2 below ground level
E	Young’s modulus
E_p	Young’s modulus under elastic conditions
E_s	Young’s modulus for the backfill soil
E_u	Undrained modulus
e	Void ratio
F_h	Lateral force
F_{sp}	Maximum spring reaction
$F_{sp\%}$	Coefficient from **Table 4.1** or **Table 4.2**, or other values from the columns for “spring load to total LL” in Appendix A
F_{ult}	Ultimate load
G	Shear modulus
G_s	Specific gravity of soil particles
H	Height of wall or end screen
H’	Depth of soil influenced by abutment movement and used in a soil-structure interaction analysis of an integral bridge
H_c	Depth of earth cover between ground level and the top surface of the roof of a buried structure
H_o	Horizontal load at ground line
h_{soil}	Height of retained soil between the top of the stem, to top of the deck
I	Moment of inertia
I_a	Abutment Second moment of inertia
I_p	Moment of inertia under elastic conditions
K	Earth pressure coefficient
K_a	Active earth pressure coefficient
K_d	Design value of K based on φ’ and including a model factor if relevant
K_H	Initial stiffness

$K_{horiz(x)}$, $K_{vert(z)}$, $K_{rot(m)}$	Stiffnesses per metre length for the strip foundation in the horizontal, vertical and rotational displacement directions respectively
K_i	Initial modulus for the lateral subgrade reaction
K_{max}	Coefficient of earth pressure applied to buried structures which takes account of pressure increases caused by structure expansion
K_{min}	Coefficient of minimum earth pressure applied when earth pressure is favourable
K_o	At-rest earth pressure coefficient
K_p	Coefficient of passive earth pressure
$K_{p;t}$	Passive earth pressure coefficient, used in the calculation for K* and determined using the design value of the triaxial φ’
K_r	Coefficient of passive earth pressure resisting overturning or sliding
K*	Earth pressure coefficient applied to integral bridge abutments subject to strain ratcheting
k	Modulus of lateral subgrade reaction
k_a	Coefficient of active soil pressure
k_h	Coefficient of lateral subgrade reaction
k_p	Coefficient of passive soil pressure
k_s	Spring stiffness
L	Length of pile
L_b	Length of bridge from the neutral point to the deck end
L_C	Characteristic length of pile
L_x	Expansion length measured from the bridge end, to the position on the deck that remains stationary under bridge expansion
LL	Live load
M	Bending Moment
M_o	Ground-line moment loading on pile
M_{up}	Maximum Abutment Moment
m_h	Modified constant of lateral subgrade reaction
n_h	Constant of lateral subgrade reaction
p	Earth pressure
p'	Mean confining stress minus the soil pore water pressure
pU,z	Ultimate lateral soil resistance
p_{atm}	The reference stress of atmospheric pressure
P_p	Passive pressure
q	Pressure on vertical plate test/ Force-displacement relationship of pile-soil-interaction

q_{ult}	Ultimate lateral soil resistance, asymptote of hyperbolic behaviour
S_u	Undrained shear strength
T	Characteristic length of pile for homogeneous case
u	Lateral deflection
u_o	Groundline deflection of pile or pile group
u_z	Pore water pressure
V	Vertical load shear
w_p	Passive pressure at the bottom level of the abutment diaphragm
y	Displacement of pile
Z	Foundation section modulus
z	Depth below ground level or top of wall
α	Coefficient of thermal expansion
β	Angle of inclination of the backfill
γ	Shear strain
γ_{EH}	Maximum load factor
γ_{soil}	unit weight of backfill soil
δ	Structure-ground interface friction angle or friction angle on a vertical or inclined virtual face
θ	Slope
θ	Skew angle of bridge
κ	Exponent providing k_s best fit to measured results
μ	Poisson ratio for the soil
ρ_d	Dry density
σ_o'	At-rest earth pressure
$\sigma_{v,z}$	Vertical effective stress
υ	Poisson's ratio
ø	Angle of backfill material internal friction
φ'	Angle of shearing resistance with respect to effective stress
φ'_{cv}	Shearing resistance critical angle
Δ	Bridge displacement
ΔT	Temperature difference between the effective bridge temperature and the original construction temperature

Table of Contents

List of Figures

List of Tables

PARAMETRIC MODELLING OF INTEGRAL BRIDGE SOIL SPRING REACTIONS

1 CHAPTER 1 – Introduction

In commonly constructed bridges, there is usually an expansion mechanism with joints accompanied by abutment or pier bearings, roller supports, and other release mechanisms that allow for the repeated thermal related expansion/contraction, shrinkage and creep (Arockiasamy et al., 2004). Bridge joints that allow for expansion are costly to incorporate into the design and serious and critical maintenance problems due to expansion joint failure and abutment bearing failure have occurred in the past. Water leakage that is contaminated with salt and de-icing chemicals makes its way through the joints and will tend to result in reinforced concrete corrosion and bearing damage underneath the deck soffit (Shah, 2007). These problems are made worse in countries where large snow-storms are prevalent and where calcium chloride and sodium chloride salts are commonly used for de-icing bridge surfaces (Krier, 2009).

The continuous maintenance and replacements costs for the bearings and joints represent considerable amounts spent by roads authorities every year. To cater for these issues, bridges with lengths of up to 60 metres, with skews less than 30° are now required in the UK to be integral with their supporting abutments and continuous at any intermediate supports (refer to BD 57, DMRB 1.3.7).

Described simply, an integral bridge is a structure which is built and designed without any expansion joints on the piers between the spans or at the abutments. The road surface is therefore continuous from one end of the deck to the other end. Integral bridges are becoming more attractive options as engineers look for methods to avoid the expensive and continual maintenance issues that are associated with bridges that have movement joints along with the accompanying water penetration issues and the problems caused by the use of de-icing salts.

It has become evident that these bridges which were originally built, in response to the deleterious effects of leaking expansion joints and increased pavement pressures, had significantly more positive aspects and less limitations than their opposition (jointed bridges). Interestingly these attributes not only reduced a bridge's capital outlay cost and life-cycle cost, but they also reduced the cost of their own future modification (eg. bridge widening) as well as their eventual replacement.

Although their jointless construction and resistance to pavement pressure, with consequent improved long-term durability appear to be the primary attributes that first motivated the construction of longer and longer integral bridges, it also appears that their simple design, good earthquake resistance and rapid construction attributes have gained them widespread favour.

In the integral bridge system, resistance to longitudinal thermal movements and braking loads are provided by the stiffness of the soil adjacent to the end supports and, in multi-span bridges the stiffness of the intermediate supports also assists. Since the earth pressure forces on opposite end abutments are resisted by deck compression, the piles supporting the integral abutments (unlike the piles supporting conventional abutments) do not need to be designed for the full earth abutment loading.

Integral abutments are often founded on a single row of piles built from steel or concrete (the use of steel piles is however not very common in South Africa) – this system results in an increase in the flexibility of the abutment, allowing the abutment to translate in the same direction as the bridge longitudinal axis. For the longer spans, an integral girder connection is generally provided by casting the girder ends into the reinforced concrete abutment. This technique develops and allows for the full

transmission of forces and moments due to temperature related displacements as well as the rotational displacement experienced by the abutment piles due to live loads.

Soil-structure interaction effects that occur between the bridge structure, the surrounding embankment backfill and the founding material are relatively complex, but in common practice they are simplified through the use of abutment and pile springs. The characteristics of the springs and their assigned model stiffness depend on a number of factors – soil type, depth below ground surface, over-consolidation ratio and the presence of a water table (for example). By making these simplifications, the engineer is able to design these types of structures with a reasonable degree of confidence in the approach taken.

1.1 Problem statement

Globally, the integral bridge structure has been well used and it is well acknowledged that the economics of the integral bridge are advantageous over the traditional jointed bridge structure. Few of these bridges are found in Southern Africa however and this may partly be due to a lack of understanding of their behaviour. Specifically, little is known about the behaviour of abutment springs, footing springs and pile springs under varying loading and span conditions. As stated above, the SSI effects due to the presence of the soil in contact with the structure are relatively complex, and their parametric behaviour not well understood. The presence of soil in contact with the abutment and the piles is commonly modelled in conventional analysis techniques using soil springs. The intention in this thesis is therefore to determine the effects on the integral bridge SSI reactions when one varies the bridge span, abutment height, temperature effects and live loading under varying soil conditions.

This thesis seeks to produce a thorough understanding of the relationship between the soil spring reactions and the soil-structure interaction effects that arise in integral bridge design under parametric variances of the bridge geometry, loading and founding soil parameters. A thorough understanding of these relationships will lead to an optimal design approach being taken by designers for the bridge deck, abutments and foundations.

If this understanding were to become more common knowledge, it would be incumbent on designers to consider this bridge type as a more commonly adopted solution, especially in areas where its implementation could lead to a more economical solution.

The underlying question therefore is: how do the spring reactions behave when the above parameters are varied?

1.2 Aims and objectives of this work

The behaviour of integral bridge springs under the parametric variances of span, abutment height, loading and founding conditions has not been widely reported thus far in the literature and the role that these variables have on the magnitude of the spring reactions for the abutments and piles (or footings) is similarly unreported. The main aim of this research is to gain an understanding of the behaviour of these integral springs under these parametric variances. This improved understanding will be useful since the designer may often be unsure where to start the conceptual design process with an integral bridge, and by considering the behaviour of the springs, the designer will be able to identify the impact that choices of the parameters of deck length, abutment height, loading and soil condition have on the overall design. How the springs behave ultimately translates into the sizing of the various integral bridge elements ie. the deck, abutment and foundations, therefore a basis of understanding for the spring reactions is a useful tool for the designer to have at the start of the design process.

The influence of the parameters of span, abutment height, loading (live load and temperature) on soil-structure reactions (as captured by the spring reactions in the models) is therefore investigated.

The research objectives of this thesis are as follows:

- To summarize the current literature on soil properties in relation to the modelling of integral bridges, in particular the modelling of the soil-structure interaction.
- To summarize and describe the types of existing simplified integral abutment models that have been formulated by previous authors.
- Determine the relationship between increasing live load and maximum spring reaction, for the same bridge geometry conditions.
- Determine the relationship between live load and maximum spring reaction, for increasing deck span or increasing abutment height.
- Determine the relationship between a positive increase or negative decrease in deck temperature, and maximum spring reaction for increasing deck span or increasing abutment height.
- Determine the relationship between a positive temperature gradient (or a negative temperature gradient) through the deck and maximum spring reaction for increasing span or increasing abutment height.
- To determine the effects of soil founding condition on the maximum soil spring reactions for increasing deck span length or increasing abutment height.
- To highlight the postulated non-linear effects of including the pile system on the spring reactions, in a piled integral bridge, by using a 3D Grillage model for varying bridge geometry, variable loading and variable founding conditions.
- To determine the relationship between the spring reactions and the applied loading in a 2D frame model for varying bridge geometry, variable loading and variable founding conditions.
- To gain an understanding of the difference in magnitude between the spring reaction for the abutments and the piles, as the bridge geometry is changed, for a variety of loading/founding situations.
- To determine whether a relationship exists between the spring stiffness and the spring reaction that is generated in the analysis, for a variety of loading/founding/variable bridge geometry situations.

Since the magnitude of the spring reactions has a direct bearing and relationship to the bending moments and shears that are then created in the abutments, deck and foundations, one can conclude that if the spring reactions are large (or small) in magnitude, the relevant element will be sized proportionately. An objective that is not explicitly covered in this thesis however, would be to determine (more exactly) the nature of the relationship between the spring reactions and the bending moments and shears that are created in the various elements under various loading arrangements. This problem could be the work of future studies in this field.

The problem is approached through the creation and subsequent analysis of a series of parametric models, in both 2D and 3D that have sufficient variation in the specific parameters ie. span, abutment height, live load and foundation conditions, to predict the spring reactions so that the relevant structural elements may be sized accordingly.

1.3 Scope of the research

This thesis focusses on the straight and orthogonal straight-ended, cast-in-situ reinforced concrete single span integral portal bridges for the range 10-40m, which is the most common range of single span integral bridge used in practice. A series of 3D MIDAS models are setup for a reinforced concrete piled structure (which, due to the presence of the piles is postulated will behave non-linearly) and 2D models are setup for integral bridges founded on footings (which are postulated to behave in a more linear fashion). Various models are subjected to live loading (expressed a % of the total dead load) and thermal loading. The assumed ends of the bridge are also symmetrical, in other words, the end screen properties - height H, and width B, of both bridge ends are equal, and the structures are modelled sans any wingwalls or approach slabs.

The superstructures considered here are beam-and-slab type deck structures. Various aspects of integral bridges have been studied by a plethora of different authors. Lehane (1999) has for example, conducted various backfill soil tests and produced a simplified 2D spring model for the restraining effects of backfill soil on integral bridges. O'Brien and Keogh (1999) describe simple 2D expansion and contraction models that allow relatively quick answers to be generated for integral bridges on footings. Dicleli and Erhan (2009) have studied the effects of superstructure to abutment continuity on the live load distribution factors in integral abutment bridge girders. Since there is relatively little research that has been done on the abutment and pile spring reactions themselves for single portal type integral structures, the 2-D and the 3-D modelling has been undertaken in this thesis to explain the relationships between the various parameters outlined in (1.2) above.

Note that in general practice, spans longer than 40m tend to involve multi span integral structures, which are not the subject of this thesis. Multi-span bridges have been specifically excluded from this study due to the variance in the properties that would need to be modelled (and the extensive number of models that would need to be generated).

1.4 Thesis Structure

Chapter 2: Literature Review

Integral Bridges introduction – A review of the different integral bridge forms such as frame abutments, embedded wall abutments, bank pad abutments (including piled abutments), flexible support abutments and semi-integral abutments is presented. This chapter also discusses the advantages and disadvantages of general integral bridge construction, examines their applications and then discusses some of the loading effects that this type of bridge should be designed for.

Summary of design guidelines and design limits set in different countries – Some of the available Codes and standards as well as the guidance documents that deal specifically with Integral Bridge designs are discussed – the main codes under consideration being the PD 6694-1:2011 Code and the AASHTO Code. The chapter looks at how certain countries have implemented the integral bridge concept. South African Practice, American Practice, Australian Practice, UK Practice, European Practice and Japanese Practices are briefly discussed.

Soil-structure interaction (SSI) in integral abutment bridges review – This chapter provides a synopsis and background to soil structure interaction considerations. Structures where SSI is relevant are discussed, p-y theory for laterally loaded piles is elaborated on and the continuum mechanics approach is briefly discussed.

Modelling of integral abutment bridges – Various 3D and 2D modelling theories relating to integral bridges are discussed in this Chapter. Finite element modelling, a bridge contraction model on flexible supports (Dobry and Gazetas, 1986), the simple foundation stiffness model (Hambly, 1991), the bridge deck expansion model using a conventional spring (O' Brien and Keogh, 1999) and the bridge deck expansion using an equivalent spring at deck level model (Lehane, 1999) are all elaborated on and described in the text. Literature relating to grillage modelling theory and how it is used for the bridge deck type (beam and slab) that has been selected for this study is included.

Details relating to abutment pile types and abutment fixity are discussed and then Wing wall considerations are described. Loading effects from environmentally related thermal cycles are discussed and the effect this has on the structure is interrogated further.

Modelling of soil behind an integral abutment bridge – The merits of various kinds of backfill are first described and then the chapter discusses horizontal stress ratios (as the soil changes its behaviour from the active to the passive state), backfill cyclic loading and granular flow behind the abutment. Items and parameters relevant to soil spring modelling are then discussed such as the coefficient of subgrade reaction, Young's Modulus for the soil, and the soil spring strength. Soil backfill pressure

effects are discussed, and the chapter ends with a discussion relating to backfill effects and approach slabs.

Conclusion - The chapter ends with a summary and conclusion of the Literature review study, and highlights the gap in the existing knowledge on integral abutment and pile spring reactions for integral bridges. The models that were used in the study are also motivated.

Chapter 3: Analysis model setup and methodology – This chapter examines the basic model assumptions used, the underlying theory assumed in the MIDAS and Prokon software, the loads assumed, the material and section properties, the boundary conditions and supports, the applicable loading combinations and the model parameters assumed. The limitations of the extents of the modelling work performed over the course of the thesis are highlighted.

Chapter 4: Analysis results and discussion – The results of the analysis models are shown in this chapter, with the trends from the reaction data being presented in a graphic format for better understanding. The results are discussed and analysed in detail throughout the text.

Chapter 5: Conclusion and Recommendations – In this chapter, the notable conclusions and inferences of the research model testing are outlined. Recommendations for future approaches to performing the work are made, and opportunities for further research into the topic of integral bridge spring reactions are discussed.

References – all references used in this thesis are listed.

2 CHAPTER 2 – Literature Review

2.1 Introduction to Integral Bridges

Integral abutment bridges are a jointless type of bridge, lately becoming the preferred construction option when installing new bridge structures for highways and rail. This type of bridge has been used all over the globe, and there are many studies that have documented their historical performance – eg Connal (2004).

Conventionally, bridges for highways and rail are built so that expansion joints divide the superstructure and substructure elements. The joints allow the superstructure to move independently from the rigid substructure as the structure experiences expansion and contraction due to the strains caused by creep, shrinkage and temperature. The numerous maintenance issues caused by expansion joints make it desirable to remove the joints completely. The integral abutment bridge structure is therefore constructed by making the superstructure and substructure continuous, as an alternative to providing expansion joints that separate the superstructure from the substructure. Under specific founding conditions, the longitudinal movement that was previously accommodated by the joints is now accommodated by a single row of piles – see below for a diagram (**Figure *2.1***) of elements related to a typical integral bridge.

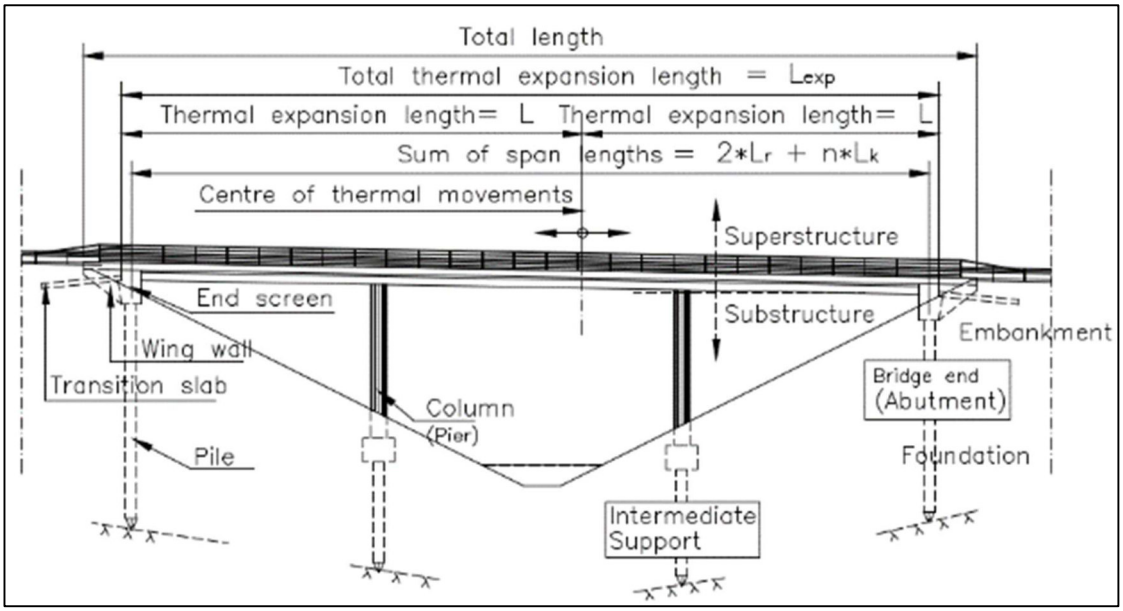

Figure *2.1*: Integral bridge elements (Laaksonen, 2011)

Since integral bridges are built without any expansion joints at the deck to abutment junction, they may be viewed as portal frame structures in their basic form. Several distinct forms of integral bridge may be identified by the height and stiffness of the abutments and whether or not a spread footing forms part of the construction.

The lateral loading on the abutments from the backfill soil is complex. The soil-structure interaction is

related and defined in terms of the deck cyclic thermal movements (expansion and contraction) resulting from the ever-changing heating and cooling environmental cycles – this governs the stresses at the abutment to backfill interface. It has been observed from the behaviour of circular biological filter bed retaining walls (England, 1994) as well as from site data from bridge abutments (Bruins and Ingleson, 1972) that an increase in the compressive soil-wall stresses occurs during successive thermal cycles, while the soil experiences extensional straining as it repeatedly changes from an active pressure condition to a passive pressure condition. Springman et al (1996) has also confirmed the presence of stress increases on retaining wall abutments in model centrifuge tests. Knowledge of these cycles and their effects on various construction materials is therefore critical to the design of the abutments and to the bridge in general.

For a single span integral bridge, the deformed shape components caused by deck live load and thermal gradients is shown in **Figure *2.2***. As can be seen from the diagram, the head of the pile is subjected to both displacement and rotation under the loading caused by the rotation of the end screen.

The stiffness relations determine the live load distribution between different structural components. The varying properties of backfill soil have been shown to have only a minor effect on the deck sagging moments at mid-span, for various deck stiffnesses and pile sizes. The influence of the backfill on the pile bending moments and the girder moments is moderate (Laaksonen, 2011).

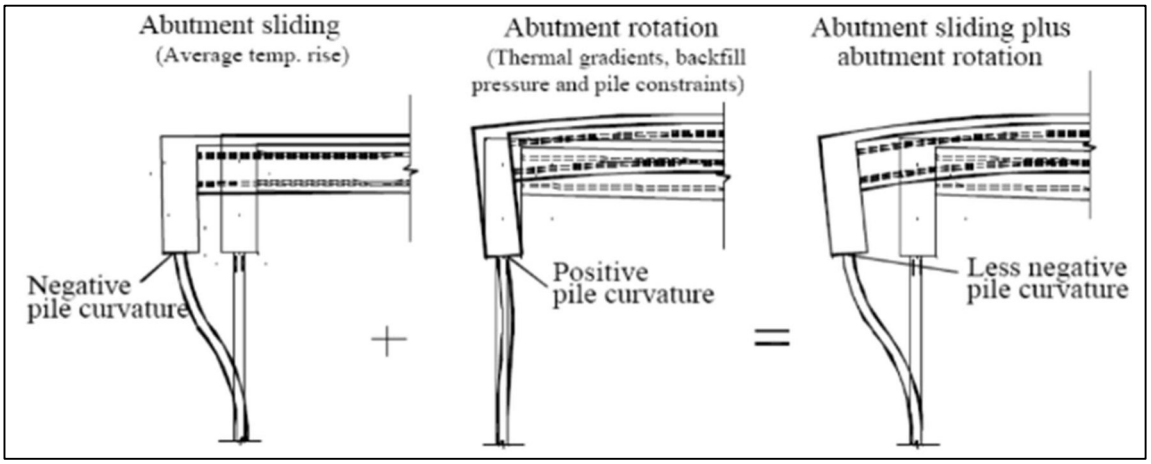

Figure *2.2*: Fully integral bridge end rotations and effect on pile curvatures (Laaksonen, 2011)

2.1.1 Integral bridge design for longitudinal movement

Integral bridges are required to be designed for a range of loading effects as a result of their continuity. These are briefly described below:

1) Bridges are required to be designed to account for the effects of not only thermal expansion but also longitudinal forces such as the thrust effects arising from traffic loading, earth pressures and friction. The axial tension from sliding or restraints also need to be catered for, this being associated with the thermal contraction effects.
2) For a 120-year return period, integral bridge abutments should limit their thermal movement in general to ± 20mm from the original as-built restraint position.
3) Expansion joints between the deck spans should not be included in multispan integral bridges. The bridge should be designed to account for the effects of the deck continuity (refer BA 57, DMRB

1.3.8) as well as axial thrust or tension.

4) The effects of temperature gradient, creep and shrinkage, should be accounted for in accordance with BS 5400: Part 4 (3), BD 24 (DMRB 1.3.1) and BD 37, (DMRB 1.3.14).

2.1.2 Integral bridge forms

The forms of integral bridge fall into three main categories of abutment that are used in the design. These three bridge forms are described in more detail below, and are also shown in **Figure *2.3***:

a) Full height frame abutments

b) Embedded wall abutments

c) End screen abutments

Note that end screen abutments include bank pad abutments (either on footings or on piles), flexible support abutments and semi-integral abutments.

A) Frame abutments

The transmission of bending moments, shears and axial forces is enabled through the abutment being structurally connected with the deck. This type of bridge is supported on spread footings or piled foundations as shown in **Figure *2.3*** (a) – (c)). The vertical loads from the bridge deck are supported by the frame type abutment, whilst it simultaneously acts as a retaining wall for the backfill and the embankment earth pressures.

B) Embedded wall abutments

The Embedded Abutment (see **Figure *2.3*** (d)), includes bored pile, sheet pile or diaphragm wall abutments, which are extended to various depths below the ground fill surface. The depth of wall embedment restrains the system against rocking while the walls are of course integral with the bridge deck.

C) End Screen Abutment

These type of abutments act only as a retaining wall for the transmission of longitudinal loads and the embankment earth pressures. The deck vertical loads are supported by separate columns which are located within 2m from the end screen – this is done in order to limit the vertical movement of the end screen during end span deflection. The supports on the ends may be structurally isolated from the end screen horizontal movements, or they may be connected to the deck, in which case they should be designed to resist, or avoid the earth pressures arising from their movement relative to the embankment.

i. Bank pad abutments

This design is effectively an extension to the deck, creating a footing that is seated on the backfill whilst acting as an end support for the bridge - see **Figure *2.3*** (e) and (f). The deck and footing slides on the foundation material in response to thermal expansion and contraction and can also rotate under live loading. The bank pad should have sufficient self-weight to provide stability to the structure, and in the multi-span design scenario, the end spans are required to have adequate flexibility to cater for any differential settlement whilst preventing uplift under traffic loading.

ii. Bank pad abutments on piles

A single row of discrete vertical piles provides the pad abutment founding conditions, these are

driven or bored through the embankment. The top of the piles are designed to be integral with the deck. During deck expansion, the ends of the deck move into the backfill and the piles flex backward into the fill.

iii. Flexible support abutments

In this instance, the bridge is supported by flexible columns or piles. Only the end screen, which is attached to the deck end, translates into the fill. The support columns or piles may be enclosed in sleeves (to allow them to bend without disturbing the adjacent soil), or they may be positioned in front of a reinforced earth wall or similar abutment.

iv. Semi-integral abutments

With the semi-integral structure, the vertical support at the end of the deck is provided by bearings that are seated on conventional abutment walls, or reinforced soil abutments that do not move into the fill during deck expansion. These abutments therefore act in a similar manner to flexible support abutments in regard to the lateral earth forces loading the end screen wall.

Further integral schemes for multi-span bridges and deck ends are elaborated on in **Figure *2.4***, which gives one an idea of the range of options available to the bridge designer.

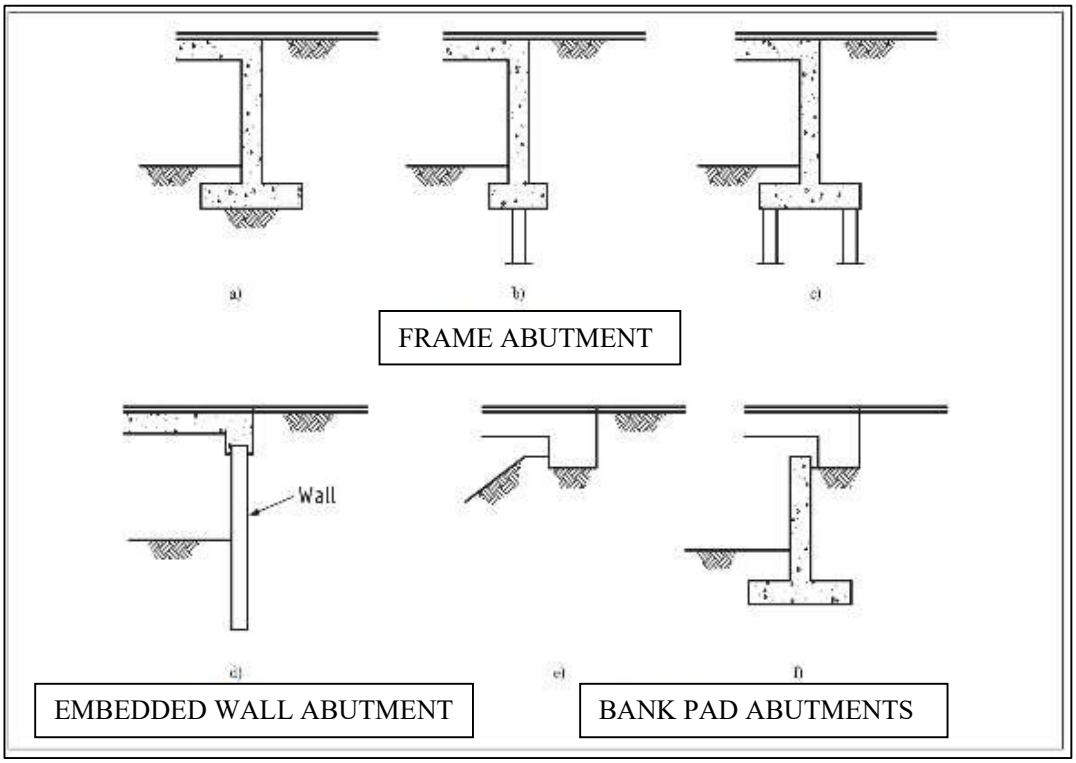

Figure *2.3*: Various abutment forms used in integral bridge construction (PD 6694-1:2011)

As there are no expansion joints, movements cannot be accommodated within the deck of the bridge alone, yet the bridge deck contracts or expands in response to the variations in the ambient temperature

on a daily basis. The thermal movements of the bridge deck will therefore be induced in the bridge abutments, causing the latter to move into and then away from the backfill soil in a movement that is both rotational and translational. This ultimately causes what is known as a 'ratcheting' effect in the abutment backfill – more on this is discussed later in this thesis. During the hot, summer seasons, the abutments are generally pushed directly into the retained backfill soil, while in the winter seasons they move back in the reverse direction towards the centre of the bridge deck.

The largest movement typically occurs at the top of the abutment and decreases down towards the foundations (Horvath, 2000). Although the amplitude of the displacement is relatively small, usually not exceeding a few millimetres, its cyclical recurrence may create substantial structural and geotechnical problems over the long term.

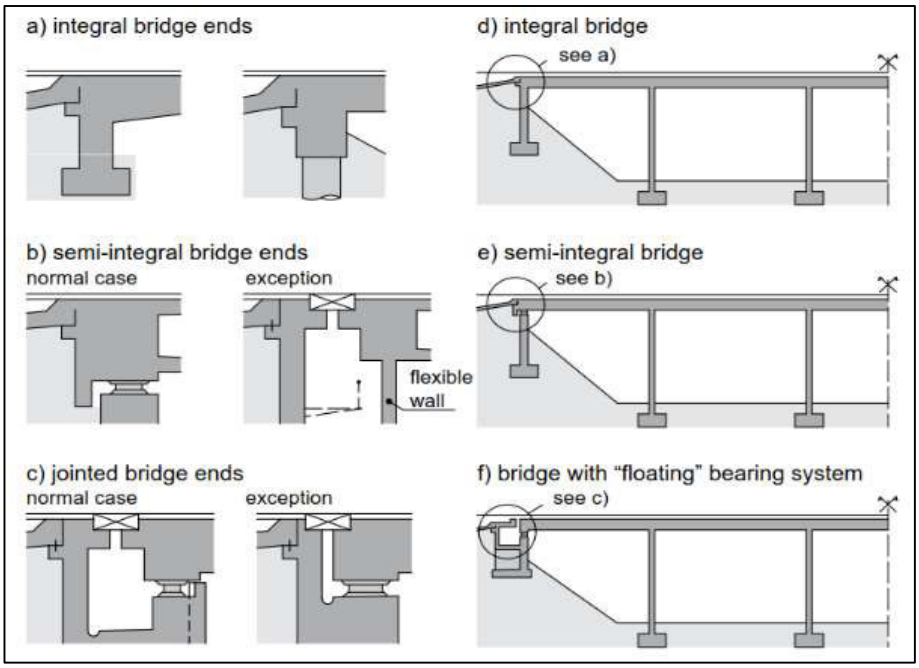

Figure *2.4*: Options for integral bridge ends (Lan, 2012)

2.1.3 Advantages and Disadvantages of Integral bridges

The principal advantages of the integral type bridge includes the following:

- The riding quality for vehicles is enhanced due to the smooth, continuous, and aesthetically pleasing deck of the integral bridge (Soltani and Kukreti, 1992).
- There is in many instances a cost saving due to the removal of expansion joints and bridge bearings and their subsequent replacement with the integral connections.
- Integral abutments may be designed to include bending moment capacity for the continuous bridge span scenario, thereby effectively reducing the bending moments on the end span with the accompanying minor savings to the end span girder costs.
- In the case of a continuous structure, integral abutments will generally provide some uplift capacity

in the end spans if necessary.

- Construction capital costs are lower since the expansion joints have been removed – refer to Yang et aI., (1985) and Greimann et aI. (1987).
- Maintenance costs are lower due to the removal of the joints – refer to Yang et aI., (1985), Soltani and Kukreti (1992), as well as Hoppe and Gomez (1996). Traditional expansion-joint type bridges, have a significant portion of the maintenance costs that relate to the damage repairs occurring at these joints.
- Performance under seismic actions is improved due to the interaction of more substructure elements and damping within the system – refer to Hoppe and Gomez (1996) and Frosch, Kreger and Talbott (2009).
- Raked piles are not required (Burke, 1996), and there are also less piles required for bridge substructure support (Soltani and Kukreti, 1992; Hoppe and Gomez, 1996).
- Construction is relatively quick and uncomplicated (Burke, 1996).
- Burke (1996), and Wasserman and Walker (1996) showed that by using integral abutments, shorter end spans may be allowed (if desired), due to the abutment acting as a counterweight and even the uplift capacity of the piles may be accounted for.
- Since there are more connected joints, there is more redundancy and absorption that will prove to be useful under the significant loads imposed during seismic events. The problem associated with maintaining the deck superstructure on its bearing supports is eliminated by using the integral system, and there is also increased inherent damping which limits the potential damage.
- In high-speed railway bridge applications, the individual structural elements such as superstructure and abutment supports can be made more slender in comparison to the traditional jointed railway bridges (Marx, 2011). This is due to the increased static indeterminacy and the related participation of all load-bearing elements in the load distribution.
- The high degree of precision tolerance erection that is normally required for the installation of bridge bearings is avoided when using integral abutments.
- The integral bridge is particularly well suited to situations where a new route may pass under an existing route, by creating a cutting underneath the newly installed bridge deck.

The following lists the <u>disadvantages</u> that are found with the use of Integral bridges:

- Temperature-induced displacements of the abutments can be the reason for settlement of the approach backfill where approach slabs have been used, which causes the formation of voids near the abutment (Burke, 1987). Needless to say, vehicular loading will also contribute to approach fill settlement over time. It should be noted here that the use of approach slabs is generally not recommended in certain European nations (eg. BA 57/01).
- Secondary forces (retained earth pressure, shrinkage, creep, settlement and temperature forces) may often be the cause of cracking in the abutments (Soltani and Kukreti, 1992). Since wing-walls are linked into the integral system, they may also exhibit cracking due to incompatibility with the rotations and contractions of the deck superstructure (Wolde-Tinsae and Klinger, 1987).
- Integral bridges with a skew will tend to cause plan rotations due to the of the cyclical earth pressure change influences on the abutment wall (Hoppe and Gomez, 1996).
- Water may enter the bridge end approach fills, causing undermining of the bridge abutments (Wolde-Tinsae and Klinger, 1987).
- Where abutment support piles are used, they will be subjected to fatigue and high service stresses as a consequence of the continuous cyclical expansion and contraction of the bridge deck. These stresses can ultimately lead to plastic hinges forming in the piles, with a corresponding reduction in their axial load capacity (Soltani and Kukreti, 1992; Yang et al., 1985; Krauthammer et al., 1994).
- Integral bridges should not be used where there are poorly compacted embankments or subsoil, and certain codes restrict their maximum allowable length, even though the maximum length is still somewhat unclear (Soltani and Kukreti, 1992).

The above limitations are generally well-known by the authorities that have built integral type bridges. In certain instances, special features involving distinct detailing practices have been applied. Some of these have been shown to work well (and are widely accepted) and others are up for debate, for example the attempt to reduce the approach fill settlement through the use of approach slabs has had very mixed results.

2.1.4 Summary - Integral bridges introduction

In this section, the integral bridge form (and variations thereof) was introduced, and the merits (and disadvantages) of this bridge type were discussed. Certain loading characteristics and design issues were highlighted and the concept of 'ratcheting' and soil-structure interaction was introduced.

2.2 Summary of design guidelines and limits set in different countries around the world

2.2.1 Applications and limits of integral bridges

The superior advantages associated with the integral type abutment bridges comes with their capability (in accordance with code range limits) to satisfy the functional and serviceability requirements in terms of their safety, durability and economy. Their use is however not recommended in certain applications, as described below.

Integral abutment bridges should generally not be used in scenarios with extreme skews (> 30^{o}) (Burke Jr, 2009). If the abutment foundation piles (where applicable) cannot be drilled through at least 3 - 4.5 m of overburden, then an integral bridge should not be used. If subsoil stability is uncertain at the site or where predicted settlement may not be insignificant, they should not be utilized. Finally, if there is any possibility that the integral bridge may become submerged, then it should not be used at the specific site under consideration, unless the superstructure is appropriately vented and restrained in order to resist uplift due to superstructure buoyancy, or both.

In general, integral bridge lengths are limited so as to minimize the passive backfill pressure effects in addition to the bridge thermal movements, to ranges that can be accommodated by the pavement cycle-control joint system or the approach slabs.

2.2.2 Review of integral bridge use in various countries

This section has been included since it is important for the reader to get a firm understanding of how widespread the integral bridge concept has been used across the World. It is noteworthy that some very different design details have successfully emerged in different countries. The differences in design approach by various countries have implications for the approach to the analysis and design of these structures. The integral bridge type has grown in its international popularity, with a diverse amount of details finding preference in different regions.

- In South Africa, the practice of designing and installing integral bridges is not particularly widespread, however it is gaining notoriety despite the lack of local guidance for this. Notable integral bridges are the 90m long Van Zylspruit bridge (**Figure *2.6***), designed by Mott

Macdonald and built in 2015. This bridge was also part of a research project funded by SANRAL which considered the temperature and soil pressure effects on the bridge (Skorpen, 2018). A further example of an integral bridge built in South Africa would be the KwaBoboza Interchange – a section at the As-built abutment is shown below (**Figure 2.5**), illustrating how the abutment walls may be tied with the approach slab in a typical integral bridge design scenario. The KwaBhoboza Interchange bridge is a 3-span underpass with spans of 18.5m, 24m and 18.5m on a skew angle of 41°. The bridge deck is 61m long and 29.2m wide.

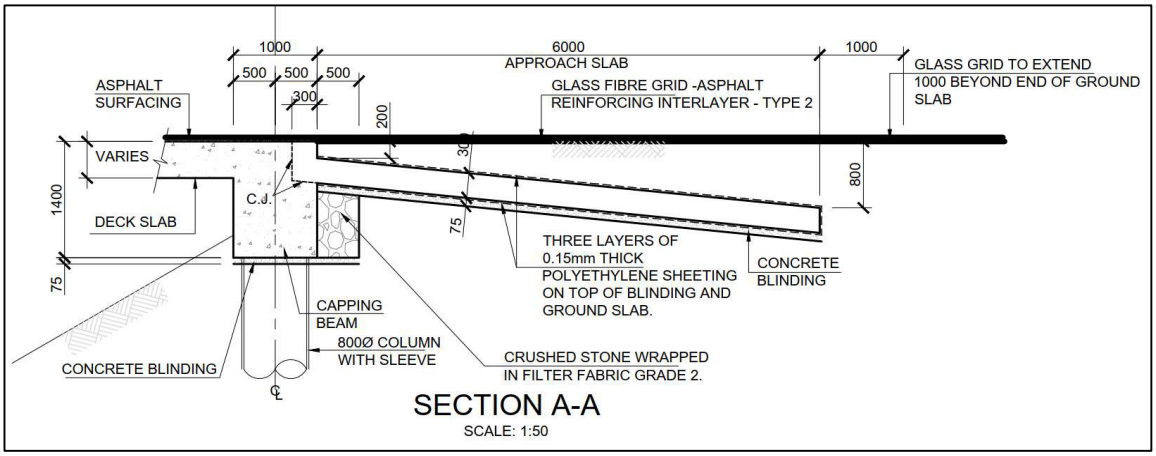

Figure 2.5: KwaBhoboza integral bridge (Source: Mott Macdonald)

Figure *2.6*: Van Zylspruit, 90m integral bridge (Source: Mott Macdonald)

- In the USA, there were 13 000 integral bridges without joints in service by 2005 (Maruri and Petro, 2005). In the USA, States prefer to use their own guidelines and have their preferred

details. The US Federal Highway Administration (FHA, 1980) has recommended that maximum cumulative (for multi-span bridges) span lengths of 91m, 152m and 183m for steel, reinforced concrete and prestressed concrete respectively are used, which are all well in excess of the recommendations contained in BA 42/96 (now superseded). Despite this, bridges extending to 240m in length have been built (Lehane et al., 1999) using progressive increases in length, and subject to lessons learnt from previous experience. There is a discrepancy between modern bridge design regulations which require a design life of 75 years vs. previously issued regulations which only required a 50-year design life, in the USA. This is still rather different in comparison to the 120-year design life required by UK authorities. One significant consequence of the UK requirement is that UK bridges will have an extended period for backfill stresses to develop and therefore increase. Bridges built in the USA have also traditionally been designed with shallower abutments founded on a single row of H-piles, with shorter retained height of fill over which the backfill forces act (Nicholson, 1998).

- In continental Europe, the Scandinavian nations have been at the forefront of integral bridge development. Integral bridges have been used on the high-speed rail network in Spain (Javier et al., 2011). Germany lacks formal guidance however some bridges have been built with lengths exceeding 100m, and one rail bridges has been built with a length exceeding 500m (Marx, 2011). In Finland, the design is based on the full passive pressure (Kerokoski, 2006) and vehicular bridges are restricted to 70m lengths. Integral bridges in Sweden have been in service for over 60 years, where both shallow and full height abutments are used (Mattsson and Sundquist, 2007). Length limitations of 60m to 90m for concrete bridges and 40m to 60m for steel, are dependent on the location (Flener, 2004). In Norway, semi-integral bridges (as opposed to integral bridges) are the norm rather than the exception (Kerokoski, 2006), whilst in Ireland, the BA42 standards are used to design integral bridges (Place et al., 2006). Switzerland relies on similar guidance as per the UK in terms of its length limit restriction of 60m (Kaufmann, 2009). Piles made of steel pipe, filled with reinforced concrete are a very common European integral bridge pile - these piles are typically between 0.7m – 1.2m in diameter. Prestressed concrete piles are also commonly in use.

- Integral bridges are increasingly accepted throughout Asia. Reinforced earth abutments are used commonly in Japan, even in rail applications (Tatsuoka et al., 2016). In 1996, Japan completed its first integral bridge, and South Korea had theirs first installed in 2002 (Burke, 2009). China's first modern integral bridge was built in 2004 (Jin and Shao, 2004) and many more have subsequently been installed across the country. In India, Panday (2015) describes various recently built integral bridges, up to a maximum of 520m long.

- In the UK and Ireland the requirement under the BD 57, DMRB 1.3.7 Code is that all new bridges that are less than 60 m long and that have a skew less than 30° shall be constructed as Integral Abutment Bridge structures with continuity over intermediate supports unless there are overruling reasons. Steel H-piles are typically specified in England and Ireland, with their strong axis aligning perpendicular to the bridge direction of expansion.

- In Australian practice, most short to medium span bridges reduce the use of expansion joints through the incorporation of thin link slabs over piers for simply supported spans. This practice is described in detail by Kumar (1998) and Gergess (2019). Link slabs at piers provide a means of transferring vertical and axial forces, however the low bending stiffness of the link slab means that there is no effective moment continuity. The resultant deck has no joints between the abutment expansion joints.

2.2.3 Standards and Codes in various countries

There is voluminous research concerning the subject of integral bridge design and the majority of the major role players in bridge codes have their own set of codes and standards that deal directly with the topic of the design of integral bridges. Note that at the time of writing, South Africa does not have its own set of guidelines for Integral bridge design, and so the tendency is to rely on the specialist advice contained in foreign codes and standards when designing integral bridges in South Africa. The following recognized codes and guidance notes play a role in today's integral bridge market:

- BA 42/96 Amendment No. 1 - The Design of Integral Bridges (this standard is now withdrawn, and is replaced by PD 6694-1:2011)
- BSI. PD 6694-1:2011 - Recommendations for the design of structures subject to traffic loading to BS EN 1997-1:2004, British Standards Institute.
- SCI Publication P356 – Composite Highway Bridge Design in accordance with Eurocodes and the UK National Annexes (Including Corrigendum, March 2014). The Steel Construction Institute.
- Richtlinien für den Entwurf, die konstruktive Ausbildung und Ausstattung von Ingenieurbauten, Teil 2 Brücken, Abschnitt 5 Integrale Bauwerke, RE-ING, 2016. (German Guidance)
- Konstruktive Einzelheiten von Brücken, Kapitel 3 Brückenende, Bundesamt für Strassen ASTRA, 2011. (Swiss Guidance).
- AASHTO LRFD Bridge Design Specifications, American Association of State Highway and Transportation Officials, Washington D.C., 2012
- AS5100.3 Bridge Design Part 3: Foundations and soil-supporting structures, Standards Australia International, Sydney, NSW., 2004
- Bridge Manual SP/M/022 3rd Edition Amendment 1. Transport Agency, Wellington, NZ, 2014.

The summary in **Table 2.1** by Rhodes (2014) relates to the recommendations contained in the PD 6694-1:2011 Code (contained in the above list). The contents of this thesis research are mostly related to the springs that are required for the Integral Abutment type models that are highlighted in the red box in the table below (ie. the full height abutment wall on a single row of piles and the bank pad on single row of piles).

2.2.3.1 PD6694-1:2011 Design approach

The PD 6694-1:2011 code describes two basic approaches to the design of an integral bridge:

- **Limit equilibrium approach**

The limit equilibrium analysis methods are applicable to abutments where:

a) The typical thermal deck end movement does not exceed 40 mm

b) The skew of the bridge does not exceed 30°

c) The depth of soil influenced by the movements of the abutment is easily identifiable without using a soil–structure interaction (SSI) analysis – an example of this is abutments founded on spread footings () or end screen abutments.

d) Abutments with pile caps **Figure *2.3*** (c) that have more than one row of piles may similarly be designed using limit equilibrium methods, with the proviso that the movement at the pile cap level is minimal enough for the at rest pressure (K_o) to be assumed to be acting at the level of the pile cap.

Integral Abutment Type	Limiting equilibrium	SSI	Notes and reference within PD6694-1 [9]
Full height wall on pad footing	Yes		Granular backfill. Assumed earth pressure distribution from Fig 5 and K* from clause 9.4.3 incorporates ratcheting.
Full height wall on piled footing	Yes		
Bank pad	Yes		Granular backfill. Triangular earth pressure distribution and K* from clause 9.4.4 incorporates ratcheting.
Embedded wall		Yes	Soil modelled using continuum. For granular soils or backfill, modify E' with depth to suit Annex A and restrict pressures to K* from clause 9.4.3. Alternatively nonlinear spring model with similar considerations.
Full height wall on single row of piles		Yes	Soil modelled using nonlinear springs. For granular backfill, modify stiffnesses and limiting pressures to suit Annex A.
Bank pad on single row of piles		Yes	Soil modelled using nonlinear springs. Reduced stiffness and limiting pressures for front face of piles. Granular backfill to end screen. Triangular earth pressure distribution and K* from clause 9.4.4 incorporates ratcheting.

Table 2.1: Guidance for integral abutment types vs modelling approaches for SSI (Rhodes, 2014). Highlighted items in red are relevant to the modelling used in this thesis.

Note that the limit equilibrium methods are not applicable in the following scenarios:

1) Abutments founded on only a single row of piles

2) Embedded wall abutments

3) Over-consolidated backfill material

4) Cohesive soils (eg. Clays)

5) Layered soils

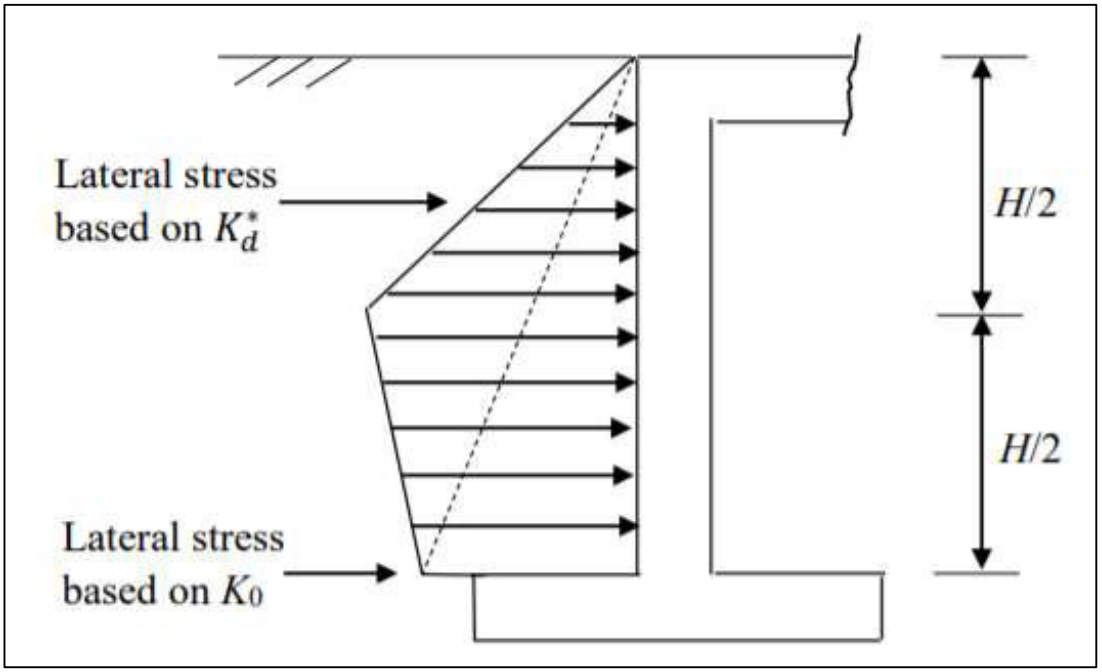

Figure *2.7*: Typical pressure diagram, PD 6694-1:2011

Figure *2.7* gives the diagram of the backfill pressure distribution assumed in PD 6694:1-2011. This Code uses the following lateral stress equation for the scenario where the abutment can rotate and/or translate due to the thermal movement:

$$K_d^* = K_0 + \left(\frac{Cd_d'}{H}\right)^{0,6} . K_{p;t} \qquad \text{(Eqn. 1)}$$

The equation below is for the calculation of lateral stresses on end screens or abutments that allow for thermal movements by translation but with no rotation:

$$K_d^* = K_0 + \left(\frac{40d_d'}{H}\right)^{0,4} K_{p;t} \qquad \text{(Eqn. 2)}$$

Where:

K_0 = coefficient of earth pressure at rest

K_d^* = earth pressure coefficient for expansion

H = height of wall or end screen

C = is 20 for foundations on flexible (unconfined) soils with E ≤ 100 MPa, is 66 for foundations on

rock or soils with E ≥ 1 000 MPa

$K_{p;t}$ = coefficient of passive earth pressure used in the calculation of K*

d'_d = deflection of an integral bridge abutment at a depth H/2 below ground level

The reader is referred to the PD 6694:1-2011 Code for further explanations in this regard.

- **Soil–structure interaction (SSI) guidance**

An indication of where SSI methods should be used is found above in **Table 2.1**. For bridges excluded by the limit equilibrium requirements, backfill earth pressures on integral abutments may be evaluated using SSI methods which incorporate an appropriate numerical model of the relevant soil properties.

The PD6694-1:2011 approach used to determine the applied pressures on the back of an abutment wall using soil-structure interaction, is iterative as indicated in **Figure *2.8*** below. The properties of the soil used in the SSI model depend on the average rotational strain in the soil (d'_d / H'). The values of d'_d / H' (and therefore the soil properties), differ between the soil in front and behind the abutment. Some iterations are required in order to determine d'_d and H'.

The SSI model needs to explicitly include all the vertical elements of the abutments and piles, with the correct horizontal, vertical and rotational springs.

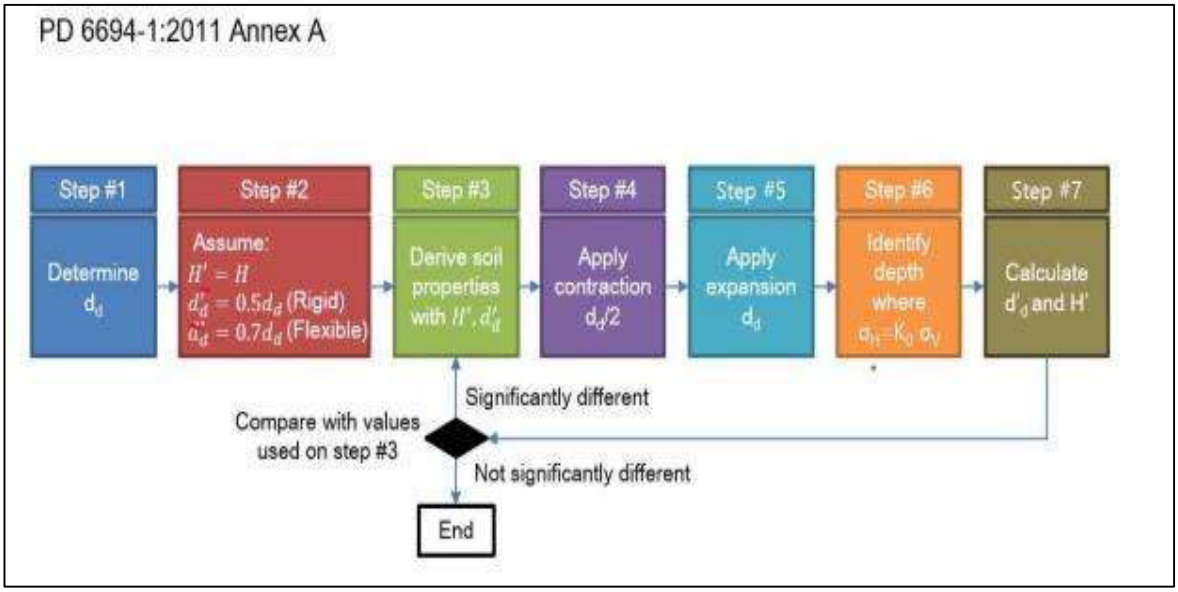

Figure *2.8*: Iterative method as described in PD6694-1

Definition of *H'* and *d'*$_d$ for the front and back of the abutment:

For the back side of the abutment (see the **Figure *2.9*** diagram):

• *H'* is the depth of soil behind the abutment, that is affected by the repeated deck expansion, which may be assumed as the depth from finished ground level to the level at which the earth pressure reduces down to its at rest (K_o) value when the deck is at its maximum expansion for the combination of actions under consideration.

• *d'*$_d$ is the horizontal deflection of the abutment wall at a depth *H'*/2 below ground level.

A 10-step process is then described in Section A.4.3 of the PD6694-1:2011 Code which demonstrates the iterative process of determining the value for *d'*$_d$ and *H'*. The reader can refer to this section of the code to get a better understanding of the steps involved. A worked example has also been published by the Highways Agency in collaboration with Arup – refer to the "HA Commentary on PD 6694-1 Issue 4" (Highways Agency / Arup, 2011).

Subsequent frame analysis

Once long-term soil properties have been obtained from the soil-structure interaction these can be used to derive the spring stiffness values and corresponding soil forces for application in the structural analysis (generally a grillage model) of the global behaviour of the bridge. The model will combine the thermal expansion / contraction loads in order to obtain compatible structural moments.

These soil pressures represent the maximum soil pressure that would be generated by bridge deck expansion and can be analysed and enveloped with other bridge loads in accordance with the envelope suggested in PD6694-1, 9.4.8.

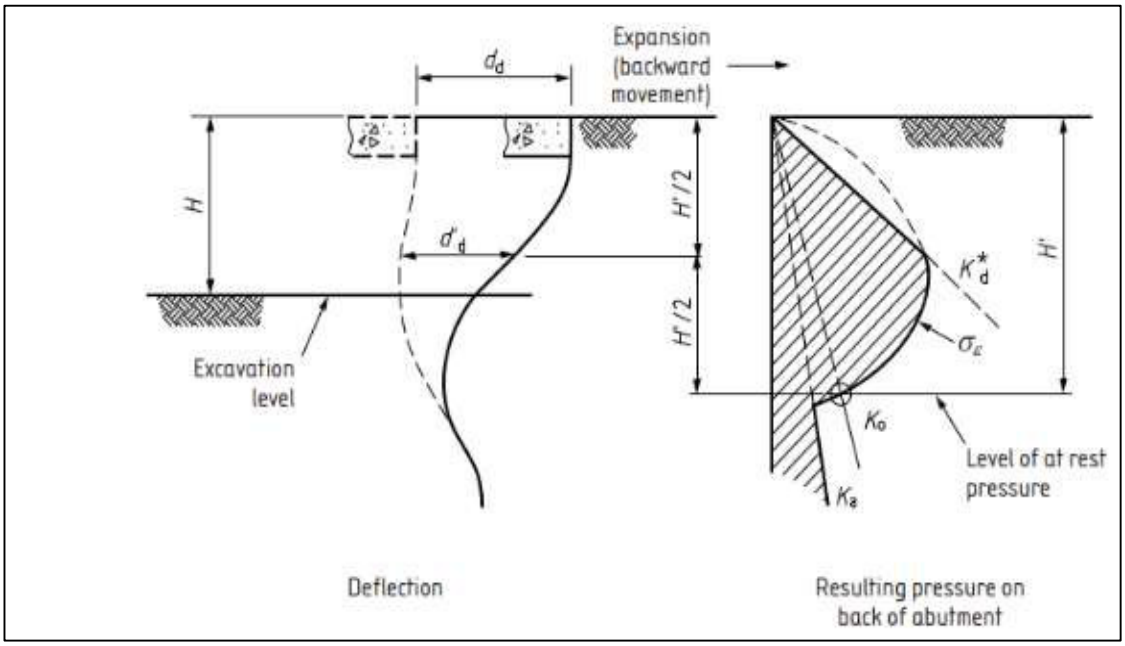

Figure *2.9*: Earth pressures applied to the back of abutment (expansion case)

2.2.3.2 AASHTO Design approach

There is minimal guidance from the AASHTO Codes of practice in regard to the design of integral bridges, the AASHTO LRFD Bridge Design specifications (2012), state that "Maximum span lengths, design considerations, details should comply with recommendations outlined in FHWA Technical Advisory T 5140.13 (1980), except where substantial local experience indicates otherwise". The document referred to above is out of date as new theories and understanding of integral bridge behaviour and soil-structure interaction have come about since its publication.

The following guidance diagram from **Figure *2.10*** and notes on assumed pressures is taken from the Minnesota Department of Transportation LRFD Bridge Design Manual, Manual 5-392, and outlays the acceptable integral bridge limits in terms of length and skew angle. Note that the diagram units are in feet.

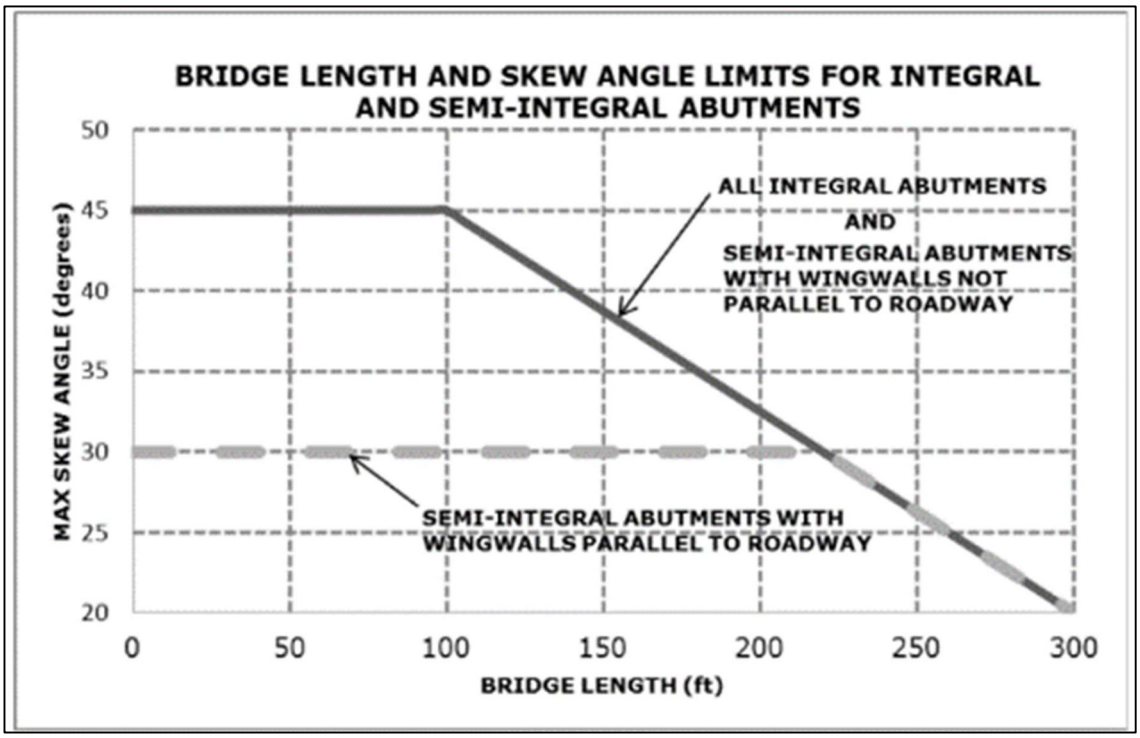

Figure *2.10*: Bridge lengths and skew angle limits (AASHTO)

Integral Abutment General Design/Analysis Method

Referring to **Figure *2.11***, the passive pressure labelled as p_p at the bottom diaphragm level, is determined using Equation's (3) and (4). This pressure is applied as a uniform pressure to the stem.

$$P_p = k_p . \gamma_{soil} . h_{soil} \qquad \text{(Eqn. 3)}$$

$$k_p = tan^2\left(45 + \frac{\phi}{2}\right) \qquad \text{(Eqn. 4)}$$

Where:

k_p = coefficient of passive pressure

h_{soil} = height of retained soil between the top of the stem, to top of the deck (see **Figure *2.11***)

γ_{soil} = unit weight of backfill soil

ϕ = angle of backfill material internal friction (use 30 degrees)

Then design the abutment for a moment M_{up} equal to:

$$M_{up} = \gamma_{EH}.\left(\frac{P_P.h_{stem}^2}{2}\right) \quad \text{(Eqn. 5)}$$

A passive earth pressure load factor is not specified by the LRFD design specifications. A maximum load factor for the active earth pressure calculation, γ_{EH} = 1.50 is therefore recommended.

The front and back face of the abutment stem is designed for the passive soil pressure caused during bridge expansion. The abutment stem is considered to be a continuous beam with supporting piles and should be designed for a maximum moment of:

$$M_{up} = \gamma_{EH}.\left(\frac{w_P.L^2}{10}\right) \quad \text{(Eqn. 6)}$$

Where:

M_{up} = Maximum Abutment Moment

w_p = the passive pressure that is determined at the bottom level of the abutment diaphragm, applied to the model as a uniform pressure to the stem of the abutment = $p_p.h_{stem}$

L = pile spacing

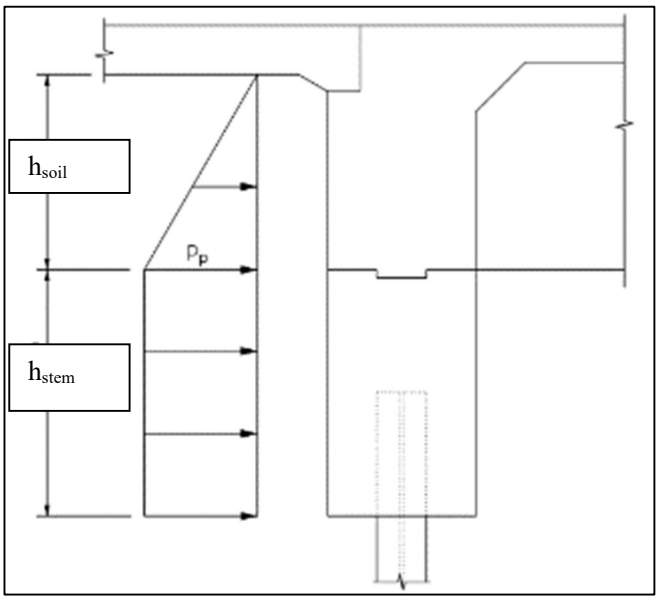

Figure *2.11*: Pressure diagram - Minnesota Dept of Transportation LRFD Bridge Design Manual

2.2.4 Summary - design guidelines and limits set in different countries around the world

This section introduced the various limits and applications that are relevant to the integral type bridge. The section also provided an overview of the Codes that are most commonly used for integral bridge design. Examples of the use of integral bridges from across the globe were illustrated, and it is obvious from the historical account that certain countries have been installing this bridge type for a number of years. Note that the PD6694-1:2011 Code is currently the most commonly used Code of Practice used for designing integral bridges across the globe, and its iterative analysis method has been highlighted in this section.

2.3 Soil Structure Interaction

2.3.1 Background to Soil-structure interaction

The simplicity inherent in integral abutment bridges unfortunately makes their idealization for modelling complex. In integral abutment bridges, the rigid connection between the superstructure, abutments, and piles requires a fully integrated (coupled) geo-structural analysis. Idealization of the soil-pile interaction in the analysis of an integral abutment bridge has been found to be problematic (Faraji et al. 2001). The lateral soil reaction not only depends on the soil type, depth, and stiffness properties, but also on the pile's lateral deflection.

Since the soil behaviour often becomes nonlinear, the soil-pile interaction usually requires an iterative analysis to determine the soil reactions and the associated pile lateral deflections. Two common approaches are therefore used to idealize the soil-pile interactions for laterally loaded piles, namely (i) the p-y approach and (ii) the continuum mechanics approach.

In a study by Dicleli (2009), the effect of soil–structure interaction on the magnitude of the internal forces in integral abutment bridge (IAB) components due to live load effects was studied. For this purpose, structural models of typical IABs were built by either including or excluding the effect of backfill and foundation soil. Models were then analysed using AASHTO live loading. In the analyses, the effects of the backfill and foundation soil on the magnitude of the internal forces in IAB components were studied for various structural, geometric and geotechnical parameters such as bridge size, abutment height and thickness, pile size and orientation, number of spans and foundation soil stiffness.

The analysis results revealed that the soil–bridge interaction had a significant effect on the magnitude of the live load moments in the components of IABs. Dicleli found that including the effect of backfill behind the abutments in the structural model would generally result in larger superstructure support and abutment moments and smaller superstructure span and pile moments. The difference between the live load moments for the cases with and without soil–structure interaction effects was found to be dependent on the foundation soil stiffness. Surprisingly, the soil–structure interaction was however found to have only a negligible effect on live load shear in the superstructure.

The process used to determine the spring stiffness and structural response of an integral abutment bridge using the p-y approach is iterative (as seen in the PD6694-1:2011 Code approach). The process normally involves two computational tools: (1) a soil-structure interaction analysis to generate the p-y curves and evaluate the soil stiffness, (2) a structural analysis to evaluate the structural responses. The spring stiffnesses in the first trial of the structural analysis are rough estimations based on the soil type and the depth of each spring. In the next step, the lateral pile deflections obtained are input into the

soil-structure interaction analysis program to determine the soil pressures or soil stiffnesses over the pile depth. In the following step, the spring stiffnesses in the structural analysis program are updated to generate a new set of deflection values for subsequent input to the soil-structure interaction analysis program. Iterations of this sequence continue until the deflections and soil stiffnesses converge.

2.3.2 Structures where Soil-structure Interaction is applicable

The soil to abutment interface stresses are governed by a soil-structure interaction that is complex, and which is characterised in terms of the cyclical thermal expansion and contraction bridge deck movements, which are /the result of solar heating. Where it is found that the stiffness of the soil and the structural interaction has a more important function in determining the behaviour of the structural system, the limiting equilibrium approach is deemed to not be appropriate. Such is the state of play for a number of integral bridge types such as those described below, commonly shown in **Figure 2.12** and **Figure 2.13**. The soil may be represented using continuum type elements or springs behind the abutment and the foundations in various FEA approaches to SSI.

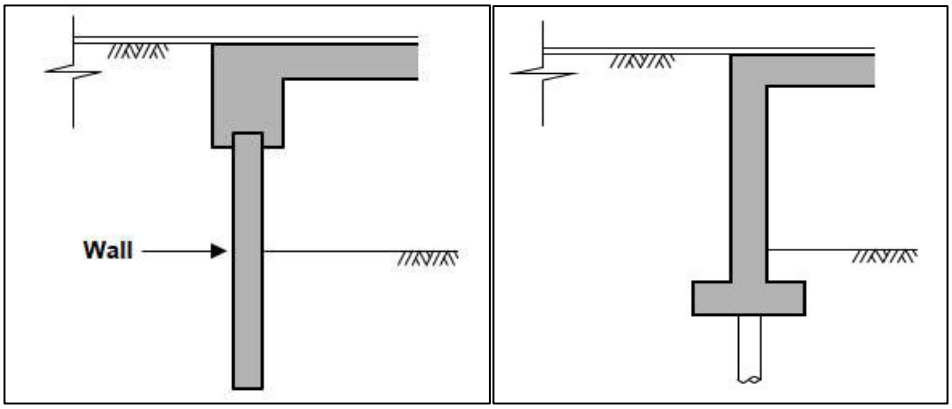

Figure 2.12: Embedded wall integral abutment (left) and Integral abutment with single row of piles, full height (right) (Rhodes, 2014)

The bank-pad abutment system is commonly supported by steel H-piles (see **Figure 2.13**), and these are often a popular form of integral bridge. In regard to these abutments, the soil stiffness is represented using springs, and is called a 'subgrade modulus' spring model. Certain authorities require that the piles are sleeved for the upper portion, so as to isolate the pile from the surrounding backfill and reduce the effects of SSI. The effect of this however is that the in and out movement of the piles in the backfill will be increased, due to the additional freedom of movement offered by the sleeves. Using this technique, one can expect that there will be increased earth pressures on the bank pads when the soil-ratcheting occurs, however the total horizontal abutment load will remain quite small due to the low pad depth. This type of bridge model is adequately catered for, using springs or K* pressures (Rhodes, 2014).

Embedded walls such as contiguous piled, secant or diaphragm - as seen in **Figure 2.12** should use the full continuum model, which is a more suitable method of analysis.

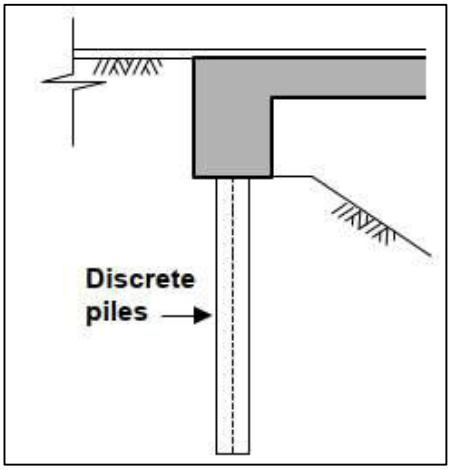

Figure 2.13: Bank pad on single row of piles (Rhodes, 2014)

2.3.3 Laterally loaded pile theory

Understanding the behaviour of laterally loaded piles that form part of the integral bridge is relevant since the soil-structure interaction effect exerts stresses on the piles. The modulus of lateral subgrade reaction distribution along the pile length has a significant effect on its behaviour, yet it is the top part of the pile in particular, that is most affected by the modulus of lateral subgrade reaction, since its effects are most prevalent here.

Lateral load capacity has been studied since the 1960's (Broms - 1964a, 1964b). Research has shown that the maximum bending moments form near the pile top, adjacent to the head of the pile especially in long, flexible piles. In slender piles, the bending moment capacity of the pile will tend to govern the design, conversely, in short and stocky piles the shear capacity of the soil will tend to govern.

For the integral bridge scenario, the piled abutments must resist considerable horizontal forces and bending moments, as a result of the thermal movements arising from the bridge deck.

For laterally loaded pile behaviour, the earth pressure is correlated with the coefficient of lateral sub-grade reaction by Eqn. 7 (and refer to Section 2.5.5 further on, in this document):

$$p = k_h . y \qquad \text{(Eqn. 7)}$$

Where:

p = earth pressure (MN/m^2)

y = displacement of pile (m)

k_h = coefficient of lateral subgrade reaction (MN/m^3)

The formula for lateral subgrade reaction behaviour is shown in Equation 8 below. Note how the formula shows how the spring stiffness for the pile is directly proportional to the pile diameter:

$$k_s = cc_s . k = cc_s . k_h . D = cc_s . n_h . \left(\frac{z}{D}\right) . D \qquad \text{(Eqn. 8)}$$

Where:

k_s = Spring stiffness

k = Modulus of lateral subgrade reaction (MN/m^2)

k_h = Coefficient of lateral subgrade reaction (MN/m^3)

cc_s = Spring division along length of pile (m)

D = Pile diameter (m)

n_h = Constant of lateral subgrade reaction

z = Depth co-ordinate (m)

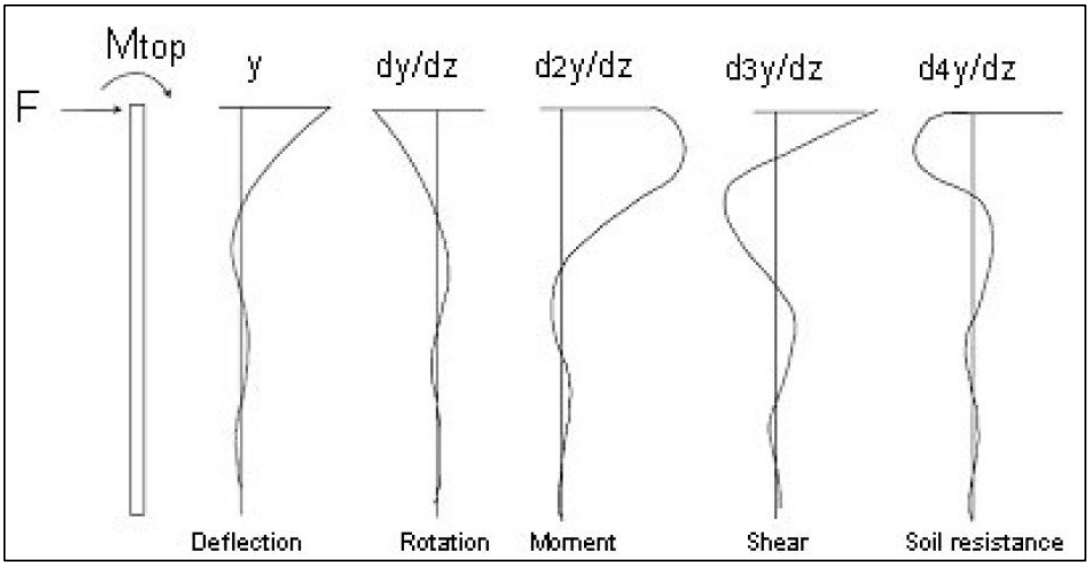

Figure 2.14: Deflections, slopes (rotations), bending moments, shear forces and soil reactions, assuming elastic conditions for laterally loaded piles (Reese and Matlock, 1956). Note the highly non-linear behaviour of the pile response to lateral loading.

If the piles are installed in an elastic medium, where lateral soil stiffness per unit length k and pile flexural stiffness E_pI_p are assumed to be constant, then the following differential equation may be described:

$$E_p.I_p.\frac{d^4.y}{d.z^4} + k.y = q \qquad \text{(Eqn. 9)}$$

Furthermore, the following relationships are used to describe the characteristics of the pile behaviour:

Lateral deflection, $u = \left(\frac{H_0.T^3}{E_p.I_p}\right).A_y + \left(\frac{M_0.T^2}{E_p.I_p}\right).B_y$ (Eqn. 10)

Slope, $\theta = \left(\frac{H_0.T^2}{E_p.I_p}\right).A_s + \left(\frac{M_0.T}{E_p.I_p}\right).B_s$ (Eqn. 11)

Bending Moment, $M = (H_0.T).A_m + (M_0).B_m$ (Eqn. 12)

Vertical load shear, $V = H_0.A_v + \left(\frac{M_0}{T}\right).B_v$ (Eqn. 13)

Soil reaction, $p = \left(\frac{H_0}{T}\right).A_t + \left(\frac{M_0}{T^2}\right).B_t$ (Eqn. 14)

Where:

$T = \sqrt[4]{\frac{E_p.I_P}{K}} = \frac{L_c}{\sqrt{2}}$ (Eqn. 15)

y = lateral deflection of pile

E = Youngs Modulus of Pile

I = Second Moment of Area of pile

H_0 = Horizontal force

M_0 = Bending Moment

A_v = Pile Shear Area

The above formulas are indicative of the pile's non-linear response to lateral loading. A and B are coefficients related to the lateral and moment loading respectively – expressions for A and B are provided in Table 9 of CIRIA Report 103 (1984). If one solves the above complex equations, the diagrams shown above in **Figure 2.14** are found (CIRIA Report 103, 1984). CIRIA Report 103 (1984) then makes a distinction between two cases for the modulus of lateral subgrade reaction distribution as shown below:

1) Constant coefficient of subgrade reaction

Long, free and fixed-headed piles

For the case where L > 1.5 L_C, the above equations may be combined to give:

$u = \left(\frac{H_0.T^3}{E_p.I_p}\right).C_y$ (Eqn. 16)

Where:

$C_y = A_y + \frac{M_0.B_y}{H_0.T}$ (Eqn. 17)

Short or stiff free and fixed-headed piles

For the case where L < 1.5 L_C, the deflection may be calculated from simple statics.

2) Coefficient of subgrade reaction increasing as depth increases

With normally-consolidated sands and clays, where the coefficient of subgrade reaction linearly varies as the depth increases, Eqn. 16 holds true.

With respect to Eqn. 18 below, the behaviour of piles that exceed 4T is similar to that of an infinitely long member. For piles with a length of less than 2T, behaviour is more like that of a short rigid member.

$$T = \sqrt[5]{\frac{E_p.I_p}{n_h}} \qquad \text{(Eqn. 18)}$$

The deflection of short piles are again calculated from statics. For free-headed piles, Broms (1964a, 1964b) found that:

$$u_0 = \frac{18.H_0.\left(1+\frac{1.33.e}{L}\right)}{L^2.n_h} \qquad \text{(Eqn. 19)}$$

For fixed headed piles,

$$u_0 = \frac{2.H_0}{L^2.n_h} \qquad \text{(Eqn. 20)}$$

Where:

e = the height of the pile above the soil level (m)

The force-displacement relationship for the lateral subgrade reaction is hyperbolic in shape and is presented in **Figure 2.15**. The force-displacement relationship is affected by the initial stiffness as well as the ultimate resistance for differing developments of strain. The Finnish guidelines assume a tri-linear behaviour force-displacement relationship for the lateral subgrade reaction – see Kerokoski (2006). The hyperbolic formula describing the behaviour is as per Eqn. 21 below:

$$q = \frac{y}{\frac{1}{k_i}+\frac{y}{q_{ult}}} \qquad \text{(Eqn. 21)}$$

Where:

K_i = Initial modulus for the lateral subgrade reaction (MN/m^2)

q_{ult} = Ultimate lateral soil resistance, asymptote of hyperbolic behaviour (MN/m)

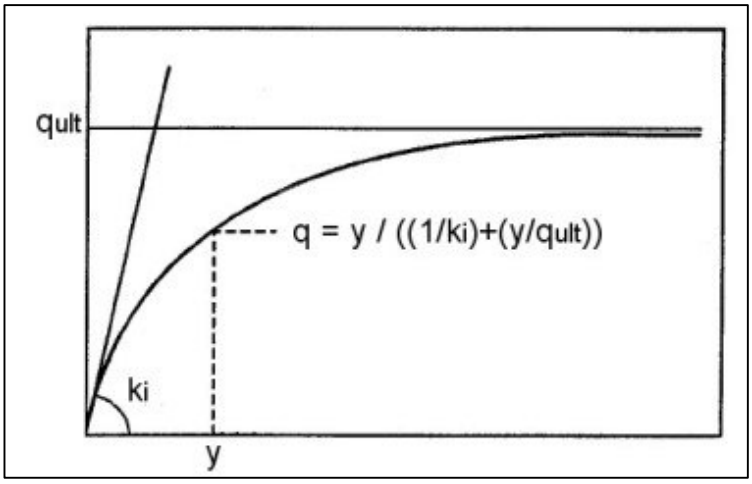

Figure 2.15: Force-displacement relationship of pile-soil-interaction, Kerokoski (2006)

Further reading on the topic of laterally loaded pile behaviour may be taken from CIRIA Report 103 (1984), Broms (1964a, 1964b) Laaksonen (2011) and Tomlinson (1994).

The modulus of lateral subgrade reaction is indeed influenced by the choice of pile diameter, although this has been the subject of much debate. The pressure bulb associated with piles with two different diameters is shown in **Figure 2.16**, below. The bulb influence length (L) is presumed to be linearly related to the pile diameter, however in the ultimate limit state load situation, it is the secant modulus that is also related to the pile diameter since the ultimate strength depends on the pile diameter.

Ashford (2005), found that when displacement levels are below the ultimate soil strength, the pile diameter has an inconsequential outcome to the p-y curves. He also found that using standard p-y curves from the literature tended to underestimate weakly cemented sand's soil resistance, for small diameter piles, however the curves tend to overestimate the resistance of the soil for the larger diameter piles. Caution and awareness of the inherent factors at play should therefore be used when using the standard p-y curves for large diameter piles in a weakly cemented sand.

For the lateral loading case, a pile group's behaviour is complex. If all the piles are vertical, of the same cross section, similar length, with similar uniform ground conditions, and the pile cap is rigid then the group capacity may be assumed to be the summation of individual capacities for horizontal loading. It is preferable however to use stiffness analysis to distribute combinations of vertical and horizontal pile cap loading to the piles.

Note that the reaction from the soil-pile interaction to lateral movement is made up of two components: (i) the normal reaction from the front and (ii) the side friction and normal reaction - this is illustrated in **Figure 2.17**.

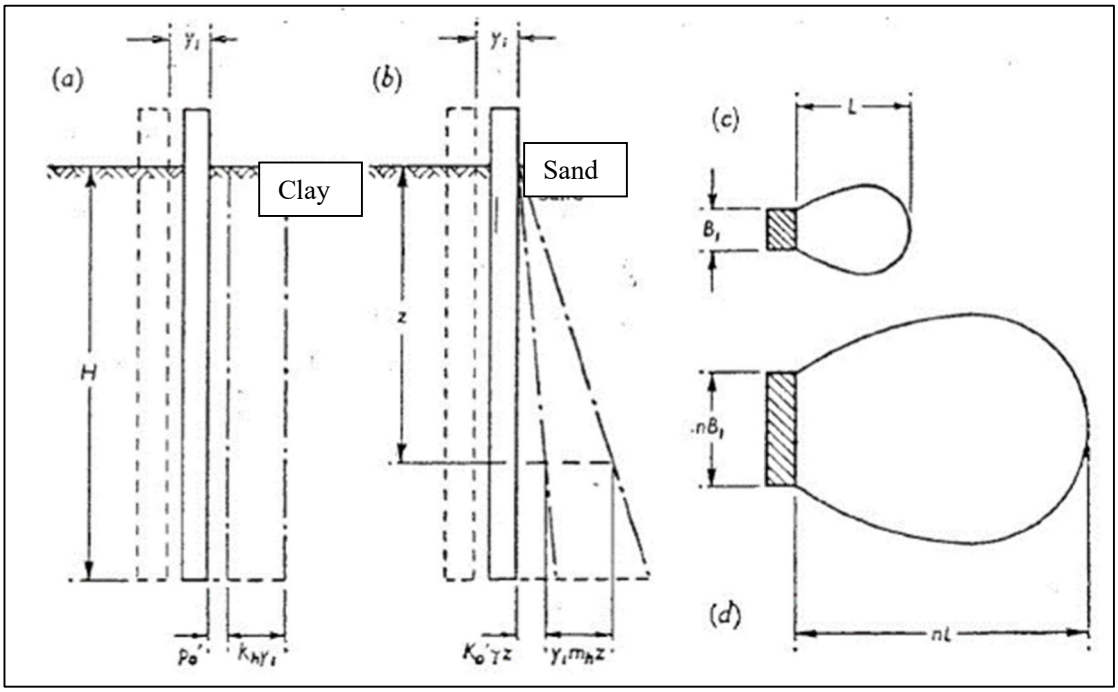

Figure 2.16: Pile Diameter effects on the Bulb Pressure dimensions (Laaksonen, 2011)

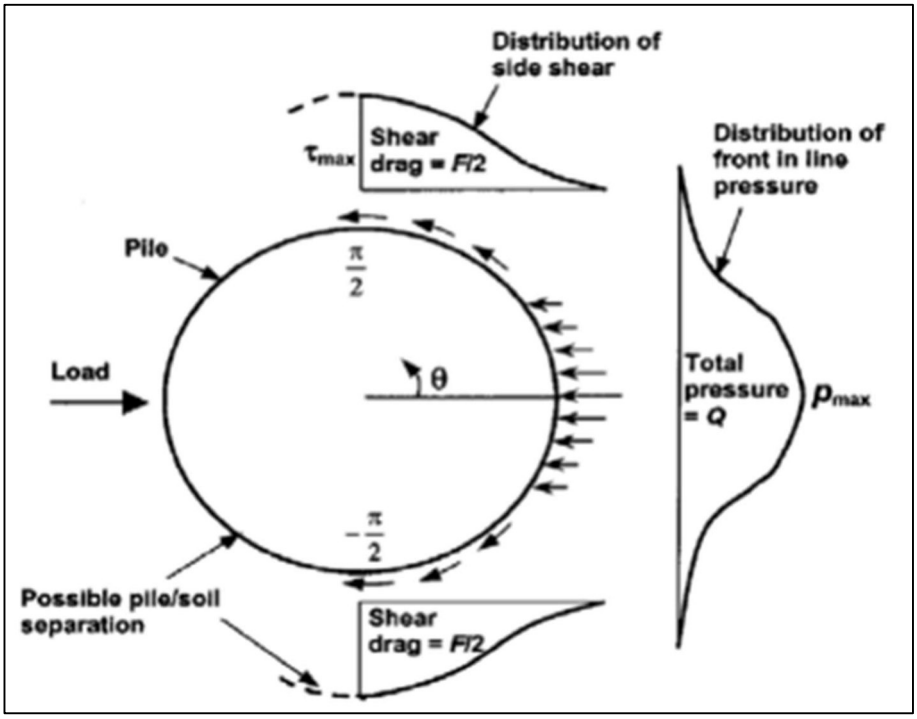

Figure 2.17: Front earth pressure and side shear distribution around a pile being subjected to lateral load (Laaksonen, 2011)

2.3.4 Continuum Mechanics Approach

As an alternative to the p-y approach, the continuum mechanics approach is generally viewed as being more rational yet versatile. This approach is usually based on finite-element or finite-difference numerical formulations (Gerolymos et al. 2009). The finite-element method requires discretization of the pile and surrounding soil. The differential equations that quantify the behaviour of the pile and soil are solved by minimizing the potential energy within the system.

The finite element method can capture the most important features of the complex pile-soil interactions, but it is rarely used in the design of laterally loaded bridge structures owing to the high computation time required (Gerolymos et al. 2009).

2.3.5 Summary - Soil structure interaction

The above section has considered the complexities inherent in the analysis of structures that interact with their adjacent soil elements, in what is termed a soil-structure interaction (SSI). Bridge structures where this SSI interaction is prevalent were highlighted. The literature survey has shown that there are several important factors such as the coefficient of lateral sub-grade reaction that play a role in a structure's response when it is embedded in soil. The two methods of analysis, namely: (i) the p-y method and (ii) the continuum mechanics method were discussed.

2.4 Modelling of integral bridges

2.4.1 Modelling theories and assumptions for 3D and 2D Models

Framed integral abutments need to be modelled so that the connection between the deck and the supporting sub-structure have complete moment continuity. The frame endscreen walls are subjected to soil pressures from the backfill material and the pressures will relate to displacements in the analysis. If the Piers are in contact with the soil, they too will be characterized by earth pressure related displacements, even though the forces involved are relatively small in comparison with the abutment forces.

A study by Kim, W. et al (2016) considered the following (i) free expansion analysis, (ii) approximate analysis, (iii) 2D static analysis, (iv) 2D time-history analysis, (v) 3D static analysis (S.A), and (vi) 3D time-history (T.H.) analysis for both 2D and 3D models. The study concluded with the following remarks:

1. Free expansion analysis can prove to be useful only for the preliminary design of piles. This analysis method is unconservative in determining pile shear force and pile head displacement but is conservative for the pile moment calculation.

2. 2D and 3D static analysis predicts only the initial girder and pile response. A 2D and 3D time-history analyses should be performed if the bridge response over time is required.

3. A 2D static analysis (S.A.) will not incorporate the soil–structure interaction and time-dependent effects. A 2D S.A. may be acceptable for pile response predictions but should not be used in the prediction of the superstructure behaviour.

4. 2D T.H. is an advanced approach that fully incorporates soil–structure interaction and time-dependent effects over a designated period of time. In the study, all of the bridge responses become stable after 15 years of simulated time. However, the maximum single member response was not available by using this approach. Apart from the girder axial force, all other responses were very similar to those obtained in the 3D-T.H.

5. Observation and comparison of 2D-S.A., 2D-T.H., 3D-S.A., and 3D-T.H. showed that time-dependent effects are significant in integral abutment bridges (IAB) and should be considered in the analysis process.

6. The abutment rotations caused by backfill pressure and time-dependent effects can significantly influence the IAB responses.

The above considerations will be born in mind when drawing conclusions in regard to the present study.

2.4.1.1 Finite Element Models

The finite element analysis technique is commonly used in the analysis of complex structures by dividing up the structure into a number of smaller elements with appropriate section characteristics and properties. Where applicable, the elements are connected to each other at distinct joints called nodes - this method has been established for use with the analysis of two-dimensional elastic structures since the 1950s (Hambly, 1991).

Numerous finite element model layouts exist, that have been tested and used, both in the two-dimensional and three-dimensional realms of analysis, with and without soil springs, piles of full length and piles with an equivalent cantilever length (Dicleli, 2000, Shah, 2007), (**Figure 2.18**) and so forth. By way of example, the integral abutment bridge models proposed Zordan et al. (2011) are shown in **Figure 2.19**.

The deck can be modelled in a traditional grillage in order to obtain realistic pile head displacements/rotations, however the end diaphragm model must have its stiffness and physical depth accurately modelled. Horizontal displacements and rotations of the pile head at the diaphragm soffit will induce the pile bending moments, therefore it is relevant that the global analysis model should capture this behaviour as accurately as possible. Note that either lateral springs located along the pile length or the 'equivalent cantilever' concept may be used in the global model. The soil resistance over the length of the ring/pipes does not need to be included in the model should the piles be situated inside rings or in pipes. Note that the equivalent cantilever concept sometimes used for modelling of the abutment piles was found to inconsistently yield either conservative or unconservative estimates of the internal forces in the components of IABs except for the superstructure shear (Dicleli, 2009).

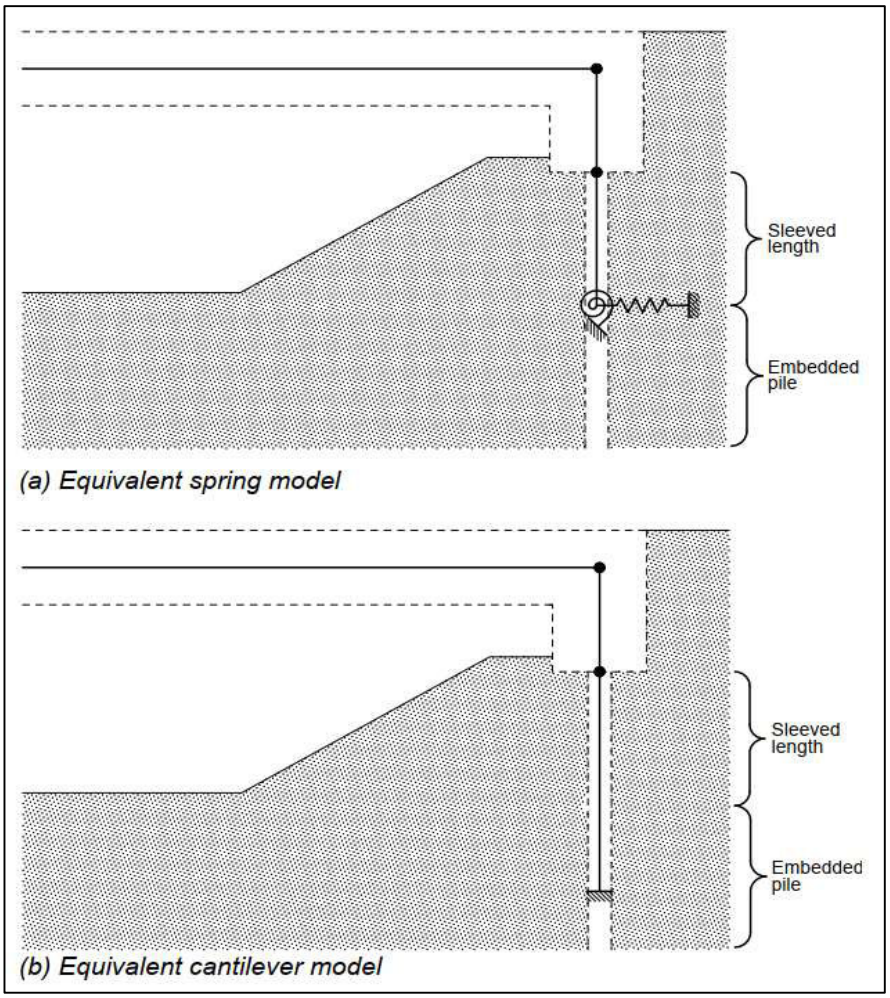

Figure 2.18: Equivalent spring and cantilever models for ends of the bridge (Iles, 2005)

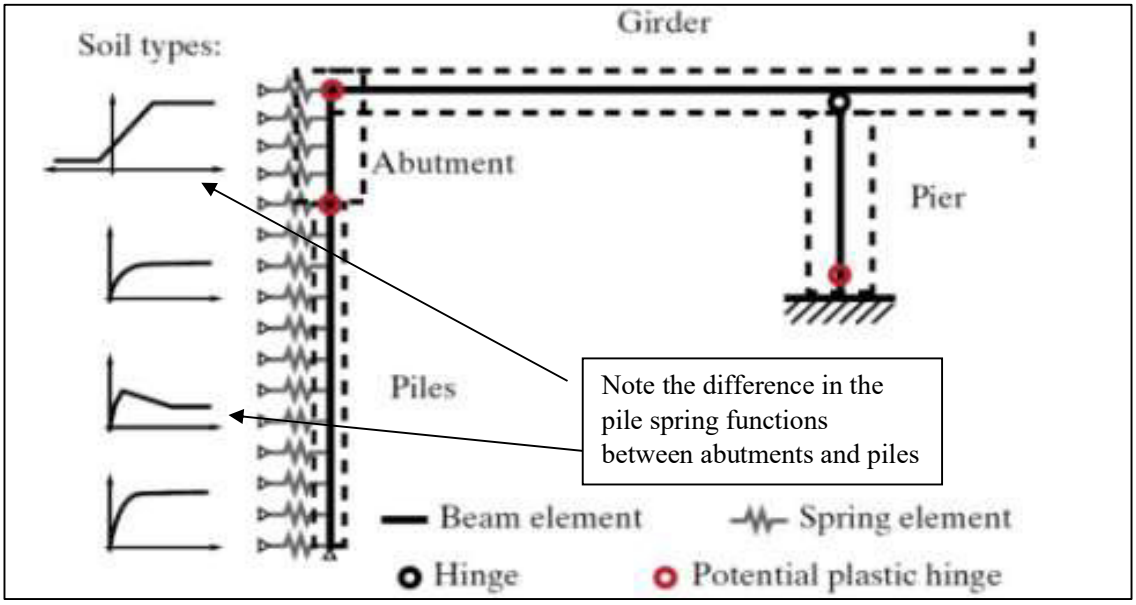

Figure 2.19: 2D finite element model with pile modelling using the soil-spring approach (Zordan et al., 2011). This diagram is crucial to understanding the approach used for the different spring types.

2.4.1.2 Bridge contraction on flexible supports

The majority of bridge structures are constructed on supports that possess some degree of flexibility. Piers and abutments are provided with foundations that bear either directly on the underlying ground or on piles that transfer loads through pile caps.

The soil that underlies a strip foundation may be simplified by using a set of linear elastic springs (**Figure 2.23**). Dobry and Gazetas (1986) provide spring stiffness expressions that relate to an elastic soil condition. Design stiffness values for springs located on the inside of the abutment, for a strip foundation of width B, that is entrenched to a depth between 0.5m and 1.0m below the finished ground level are provided in the following equations:

$$K_{vert} = 0{,}4.E_s \quad \text{(Eqn. 22)}$$

$$K_{horiz} = 0{,}5.E_s \quad \text{(Eqn. 23)}$$

$$K_{rot} = \frac{E_s.B^2}{6} \quad \text{(Eqn. 24)}$$

where k_{vert}, k_{horiz} and k_{rot} are the stiffnesses per metre length for the strip foundation in the vertical, horizontal and rotational displacement directions respectively.

An upper bound estimate for the secant Young's modulus of elasticity, E_s, can be conservatively calculated by using Equation 53 assuming a p' value equivalent to the foundation bearing pressure, with a shear strain (γ) of 0.001.

A typical temperature contraction model that uses the above springs with their stiffnesses is shown in **Figure 2.20** below.

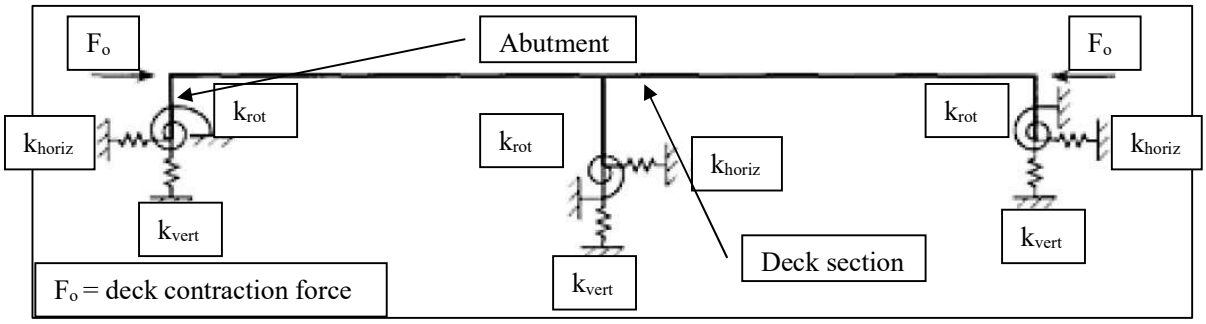

Figure 2.20: 2D bridge contraction on flexible supports, finite element model for footing modelling using the soil-spring approach (Dobry and Gazetas (1986))

2.4.1.3 Foundation stiffnesses (Hambly)

Equations for shallow footing foundation stiffnesses are found below. These are derived from elastic half space theory and are approximate. The equations are as described by Hambly (1991).

Shear Modulus $G = \frac{E}{2(1+\nu)}$ (Eqn. 25)

Vertical stiffness $K_s = \frac{2{,}5.G.A^{0,5}}{(1-\nu)}$ (Eqn. 26)

Horizontal stiffness $K_x = 2.G(1+\nu).A^{0,5}$ (Eqn. 27)

Rocking stiffness $K_m = \frac{2{,}5.G.Z}{(1-\nu)}$ (Eqn. 28)

Where:

G = Shear modulus for soil

E = Young's modulus for soil

υ = Poisson's ratio for soil

A = Foundation area = bd

Z = Foundation section modulus = $bd^2/6$

If the value of υ lies between 0.3 to 0.5, then these equations can be simplified to the following:

$K_z = 1{,}5.E.A^{0,5}$ (Eqn. 29)

$K_x = E.A^{0,5}$ (Eqn. 30)

$K_m = 1{,}5.E.Z$ (Eqn. 31)

The vertical and rotational stiffnesses may be represented often by two parallel springs (see **Figure 2.21**), spaced at a distance of l between each other. The stiffness and the space between the vertical spring supports are given by the following equations:

$$K = 0.5K_z, \quad \text{(Eqn. 32)}$$

$$l = 2.\left(\frac{K_m}{K_z}\right)^{0,5} = 0{,}82.b^{0,25}.d^{0,75} \quad \text{(Eqn. 33)}$$

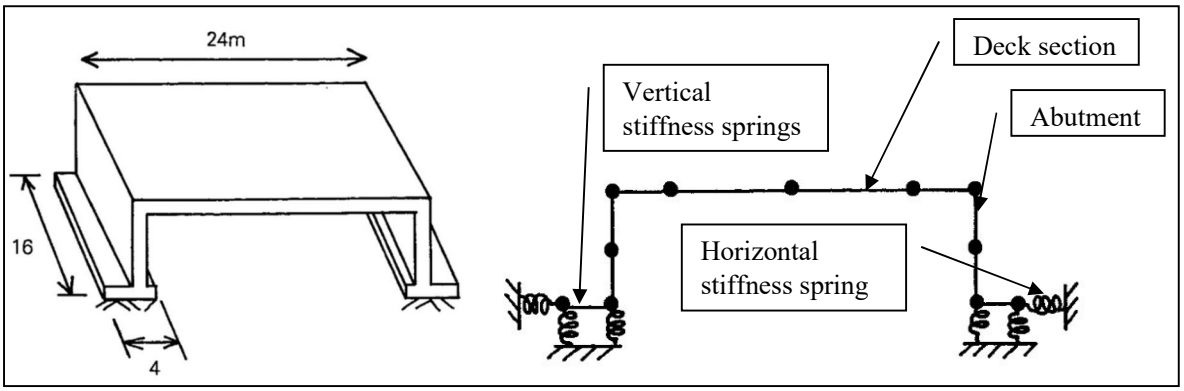

Figure 2.21: 2D finite element model for footing modelling using the foundation stiffness soil-spring approach (Hambly, 1991)

The simplifications inherent in the elastic half space theory may differ substantially from real ground conditions. The equations above also provide no indication of the stiffness interactions of the structure when it is subjected to complex loading, and therefore a stiffness matrix is required in order to be more accurate. Caution should therefore be exercised with the above equations, however they will nonetheless give a rapid means of calculating the foundation stiffness magnitudes.

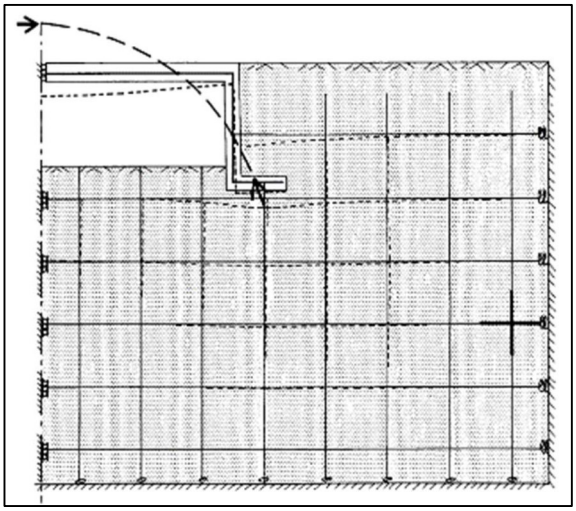

Figure 2.22: Section of portal space frame with line of thrust under live load indicated (Hambly, 1991)

In reality, the reacting force routes determine the ground stiffness under a particular foundation. The loading on adjacent foundations makes the vertical movement of a particular foundation slightly uneven, which is in contrast to the balance that is achieved under arch type force action, where horizontal forces and moments are balanced between opposite foundations (see **Figure 2.22**).

Note that if there is a short load path through the ground between foundations, then the horizontal stiffnesses as well as the moment stiffnesses may be increased. In scenarios where unbalanced reactions are applied to the foundations, the horizontal stiffness will be reduced – this is typically where any concurrent loading occurs on adjacent foundations, for example if horizontal loading from vehicle braking is applied to the system. It is not really practical to attempt to account for all the loading nuances when determining the foundation stiffnesses, however it is advisable to consider any balancing force load paths that may arise. In the design, compacted layers of fill, ground beams, piles or ties will tend to increase the horizontal stiffnesses of the foundations.

Since isolated foundations attract a lot of their stiffness from the propagation of forces laterally, it is always more accurate to characterise the ground material as a 3-D solid rather than as a simple 2-D vertical plane. Despite the above, the crudest of 3-D finite elements still lack the ability to model actual soil behaviour, even though they are capable of rapidly determining the effects from the inclusion of different soil layers and various other interactions with foundations. Where pile foundations are applicable, and especially where they derive their stiffnesses from the pile bending interaction and horizontal soil stresses (as opposed to axial pile compression only), the stiffnesses are more complex.

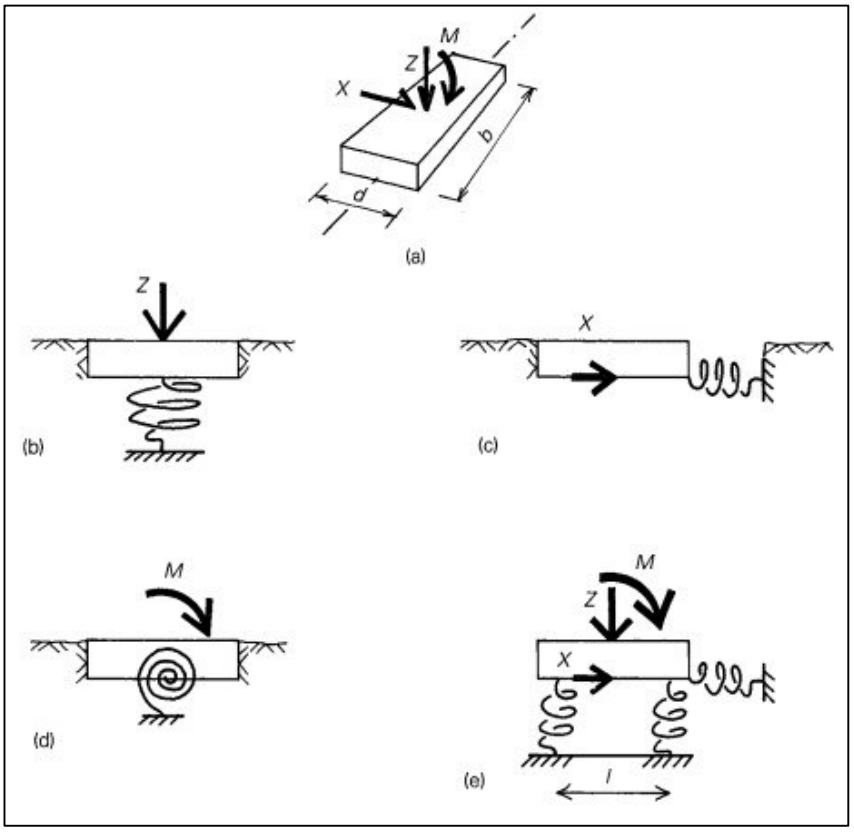

Figure 2.23: Footing stiffnesses (Hambly, 1991)

2.4.1.4 Bridge deck expansion - conventional spring model

This simplified method shown below (and see **Figure 2.24**) is described by O'Brien and Keogh (1999). Noting that the abutment backfill material is compacted up to the underside of the jockey slab - under deck expansion, the abutment backfill provides significantly more resistance than during the contraction case. The properties of the abutment backfill will therefore impact the stresses that are created by any deck temperature increases in a significant manner.

The selection of a suitable soil stiffness value (E_s) is essential for the accurate modelling of the backfill. The following conclusions were made by Springman et al. (1996), and others:

1) Deck expansions and contractions, (arising from the cyclic temperature fluctuations) causes the backfill to become denser over time, and the density reaches an equilibrium which matches the strain amplitude that the backfill is exposed to. The field and lab evidence suggests that granular type backfill over this period will have increased in its compacted density by a maximum of about 20% from its as-placed density for loose fills and by a maximum of about 10% for well compacted fills.

2) Horizontal stresses in the abutment follow the deck cyclic expansions and contractions yet are found to be approximately uniform for depths up to 6m from road level and commonly have a stress range between 25kN/m^2 and 50 kN/m^2 – note that this is dependent on the equipment type used for compacting the fill. These observations suggest that it is acceptable to use a constant soil stiffness value with depth (for a certain strain) up to a depth of 6m.

3) The stiffness of the soil is influenced by the backfill shear strain (see also previous section "Backfill cyclic loading"). The extreme shear strains induced in the backfill when the deck pushes out the abutment a distance δ is approximately 2δ/H, where H represents the height of the retained fill. To adopt a single soil stiffness value, an average shear strain is assumed. The average shear strain in the backfill must be less than 2δ/H, and this may conservatively be assumed as about 2δ/3H. Non-linear elastic finite-element analysis results by Springman et al. (1996) supports the validity of this assumption.

4) The conventional spring model represents the backfill soil as well as the soil beneath the abutment by a series of spring supports. Such a model is somewhat inaccurate as it does not allow for the shear transfer within the soil since there is no interaction between the springs. The approach does however have the advantage of simplicity. For the backfill material behind an abutment with height H and transverse width L, an approximate equation, that assumes linear elasticity has been conceived for the modelling of the horizontal spring stiffness/m^2:

$$K_{horiz} = \frac{\sqrt[4]{\pi.E_S}}{\left(\frac{L}{H}\right)^{0,6}.H} \text{ kN/m/m}^2 \qquad \text{(Eqn. 34)}$$

Where:

L = Bridge span

H = Abutment height

E_s = Young's modulus for the backfill soil

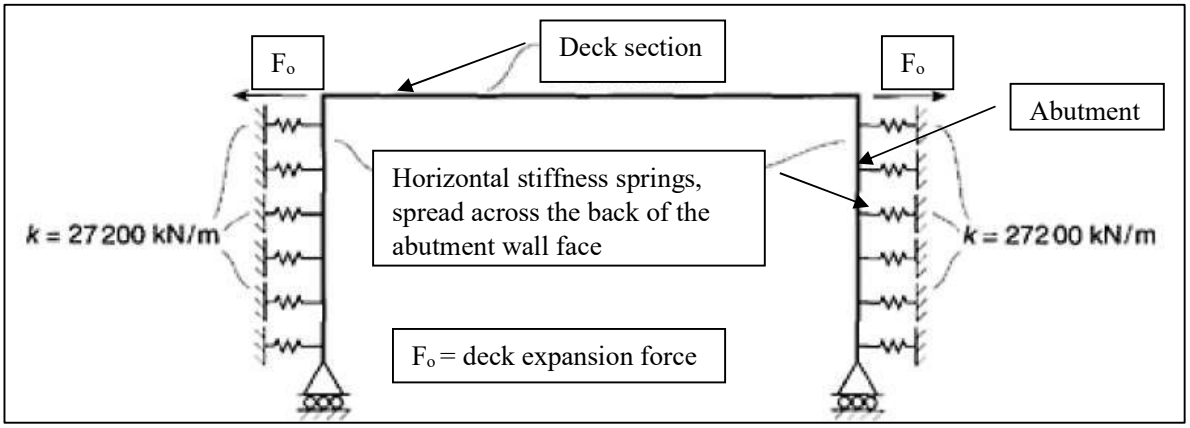

Figure 2.24: Example of a conventional spring model for deck expansion – note how the spring stiffness is distributed down the height of the abutment

2.4.1.5 Bridge deck expansion modelling - equivalent spring at deck level approach

An alternate model to the traditional spring type model is the spring at deck level (see **Figure 2.26**) which has some benefits over the conventional method. The technique's approach is to model both the surrounding soil and the abutment with a simple equivalent rotational and lateral spring, stationed at the level of the deck. Details concerning the abutment moment distribution, or the soil pressure distribution are not provided for in this method, however it is nevertheless useful for estimates of deck and top of abutment forces.

Where there is retained backfill, Lehane (1999) determined the top of an abutment forces and moments allied with the lateral movements and rotations (under deck expansion). A set of finite-element analysis models were created which investigated the effects at the top of the abutment of (i) an applied horizontal displacement δ (with zero rotation), and (ii) a rotation θ (but with zero horizontal displacement) – see **Figure 2.25**.

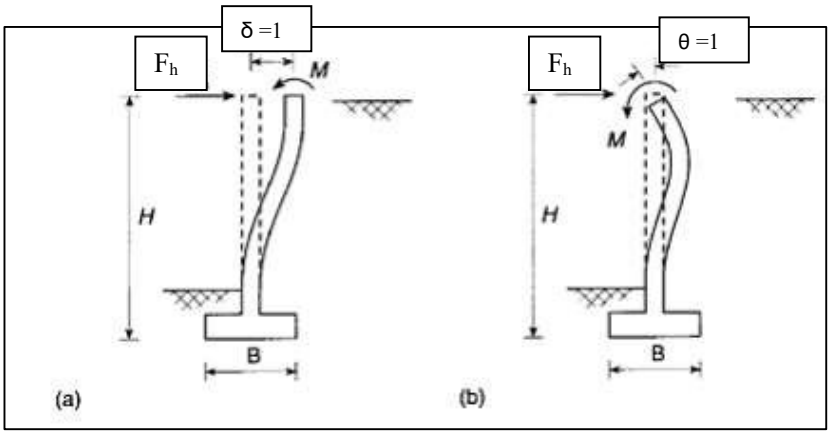

Figure 2.25: Stiffness variables for top of the abutment wall: (a) unit translation; (b) unit rotation

The flexural rigidity of the abutment (EIa) was found to relate to the abutment backfill soil modulus by the ratio, r, as defined below:

$$r = \frac{E_s}{E.I_a} \qquad \text{(Eqn. 35)}$$

Where:

E_s = Young's modulus for the backfill soil

E = Young's modulus for concrete

I_a = Abutment Second moment of inertia

r is the most significant factor determining the lateral forces size (F_h) and moments (M) located at the top of the abutment wall. As the base width (B) was made larger and the height (H) was reduced, the values of F_h and M were also noted to increase.

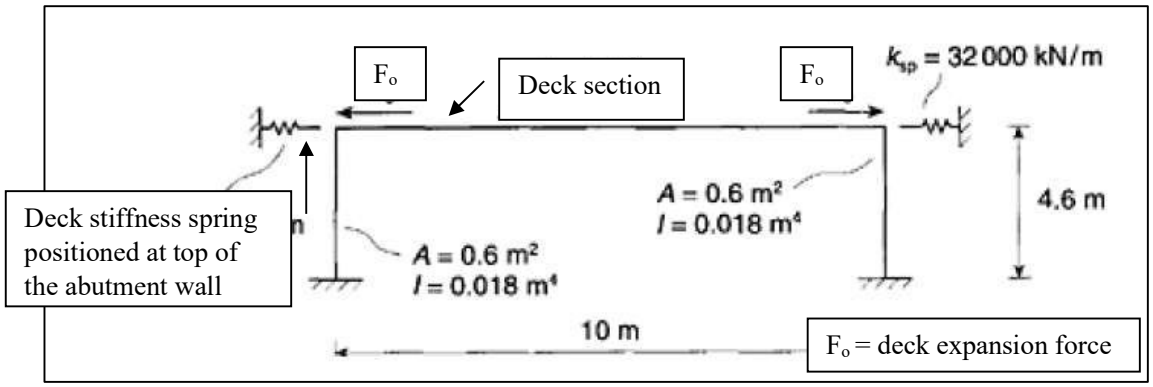

Figure 2.26: Example of a single-equivalent spring model for deck expansion – note how the spring is located only at the top of the abutment

O'Brien and Keogh (1999) provide details of the best-fit expressions that the analysis results showed for F_h and M for a variance in the parameter values. The expressions are shown below in matrix form:

$$\begin{bmatrix} F_h \\ M \end{bmatrix} = E.I_a \begin{bmatrix} f_1.r^{0,75} & f_2.r^{0,5} \\ f_2.r^{0,5} & r^{0,25} \end{bmatrix} \begin{bmatrix} \delta \\ \theta \end{bmatrix} \qquad \text{(Eqn. 36)}$$

Where:

f_1 and f_2 are dependent on the ratio, H/B which are given below in Equations 37 & 38 for $r > 0.05\ m^{-3}$.

If friction between the abutment and the soil can be considered to be negligible, then all the values in the stiffness matrix may be reduced by 15%.

An equivalent abutment height is then calculated as:

$$f_1 = \frac{0{,}85\ \frac{\sqrt{H}}{B}}{\frac{3.\sqrt{H}}{B}} \quad \text{(Eqn. 37)}$$

$$f_2 = \frac{0{,}5+\frac{\sqrt{H}}{B}}{\frac{2{,}5.\sqrt{H}}{B}} \quad \text{(Eqn. 38)}$$

$$H_{eq} = \left(\frac{3}{2.f_2}\right).r^{-0{,}25} \quad \text{(Eqn. 39)}$$

Expansion of frames with deep abutments

In the deep abutment scenario, the equivalent spring at deck level model may be further reduced in complexity. Where (H/B) > 10, the parameters f_1 and f_2 tends towards minimum values of 0.33 and 0.40 respectively. The corresponding abutment second moment of area may consequently be set equal to the actual second moment of area without incurring a substantial increase in the outcome's level of inaccuracy:

$$I_{eq} = I_a \quad \text{(Eqn. 40)}$$

Finally, substituting for f_1 and f_2 in the above equations results in a spring stiffness of:

$$k_{sp} = \frac{E.I_a.r^{0{,}75}}{8{,}5} \quad \text{(Eqn. 41)}$$

The equivalent frame model properties for integral bridges with deep abutments may be estimated using the above equations.

2.4.2 Abutment Pile types and considerations for modelling

Abutment piles for integral bridges are required to have a combination of acceptable vertical resistance, and low stiffness, so that the flexural effects of thermal and other movements are minimized. For the case where there are fully connected integral abutments, it is presumed that the superstructure will transmit all moments, as well as all vertical and horizontal loads arising from the complete spectrum of superimposed dead loads (loads applied after moment continuity begins), live load and impact forces, centrifugal and braking forces, temperature, creep, shrinkage and seismic loads (if relevant).

The ability of the abutment piles to sustain both the vertical loads and the cyclical temperature-induced displacements over many cycles is a critical factor of consideration in the pile design for an integral bridge. The lateral displacements will tend to reduce the vertical-load carrying capacities of the piles (Greimann and Wolde-Tinsea, 1988). In fact, the maximum length possible for an integral bridge is determined by the pile's ability to accommodate the lateral displacements.

Piles should therefore be sized in order to keep the stresses low. Weak-axis bending orientation for the piles can be used and further strategies may be implemented such as the predrilling of oversize holes filled with loose sand (Yang et aI., 1985). Predrilling is recommended in stiff to very stiff soil conditions. Yang, Wolde-Tinsea and Greimann (1985) investigated this issue through the use of FEA modelling and found that predrilling significantly increased the carrying capacity of the piles in the

vertical direction. A further significant factor was the length of the predrilling, with 1.8m - 3m generally being used.

It is quite common that piles are installed in a single row to support the abutment, with the piles being aligned so as to ensure that the longitudinal bending occurs along the pile's weak axis (see **Figure 2.27** (b)). If the anticipated movements are excessive, then it may be useful to pre-bore the piles and fill the gap with a compressible material surrounding the pile – this will reduce the large shear forces and moment effects prevalent in the upper pile regions.

A reduction of the pile moments can be achieved by using a pin connection to the underside of the abutment – this is discussed later on in this thesis, under Section 2.4.3. A pin connection transfers the vertical and shear forces, but no moment. Pile bending moments are hence reduced, and the pile bending due to vehicular live loads is removed, with fatigue loading also being reduced.

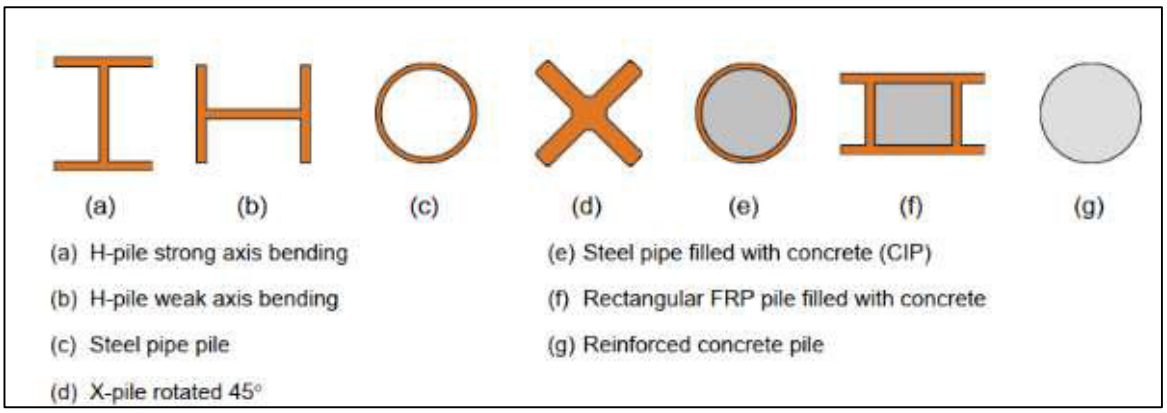

Figure 2.27: Pile types used for Integral bridge abutments (INTAB, 2010)

In Finite Element (F.E) modelling, some designers use the actual installed length of the piles, while other designers prefer using an equivalent cantilever model (see **Figure 2.18**). For various reasons, the equivalent cantilever concept is not preferred.

The equivalent cantilever approach can be useful for certain analytical models and may even be used for determining the lateral strength and ductility demand of the yielding soil-pile system. Note the full length pile is used in the modelling in this thesis - this enables the determination of the pile and the structure behaviours in both the ultimate limit state (ULS) as well as the serviceability limit state (SLS).

2.4.3 Abutment Pile fixity effects and considerations for modelling

Hinged joints may be preferred in the bearing design of semi-integral bridges. The hinge is designed to transfer only shear and vertical forces to the piles (no bending moment transfer). An example of a bridge that uses this type of bearing and abutment design is the Gillies Street Bridge in Australia (Connal, 2004). **Figure 2.28** shows a sketch of one of the abutment joints from this bridge as well as the hinged dowel bar connector that was used to join the abutment to the piles.

For this hinged joint design, the joint filling was specified as polystyrene sheets, in order to reduce concrete crushing during pile cap rotations due to bending. The pin type connection was created by anchoring the concrete pile and the pile cap to each other through the use of galvanized dowel bars. To ensure that the lateral forces are not excessively large towards the top of the concrete piles, the upper 2m of the pile were wrapped in 50 mm thick compressible material.

A variation of the above type of hinge was used by the Virginia Department of Transportation (VDOT), using a shear key in the joint as shown in the left, of **Figure 2.29**. Testing of this joint detail however, showed that the abutment and the pile cap rotated as one singular unit until failure, and did not operate as a hinge. After some experimentation, the hinge was modified as shown on the right of **Figure 2.29**. This produced a result that made a more flexible joint (as originally intended). The joint has neoprene strip bearing material adjacent to both sides of the dowel line. Joint filler (such as sponge rubber) is used to fill the remainder of the joint. Vertical forces are then transmitted down the abutment, through the neoprene strips and further into the piles, with the dowels transferring any shear forces.

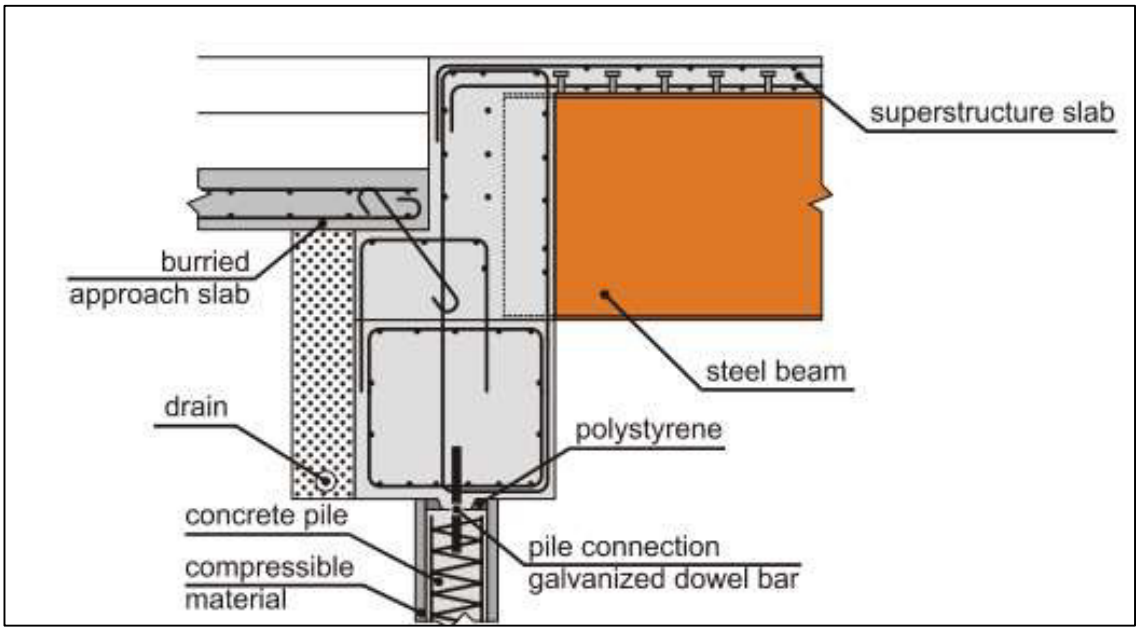

Figure 2.28: Hinged pile connection to the abutment (Connal, 2004)

Since the bridge end rotates under loading and the bridge has an inherent stiffness resisting the rotations it means that the pile tops are not prevented from rotation, even though the supporting piles of the integral bridge ends are monolithically attached to the end of the deck or to the end screen of the bridge. Note that bridge abutment rotation (or end screen rotation) will tend to decrease the top of pile curvature – see **Figure *2.2***.

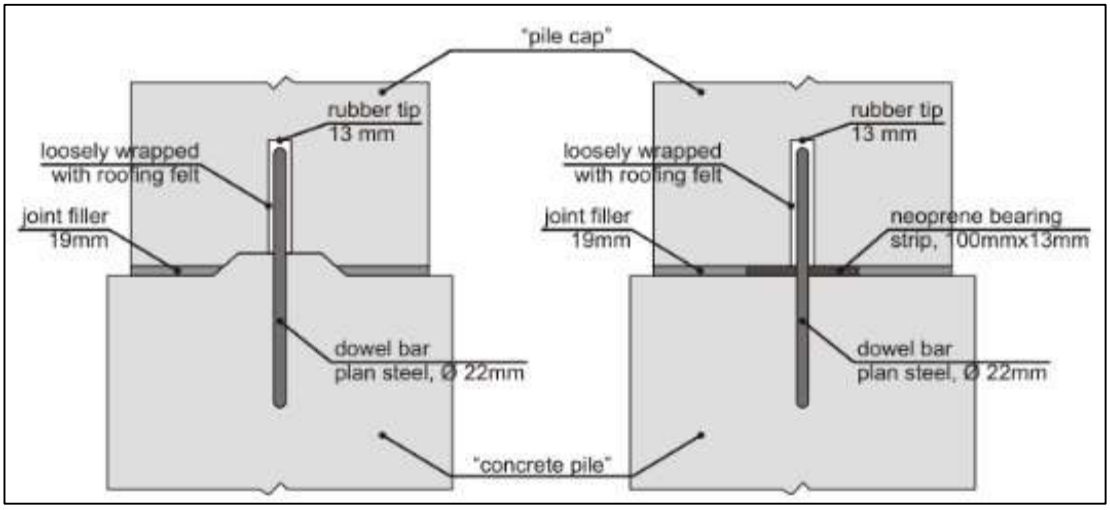

Figure 2.29: VDOT initial hinge design (left) / altered hinge detail (right) (Connal, 2004)

2.4.4 Wing wall modelling considerations

Currently, wing walls are often viewed in isolation and are designed only for the forces applied to them alone, however the wing wall forces may be exerting effects on the overall structure that do not typically receive much attention from the designer. The integral bridge should however be designed as a complete system (rather than as a series of individual components) that work together, to ensure reliable and safe performance.

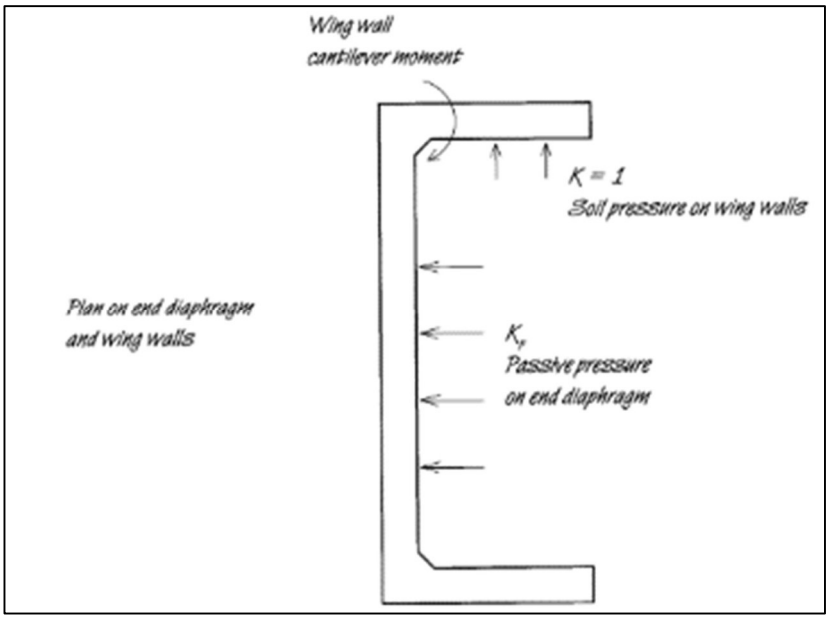

Figure 2.30: Typical soil pressures for end diaphragm and wing walls (Nicholson, 1998)

Each component should be investigated to determine how it affects the overall structure performance. Wing walls and their supporting foundations have the ability to restrict and resist the rotations and translations of the bridge deck and abutment wall, which can detrimentally affect the overall bridge performance and should therefore be accordingly investigated.

Additional forces are introduced into the overall structural system when piles are placed beneath any wing walls. Piles create points of fixity and a moment couple that prevents rotation of the abutment wall. These restrained rotations create internal forces that must be accommodated somewhere within the structural system.

There are various options for the type of wing wall that one may use for the integral bridge system. The smaller and more compact wing walls take preference with integral bridges since the skewer wing walls tend to be larger and therefore create significant passive earth pressure forces that are positioned at a sizable lever arm relative to the abutment. If long wing walls are really required, then they should be installed as free standing, not being connected to the abutment.

Nicholson (1998) recommends that the end diaphragm should be designed for the full passive soil pressure, and reasoned further that a pressure coefficient of at least one should be applied to the adjacent wing walls. Therefore, to maintain consistency, the wing walls are to be designed with soil pressures based on a K = 1 value applied to them (see **Figure 2.30**).

Figure 2.31 shows that as the skew bridge angle increases, the more the pressure exerted on the one wing wall side tends towards the passive lateral earth pressure.

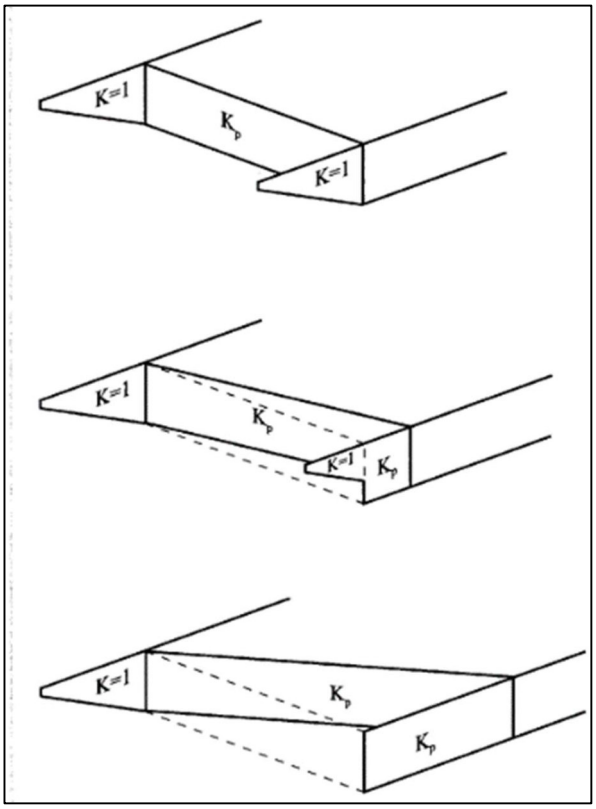

Figure 2.31: Soil pressure effects from Skew angles on wing walls (Nicholson, 1998)

2.4.5 Thermal effects for modelling

As alluded to earlier, bridge deck contraction and expansion is the result of the continuous changes in solar radiation effects as well as the daily and seasonal fluctuations to the ambient temperatures (see **Figure 2.32**). Differences of the bridge material thermal properties, as well as the differing inertias for concrete and steel, mean there is a variation in the response of different integral bridges to environmental changes. It is for these reasons that longitudinal deck movements are difficult to predict from the surrounding shade temperatures (England, 2000).

Effective bridge temperature's (EBT's) will vary throughout the year. The daily variation in the EBT's in winter is in general about one-third to one-fifth of that in the summer. The soil mostly behaves in an active stress state over winter, and hence even small wall movements can induce significant ratcheting strains in the soil.

The EBT generally lies within the shaded area of **Figure 2.33**, for a given bridge and geographical location. These daily variations are thus bounded by the two curves, (max. EBT profile and min. EBT profile) as shown.

The characteristics and scale of the cyclical abutment movements depend on the environmental temperatures as well as the nature of the bridge deck construction itself. Emerson (1973, 1977) showed that the EBT of a steel beam bridge deck (with composite concrete slab) relates to the ambient temperatures for the preceding 8 hours only, while the EBT of a purely concrete deck strongly correlates with the ambient temperatures recorded for the previous 48 hours.

The movement ratio for a season when comparing a composite bridge deck to a concrete deck is about 1.21, for the same location and for a similar deck length. In addition, for the same scenario, the maximum daily deck movement of a composite bridge is roughly 3x the movement found in a concrete bridge. The thermal attributes for the different bridge types indicate that the stress histories and characteristics of the backfill soil are unique and complex for each type of bridge.

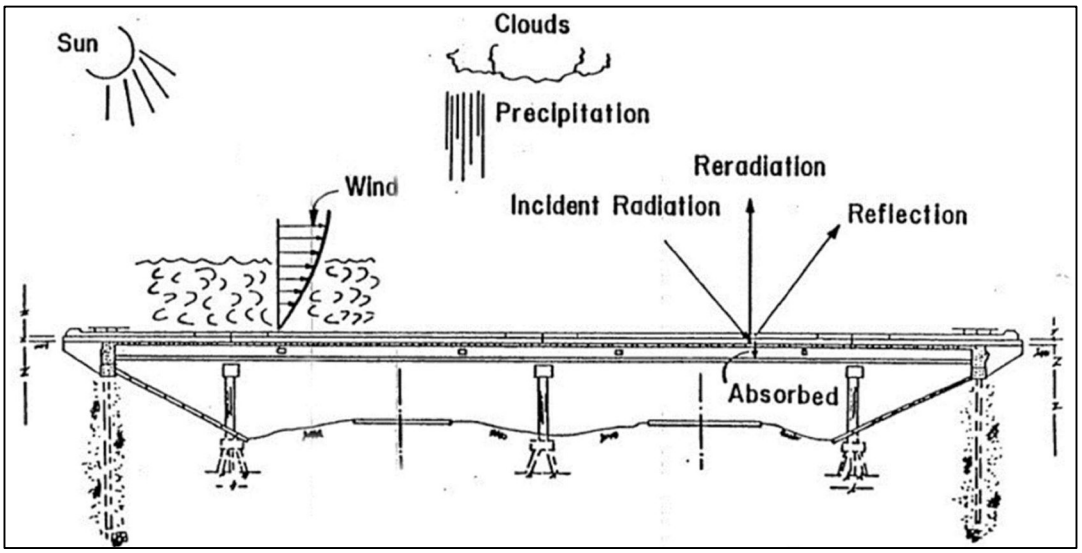

Figure 2.32: Environmental effects impacting bridge temperatures (England, 2000)

Internal deck forces and stresses are caused by the thermal gradients that occur throughout the deck depth. These effects are of significance in the design of the deck, and the temperature variation related stresses are one of the main differences between integral bridges and jointed bridges. If the foundations are restraining the thermal displacements, then a significant axial load in the deck is developed, which will be transmitted through into the bridge abutments.

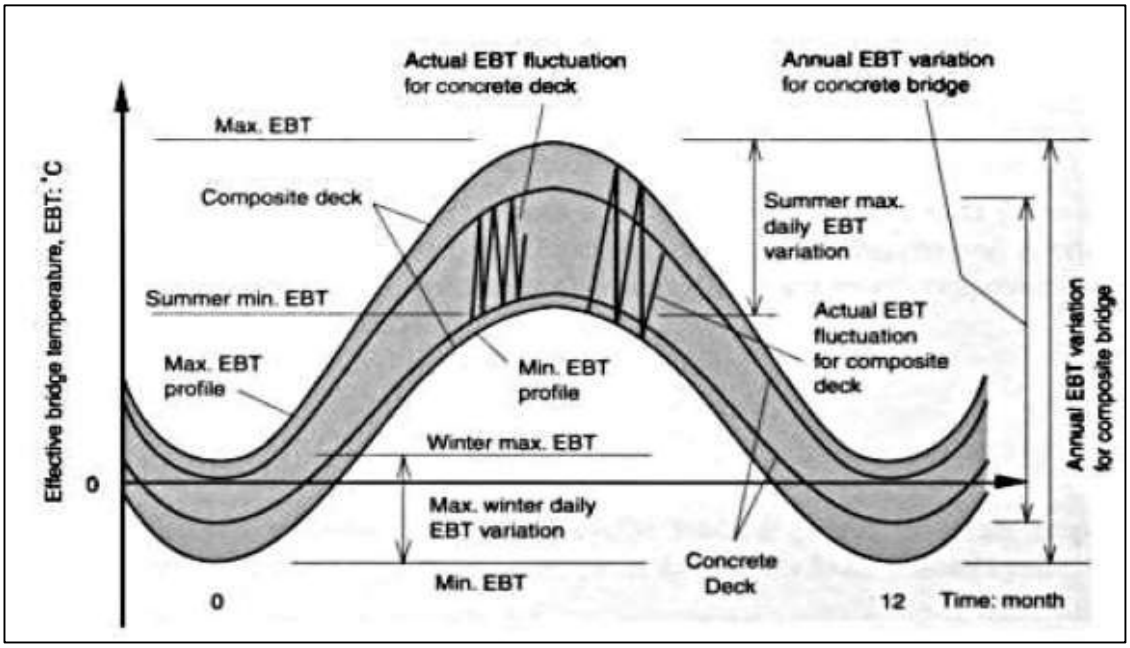

Figure 2.33: Composite deck and concrete deck effective bridge temperatures (EBTs), demonstrating the daily and seasonal fluctuations (England, 2000)

Secondary moments throughout the deck as well as at the supports are caused by the thermal differences throughout the depth of the bridge superstructure, which result in sizeable rotations. **Figure 2.34** gives an indication of the deformations in two to five-span integral bridges that are the result of the superstructure differential thermal gradients, as described by Burdet (2010).

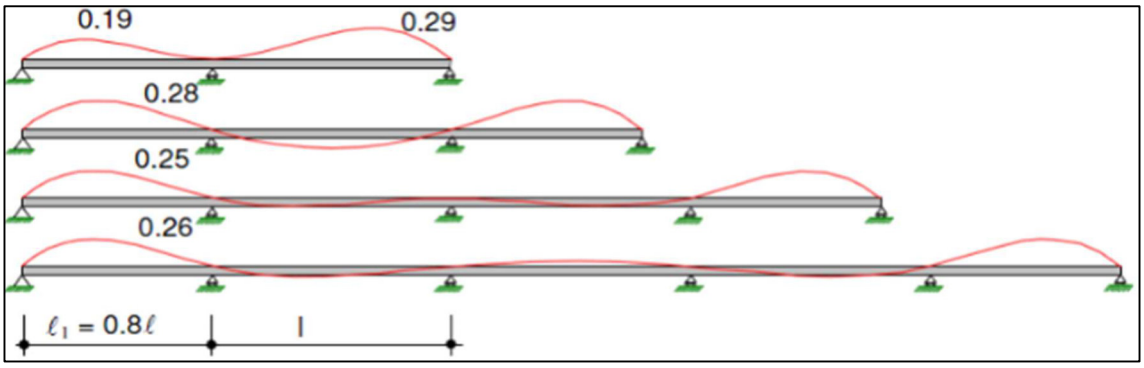

Figure 2.34: Schematic deflection of superstructure of integral bridges due to change of temperature (Wood et. al, 2015)

The soil-structure interaction resulting from these deformations is nonlinear and complex, and is compounded by the secondary stresses caused by creep, shrinkage and certain other loading effects. Shah et al (2008) found that the mode and scale of deformation as well as the structure's overall behaviour are significantly influenced by the compaction level of the granular abutment backfill, and the soil material that provides the friction resistance around the piles along their length, the bending stiffness of the deck of the bridge, the abutment wall stiffness, the foundation pile stiffness, the bridge length and skew, the horizontal soil pressure behind the abutment wall and the stress of confinement in the backfill material.

Thermal expansion creates substantial earth pressures that are generated behind the bridge abutments, which are more often than not the critical loadcase. Thermal contraction however generates rather small active earth pressures at the same positions, leaving a gap behind the abutments. This gap will be relatively small for bridges with lengths less than 100m. The real earth pressure should be calculated using the soil-spring model using accurate soil parameters (examined in this thesis), and is usually smaller than the full passive pressure. For the typical design case, Upper and Lower bound values for the springs are used in the analyses, in order to determine the sensitivity of the structure to the soil parameters used. The effects of the soil properties tend to be more significant for full-height abutments in comparison with piled foundations/abutments.

2.4.6 Modelling of the deck - Beam and slab bridges

In the 10m to 50 m span range, the most commonly adopted bridge type is the slab-on-girder bridge. These bridges have hence been chosen as a suitable bridge type to use for this study. These bridge decks have multiple longitudinal beams, spanning (often prestressed) between the abutments with a thin transversely spanning deck slab on top (see **Figure 2.35**), over the girders. The longitudinal beam load sharing occurs due to the presence of the top slab or a combination of top slab and transverse diaphragm beams. The slab stiffness essentially determines the load sharing extent. It is therefore important that the slab be suitably modelled/idealised to avoid incorrect load sharing predictions between the adjacent beams, which may present a false load sharing narrative. Wide diaphragms will also improve the shear characteristics.

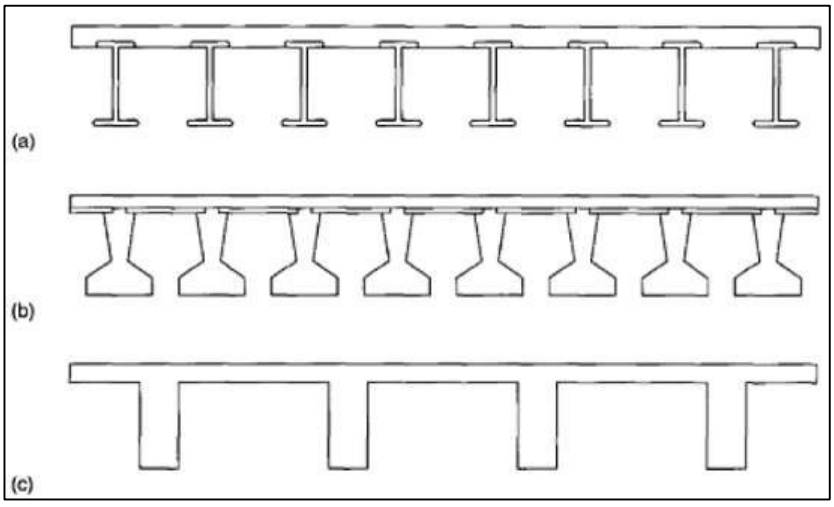

Figure 2.35: Beam and slab construction options (O'Brien and Keogh, 1999)

In the beam and slab category, T-beam bridges are widespread and popular examples due to their simplified geometry and low cost in fabrication, easy casting and erection, and reduced self-weight loading. If the overall section depth is not a dominating factor in terms of vertical clearance considerations, then T-beams prove to be economical.

The girder spacing 'S' in **Figure 2.38** is usually in the range between 2 to 3 m for these bridges, with the span to depth ratio generally being maintained at 20, for the simple supported beams case and to 25 for the continuous span bridges using prestressed concrete girder bridges.

Beam and slab decks can be created using a number of different approaches, with some common methods being in-situ concrete slabs cast ontop of structural steel beams, or concrete precast beams with in-situ deck slab – see **Figure 2.39** (a) and (b). Other available methods include an in-situ beam with in-situ deck slab, as shown in **Figure 2.39** (c).

During construction the beams will usually have a period when they are self-supporting and therefore they should be able to carry their own self-weight, along with the slab weight as well as any live loads during construction. Once composite action is achieved and the slab has hardened, the slab transmits the applied loads to the girders by transversely spanning between them.

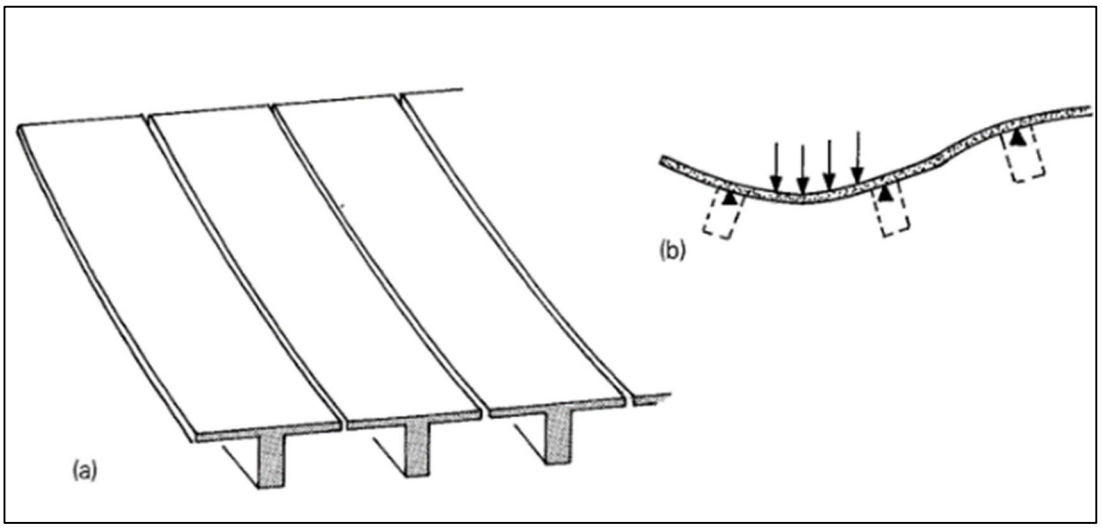

Figure 2.36: Beam-and-slab deck action in (a) flanges of T-beams in longitudinal bending and (b) continuous beam in transverse bending (Hambly, 1991)

The slab will act as the top flange of the beams in longitudinal bending, whilst the deck slab may be understood to act as a set of T-beams that are coupled along their flange edges. As the slab has a significantly smaller bending stiffness to that of the main beams, its rotational curvatures will be higher transversely as opposed to longitudinally. By spanning between the beams, the slab behaves as though it were a number of transverse spanning beams (see **Figure 2.36**). The close vicinity of a concentrated load is the only position where the slab torques and longitudinal moments are of a similar scale to the transverse moments.

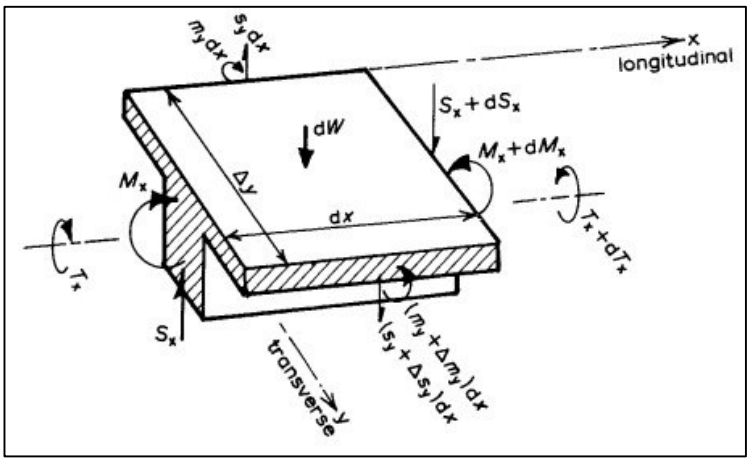

Figure 2.37: Elements of beam-and-slab deck (Hambly, 1991)

Figure 2.37 depicts an element of the deck, providing support for load dW of the locally dispersed load. Moment M_x, shear force S_x and torsion T_x are transmitted by the beam. The slab however transfers the transverse moment m_y and shear force s_y (per unit width of slab) only. The following equations relate these forces accordingly:

$$\frac{dS_x}{dx} + \Delta s_y = -W\Delta y \qquad \text{(Eqn. 42)}$$

$$\frac{dM_x}{dx} = S_x \qquad \text{(Eqn. 43)}$$

$$\Delta m_y + \frac{dT_x}{dx} = S_y.\Delta y \qquad \text{(Eqn. 44)}$$

The torsion in the thin slab is relatively small and hence it has been omitted. Furthermore, beams that are made up of thin I-section webs have a small torsional stiffness, so that effectively, T_x may be treated as zero. The slab can be treated as a continuous beam that is supported on the longitudinal beams, which are modelled as elastic supports. If the beams have a torsional stiffness that is high, then T_x will be large and the moments in the slab will be discontinuous over each longitudinal beam support.

Longitudinal grillage members should not be positioned very much further apart than about 1/10 of the span since the distribution characteristics of beam-and-slab decks are not very good, otherwise the moment concentration will not be visible in the analysis of the grillage. The spacing recommendations of Section 2.4.7.2 also refer in this regard. The transverse members that are representative of the thin slab will therefore be given a lower stiffness in comparison with the members that represent the main beams.

Longitudinal members of nominal stiffness may be conveniently positioned along the outer deck edges in order to define the overall width for the load application. **Figure 2.38** depicts three beam-and-slab cross-sections as well as the section of each deck being represented by each grillage member.

Each grillage member's flexural inertia is calculated about the section centroid that it represents, and it is often the case that different centroid levels are applicable to internal and edge member sections.

Note that the effective width of slab acting as a flange to each beam may be reduced by shear lag, if the edge cantilever exceeds 1/12 of the effective span or if the deck beams are spaced apart further than 1/6 of the span. A reduced width of slab for the grillage inertia calculation should then be used.

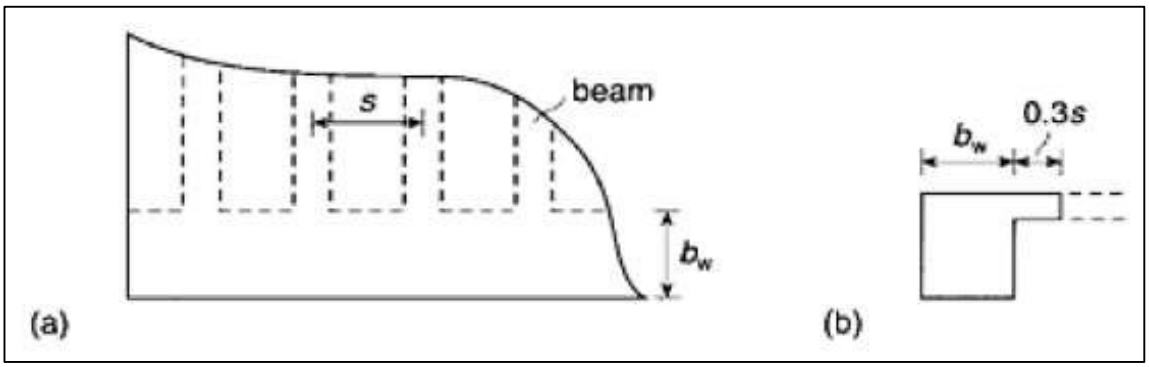

Figure 2.38: Effective width of flange for diaphragm beam: (a) deck end plan view; (b) L-beam section (O'Brien and Keogh, 1999)

At diaphragm beam locations, transverse grillage members should be located. The slab acts as a flange in these beams, making their shape a T- or L-section. From the beam spacing, s, Hambly (1991) describes how an effective flange width of b_w+0.3s be used for L-sections as illustrated in **Figure 2.38**.

The slab transverse stiffness is required to be represented by the transverse members and the transverse element spacing should lie between one to three times the longitudinal member spacing, for beam and slab decks. There is no significant loss in accuracy with larger spacings (>3s). The relevant diaphragm beam or slab properties are calculated by using the properties of the transverse grillage elements as applicable, with each member acting about its own axis.

In **Figure 2.39** below, the 'beam' parts (darker hatching) perform like beams that are subjected exclusively to longitudinal torsion when the various decks are subjected to torsion, while the slab elements act like slabs acted on by torsion in the two principal directions. The constant (C) for torsion of any particular grillage element is therefore the summation of the torsion constants for the slab and for the beam. Certain beams can have very small torsion stiffnesses in contrast with their bending stiffnesses - this is the scenario shown in **Figure 2.39** (b) and (c), and in such cases, for design purposes, it is possible to omit the inherent grillage torsion.

The typical transverse grillage element section properties (representing only slab) are therefore calculated as for a normal slab. The following equations apply for the transverse members:

$$I = \frac{b.d^3}{12} \qquad \text{(Eqn. 45)}$$

$$C = \frac{b.d^3}{6} \qquad \text{(Eqn. 46)}$$

On numerous bridges it is the case that the beams have bending stiffnesses that are significantly larger than their torsion stiffnesses. A composite steel beam from **Figure 2.39** (b) has a torsion constant (C)

of less than 1/60 of its own bending inertia, and the (2x) precast beams of **Figure 2.39** have torsion constants of less than 1/10 of their bending inertias.

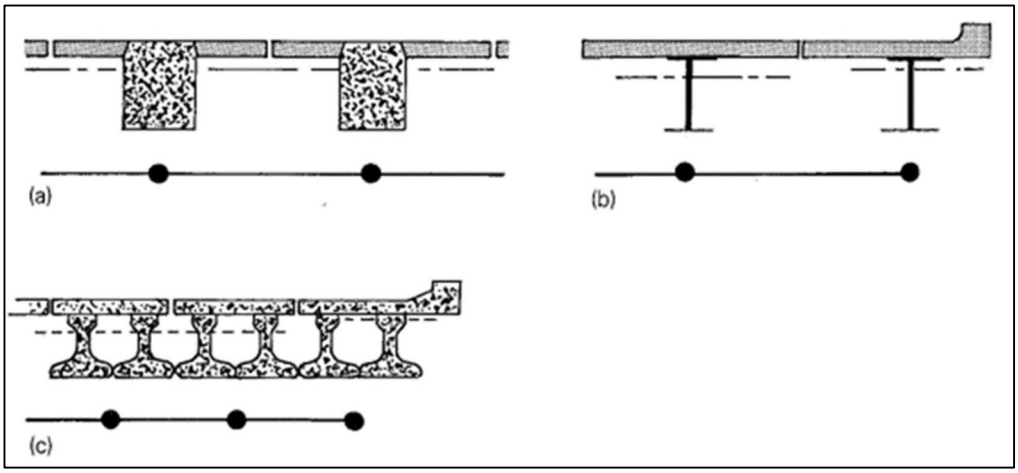

Figure 2.39: Sections represented by longitudinal grillage members (Hambly, 1991)

Research by Hambly (1991) showed that the analysis of these bridges may be safely simplified, if the effects of torsion are totally ignored. In the 'torsionless' deck grillage analysis, the load distribution is somewhat less, (and therefore not quite as effective), which results in the calculated bending moments being slightly higher than with full torsion design. It should be recognized that where the beams have a high torsion stiffness, ie. torsion constants of a similar size as their bending inertias, torsionless design should not be used.

2.4.7 Grillage modelling theory

Grillage Analogy method is the most common analysis method for analyzing the decks of bridges and has been proven to be reliable and precise for an extensive set of bridge types. In instances where bridges have complex features like edge stiffening, isolated supports and extreme skew, this method is still appropriate. The deck of the bridge is assumed to be an assembly of structural members connected together by individual nodes that form a grid. The beam element deformations at the two ends are affected by the applied bending and torsional moments through their bending and torsional stiffness (Hambly, 1991). The grillage method has been shown to be reasonably accurate for a wide variety of bridge decks.

The method consists of adapting the structure to a system of skeletal members connected rigidly to each other by nodes. In general, a grillage with 'n' number of nodes will have 3n degrees of freedom, in other words, the structure will have three degrees of freedom at each node. This would include the freedom for vertical displacement and freedom for rotation about two mutually perpendicular axes in the horizontal plane. All loadings from the span are converted into the nodal load equivalents by computing the fixed end forces and transferring them to the global axis.

It should be noted that the deck idealization is not without pitfalls and the grid lines used in one case may not be applicable in another similar case – therefore the experience and judgment of the designer will always be required. It is challenging to make exacting general rules for choosing the grillage mesh as it is dependent upon the nature of the deck to be analyzed, the support conditions, accuracy required, magnitude of computing facility available etc. and only a set of guidelines can be suggested for the setting out of grid lines.

The interconnected grillage beams are assigned the flexural and torsional stiffnesses appropriate to the segment of the structure they represent in the model. The bending moments, torques and shear forces of the grillage beams at the nodal joints are then able to be determined. The grillage analogy is the most widespread method of analysis amongst the bridge engineer fraternity, and it has been used in an extensive range of concrete and composite bridge structures. Simple guidelines for direction, location, number, spacing etc. of the longitudinal and transverse grid lines that create the idealized grillage mesh, are described below.

2.4.7.1 Location and Direction of Grid Lines

Grid lines should be created along 'Lines of Strength'. Longitudinally, these grids should be located along the centre lines of girders, edge beams or longitudinal webs, wherever these may be found. Where individual bearings are used, the grid lines should be chosen along lines that join the centers of the bearings (not applicable to the structures modelled in this thesis). Transversely, the grid lines should be adopted, one at each end, so as to connect the centres of any bearings as well as along the centre lines of the transverse beams, where these may exist. The grid lines are chosen so as to coincide with the centre of gravity of the sections, however some shift is permissible, when the shift simplifies the grillage grid layout or if it more understandably assigns sectional properties of the grid members in the other orthogonal direction.

2.4.7.2 Number and Spacing of Grid Lines

A minimum number of three longitudinal grid lines should be provided and a minimum number of five transverse grid lines per span should be used in the model.

The spacing ratio for transverse grid lines to those of the longitudinal grid lines may be selected to lie between 1.0 and 2.0. This ratio should also relate to the bridge span-width ratio. In other words - for a short bridge span with a wide deck, it should be near to 1.0 and for a longer span with a narrower deck, the ratio may approach 2.0. For example, it is more accurate to use closer transverse grid line spacing near a continuous support since the longitudinal moment gradient is steep at such locations.

It should be noted that the accuracy of the computations will increase as the number of grid lines increases, however there is more effort required and the scenario becomes a case of diminishing returns. For slab bridges, the grid lines are not required to be closer than two to three times the depth of the slab.

2.4.7.3 Slab Bridge Grillage Idealization

The following further grillage related advice by Hambly (1991) is provided for the grid line setting out in slab decks with line supports on either end:

i) The longitudinal grid line directions are normally parallel to the deck free edges.
ii) The spacing of the longitudinal and transverse grid lines are kept uniform, as far as possible.
iii) A single longitudinal grid line is recommended to be used along the centre line of each edge beam (if present), and where bridges are supported by discrete bearings, longitudinal grid lines should be positioned along the centres of each bearing position.
iv) The maximum space between longitudinal members should not exceed a quarter of the effective span.
v) Transverse grillage members should generally be orthogonal to the longitudinal members. However, where bridges have a skew angle less than or up to 15° or where the transverse directions of strength, such as reinforcement or prestressing are skew, the transverse member grid lines should be oriented parallel to the supports.
vi) It is particularly important that the grillage is supported at similar positions to the actual deck.

2.4.8 Summary - Integral bridge modelling

The above extensive literature survey on integral bridge modelling has discussed various kinds of models that allow the engineer to understand the different effects of the various loading that integral bridges are subjected to (in particular, thermal loading being one of the more important loads to understand). The models used can vary in complexity from simplified 2D models to far more complex 3D models that rely on springs and SSI. The 3D models will of course provide the more accurate results due to their more accurate loading distribution nature. In addition, abutment pile types and abutment fixity conditions, as well as Wing wall considerations were discussed. In relation to bridge deck modelling, the theory behind beam and slab bridges was discussed as well as general grillage modelling theory, which remains a very common method of analysis used for bridges. Another option that could have been looked at is the use of shells for finite element modelling (O'Brien and Keogh, 1999), however this is computationally onerous and therefore has not been deemed as a good alternative for the models considered in this thesis. Note that beam and slab type bridges were selected for use in this thesis since they are a very common bridge type used in practice, for the span lengths under consideration. This type of deck, when compared to a box girder (for example) also suffers less from the effects of shear lag, and therefore was deemed a suitable deck type to use for the modelling.

2.5 Modelling of soil behind the abutment

2.5.1 Abutment Backfill

The installed backfill solution must address both the seasonal and longer duration accumulated increase in the abutment horizontal earth pressures and must account for road-surface settlement adjacent to the

abutments, which occurs due to the cyclical deck expansion and contraction (Horvath, 2005).

The popular choice of abutment backfill for bridge authorities constructing integral bridges is the granular porous type. Compacted gravel (or sometimes even sand) is the most common backfill material specified in European countries. The USA has differing opinions on whether the granular backfill should be well compacted or not, with 69% of the States requiring the fill to be well compacted, and 15% requiring the backfill to be left loose. The idea of leaving the fill loose is that this can reduce the forces acting on the abutment (White, 2007). Although not widespread, it is thought by some that a compressible material behind the abutment stem will also reduce the soil pressure on it.

Using granular backfill has two main benefits:

1) Granular material is easier to compact in close spaces

2) This material will aid in dispersing intrusive water away from the backfill and the abutments. Well-graded material is desirable since uniformly graded material compacts poorly with less particle interlock.

For full height integral frame type abutments, research conducted by Clayton et al. (2006) and Xu et al. (2007) showed that different considerations would apply to the use of stiff clay backfill vs. sand backfill. Although daily and seasonal changes in temperature will result in significant horizontal stresses behind monolithic integral abutments, an increase in horizontal stress is not anticipated with stiff clay the ratcheting effects can be safely ignored – this is also stated in PD6694-1:2011, Clause 9.4.5.2. The full passive earth pressure over the entire abutment height should be used for design, when granular sand backfill is specified, as there is an increase in the horizontal stresses over time with strain cycling over a wide range of density variations.

Between the European countries, there is little agreement on how the abutment soil pressure should be calculated, for example - Germany uses the full passive pressure while England and Ireland use displacement driven soil-interaction formulas in their codes. Sweden also uses the full passive pressure, but only if the movement exceeds 0.005 times the height of the abutment stem.

Backfill options

Five abutment backfill options are considered below for discussion.

1) 6N/6P granular backfill

This is the most commonly specified option for backfill material behind integral abutments. In the UK, the material is known as 6N (and 6P) material which is described in Table 6/1 of the 'Manual of Contract Documents for Highway Works - Volume 1 – Specification - Series 6005'. Having become a standard design solution, this material is widely used and is one of the most well researched backfill materials. One must note however that given its high density (19kN/m^3), its use will result in substantial moments being induced in the abutment piles, as well as significant hogging moments being transferred at the deck/abutment interface, for cases where the abutment height is higher than normal. This may prompt certain designs to resort to the use of alternative lightweight-backfill options. As stated earlier, granular backfill has a ratcheting effect (causing a pressure increase over time) when subjected to the repeated deck thermal cycles.

2) Expanded clay

Railways, roads and ditches have been using expanded clay material since the 1950's to provide insulation. Natural marine clay is heated in a rotary kiln at temperatures up to 1150^o C, and the material is thus formed. A hard, ceramic shell granule with a porous core and of various sized granules is the product of this process, and this is used as lightweight backfill material. Thus transformed, the material

has excellent properties for insulation, with a density of approximately 4 kN/m^3. This results in a significantly reduction of the backfill horizontal pressures acting on the abutments and wing walls.

The internal angle of friction (φ) for this clay material is greater than with granular material however, and this leads to a marginally increased passive earth pressure. Since a capping layer of 6N granular backfill is still required, the end result is a reduction of the initially anticipated savings (Davies, L., Bull, J. and Kucki, T., 2014). There are also certain considerations that deserve attention if one is specifying expanded clay type backfill:

• The particles are porous and absorb moisture after installation, thereby increasing the backfill weight.

• Due to their low density, the expanded clay particles may become buoyant and therefore should not be stationed below the water table or in areas that are prone to being submerged.

• Testing methods such as the California Bearing Ratio (CBR) test are not applicable since the expanded clay particles have a much lower crushing strength when compared to normal soils.

• In order to spread traffic loads, a capping layer is recommended to ensure that particle crushing limits are not exceeded.

3) Expanded polystyrene (EPS) blocks

Horizontal pressures on bridges and other civil structures can be substantially reduced by using EPS. Surcharge loading is directed mostly vertically to the ground beneath. Cyclical temperature movements and vehicle braking forces still create lateral pressures which are applied to the abutment walls by the EPS blocks. These lateral stresses include corresponding strains within the EPS blocks.

As a fill material, EPS has a history of use since the 1970's, and has been used in embankment construction, offering the benefits of reduced foundation dimensions, the elimination of lengthy surcharge periods (for induced settlement) and reduced settlement problems after construction.

Design considerations that need to be taken into account when using EPS blocks are as follows (Davies, L., Bull, J. and Kucki, T., 2014):

- UV resistance.
- Fire protection.
- EPS is highly susceptible to hydrocarbon chemical attack. If used in railway or highway embankments, EPS should therefore be protected by high-density polyethylene (HDPE) sheets or by concrete encasement.
- It is possible to specify higher grade EPS blocks that have a higher density – these blocks have increased load bearing capacities.
- As with expanded clay, a capping layer of granular backfill is required to spread the applied vehicle loads, thereby preventing localised damage to any EPS blocks (or HDPE membrane sheets).

4) Geosynthetics

Studies have indicated that various pressure and settlement issues may be solved through the use of uncomplicated, optimally costed geosynthetics design and ground improvement techniques. Hoppe (2005) conducted a study which showed that the field measurements for an integral bridge abutment that included an elastic material block positioned between the backfill and the abutment, demonstrated a reduced lateral earth pressure, with acceptable settlements for the fill used in the approaches.

This type of design has been used in Japan (Tatsuoka et al., 2016) for high-speed railway bridges, and their performance under seismic conditions has been positive. In Japan, this type of abutment is known

as a GRS (Geosynthetic-reinforced soil) retaining wall. The reason for the preference for GRS in Japan is its high cost-effectiveness coupled with its high performance. There are over 1,050 sites where GRS structures have been constructed with no serious problems having been experienced despite exposure to heavy rainfall and severe earthquakes.

5) Tyre-derived aggregates

This type of aggregate is somewhat of a novel mechanically stabilised backfill abutment system (Caristo, Mitoulis and Barnes, 2018) for integral bridges in which there are two additional items added: (i) Geogrids and (ii) Tyre-derived aggregates (TDA) that behave as a compressible medium (isolator). Dynamic testing of this material has previously shown good results. The isolator material is added vertically between the backfill and the abutment wall, and acts as a compressible layer.

Materials	**6N Granular Backfill**	**Expanded Clay**	**EPS Blocks**
Advantages	• Well understood material • Cheap and readily available • Ability to use normal compaction plant and testing methods	• Eliminates settlement period • Free draining • 1m compaction layers • Chemically inert • Resistant to fire and frost • Re-usable, no special requirements for disposal • Placed using same methods as normal backfill	• Placed by hand • No compaction required • Inhibited water absorption • Immune to attack from bacteria and mould • Minimizes settlement issues • Can be recycled
Disadvantages	• High unit weight • 0.25m compaction layers • Susceptible to settlement issues • Susceptible to frost heave issues	• Heavy winds can blow the finer materials increasing dust levels • Aggregate dust containing quartz can constitutea long-term health risk • No accepted test for measuring density in-situ	• Susceptible to attack from hydrocarbons • Expensive
Unit Weight ϒ(kN/m^3)	19	4	0.5
Angle of Friction ø'	35	37	N/A
Cost (£/ m^3)	35	40 - 50	60- 80

Table 2.2: Backfill materials comparison (adapted from Davies, L., Bull, J. and Kucki, T., 2014)

Specific details relating to the laboratory triaxial testing for TDA properties may be found in (Mitoulis et al., 2016), as well as results for differing arrangements of the compressible TDA layer. Overall, the TDA system has demonstrated itself to be a sustainable and effective system capable of isolating the bridge from the abutment backfill, with a significant reduction to the lateral pressures on the abutments as well as reduced settlements.

The table above (**Table 2.2**) provides some guidance on the advantages and disadvantages of three of the above choices of backfill.

2.5.2 Horizontal stress ratios

The relationship between vertical and horizontal stress is defined as K_o, when soil is retained by a structure, it has not moved horizontally and is essentially at rest. If the wall translates and rotates sufficiently then the horizontal stress in the wedge of soil decreases to what is called an active pressure, K_a.

The K_o (or at-rest) ratio depends principally on the soil type, the loading-unloading history (in effect, the consolidation ratio) and the soil density. The formulas for the different cases of K_o is as follows:

1) In the zero lateral strain scenario, the horizontal and vertical stresses are associated with the soil's Poisson ratio (μ) as follows:

$$K_0 = \frac{\mu}{1-\mu} \quad \text{(Eqn. 47)}$$

2) With a normally consolidated soil, and zero degree backfill with variable internal friction angles of soil (Φ) (Jaky, 1948):

$$K_0 = 1 - sin\phi \quad \text{(Eqn. 48)}$$

3) In the case of a normally consolidated soil, having a sloping backfill at variable angles of slope (Danish Geotechnical Institute, 1978):

$$K_0 = (1 - sin\phi).(1 + sin\beta) \quad \text{(Eqn. 49)}$$

Where β is the backfill angle to the horizontal.

4) For an over-consolidated (OCR) soil with variable OCR ratios (Mayne & Kulhawy, 1982):

$$K_0 = (1 - sin\phi).(OCR)^{sin\phi} \quad \text{(Eqn. 50)}$$

Where:

ϕ = Soil internal friction angle

OCR = Overconsolidation ratio

μ = Poisson ratio for the soil

More information pertaining to the derivations of passive (K_p) and active (K_a) earth pressures can be found by the reader in Craig (1997) or in various other soil mechanics textbooks. Generally speaking however, the soil's passive pressure will be larger than the active pressure. The transition curves from active to at-rest to passive pressures is shown in **Figure 2.43**.

2.5.3 Effects of cyclic loading on backfill

For an element of soil that lies adjacent to an abutment wall (see element A in **Figure 2.41**), the collective effect of the soil to wall friction and the shifting lateral earth pressures is to create a combination of cyclic rotations (the characteristics are described in **Figure 2.41**) in the major principal stress directions with corresponding cyclic changes to the ratio of principal stresses. **Figure 2.41** also depicts the initial stress condition for the soil element after backfilling has been completed. Shear stresses on the element are reduced during the bridge deck contractions, with possible reversal of their directions. During the subsequent deck expansion, the initial stress is reinstated. The abutment rotations under expansion / contraction were studied by Arthur et at. (1980, 1991) and Dunstan et al. (1988) who identified the combination of critical rotation angles matched by different stress ratios that gave rise to an increased soil fluidity. The additive influence of the friction arising at the wall-soil boundary as well as the cyclical transverse wall movements can be expected to encourage significant granular flow with increasing compaction of the soil material lying adjacent to the abutment.

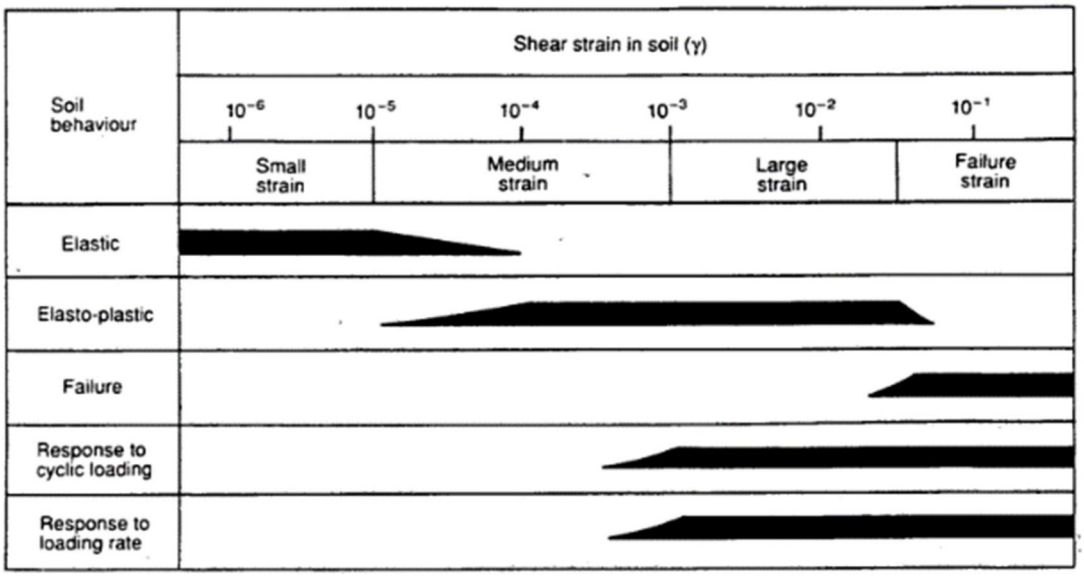

Figure 2.40: Changes in soil behaviour with shear strain (lshihara 1982)

It is well recognised (Card G B, Carder D R., 1993) that soil behaviour under cyclic loading is influenced by the following variables in the integral bridge system:

- initial density (if cohesionless)
- ground water presence
- soil type (cohesive or non-cohesive)
- shear strain magnitude
- loading frequency and magnitude

In cohesive low permeability soils, the dissipation rate for the pore water will be slow, and the soil behaves as if it were undrained. In this situation, the soil is likely to respond to cyclic loading. Anderson et al (1980) showed that under these conditions, with increasing shear strain the undrained shear strength

is reduced and the soil softens, reducing in stiffness. However, if partial or full drainage of the soil occurred the result was further consolidation and strengthening of the soil as well as an increase in its stiffness.

Cyclic loading of non-cohesive soils (eg. silts, sands and gravels) causes a change in pore water pressure that is easily dissipated within the material due to its high permeability. This brings about a densified soil mass and an increased stiffness. This behaviour will continue to the soils' densification limit where full dissipation of pore pressure is prevented after each loading cycle. Further cyclical loading causes pore pressure build-up where the soil loses strength until ultimately liquefying (Terzaghi and Peck, 1967).

Cyclic wall movements (see **Figure 2.45**) will thus change the distribution of friction in the upper portion of the wall, causing further vertical loading to be transferred to the lower portion. The probable consequence of the soils' densification will be to cause the location of the cut-off point (X-X above) to rise. This in turn will improve overall stability but impose higher bending stresses in the upper part of the piled abutment.

In many situations the bridge deck thermal movements will tend to cause a rotation about the toe of each abutment. Soil strains associated with this arrangement of abutment strain may be defined by Eqn. 51 below.

$$\gamma = \frac{2\delta}{H} \qquad \text{(Eqn. 51)}$$

Where:

γ = Backfill shear strain

δ = Horizontal deformation at top of the abutment

H = Abutment height

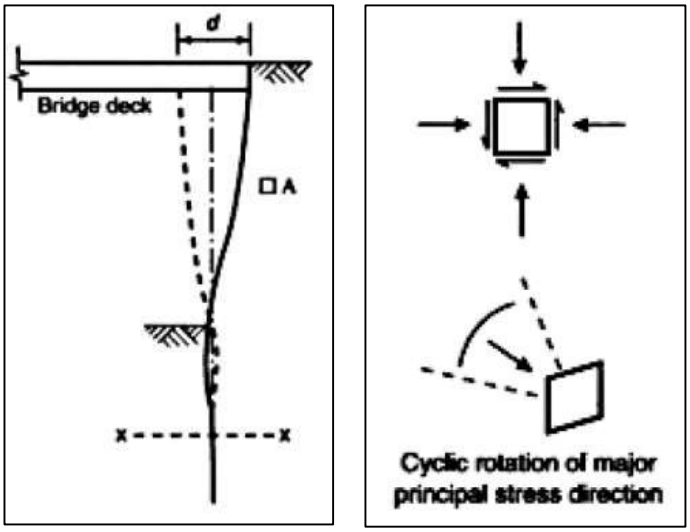

Figure 2.41: Sheet pile abutment retaining wall showing the cut-off point at depth x-x. The soil element A lies near the retaining wall and supports the stress states as shown on the right-hand side diagram (England, 2000)

Ishihara (1982) correlated the magnitude of the induced cyclic movements/shear strains in soil with their properties and behaviour (see **Figure 2.40**). Below a shear strain of the order of 10^{-5}, the behaviour of most soils (whether cohesive or non-cohesive) is elastic (and is therefore recoverable). A model with elastic soil properties is applicable and in this simple case the shear modulus, G_{max} is an important factor to be understood, to model the soil's behaviour. The soil behaviour becomes elasto-plastic for shear-strains in the range 10^{-5} to 10^{-3}. In this range, the shear modulus tends to decrease, with increasing shear strain. In going beyond shear strains of approximately 10^{-3}, the number of cycles also affect the soil properties as well as the rate of loading, which becomes significant in its effect on the soil's strength and stiffness behaviour.

The shear strains induced in the backfill soil during typical daily thermal movement cycles of +/- 3mm could be in the range 1 x 10^{-3} to 5 x 10^{-3} and for a yearly seasonal cycle of +/- 40mm, strains would be between 1 x 10^{-2} to 5 x 10^{-2}. From **Figure 2.40** this would place the soil in the elasto-plastic range, approaching failure conditions.

For active pressures to be reached, the horizontal strain required is generally less than 0.5%. As the principal horizontal to vertical stresses increase in the backfill, the soil's state changes from an active to a passive condition and the horizontal soil strain progressively increases as shown in **Figure 2.42**. Similarly, as the abutment horizontal movements change daily and seasonally, the soil's stress state changes as seen in **Figure 2.43**. The Mohr circle stress diagram relating to a cohesionless soil is demonstrated in **Figure 2.44**, which shows the variance in principal stresses.

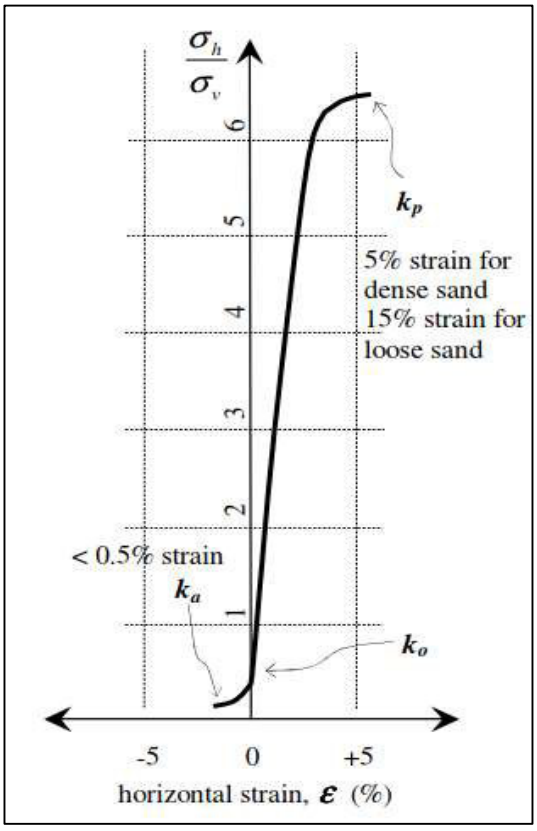

Figure 2.42: Strains vs soil pressures (Haynes, 2014)

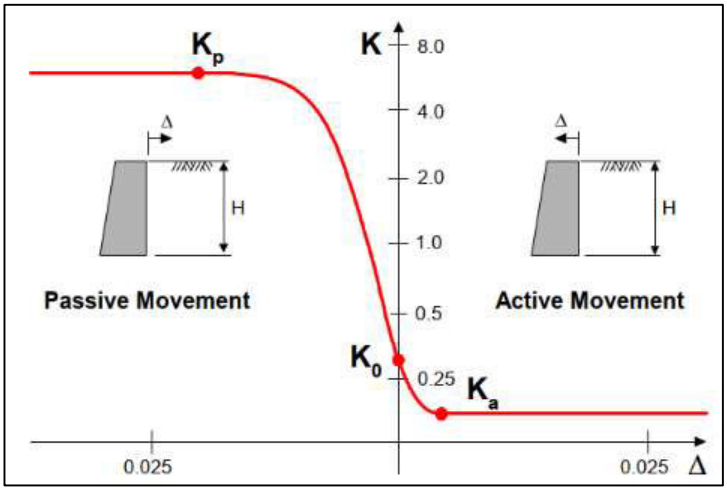

Figure 2.43: Passive and active movements vs horizontal deflections (Rhodes, 2014)

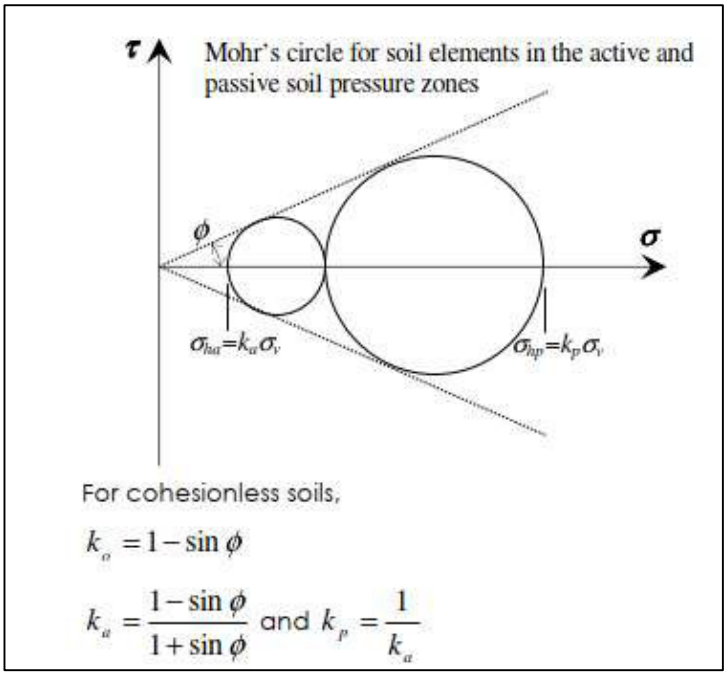

Figure 2.44: Mohr stress circle diagram depicting the difference between active and passive pressure lines (Haynes, 2014)

2.5.4 Granular flow behind the abutment

England (2000), describes how the performance of drained granular soils subjected to cyclic loading (imposed stresses or strains) may be characterized by the following properties during any loading/unloading cycle:

- volumetric changes (either compaction or dilation)

- the soil fabric's development and collapse of interparticle load-carrying structures

- shape changes due to ratcheting shear strains as well as the flow of granular particles

The specific characteristics of the loading for any given situation determines the possible dominance of any one of the above phenomena. It is therefore important to distinguish between cycles of stress with and without changes in the directions of principal stress, and between imposed stress or strain fluctuations. This leads to two main descriptions for the fluctuating stresses at the soil to abutment interface:

- stress increment reversal loading (with no change in principal stress direction)
- 90° jump changes in the direction of principal stress during a cycle

England (2000) describes how the volume changes, soil fabric development (and collapse) as well as shape changes are related to the two descriptions above for the soil fabric's behaviour during fluctuating stress cycles.

Figure 2.46 shows the cyclic stress path of the backfill soil, for an element of soil close to the wall as well as for an element further away from the wall (they are different). The relatively stiff wall of an abutment, seated on a pinned base, showing the nature of wall rotations is provided in **Figure 2.46**.

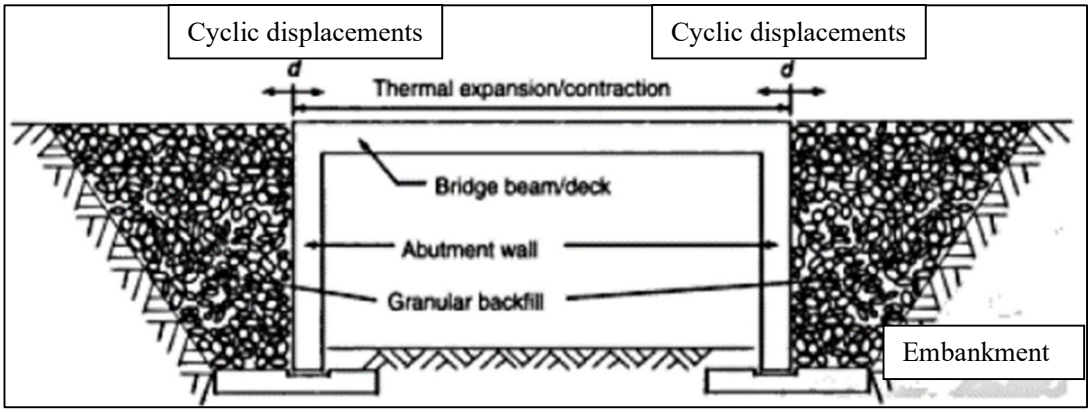

Figure 2.45: Typical cyclic displacements for an integral bridge (England, 2000)

2.5.5 Coefficient of subgrade reaction vs soil conditions

Often it is the case that the 2D plane-strain model is not suitable for certain bridge types, making the spring model approach a more attractive one. Frank et al (2004) advocates the yielding spring approach for use in integral bridge analysis, and EN1997-1, clause 9.5.4 also suggests the use of spring models. The Winkler spring or subgrade reaction type of model is the terminology widely given to an SSI analysis where the soil and its vertical and horizontal resistance is modelled using springs. In the integral bridges and retaining structures context, the horizontal stiffness, the 'spring stiffness', k_h (force/length^3), is of relevance. Nonlinear springs may be used in a Finite Element model to simulate the horizontal earth pressures in a retained earth wall type of design, assuming the assigned pressure/deflection relationships are similar to that shown in **Figure 2.43** (for example).

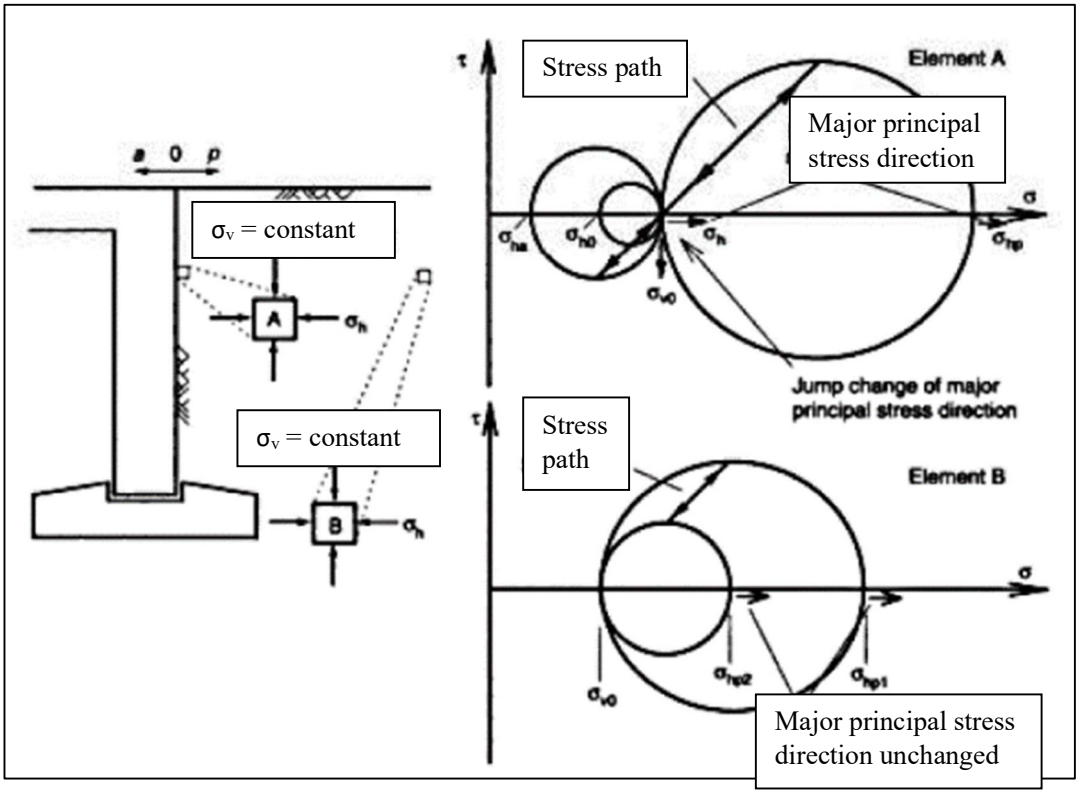

Figure 2.46: Cyclic stress variations in soil elements (England, 2000)

Note that **Figure 2.43** above includes the modulus of subgrade reaction (k_h) and the at-rest earth pressure (σ_o', related to K_o). These quantities are significant items in an SSI analysis even though they are not utilized when designing retaining walls, using the limiting earth pressure methods (see CIRIA C580, section 5.1). The salient points shown above in **Figure 2.43** (the active and passive 'yield points' including the at-rest pressures), will typically vary with depth.

In cohesive soil materials, it can usually be assumed that spring stiffnesses can be taken as constant with depth (Rombach, 2011). A linear variation with depth is applicable for granular soils, as is suggested by Bowles (1997) and Rombach (2011). Finnish guidelines assume that there is a linear progression in granular stiffness up to a depth of 10 x pile diameter and thereafter the subgrade stiffness remains a constant value. The following polynomial equation is used by Bowles (1997):

$$k_s = A + B.z^k \qquad \text{(Eqn. 52)}$$

Where:

k_s = coefficient of lateral subgrade reaction (MN/m^3)

A = a constant value relating to a horizontal or vertical member

B = depth variation coefficient

Z = relevant depth below ground (m)

κ = exponent providing k_s best fit to measured results

Rombach (2011) suggests the typical variations of κ with depth for different soil types – these are illustrated below in **Figure 2.47**.

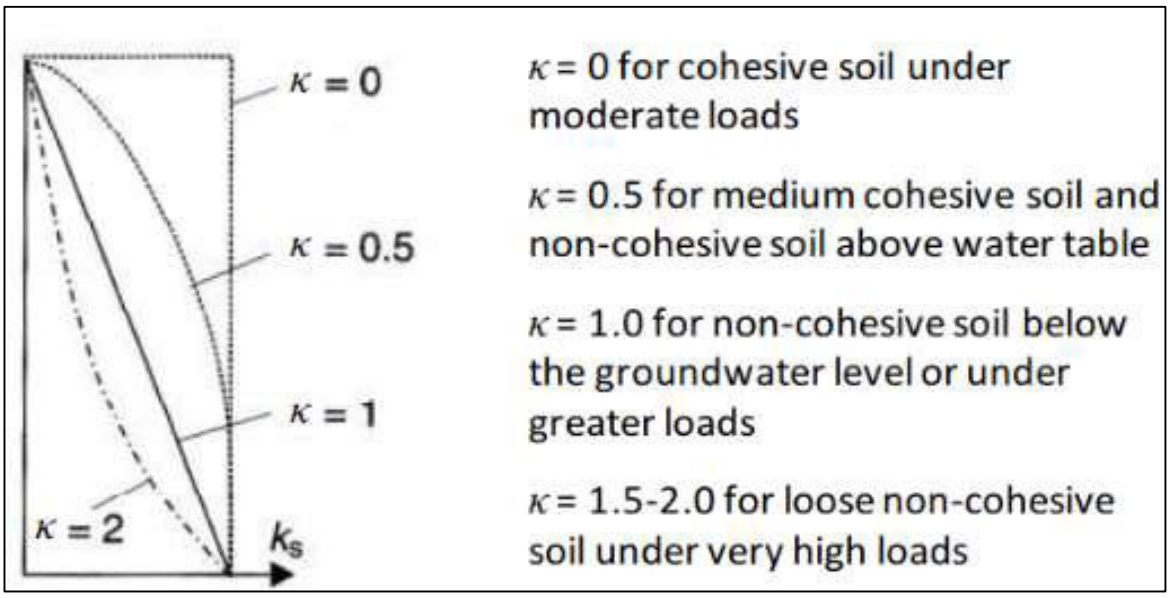

Figure 2.47: Variations of κ with depth for piles (adapted from Rombach, 2011)

There is some variance in the initial recommended subgrade lateral stiffness for sand, as provided by various researchers (similarly for clay). As may be seen below, the lower bound and upper bound values of 2 000 kN/m^3 and 12 000 kN/m^3 respectively, as reported by Bowles (1997) are similar to the recommended lower bound and upper bound values by Terzaghi and Peck (1967) – see **Table 2.3**. CIRIA 103 (1984) also makes the distinction between submerged and dry sand as being 2 000 kN/m^3 and 1 000 kN/m^3 for loose sand (dry and submerged respectively), and 17 000 kN/m^3 and 10 000 kN/m^3 for dense sand (dry and submerged respectively) – see **Table 2.4**.

Soil type	**Terzaghi**			**Bowles**		
	Subgrade Modulus (kN/m^3)	Density (kN/ m^3)	Friction angle (ø)	Subgrade Modulus (kN/m^3)	Density (kN/ m^3)	Friction angle (ø)
Loose sand	1 930	17	30	2 000	16	30
Medium sand	6 790	18	35	6 000	18	35
Dense sand	13 850	20.3	40	12 000	20	40

Table 2.3: Different types of soil properties, adapted from Nikravan (2013)

The table below from CIRIA 103 provides the coefficient of subgrade reaction values for clays – note these are presumed as being constant with depth (unlike with sandy material).

Consistency of clay	Firm to stiff	Stiff to very stiff	Hard
C_u (kN/m^2)	50 to 100	100 to 200	>200
K (MN/m^2)	3 to 6	6 to 12	>12

Table 2.4: Values for coefficient of subgrade reaction (K) for clays, adapted from CIRIA 103 (1984)

2.5.6 Youngs Modulus for soils, Es

Large-diameter plate bearing tests are used for best estimates of stiffnesses. Retrospective analysis of the characteristics of similar bridges in similar founding conditions may even be utilized. Guidelines for the Soil modulus estimates are shown below in **Table 2.5**.

Soil type	Young's modulus, E (MN/m^2)		Poisson's ratio, v
Loose sand	5 to 20		0.3 to 0.4
Medium dense sand	16 to 20		0.2 to 0.35
Dense sand	30 to 100		0.15 to 0.3
	Undrained	Drained	
Soft clay	2 to 6	1 to 4	0.5 for undrained conditions, 0.1 to 0.3 for drained conditions
Firm clay	5 to 12	3 to 8	
Stiff clay	10 to 20	5 to 15	

Table 2.5: Youngs modulus and Poisson's ratio for various soil types - adapted from CIRIA 103 (1984)

Table 2.6 taken from Hambly (1991) also provides an estimated guideline to variations in the scale of Young's modulus for a range of soil types. This data is best corroborated with an on-site investigation to determine the specific foundation conditions. In this table, note that the undrained modulus is E_u and the undrained shear strength is S_u.

Type of soil	Approximate strength	Young's modulus relating to strength
Stiff clay	S_u = 100 kPa	40 – (120) MPa
Very stiff clay	S_u = 200 kPa	80 – (240) MPa
Loose sand*	Ø = 30°	20 – 60 MPa
Medium sand*	Ø =35°	40 – 120 MPa
Dense sand*	Ø =40°	80 – 240 MPa
Dense gravel*	Ø =45°	160 – 480 MPa
*Under vertical pressure of approx. 200 kPa		

Table 2.6: Young's Modulus for soil types beneath spread footings under short term, low strain loading (Hambly, 1991)

The clay modulus for a material under consideration is determined by the duration of time that the material has had to drain under loading, as well as the amount of strain caused over this time. The

Table 2.6 values essentially relate to quick live loading conditions which do not allow much time for soil drainage to occur. Shear stresses are minor in relation to the soil's ultimate shear strength under quick live load conditions, and the secant modulus can be assumed to be approximately half the values of **Table 2.6** when the short-term loadings are large.

Under long-term drained conditions, the Youngs modulus (E) for various clays is significantly smaller than that for the short-term condition. The loading history of the ground under consideration determines the modulus value, for example if the soil had been unloaded prior to the re-application of load.

The values in **Table 2.6** relate to a vertical confining pressure of approx. 200 kPa and the soil confining pressure determines the sand and gravel moduli. Hambly (1991) provides references that elaborate on how E can vary in accordance with either the pressure, or the square root of the pressure.

For undrained conditions, Poisson's ratio is usually taken to be 0.5 and the shear modulus is then G = E/3. In drained conditions, Poisson's ratio is presumed to be 0.3 for sands and 0.2 in the case of medium to stiff clays, so that G = E/2.5.

Hambly (1991) refers to previous studies that show that the ratio E_u / S_u has the following characteristics:

1) For highly plastic or organic clays, E_u / S_u has values that range from 400 to 800.
2) For lean inorganic clays, E_u / S_u is in the range 1000 to 1500.

Table 2.6 shows E_u values, based on (E_u / S_u) = 400 with the values in brackets based on (E_u / S_u) = 1200. Since spread footings on soft clay are highly unlikely to be used for a bridge (piles would more be more appropriate), soft clays are not included in **Table 2.6**.

At strains in excess of about 50×10^{-6}, the soil stress-strain relationship becomes non-linear and it is common to refer to a secant modulus. For a typical cohesionless soil (eg. granular type generally used for integral bridge backfill), the Secant modulus value for a given strain mostly depends on its density, void ratio, loading history and the level of confining stress (in other words, this equation would supposedly account for the ratcheting effects over time). The following approximate equation for Secant modulus has been proposed by Lehane et al. (1999). In this derivation, the Shear moduli (G) is substituted with an equivalent Young's modulus (E_s) using $\nu = 0.25$ and $E_s = 2G(1+\nu)$:

$$E_s = 2{,}5.G.(approx.) = 150.F.e.\left(\frac{p'}{p_{atm}}\right)^{0.5}.\left(\frac{0.01}{\gamma}\right)^{0.4} \qquad \text{(Eqn. 53)}$$

Where:

E_s = Secant Young's modulus in kN/m^2

$F(e) = (2.17 - e)^2 / (1 + e)$

e = Soil void ratio

p' = Mean confining stress minus the soil pore water pressure (which varies with abutment height)

p_{atm} = The reference stress of atmospheric pressure (100 kN/m^2)

γ = Shear strain which is taken to lie within the range 50×10^{-6} to 0.01

The on-site backfill degree of compaction is often specified in terms of the dry density, ρ_d, which is associated with the void ratio (e), by the following formula:

$$\rho_d = \frac{G_s \rho w}{1+e} \qquad \text{(Eqn. 54)}$$

Where:

G_s = the specific gravity of soil particles (typically 2.65)

ρ_w = the density of water

Therefore, the specification of the dry density effectively dictates the void ratio (e). The Secant Young's modulus, derived using Equation 53, is plotted in **Figure 2.48** for a variety of in-situ dry densities (ρ_d), confining stresses (p') and shear strains (γ). Equation 51 or **Figure 2.48** can be used to estimate the secant Young's modulus for a cohesionless soil. Note that Equations (61) to (64) in Section 3.8.1 are based on the above equations (53) and (54), with some additional cycle factors included.

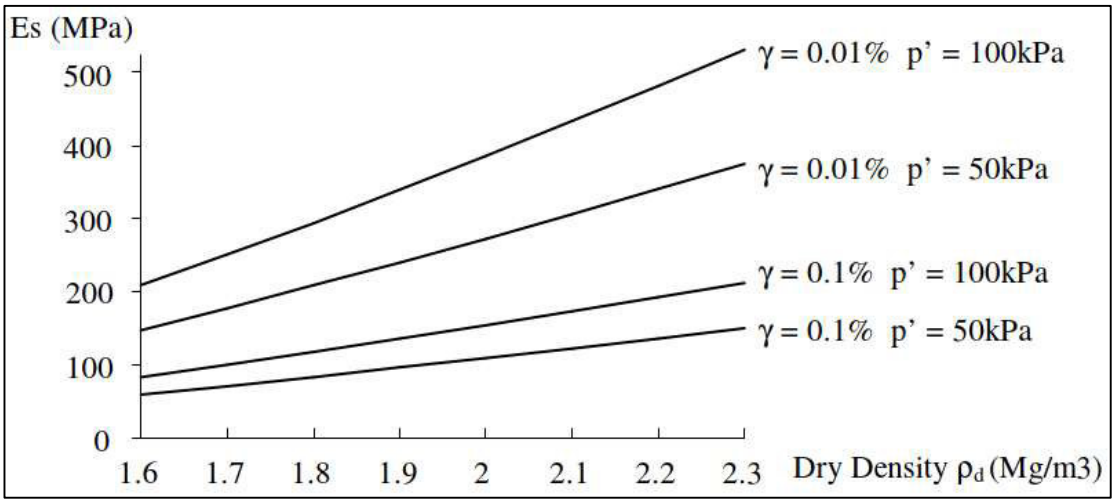

Figure 2.48: Backfill soil Young's Modulus (E_s) of for a selection of In-Situ Dry Densities (ρ_d), Mean Effective Stresses (p') and Average Shear Strain Levels (γ)

2.5.7 Soil Spring Strength

Bohnhoff (2014), studied buried posts or piers and provided a formula for the ultimate resistance load that an individual soil spring can provide as follows:

$$F_{ult} = pU, z.t.b \qquad \text{(Eqn. 55)}$$

Where:

F_{ult} = Ultimate load arising from an individual spring at depth z, (kN)

pU,z = Ultimate lateral soil resistance for soil at depth z (unexcavated condition), (kN/m^2)

b = Post/pile footing or collar width of the face that loads the soil when the foundation moves horizontally (m)

t = Soil layer thickness, represented with a soil spring of stiffness K_H (m)

z = Distance of spring below ground level (m)

SOIL TYPE	Unified Soil Classification	Consistency	Moist Unit weight, ϒ	Undrained soil shear strength, S_U	Young's Modulus for soil, E_S
			kN/m^3	kN/m^2	kN/m^2
Homogenous inorganic clay, sandy or silty clay	CL	Soft	19,64	24,1	27 027,5
		Medium to Stiff	20,42	48,3	42 471,7
		Very Stiff to Hard	21,21	96,5	57 916,0
Homogenous inorganic clay of high plasticity	CH	Soft	17,28	24,1	11 583,2
		Medium to Stiff	18,07	48,3	19 305,3
		Very Stiff to Hard	18,85	96,5	30 888,5
Inorganic silt, sandy or clayey silt, varved silt-clay-fine sand of low plasticity	ML	Soft	18,85	24,1	27 027,5
		Medium to Stiff	18,85	48,3	42 471,7
		Very Stiff to Hard	18,85	96,5	57 916,0
Inorganic silt, sandy or clayey silt, varved silt-clay-fine sand of high plasticity	MH	Soft	16,49	24,1	11 583,2
		Medium to Stiff	16,49	48,3	19 305,3
		Very Stiff to Hard	16,49	96,5	30 888,5

Table 2.7: Table - Properties for Silt and Clays (Cohesive) Soils, adapted from Bohnhoff (2014)

SOIL TYPE	Unified Soil Classification	Consistency	Moist Unit weight, ϒ	Drained soil friction angle, Ø'	Increase in Young's Modulus per unit depth, A_E
			kN/m^3	Deg	kN/m^2/m
Silty or clayey fine to coarse sand	SM, SC, SP-SM, SP-SC, SW-SM, SW-SC	Loose	16,49	30,0	9 953,2
		Medium to Dense	17,28	35,0	14 929,9
		Very Dense	18,07	40,0	19 906,5
Clean sand with little gravel	SW, SP	Loose	18,07	30,0	19 906,5
		Medium to Dense	18,85	35,0	29 859,7
		Very Dense	19,64	40,0	39 813,0
Gravel, gravel-sand mixture, boulder-gravel mixtures	GW, GP	Loose	21,21	30,0	59 719,4
		Medium to Dense	21,21	35,0	79 625,9
		Very Dense	21,21	40,0	99 532,4
Well-graded mixture of fine- and coarse grained soil: glacial till, hardpan, boulder clay	GW-GC, GC, SC	Loose	18,85	30,0	29 859,7
		Medium to Dense	19,64	35,0	39 813,0
		Very Dense	20,42	40,0	49 766,2

Table 2.8: Properties for Sand and Gravel (Cohesionless) Soils adapted from Bohnhoff (2014)

ANSI/ASAE EP486.2 (2012) covers the equations for calculating pU,z by using pre-bored pressuremeter test (PMT) plots of results and cone penetration test (CPT) results. Alternatively, pU,z may be derived for cohesionless soils (sands and gravels) as follows:

$$pU,z = 3\sigma_{v,z}.k_p = 3(y.z - u_z).k_p \quad \text{(Eqn. 56)}$$

For cohesive soils (silts and clays) the following expressions are applicable:

$$pU,z = 3S_U \quad (1 + z/(2b)) \text{ for } 0 < z < 4b \quad \text{(Eqn. 57)}$$

$Pu, z = 9S_U$ for z > 4*b* (Eqn. 58)

Where:

K_P = Coefficient for the passive earth pressure (dimensionless)

= (1 + sin Ø)/(1 – sin Ø)

Ø = Soil friction angle, degrees

$\sigma_{v,z}$ = Vertical effective stress at depth *z*, kN/m^2

= $\gamma z - u_z$

γ = soil moist unit weight, kN/m^3

u_z = pore water pressure at depth *z*, kN/m^2

S_U = undrained shear strength at depth *z*, kN/m^2, equal in value to the cohesion, *c*, of a saturated clay soil.

In the absence of any materials testing, values may be assumed from **Table 2.7** or **Table 2.8**, which provide values of Young's Modulus for various categories of soil condition. To calculate the spring stiffness, the following equation is provided:

$K_H = 2{,}0.t.E_S$ (Eqn. 59)

Where:

K_H = initial stiffness of an individual soil spring located at depth z, kN/m

E_S = Young's modulus for soil, located at depth z, kN/m^2

2.5.8 Soil backfill pressure effects on the superstructure design

The soil backfill lateral pressure at the back of the abutment (see **Figure 2.49**) can vary linearly with depth (depending on what code one uses), therefore the pressure centre on an end screen wall is positioned at roughly 2/3 of the height from the top of the wall to its underside. For the fully integral (or semi-integral) bridge or one on piles, there is thus a lever arm between the backfill pressure centre and the girder (or deck) centroid as per the diagram below, which creates additional hogging moments and axial forces on the structural system.

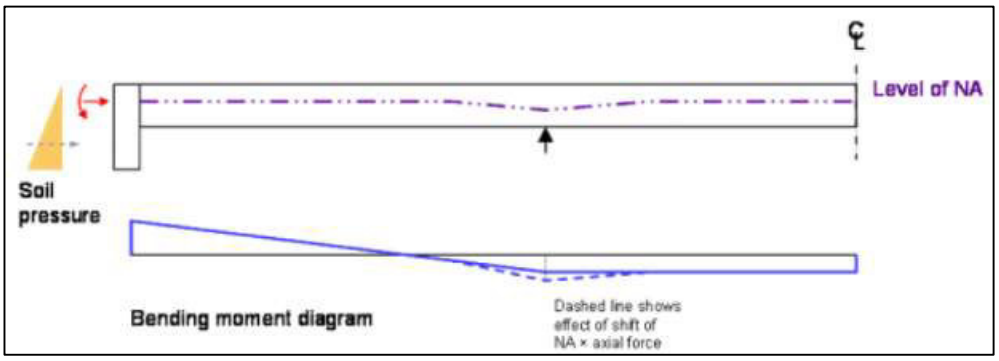

Figure 2.49: Effects of axial force due to soil pressure (Iles, 2005)

2.5.9 Backfill effects related to the Approach Slab system

It is a widespread practice to build approach slabs that are connected behind the abutment with integral abutment bridges, despite being banned in certain European nations. It is preferable to locate the slab at pavement level as opposed to burying it at a level below the pavement layers. The approach slab is recommended to be a minimum of 3m long, (preferably 5m long) and should have a similar skew alignment as per the abutment.

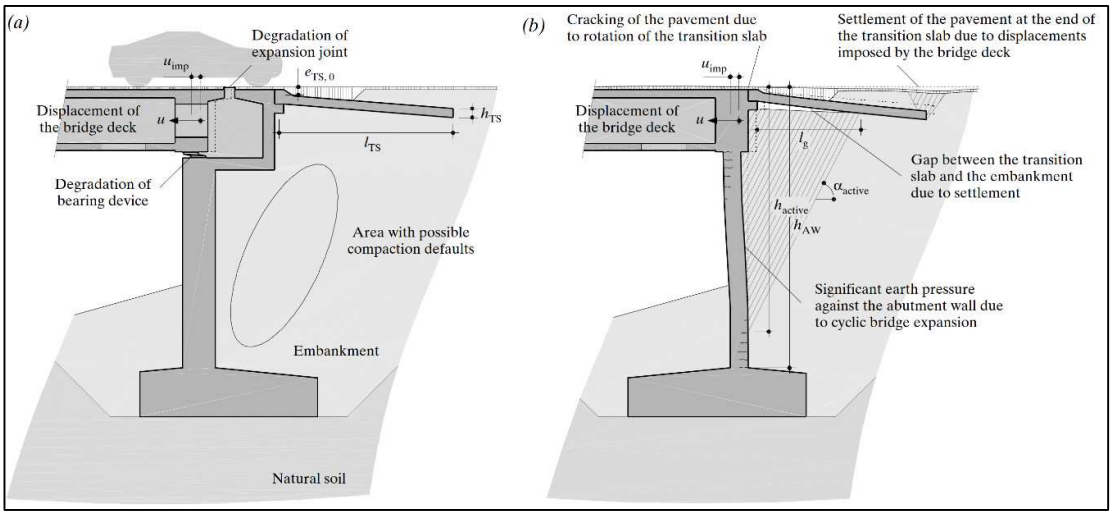

Figure 2.50: Types of structural damage due to longitudinal displacement of the bridge deck (Dreier, Burdet, Muttoni, 2011)

The approach slab aims to achieve the following goals (Briaud et al., 1997):

1) Prevention of continued settlement of the bridge backfill due to sustained vehicular loads.
2) Provision of a smooth transition, enabling the abutment rotation and translation.
3) Preventing water penetration of the abutment soils, which can result in erosion and piping of the backfill behind the abutment. This is achieved when using a continuous connection between the deck approach slab and the abutment rear wall.
4) The prevention of moisture carrying salts from obtaining access to the lower abutment regions as well as to the bearings in the case of semi-integral abutments. This is achieved by the continuous connection between the approach slab and the bridge deck.
5) Spanning over any voids that might be created below the slab (see **Figure 2.50**).
6) To provide a transition ramp for any differential settlement occurring between the embankment and the abutment.

By connecting the approach slab to the abutment, the bridge movements do not disappear in the system, but must be allowed for at the far ends of the approach slab. With short length bridges, the anticipated movements are insignificant and therefore there is no need for the use of expansion joints. However, where large movements are predicted, a control joint may be used between the approach slab ends, and the adjacent road pavement. A small footing slab positioned underneath the joint is usually provided.

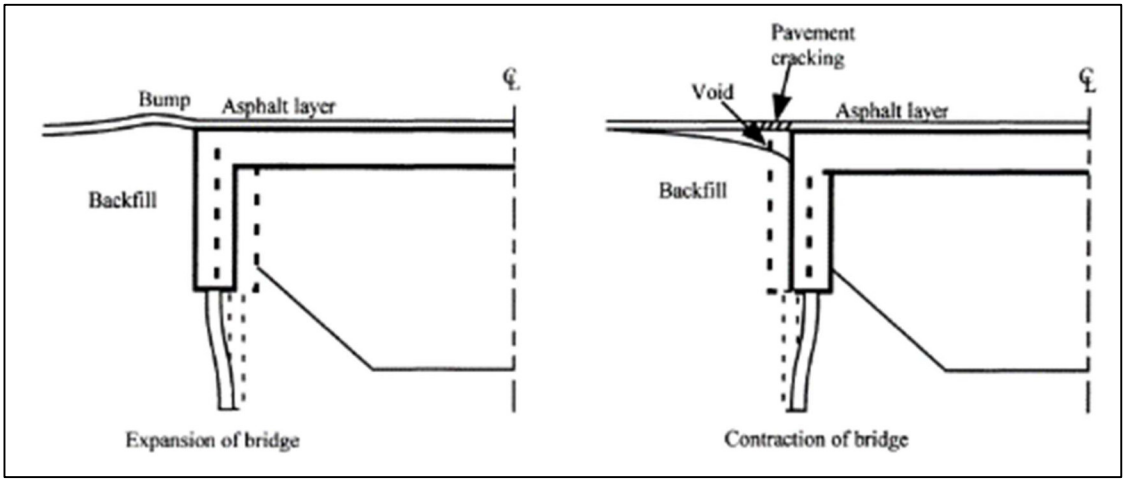

Figure 2.51: Expansion and contraction movements of a bridge with no approach slab (Arsoy et al., 1999)

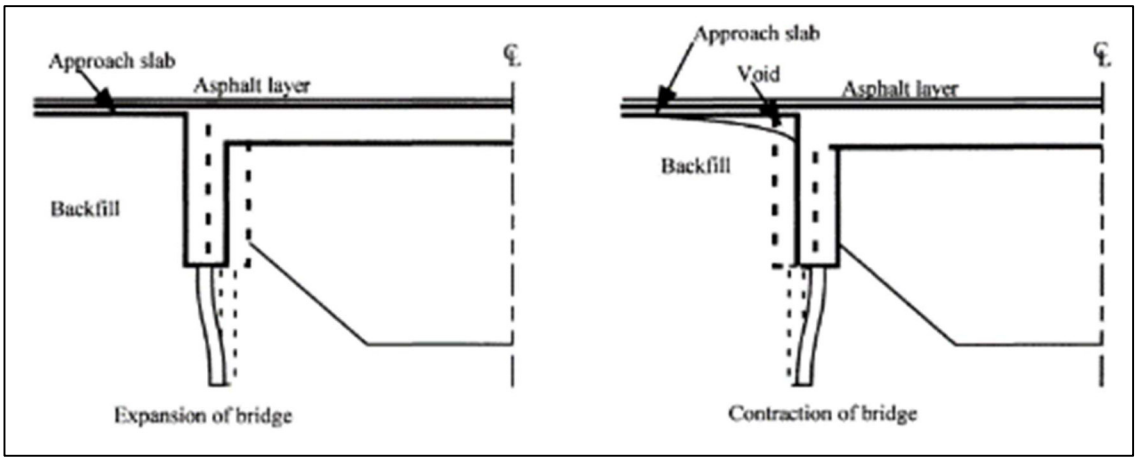

Figure 2.52: Expansion and contraction movements of a bridge with an approach slab (Arsoy et al., 1999)

The literature review conducted by Arsoy (1999) concluded that there is no single over-riding factor that may be held responsible for integral bridge settlement in the approach fill – rather, there are many factors that cause the issue, and remedial measures need to be taken to reduce the impact of these factors. The most significant factors are the following (Arsoy,1999):

1) Poor compaction and drainage cause settlement of the approach fill, which can be significant over time.
2) Foundation founding material can be soft and compressible, causing settlement of the approach fill.
3) Pavement growth and other factors such as excessive vehicular loading.

Figure 2.51 and **Figure 2.52** show the effects of the expansion and contraction cycles on an integral

abutment bridge with and without an approach slab. As can be seen in the expansion case where there is no approach slab (**Figure 2.51**), a bump in the road is formed as the deck thermal extension is reflected back into the backfill and road surfacing. In both cases, over time, a void in the backfill may be formed behind the abutment to the expansion and contraction of the deck movement cycles.

Burke (1987) provides commentary and critique of various approach slab details and shows that several of them have many faults and are inadequate for the task of achieving the goals for the approach slab that are listed above. Burke (1987) also states that many designs are limited in their ability to fulfil their function, warning that agencies that are building integral bridges without cycle-control joints should expect to see high pressures in and fractures of rigid-approach pavements with distress and deterioration of flexible-approach type pavements.

2.5.10 Summary - Modelling of Soil behind the abutment

In this section of the literature review, a focus was put on the geotechnical considerations relating to the backfill material as well as the derivation of the parameters of importance such as the soil's Young's Modulus and Coefficient of Subgrade reaction. Note that equation No. 53 by Lehane (1999) supposedly accounts for the effects of strain ratcheting and thermal movement over time for a granular material. The Young's Modulus and Coefficient of Subgrade reaction parameters are highly dependent on the soil type and (often) the depth under consideration. The merits of various kinds of backfill material were also tabulated and the effects of the stress cycles induced by the thermal movements on the backfill material were highlighted. The most commonly specified backfill material for the integral bridge type is the 6N/6P granular backfill, which is a well researched material, and which displays the ratcheting effect. The effects of pore water pressure and compaction density were also discussed and it is clear from the tables that there are differences in the Youngs modulus and Subgrade Coefficients that relate back to the soil type, as well as the reference used (hence field testing is preferred). Also of importance to note is the concept of a finite soil spring strength value – this is the reason why analysis programs should allow (to be more accurate) for their non-linear behaviour. In regard to the approach slab system, it should be noted that these slabs are banned in certain countries in Europe since they can often give ongoing maintenance issues. There are also variances in the positioning of the approach slab – some designers prefer the slab to be near the surface, whilst others prefer it to be buried under some of the backfill. From the authors experience, the inclusion or exclusion of an approach slab does not in general make a large difference to the design moments in the abutment, although it will create some additional friction that needs to be overcome when the abutment tries to move during its daily (and seasonal) thermal cycles.

2.6 Summary - Literature review conclusion

The integral bridge represents a structure where a dynamic interplay exists between both the structural and geotechnical characteristics of the surrounding soil medium.

An extensive literature survey (with the key findings from previous authors being noted) was undertaken in order to provide a framework for understanding the behaviour of integral bridges, the soil-structure interaction, as well as how various authors have attempted to model the behaviour of select types of integral bridge. The iterative nature of the soil-structure analysis was described, as well as the approach taken by various codes of practice to account for these requirements. Various 2D models with simplified assumptions have been looked at in the review, as well as more advanced 3D

models with more accurate soil-spring characteristics. The grillage method of bridge analysis has been discussed in the literature review and this is used in the 3D models that were created for this thesis. Simple 2D models based on the various approaches used by previous authors rely on a frame analysis with springs, and this is therefore what has been used in the modelling that is described in the next section.

The literature review showed that there is a wide variance in soil and backfill characteristics which can have a profound effect on the overall integral bridge behaviour.

The literature review showed that to date, there have been relatively few studies made of the spring reaction characteristics themselves, and hence the parametric study in this thesis was deemed appropriate and necessary to fill in the research gap.

In the next Chapter, the characteristics and parameters of the models used in the thesis are described.

3 CHAPTER 3 - Analysis model setup and methodology

In order to satisfy the requirements for the aims and objectives of this investigation – which concerns itself with studying and revealing the behaviours of integral bridge spring reactions, it is necessary to create a series of parametric models in both 2D and 3D.

In South Africa, the reinforced concrete bridge deck is very common, and so this thesis has focussed on the concrete deck solution as opposed to the composite steel solution which is quite popular in various other countries. In general, deck spans from 10m - 40m represent the most common limits that the single span integral bridge is built to locally and abroad (longer spans are more often than not designed as multi-span bridges), and therefore these have been considered in the 3D Grillage models whilst spans from 10-30m have been used in many of the 2D Frame models – this was simply due to time constraints in creating the models, (40m spans would have been preferred to have also been included in the 2D models). Abutment heights of between 3m and 9m were considered for the study, although a 9m high abutment would be quite rare to see in practice, it was included since it was the next multiple in the series and certainly assisted in revealing the spring behaviour. A Deck width of 9.6m has been chosen as it allows for neat nodal spacing of the longitudinal and transverse beams, allows for two-way flowing traffic and is wide enough for transverse effects to take place.

The underlying theme in the creation of the various bridge models is that the element sizes should increase as the span increases, since this is what would happen normally in practice - the spring reaction results are therefore indicative of what would take place in the normal design practice scenario. This standardization of the method of element sizing (through the application of various element sizing rules) is necessary in order to provide a degree of realism to the results obtained. Other choices in modelling approach were made in order to simplify the model and remove further opportunity for variance (eg. not including wing walls and approach slabs).

Beam depths and corresponding abutment thicknesses are therefore increased from model to model based on span/depth ratios and second moment of area ratios between the deck and the abutments. Pile sizes are determined (and increased) based on a set working stress – they therefore increase in size as the span is increased. See Section 3.2, **Table 3.2** and **Table 3.3** for further information concerning the sizing of the elements used in the models. The details of the exact calculations used to create and size the elements form a very large spreadsheet, therefore (for ease of reading) only parts of this spreadsheet are reproduced in Appendix A. Note that a further reason for the above approach is to avoid the need for a full design check of each bridge model (reinforcement and/or prestressing would need to be assumed), which would consume a considerable amount of time, and may not even result in a standardized set of models.

As part of the above exercise, the calculation of the spring stiffnesses is crucial to the creation of the boundary conditions in each of the models. The information showing the calculations for this are shown below in **Table 3.5** to **Table 3.9** below, however there are further calculation tables in Appendix A. With reference to **Figure 2.19**, the spring stiffnesses for the abutments and the foundations are dependent on quite different variables, theory and equations. For example, from Equations 61, 62, 63, 64 (see further in this Chapter) it is clear that the abutment spring stiffness as calculated in the 3D Grillage modelling is inversely proportional to the deck length, as well as the change in deck temperature. Equation 34 shows an inverse relationship of the spring stiffness to the abutment height in the simplified 2D model whilst Equation 8 relates to the P-Y theory formulations and shows a directly proportional relationship of spring stiffness to the pile diameter.

In broad terms, the 2D models that have been setup are based on the simplified theories published by Hambly (1991) and O'Brien and Keogh (1999) which account for deck contraction and expansion or live loading. These 2D Frame models (and the diagrams that describe them) as well as the 3D Grillage model has been discussed in the Literature review and is highlighted in **Table 3.1**.

In these simplified models, either the soil spring is modelled as a single spring positioned at the level of the deck, or it is distributed along the height of the abutment. In other instances, the footing is simplified as a set of two springs, spaced a distance apart from each other. These 2D frame models have been selected for the study since they have few variables and are easy to create, therefore they are ideal for use in the study. The 3D grillage model is used as it is a common method of analysis for bridges (Hambly, 1991) and presents a more accurate set of answers that capture the transverse bending that is not found in a 2D model, assuming the grillage layout has been created in accordance with the principles outlined in Section 2.4.7.

Note that the 3D Grillage models that were created mostly include for the effects of ratcheting since they use the Lehane (1999) and Broms (1971) formulations for the calculation of the secant Young's modulus (see further on, in Section 3.8.1). The only model which does not include for these ratcheting effects is the Hambly (1991) foundation stiffness model, which uses a Young's modulus value taken from a standard reference table.

Note that for the 2D models that were created, the same footing size was used between the models (to cover a range of eventualities), as it was postulated that this would standardize this aspect of the spring reaction effects. This could have been done differently however, and each footing could have been made larger as the span/load increased (as has been done with the piled type of bridge design). Slightly differing answers would indeed have been produced if this route had been followed.

3.1 Model Types

Five main kinds of linear (as opposed to non-linear) integral bridge models were studied in the series of analysis models that were created for this thesis, and are as per the characteristics that were described in the literature review (see the Reference column below in **Table 3.1**):

	2D / 3D Model descriptions						
	Description	**Primary Loading for model**	**Reference**	**Type**	**Analysis package used**	**Foundation type**	**Reference Figure**
1	**Shallow strip footing foundation stiffness**	Live load	Hambly (1991)	2D Frame	PROKON	Pad footing	Figure 2.21 and Figure 2.23
2	**Spring model on flexible supports**	Contraction	Dobry and Gazetas (1986)	2D Frame	PROKON	Pad footing	Figure 2.20
3	**Conventional spring model for deck expansion**	Expansion	O'Brien and Keogh (1999), Springman et al (1996)	2D Frame	PROKON	Piles / Pad footing	Figure 2.24
4	**Equivalent spring at deck level model**	Expansion	Lehane (1999)	2D Frame	PROKON	Pad footing	Figure 2.26
5	**Full height abutment spring modelling**	Contraction & Expansion + Live Load	Hambly (1991), Dicleli (2009)	3D Grillage	MIDAS	Piles	Figure 3.1

Table 3.1: Model types used in the various analysis models for this thesis (refer also to Literature review section)

3.2 Methodology for model component and spring sizing

The methodology described below was followed in order to create all of the analysis models that were generated for the model testing (and see **Figure 3.1** and **Figure 3.2**):

The rationale and workflow used in the development and derivation of the various model dimensions (see Appendix A) is as follows:

1) As described earlier, spans from 10m to 40m and abutment heights from 3m to 9m were considered. Soil conditions varied from stiff clay to loose sand.
2) From the assumed spans, the beam depth is determined. The combined depth of slab and beam is kept between a narrow range of 21 < Span / Beam depth < 22. This range was deemed to be a suitable range for an integral type bridge of this nature after studying some examples of previous integral bridge projects. Examples of bridges known to the author that were considered in this study are the Kwa-Bhoboza interchange bridge, Van Zylspruit N1 bridge - South Africa, Yeading Brook bridge – England, and others. In design practice, this range will vary from project to project, and will depend on items such as allowable deflection, deck type, beam class, designer preference and the presence of prestressing or not.
3) The Second Moment of Area for the combined beam and slab system, Ixx is compared with the abutment Second Moment of Area, and are made as similar as possible, within a narrow band of tolerance (5% is used). This check enables the determination of the Abutment thickness. This check is necessary since the ends of the deck and the abutment are required to resist similar magnitude moments at the joint.
4) A pile size (where applicable) is assumed (must be smaller in size than the abutment thickness) and the weight of the structure is calculated, with the stress on the pile being checked for vertical load (Dead load + SDL + Live load) only. A maximum stress of between 7 – 8 MPa has been selected to ensure that the pile is reasonably sized. This allowable stress has been derived from guidance contained in the publication by Byrne et al. (2019), which provides notes to the designer for the initial sizing of auger piles based on their vertical loading and allowable working stress only.
5) Springs are assigned to the structure, based on either the Young's Modulus (hand calculations for 2D models), or are calculated by MIDAS, once the properties of **Table 3.10** have been used as input to the spring assignment function. 2D model properties are taken from **Table 3.11**, with further calculations being required, as per the **Table 3.6** to **Table 3.9** information.
6) Typical dead and superimposed dead loads are calculated, so that the corresponding % live loads can be assigned to the deck longitudinal beams in a parametric manner (see 'Loading' in Section 3.6). Temperature loads (+/- 15^{o}C) are also applied to the deck, as well as temperature gradient (positive and negative) loads for some selected instances.

3.3 Model description and characteristics

The following model characteristics have been chosen as being suitable for the set of analysis testing that was undertaken:

1) For reasons of simplification, the deck has no vehicle impact barriers included. There is a large variance in the types of vehicle impact barriers that are available (pedestrian and vehicle impact barriers are available), with a corresponding variance in self weight, therefore it was deemed preferable to omit any vehicle barriers.

2) A uniformly distributed live loading was applied only to the longitudinal beams in the grillage – this would be considered normal practice.
3) A similar number of piles have been provided as per the number of longitudinal beams (8 No. of in this instance).
4) A beam and slab grillage model, as described in Section 2.4.7 has been used in the MIDAS analysis models.
5) For the 2D frame analysis models, a section with 8 beams has also been assumed.
6) The abutment is modelled using shell elements in this scenario. Further models are presented in Appendix B.
7) A simple 2D frame analysis (see **Figure 3.7**), where the entire section is considered as being represented by a line element) is used for the Prokon models. The figures below give one an idea of the shape and size of the various models that have been used. The reader is referred to Appendix B for more details of the models.
8) A pile length of 12m was chosen as this represents an average pile length that would be found in the field, and the length is long enough to be reasonably flexible. To understand the sensitivity of results, some select models were also tested for a 6m pile length (refer to Chapter 4).

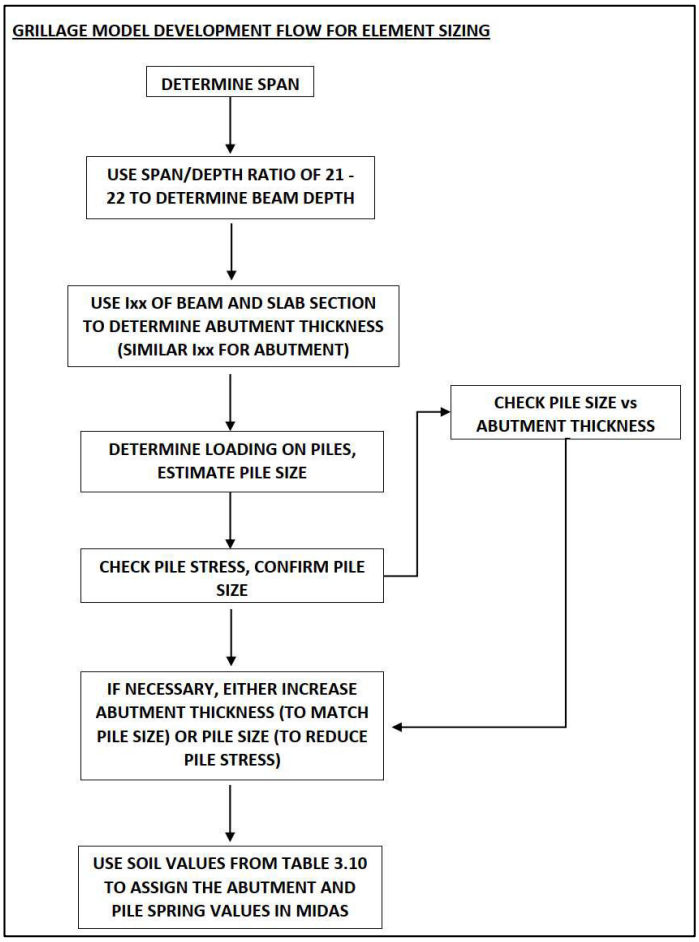

Figure 3.1: Typical flow used to generate models for the 3D MIDAS Grillage

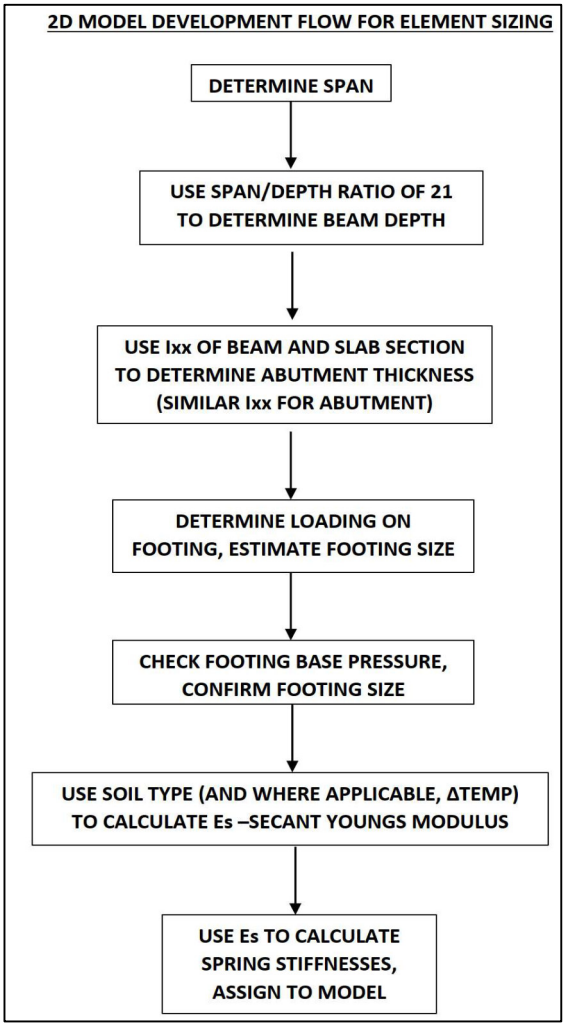

Figure 3.2: Typical flow used to generate models for the 2D Frames

9) The augered piles are a common design solution in South Africa (hence they have been chosen for use in this thesis) and are assigned spring functions down their length, which are simulating a pile with skin friction and some end bearing capacity. An allowable pile stress of 7-8 MPa was selected as being appropriate for the sizing of the abutment piles - see guidance from Byrne et al. (2019).
10) Wing walls are excluded from the modelling due to the variability that these items have in practice (parallel wing walls, splayed wing walls, cantilever walls and no wing walls are all possible design choices).
11) Approach slabs are excluded since they are not a standard practice in all parts of the world, their size is variable, and there is also a variability in their positioning relative to the top of the abutment wall.
12) All elements are RC concrete – beams, deck slab, abutments and the augered piles or footings as the case may be.

Table 3.2 below (extracted from Appendix A) shows the relationship between the assumed spans vs. the beam depths used for the analysis models. Note that a span / depth ratio of between 21 and 22 has been used in order to calculate the beam depth in these tables.

Bridge Span	No. of Longitudinal beams	Slab thickness	Beam Depth	Total Depth (beam + slab)	Actual Span/depth ratio	Beam width	Beam spacing, S	Total deck width	Gap between Beams
m	No. of	m	m	m		m	m	m	m
10,000	8	0,250	0,225	0,475	21,053	0,500	1,200	9,600	0,700
20,000	8	0,250	0,700	0,950	21,053	0,500	1,200	9,600	0,700
30,000	8	0,250	1,175	1,425	21,053	0,500	1,200	9,600	0,700
40,000	8	0,250	1,650	1,900	21,053	0,500	1,200	9,600	0,700

Table 3.2: Beam properties showing the relationship between assumed beam depth and span (used across all the modelling, 2D and 3D)

The following basic characteristics have been assumed in the bridge modelling (a more detailed breakdown is provided in the examples shown in Appendix A):

Item	Value	Unit
Beam width	500	mm
Horizontal spacing between beams (and shell nodes down abutment)	1200	mm
Slab thickness	250	mm
Longitudinal beam node spacing	1000	mm
Abutment vertical node spacing	1000	mm
Typical transverse beam width	1000	mm
No. of longitudinal beams	8	No. off
Total depth of beam + slab	Varies	mm
Total deck width	9600	mm
Span/depth ratio(max)	22	
Span/depth ratio(min)	21	
Maximum allowable footing stress	250	kPa
Maximum allowable pile stress	7-8	MPa
Pile Length	12 000 and 6000 (for certain models)	mm
Pile/Abutment Spring vert. spacing	1000	mm
Abutment Spring horizontal spacing	1200	mm

Table 3.3: Beam, deck and model assumptions

In the modelling setup for this thesis, MIDAS CIVIL 2020 (version 3.1) has been used to model a series of parametrically varied integral bridge models with various parameters examined for the variation of their values and the effects that this has on the calculated spring reactions.

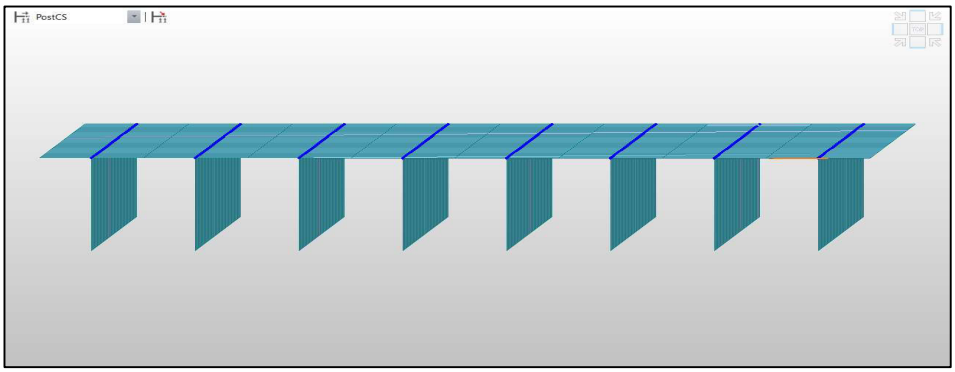

Figure *3.3*: Typical section taken through MIDAS model showing the T-Beam model layout

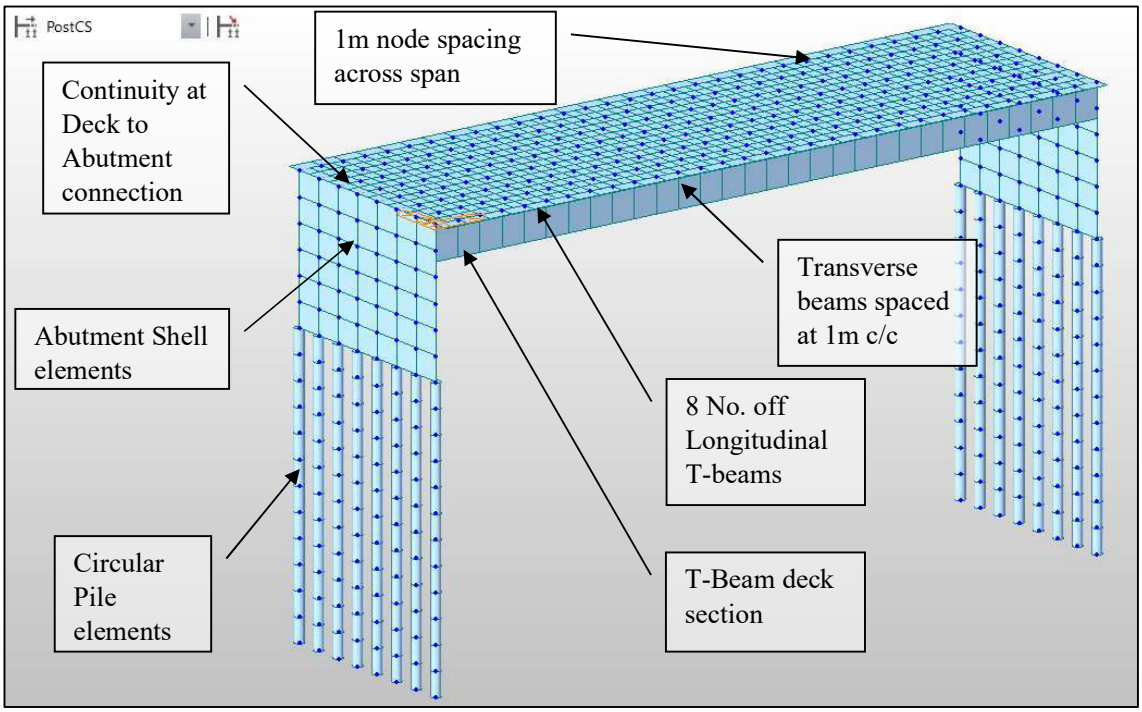

Figure *3.4*: Typical MIDAS Integral bridge model created for the parametric modelling

The springs are positioned behind the abutments as well as along the length of the piles in the 3D MIDAS model. 3D MIDAS models are used to simulate the 3D effects, considering the deck width, the foundation piles and the non-linearity of the spring system.

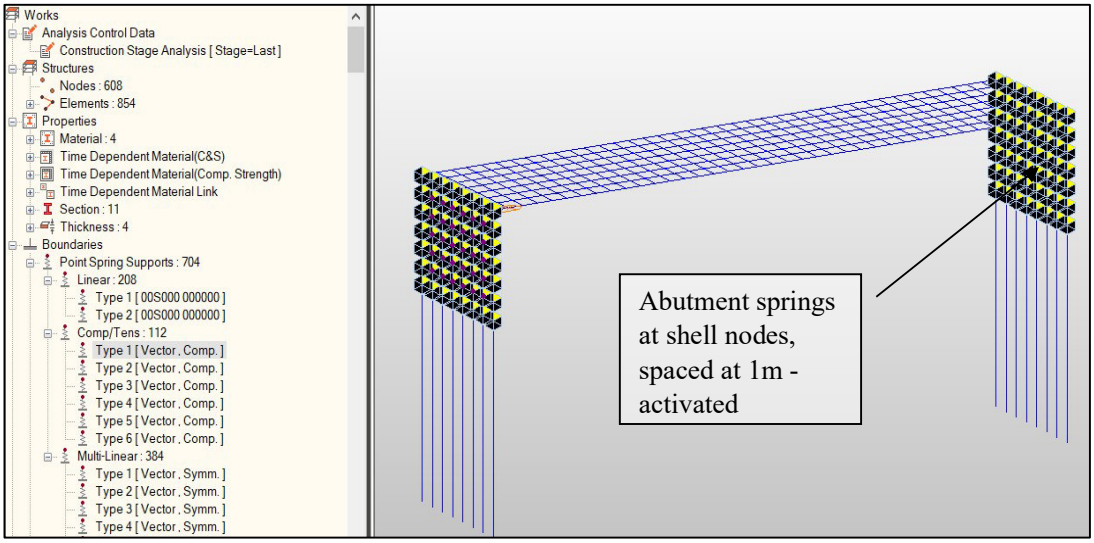

Figure *3.5*: Typical Integral bridge MIDAS model with Abutment Spring reactions activated and Compression/Tension Functions shown

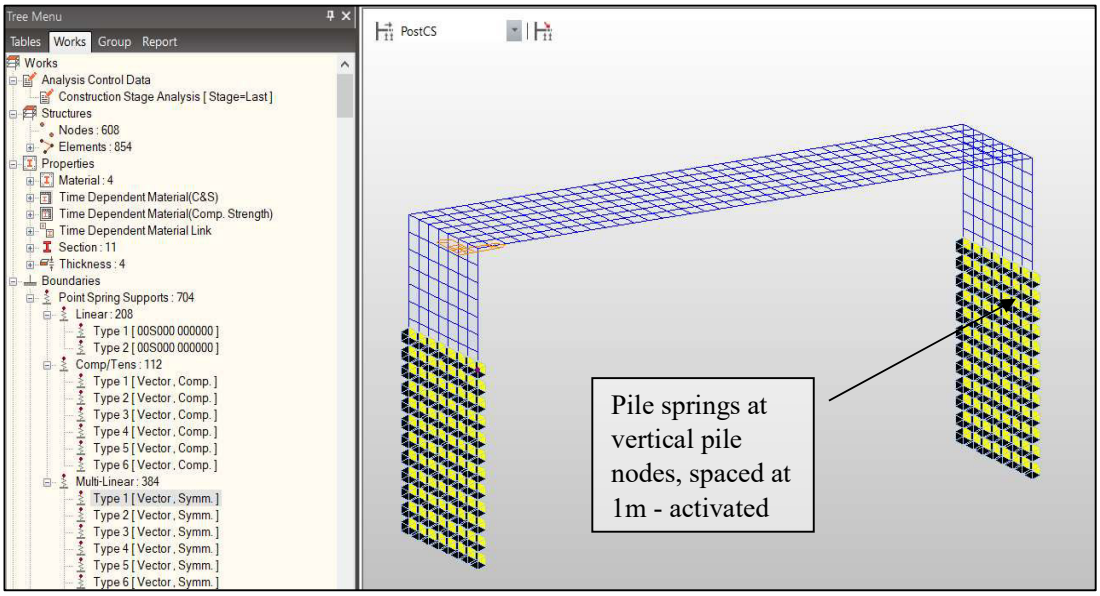

Figure *3.6*: Typical Integral bridge MIDAS model with Pile Spring reactions activated and Multi-linear Functions used for Pile springs

Figure *3.4* shows a typical 3D MIDAS grillage model. The diagram shows the typical shell elements used for the abutments, the longitudinal beams, the transverse beams and the 12m deep circular piles. Note that in order to create the integral abutment continuity, the connections between the longitudinal beams and the abutments are fixed. **Figure *3.5*** and **Figure *3.6*** show the distribution of abutment and pile springs respectively across the various elements. The different springs can be separately activated

in the model as shown in the two diagrams. **Figure *3.3*** shows a transverse section through a typical 3D MIDAS Grillage deck model. Note that 8 beams have been consistently used for all the models in this thesis, whether considering a 2D Frame analysis model or 3D Grillage model.

The 2D frame models (Prokon version 3.1.08) as described in **Table 3.1** are used to simulate the integral bridge behaviour, as per the theories of the authors listed in **Table 3.1**. Note that in all instances where the 2D frame is used, the foundation is a footing, not a pile foundation, and a single span structure has been assumed in each instance.

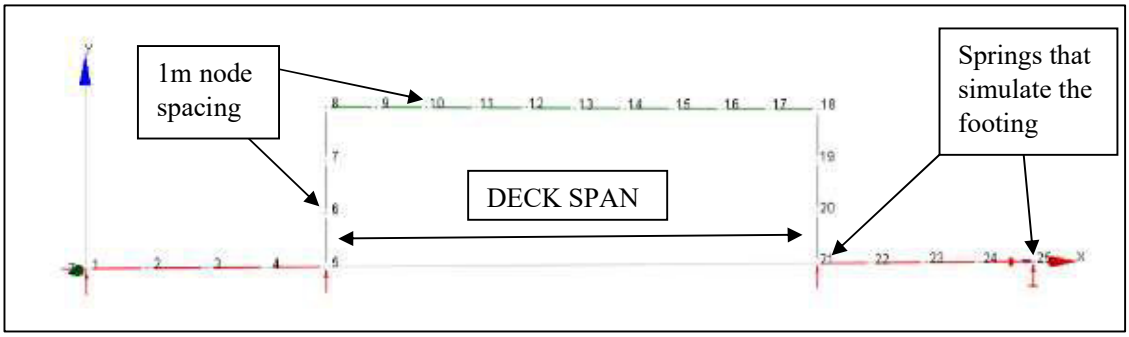

Figure 3.7: Typical 2D Frame model (Prokon)

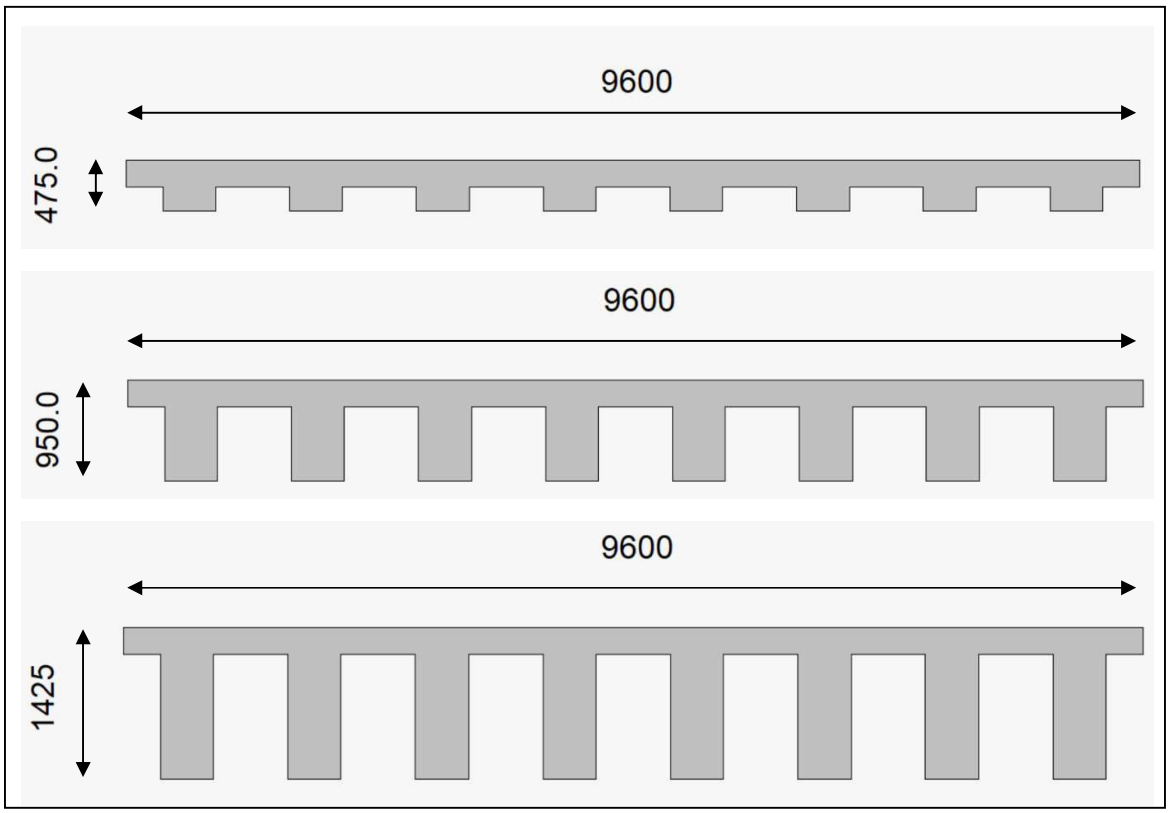

Figure *3.8*: Deck sections for *2-D* Prokon models, 8 longitudinal beams with varying depths

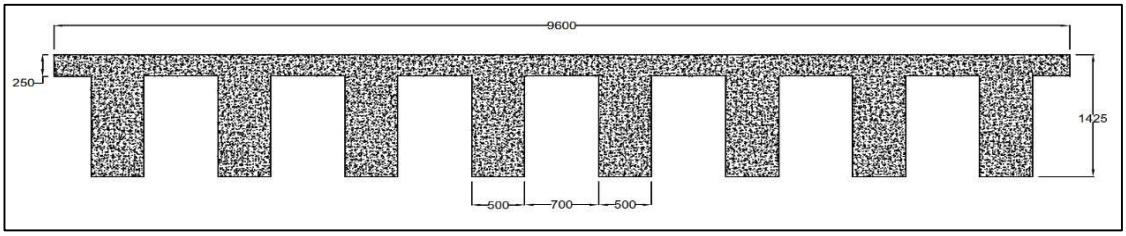

Figure *3.9*: Typical T-beam composite section assumed in the analysis modelling (both 2D and 3D)

A section through a typical deck slab used in Prokon is shown above in **Figure *3.8***. The beams are standardized between the 3D MIDAS model and the 2D Prokon model, with the only variance being the depth of the beam. Each longitudinal beam is 500mm wide, spaced at 1200mm, and the deck slab is 250mm deep, as shown in.**Figure *3.9***.

3.4 Structural material properties

The concrete beam and slab model has been used for the modelling process, with the properties that are described in **Table 3.4**. For simplicity, the same concrete strength has been used for the slab, beams, abutments and piles/footings. Note that many factors will influence the effect of creep and shrinkage on the response of concrete members in integral bridges. Factors influencing concrete shrinkage include water-cement ratio, water content, workability, type and content of aggregate, and relative humidity. Factors that will affect concrete creep include the nature of the sustained stress, concrete strength, type, size and content of aggregate, water-cement ratio, slump, air content, loading age, relative humidity, volume-surface ratio and temperature.

Material property	Symbol	Value	Unit	Reference
Concrete self-weight	γ_c	**25,50**	kN/m^3	**TMH7 (1&2): 2.2.1**
Asphalt self-weight	γ_{as}	**20,60**	kN/m^3	**TMH7 (1&2): 2.3.1**
Asphalt thickness	T_a	**0,10**	m	
Concrete beam and abutment strength	f_{cu}	**40,00**	MPa	
Concrete slab strength	f_{cu}	**40,00**	MPa	
Concrete pile strength	f_{cu}	**40,00**	MPa	
Youngs modulus, concrete	E_c	**31**	GPa	**TMH7 (3): Table 3**
Abutment backfill Specific gravity	Gs	**2,65**		**Lehane (1999)**
Coefficient of linear expansion for concrete	α_c	**1,20E-05**		**TMH7 (1&2): 4.5.6**
Water density	ρ_w	**10,00**	kN/m^3	**SANS 10160-2:2010, Table A.7**

Table 3.4: Material properties used in Spreadsheet calculations of Appendix A and various 2-D and 3-D analysis models – references have been listed where applicable

3.5 Model input for springs

Table 3.5 to **Table 3.9** show the typical input calculations for the spring properties that are utilized for the five model types as described in **Table 3.1**. The columns containing all the calculations can be referred back to the literature study that was done, where these models were discussed and the equations for the spring modelling presented.

Bridge Span	Void ratio (e)	Differential Deck Temp. ΔT	Ground Level	Pile diameter (D)	Unit weight of soil	Earth Pressure Coefficient at rest (Ko)	Coefficient of Subgrade Reaction (Kh) (Terzaghi - CIRIA 103)	Initial Soil Modulus (K1) (MIDAS)	Undrained Cohesion (Cu)	Internal friction angle (ϕ)
m	m	m	m	m	kN/m^3		kN/m^3	kN/m^3	kN/m^2	Degrees
10,000	0,38	30,00	-3,0	0,300	19,0	0,42	30 000,0	N/A	100,0	N/A
20,000	0,38	30,00	-3,0	0,350	19,0	0,42	30 000,0	N/A	100,0	N/A
30,000	0,38	30,00	-3,0	0,400	19,0	0,42	30 000,0	N/A	100,0	N/A
40,000	0,38	30,00	-3,0	0,500	19,0	0,42	30 000,0	N/A	100,0	N/A

Table 3.5: Typical Model spring property input for the 3D MIDAS grillage modelling (this particular input is for stiff clay founding conditions for the piles)

Bridge Span	Pile Vertical Spring (adj) $K_z = 1.5EA^{0.5}$	Pile Horizontal Spring $K_x = EA^{0.5}$	Pile Rocking Spring $K_m = 1.5EZ$	$l = 2(K_m/K_z)^{0.5}$
m	MN/m	MN/m	MN/m	m
10,000	965,981	1 287,975	5 184,000	4,63
20,000	965,981	1 287,975	5 184,000	4,63
30,000	965,981	1 287,975	5 184,000	4,63

Table 3.6: Typical spring property input for the shallow strip footing stiffness model, as per Hambly (1991)

Bridge Span	ΔT	$\delta = \Delta T \alpha_c L$	$\Upsilon = 2\delta/3H$	$E_s = 150\,000(2.17-e)2/(1+e)(p'/p_{atm})^{0.5}(0.0001/\Upsilon)^{0.4}$	$k_{vert} = 0.4E_s$	$k_{horiz} = 0.5E_s$	$k_{rot} = E_s B^2/6$	$F_o = A_d \Delta T \alpha_c E_c$
m	°C	m		kN/m^2	kN/m	kN/m	kN.m/m	kN
10,000	30,00	1,80E-03	4,00E-04	133 066,33	510 974,69	638 718,36	1 916 155,08	36 828,00
20,000	30,00	3,60E-03	8,00E-04	148 371,13	569 745,13	712 181,41	2 136 544,23	58 032,00
30,000	30,00	5,40E-03	1,20E-03	166 627,21	639 848,47	799 810,59	2 399 431,77	79 236,00

Table 3.7: Typical spring property input for the bridge contraction on flexible supports model, as per Dobry & Gazetas (1986)

Bridge Span	ΔT	δ = ΔTα$_c$L	Υ = 2δ/3H	E_s = 150 000(2.17-e)2/(1+e)(p'/p_{atm})^0 $^{.5}$(0.0001/Υ)$^{0.4}$	p'	L/H	k_{horz} = (4/π)E_s/(L/H)$^{0.6}$H	F_o = A_dΔTα$_c$$E_c$
m	°C	m		kN/m^2	kN/m^2	m/m	kN/m/m^2	kN
10,000	30,00	1,80E-03	4,00E-04	141 388,01	50,00	3,33	279 734,11	36 828,00
20,000	30,00	3,60E-03	8,00E-04	107 152,07	50,00	6,67	139 867,06	58 032,00
30,000	30,00	5,40E-03	1,20E-03	91 109,59	50,00	10,00	93 244,70	79 236,00

Bridge Span	ΔT	δ = ΔTα$_c$L	Υ = 2δ/3H	E_s = 150 000(2.17-e)2/(1+e)(p'/p_{atm})^0 $^{.5}$(0.0001/Υ)$^{0.4}$	p'	L/H	k_{horz} = (4/π)E_s/(L/H)$^{0.6}$H	F_o = A_dΔTα$_c$$E_c$
m	°C	m		kN/m^2	kN/m^2	m/m	kN/m/m^2	kN
10,000	30,00	1,80E-03	2,00E-04	186 562,60	50,00	1,67	279 734,11	36 828,00
20,000	30,00	3,60E-03	4,00E-04	141 388,01	50,00	3,33	139 867,06	58 032,00
30,000	30,00	5,40E-03	6,00E-04	120 219,82	50,00	5,00	93 244,70	79 236,00

Bridge Span	ΔT	δ = ΔTα$_c$L	Υ = 2δ/3H	E_s = 150 000(2.17-e)2/(1+e)(p'/p_{atm})^0 $^{.5}$(0.0001/Υ)$^{0.4}$	p'	L/H	k_{horz} = (4/π)E_s/(L/H)$^{0.6}$H	F_o = A_dΔTα$_c$$E_c$
m	°C	m		kN/m^2	kN/m^2	m/m	kN/m/m^2	kN
10,000	30,00	1,80E-03	1,33E-04	219 412,36	50,00	1,11	279 734,11	36 828,00
20,000	30,00	3,60E-03	2,67E-04	166 283,47	50,00	2,22	139 867,06	58 032,00
30,000	30,00	5,40E-03	4,00E-04	141 388,01	50,00	3,33	93 244,70	79 236,00

Table 3.8: Typical spring property input for the conventional spring bridge deck expansion model, as per O' Brien & Keogh (1999). Note that the abutment heights are 3m, 6m and 9m from top to bottom for the above three tables respectively

Bridge Span	ΔT	δ = ΔTα$_c$L	Υ = 2δ/3H	E_s = 150 000(2.17-e)2/(1+e)(p'/p_{atm})^0 $^{.5}$(0.0001/Υ)$^{0.4}$	r = E_s/EI_a	H_{eq} = 3.75/r$^{0.25}$	k_{sp} = EI_ar$^{0.75}$/8.5	F_o = A_dΔTα$_c$$E_c$
m	°C	m		kN/m^2	kN/m^2	m	kN/m	kN
10,000	30,00	1,80E-03	4,00E-04	133 066,33	0,67	4,14	166 069,11	36 828,00
20,000	30,00	3,60E-03	8,00E-04	148 371,13	0,09	6,78	303 055,57	58 032,00
30,000	30,00	5,40E-03	1,20E-03	166 627,21	0,03	8,93	448 113,57	79 236,00

Table 3.9: Typical spring property input for the equivalent spring at bridge deck expansion model, as per Lehane (1999)

Note that two kinds of springs are used in the 3D MIDAS Modelling (see **Figure *3.5*** and **Figure *3.6***):

1) Abutment springs (backfill soil is defined as compression-only springs). The theory for this is derived from the experiments and equations by Lehane (1999) and Broms (1971).

2) Pile springs are defined as symmetric nonlinear elastic springs for lateral springs (P-y curve theory for the lateral loading of piles is used for the calculation of the spring stiffnesses in this instance) whilst vertical springs are modelled as linear elastic.

The following **Table 3.10** is used for the MIDAS input for the soil spring properties. The information is derived from recommendations contained in CIRIA Report 103 as well as the recommendations in the paper by Bohnhoff (2014) and the textbook by Craig (1997).

The typical input for the Abutment and Pile springs is shown below (see **Figure *3.10***). Note that this information is repeated in a different format, in the model input tables of Appendix A, which show samples of the calculations (due to their size, not all the calculations have been included).

The theory used in regard to calculating the spring stiffnesses for the various 2D models is described earlier in this thesis, in Section 2.4.1 and Section 2.5.

	Coefficient of Subgrade Reaction (Kh)	Internal friction angle (φ)	Undrained Cohesion (Cu)	Earth Pressure Coefficient at rest (Ko)
	kN/m^3	Degrees	kN/m^2	
Loose Sand	2 000,0	30,0	N/A	0,60
Dense Sand	17 000,0	40,0	N/A	0,35
Soft Clay	15 000,0	N/A	50,0	0,60
Stiff Clay	30 000,0	N/A	100,0	0,42

Table 3.10: Soil properties used in MIDAS modelling for Spring property calculations – refer to CIRIA 103 (1984)

In terms of the 2D Prokon models that are used for examining the effects of live load and temperature loading on an integral bridge with a footing foundation, **Table 3.11** (taken from Hambly, 1991) provides the basis for the soil values that are used in the spring stiffness calculations.

Note that an Upper bound and a Lower bound material value has been used in some of the 2D Modelling. In practice, for a specific bridge design solution, one would consider both the Upper and the Lower bound values in order to draw conclusions about the worst-case forces to design for. This rationale has been included in these 2D models only, so as to provide an appreciation for the spread of results that is possible given the variance in material property (thus for interest only). This approach (using Upper and Lower bound material properties) and the additional effort required has not been included in the 3D Grillage modelling as we are not designing for a specific bridge solution here, and it would add a significant (and unnecessary) complexity in interpreting the graphs presented for the 3D models in Chapter 4.

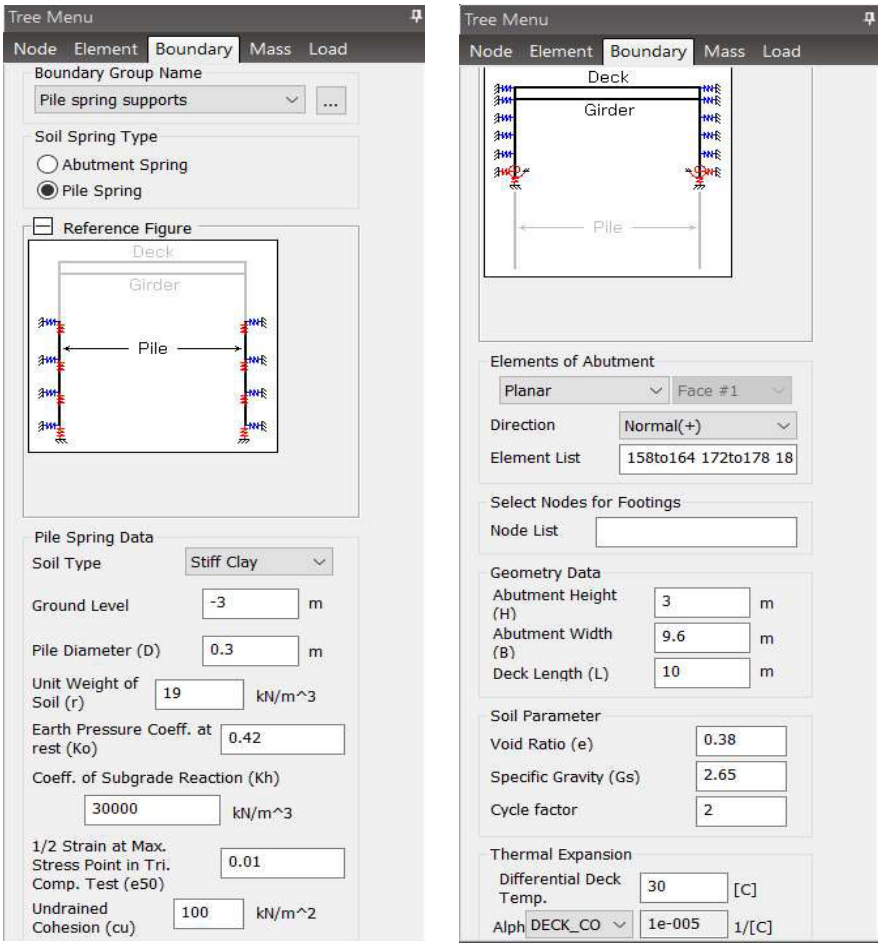

Figure *3.10*: Integral bridge Pile and Abutment spring information input

Ground conditions	Approximate Strength (kPa)	Young's Modulus (Lower bound) MPa	Young's Modulus (Upper bound) MPa
Soft clay	**50,0**	**20,0**	**60,0**
Stiff clay	**100,0**	**40,0**	**120,0**
Very stiff clay	**200,0**	**80,0**	**240,0**
Loose sand		**20,0**	**60,0**
Medium sand		**40,0**	**120,0**
Dense sand		**80,0**	**240,0**
Dense gravel		**160,0**	**480,0**

Table 3.11: Soil properties used in Prokon 2D modelling for Spring property calculations – refer to Hambly (1991)

3.6 Loading

The following parameters and variations of parameters were studied, with the focus on examining the effects on the maximum spring reactions in each instance:

1) Live load variability (for constant span)
2) Span variability (for constant live load)
3) Abutment height variability (for constant span)
4) Ground condition variability (for constant span). Note that this is the footing or pile founding condition, not the backfill condition, which remains constant.
5) Temperature variance effects (effective temperature and temperature gradient)

The basic loading scenarios that are investigated in this set of models are as follows:

- Live load (20% DL, 40% DL, 60% DL, 80% DL) – see example below in **Figure *3.11***.
- Temperature Max (+15ºC rise, from 20ºC ambient)
- Temperature Min (-15ºC drop, from 20ºC ambient)
- Temperature Gradient (in accordance with TMH7 Parts 1 &2 - Section 4.5.5, Figure 22 and Table 16). This loading has only been applied to selected models however.

Note that the temperature rise and fall of 15ºC (which adds up to a variance of 30ºC) was specifically chosen to simulate what happens in the field. This would be an average temperature variance over the course of the seasons that a bridge would be subjected to – it is not the maximum temperature difference, but is more realistic, as per the average sort of daily temperatures that a bridge would be subjected to.

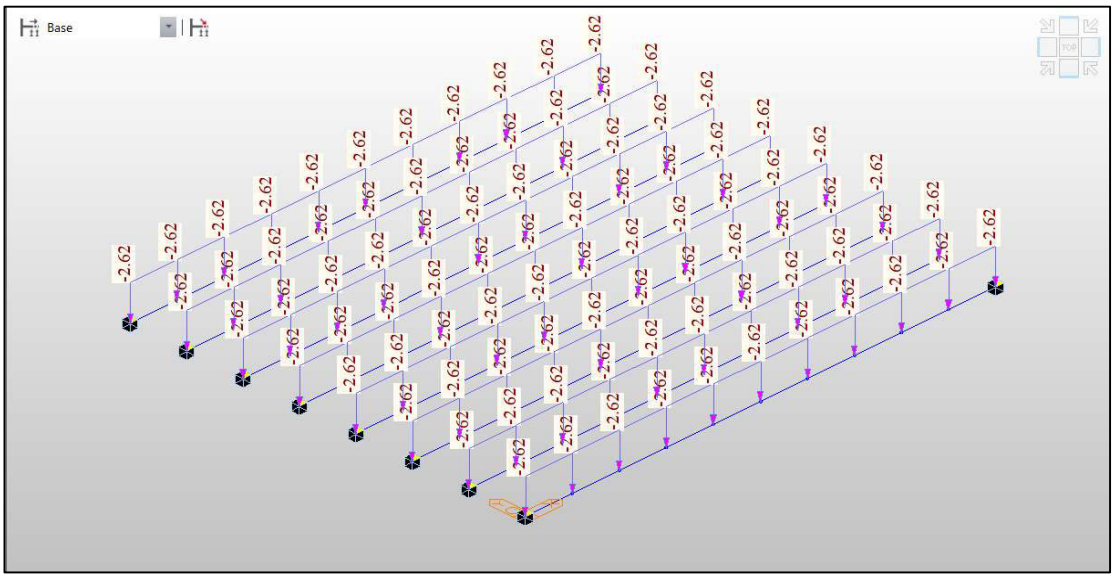

Figure *3.11*: MIDAS model Loading for 20% Live Load, 10m span bridge deck

Various %'s of live loading (% live load in relation to the Dead + Superimposed Dead Load) have been applied to the 3D grillage and 2D models that have been created. The calculations for these loads are shown in the sample spreadsheets in Appendix A. No specific code has been used in these parametric

models, line loads only have been used, which are applied only to the T-beams. Note that the total dead load calculation includes the loads from the following items:

- Beam and slab (DL)
- Asphalt (SDL)

The following figures give one an idea of how the loading has been applied to the various models, **Figure *3.11*** shows the line loads applied to the longitudinal beams of the 3D Grillage for the case of 20% Live load for a 10m span bridge deck.

Figure *3.12* and **Figure *3.13*** shows the maximum and minimum temperature loads applied to all the longitudinal beams of the 3D Grillage for a 10m span bridge deck with 3m high abutments.

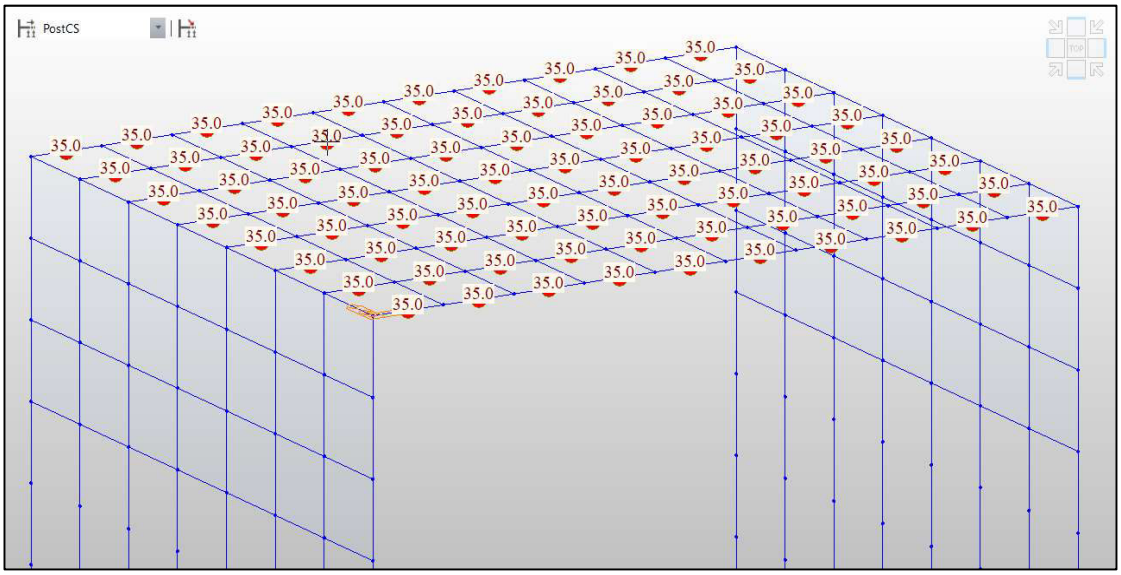

Figure *3.12*: MIDAS model Loading for 15° Temperature increase (from baseline temperature of 20°)

Figure 3.14 shows how the live load is applied across the span section in the 2D Frame models – the example shown is for the foundation stiffness model (Hambly, 1991).

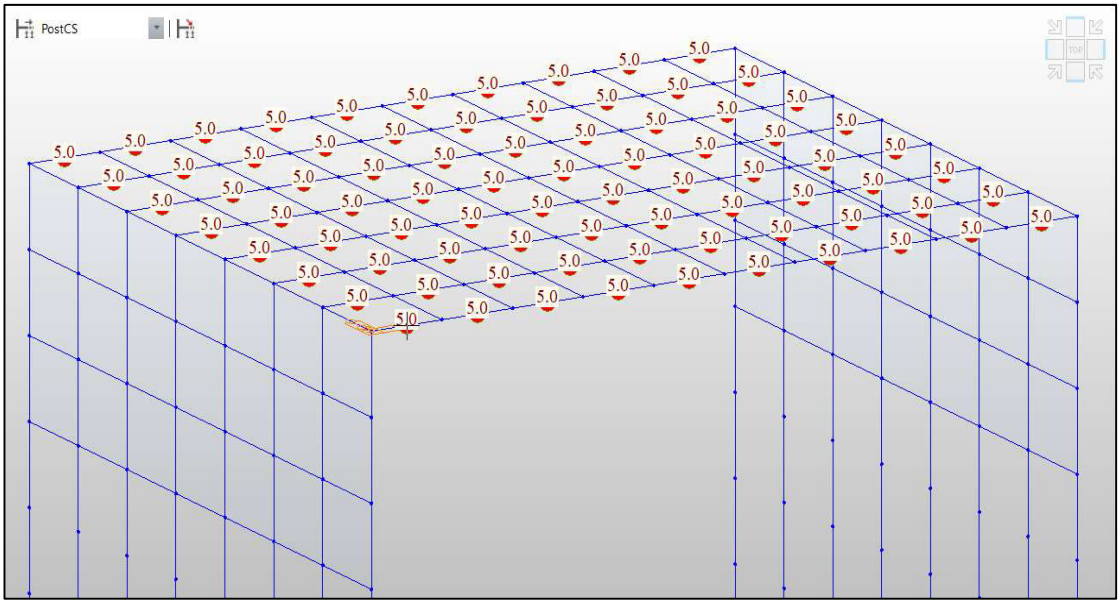

Figure *3.13*: MIDAS model Loading for 15° Temperature decrease (from baseline temperature of 20°)

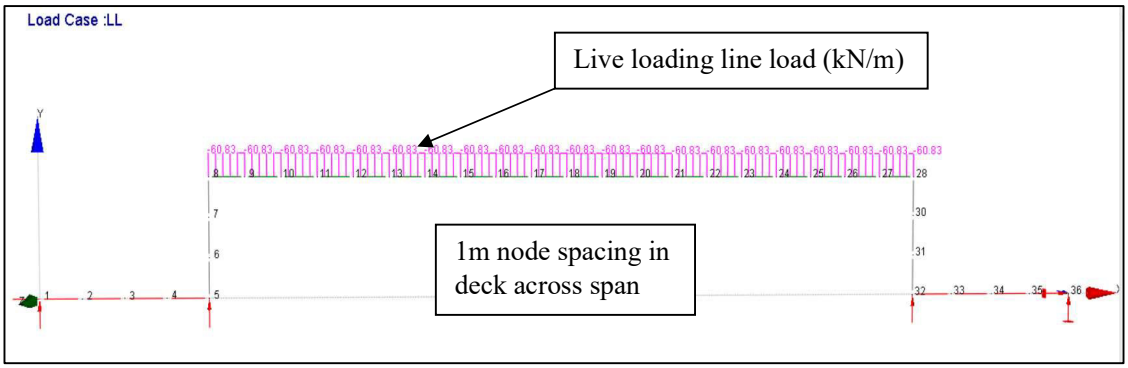

Figure *3.14*: Live loading for Model 5, Prokon Model

The bridge contraction and expansion models rely on a point load to be applied (see F_o in **Figure 2.20**, **Figure 2.24** and **Figure 2.26** to simulate the effect of the temperature related load increase or decrease (as the case may be). This point load is easily calculated as follows:

$$F_o = A_d.\Delta T.\alpha_c.E_c \qquad \text{(Eqn. 60)}$$

Where:

F_o = temperature force induced in the structure, and applied to frame

A_d = area of deck section

α_c = Expansion coefficient for concrete

E_c = Young's modulus of the beam section (concrete in this instance)

ΔT = Change in deck temperature

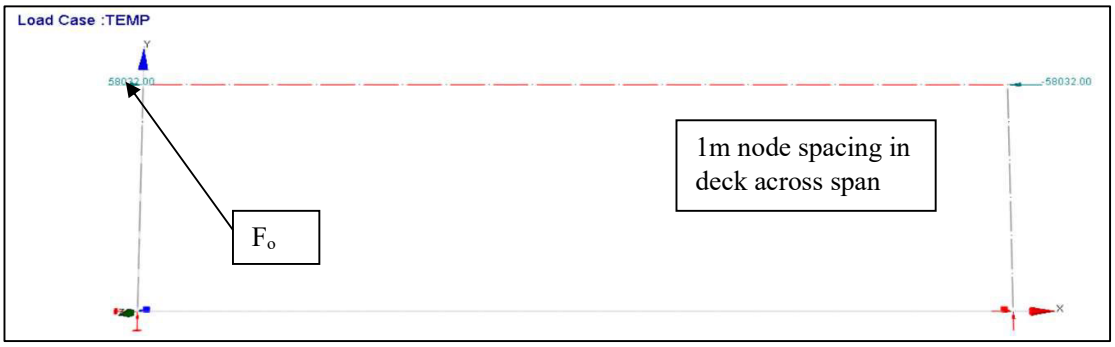

Figure *3.15*: Temperature contraction loading on flexible supports for Model 71 (Dobry & Gazetas, 1986) Prokon Model

Figure *3.15* and **Figure *3.16*** show the frame models with their temperature induced point load forces applied to their ends.

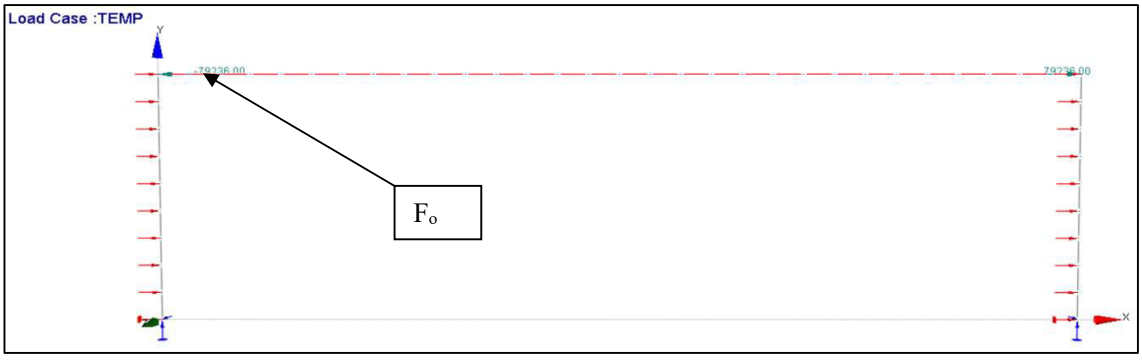

Figure *3.16*: Temperature expansion loading for Model 84, conventional spring model, (O' Brien & Keogh, 1999) Prokon Model

The temperature gradient loadcase simulates the effect that the difference in temperature between the deck soffit and the top of the deck surface has on the structure and on the deck in particular. A gradient loading condition known as a positive temperature gradient is applied to account for the warmer summer environmental conditions that the bridge structure will be subjected to. The negative temperature gradient condition is therefore applied as a loadcase to account for the cooler winter months, where the deck is often subjected to sub-zero temperatures. Due to the amount of input required, the temperature gradient loadcase has been applied to only a limited number of models in this thesis. The temperatures for the deck cross section are obtained from TMH7 Parts 1 &2 - Section 4.5.5, Figure 22 and Table 16.

This information has been used to produce the temperature points table shown in **Table 3.12** which accounts for both the positive and the negative temperature gradients applied to the deck section.

	SPAN	10,000	20,000	30,000	40,000	m
	Beam depth, H	0,475	0,950	1,425	1,900	m
	Slab depth	0,250	0,250	0,250	0,250	m
	Beam depth	0,225	0,700	1,175	1,650	m
	Beam width	0,500	0,500	0,500	0,500	m
	Slab width	1,200	1,200	1,200	1,200	m
	+ve temp gradient (°C)					
h1	0,3H	0,143	0,285	0,428	0,570	m
h2	0,3H	0,143	0,285	0,428	0,570	m
h3	0,3H	0,143	0,285	0,428	0,570	m
	T1	17,2	17,8	17,8	17,8	°C
	T2	4,6	4,0	4,0	4,0	°C
	T3	1,4	2,1	2,1	2,1	°C
	-ve temp gradient (°C)					
h1	0,2H	0,095	0,190	0,285	0,380	m
h2	0,25H	0,119	0,238	0,356	0,475	m
h3	0,2H	0,095	0,190	0,285	0,380	m
h4	0,25H	0,119	0,238	0,356	0,475	m
	T1	6,4	10,3	10,6	10,6	°C
	T2	2,3	2,1	0,7	0,7	°C
	T3	0,6	1,2	0,8	0,8	°C
	T4	3,2	6,3	6,6	6,6	°C

Table 3.12: Temperature gradient points and depths for positive and negative temperature gradients (refer to TMH7 Parts 1&2, Section 4.5.5)

Figure 22, from TMH7 Parts 1 &2 is reproduced here in **Figure *3.17*** to give an idea of what the deck temperature profile looks like for the two gradient conditions, as well as the values of certain temperature profile points.

3.7 Loading combinations and loadcases

No loading combinations as per any particular code have been used in general, in the parametric modelling that has been done in this thesis. Dead Loads and Live loads are parametrically varied between the various models and have been considered individually so that their effects may be uniquely understood. Temperature expansion and contraction as well as positive and negative gradient loadings, are also considered individually and have not (in this study) been combined with other load cases.

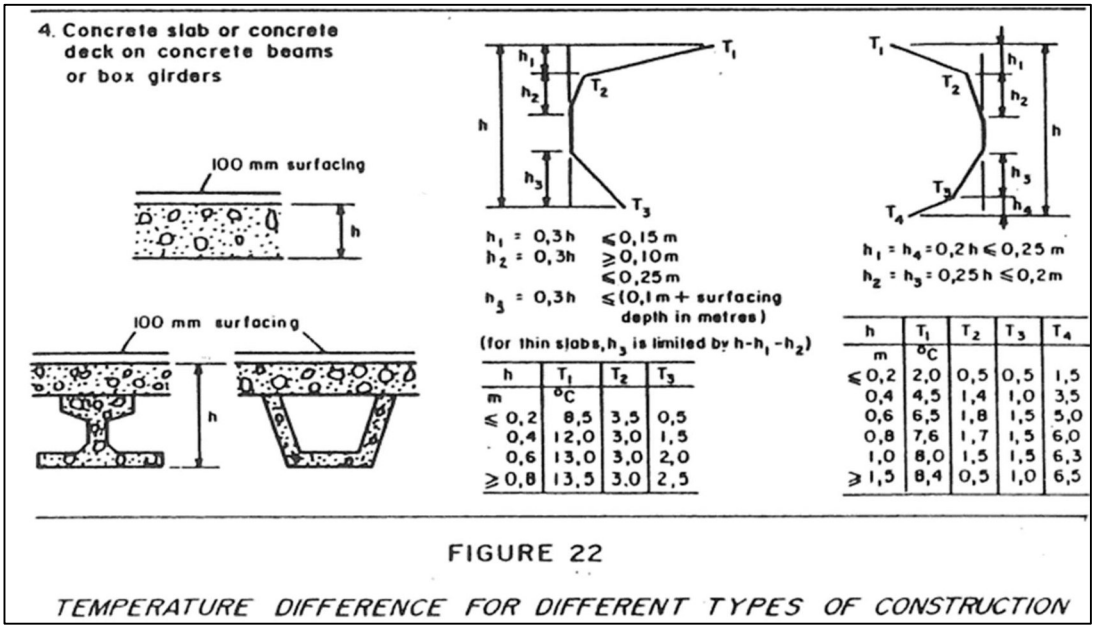

h m	T1 °C	T2	T3
≤ 0,2	8,5	3,5	0,5
0,4	12,0	3,0	1,5
0,6	13,0	3,0	2,0
≥ 0,8	13,5	3,0	2,5

h m	T1 °C	T2	T3	T4
≤ 0,2	2,0	0,5	0,5	1,5
0,4	4,5	1,4	1,0	3,5
0,6	6,5	1,8	1,5	5,0
0,8	7,6	1,7	1,5	6,0
1,0	8,0	1,5	1,5	6,3
≥ 1,5	8,4	0,5	1,0	6,5

FIGURE 22

TEMPERATURE DIFFERENCE FOR DIFFERENT TYPES OF CONSTRUCTION

Figure *3.17*: Temperature gradient loading with positive and negative temperature gradients

The only applied loading that has been derived from any code of practice is the temperature gradient loadcase, which has used the South African TMH7 Code as the basis for creating the positive and the negative temperature gradient profiles at different points across the deck profile. This loadcase is not applied in combination with any other loadcases however, since we are only interested in this thesis in studying the effects of raw load cases. Note that in the TMH7 Code, the temperature gradient load may be combined with the temperature expansion / contraction loadcase in certain circumstances (see Combination 2 and 3 of Table 17 of TMH 7, Parts 1&2).

3.8 Integral bridge theory used in MIDAS software

3.8.1 Abutment Springs

As stated above, the backfill soil is defined as compression-only springs. This type of spring is created once assigned from the spring definition environment shown in **Figure *3.10***.

Expansion and contraction of the integral bridge deck affects the backfill soil adjacent to the abutments. Backfill compaction due to deck expansion and soil slide due to deck contraction are continually repeated over time. Due to the repeated cycles of backfill compaction and soil slide, the modulus of subgrade reaction and the pressure distribution of backfill will tend to vary with depth, and over time. Note that the equation for the Young's Modulus depends on the confining stress p' which depends on the abutment height.

A Cycle is the period from a deck expansion to a deck contraction. If cycles are repeated infinitely, the modulus of subgrade reaction of backfill becomes constant. Using the formulation proposed by B.M. Lehane (1999) and Broms (1971), soil springs can be assigned which account for this effect (equation

No.61). According to Broms (1971), the lateral stress-displacement relationship for the abutment backfill of an Integral Bridge will not behave exactly as modelled – the diagram in **Figure *3.19*** illustrates this concept. To account for this characteristic of the soil, lateral abutment springs are modelled as compression-only springs and vertical springs are modelled as linear elastic springs for the bridge Abutments. The following Equations (61 - 64) have been used by MIDAS to calculate the abutment spring stiffnesses:

$$K_s = \left(\frac{3.5G_{eq}}{H\sqrt{(\frac{B}{H})}}\right) \quad \text{(Eqn. 61)}$$

$$G_{eq} = p_{atm}.600.f_{cyc}.F(e).\left(\frac{p'}{p_{atm}}\right)^{0.5}.\left(2.5\,H.\frac{0.0001}{\Delta}\right)^{0.5} \quad \text{(Eqn. 62)}$$

$$F(e) = \left(\frac{2.17-e}{1+e}\right)^2 \quad \text{(Eqn. 63)}$$

$$\Delta = \left(\frac{\alpha\,.\Delta T\,.L}{2}\right) \quad \text{(Eqn. 64)}$$

Where:

K_s = Stiffness per unit area

f_{cyc} = Cycle factor

L = Deck length

B = Abutment width

H = Abutment height

ΔT = Change in effective deck temperature

The other variables in the above equations (61 to 64) that are not defined above are already defined in Equation 53 and 54 previously. One important item to note from the above equations is that the spring stiffness per unit area depends on the deck length (an inverse relationship exists).

3.8.2 Pile Springs

Springs for the soil adjacent to the piles are assigned using the MIDAS Integral spring assignment function, as per the input requirements shown in **Figure *3.10***, however the theory is quite different from the theory used for the abutment springs (refer to Section 2.5.6). The pile springs are modelled as symmetric nonlinear elastic springs (see **Figure *3.18*** for a diagram of the non-linear behaviour associated with the assigned pile functions) and vertical springs for the soils adjacent to piles are modelled as linear elastic springs. The Force-Deformation Function as seen in **Figure *3.18***, is the manner in which MIDAS accounts for the hysteresis characteristics of a multi-linear hysteresis stiffness spring. The underlying P-Y type behaviour of the pile (as seen in **Figure 2.14**) is distinctly non-linear in nature and this must be borne in mind when interpreting pile spring reaction results.

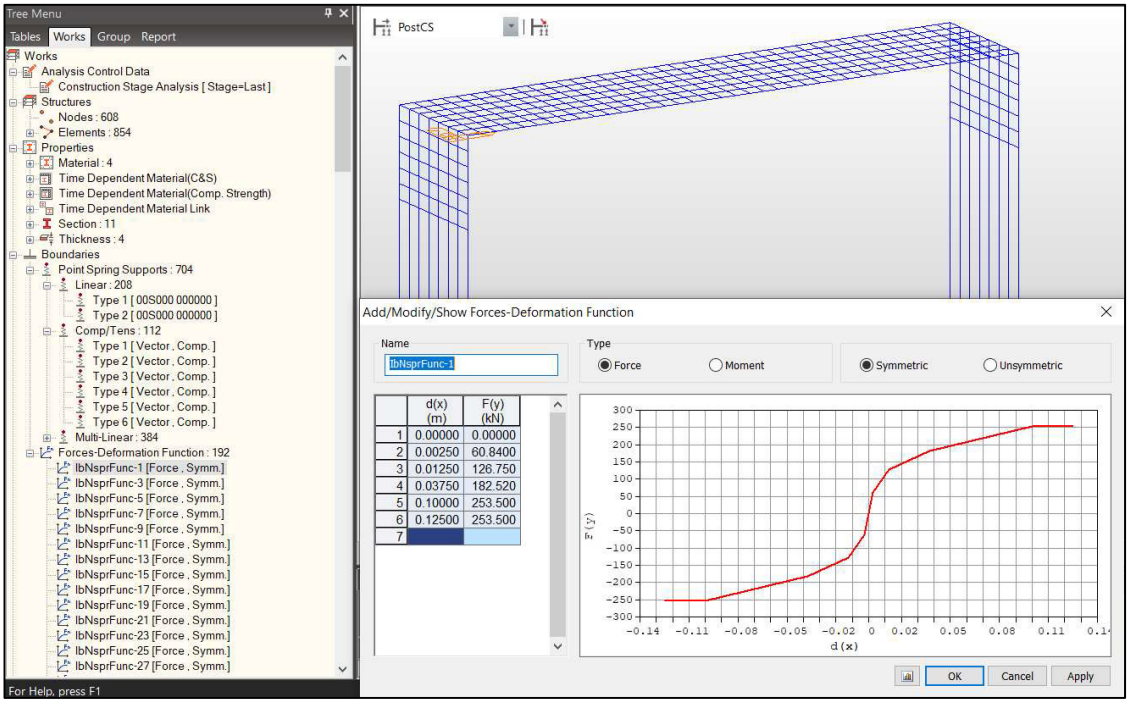

Figure *3.18*: Non-linear force-deformation P-Y function used for pile springs definition

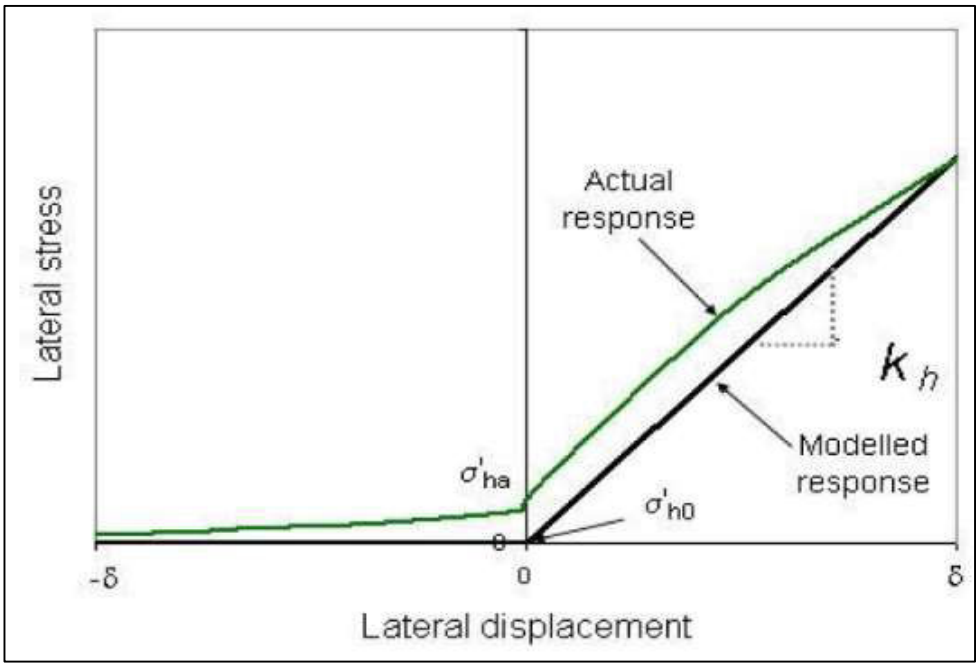

Figure *3.19*: Lateral stress vs displacement (Broms 1971), note how the actual response differs from the modelled response for varying directions of lateral displacement of an abutment

3.9 Model Tables

A sample list of the model details used in the parametric study is found in Appendix A and B. These tables describe the results from the study, as well as the grouped properties of the models.

3.10 Limitations of the modelling simulations

The following summary describes the limitations of the analysis and modelling procedures that were followed in this thesis - these should be born in mind in regards the interpretation of the results.

1) The effects of live load and temperature only were investigated. The effects of post-tensioning of the slab and beams were not considered.
2) The spans considered were limited up to 40m. It is unclear how the results would change when considering the effects of super long spans, such as have been constructed in Germany (500m +) (Marx, 2011). These lengths of bridge would of course involve the use of intermediate piers.
3) The graphs that are shown in the following chapter are quite coarse (only 3 – 4 points have been used to draw each of the curves) and can be further refined in order to adequately develop equations that describe them.
4) Only single span bridges were considered, the characteristics of springs for multi-span bridges were not considered.
5) Concrete bridges only were considered, the effects of steel composite construction were not investigated.
6) Combinations of loading were not considered – eg. (Dead load + Temperature) loading was not considered as a load case since the aim was to examine the 'raw loading' characteristics and effects. Parametrically varied ratios of Live load (derived from the dead load calculation) were however considered, but Dead load effects were not reported on (but certainly could be).
7) The variance of the deck width was not investigated. As can be seen in **Figure 4.2** (for example), the abutment spring reactions are not uniform across the abutment, they tend to vary with height and across the width of the abutment. The same can be said for the pile reactions.
8) The presence of Wing walls was not included in any of the analysis models (and these are not always present in practice). This modelling approach matches what is often done in practice, with the wing walls being considered as separate structures. As has been mentioned previously, it is however more accurate to include the wing wall effects in the analysis.
9) Approach slabs have not been included in the modelling due to the variance in their design and the limited impact that including them would have. Note however that despite the fact that they are used commonly in South Africa, they are in fact banned in certain countries in Europe.
10) The variance of abutment backfill properties was not considered in the MIDAS modelling – a standard crushed gravel backfill has been used in all the MIDAS analysis models, with the variance in soil properties being found only in the pile boundary conditions. Variance in backfill and founding condition properties was however used in the 2D Prokon models due to the positions of the springs. Note that it is not usually practical however to use clay backfill for an integral bridge, due to the difficulty with installing such material.
11) The effects of the variance of pile size were not investigated in these models.
12) The footing foundation condition (as opposed to the piled foundation condition) was examined only in the 2D analysis, and not in the 3D MIDAS modelling. No footings were modelled in the 3D MIDAS modelling, and conversely no piled foundation integral bridges were modelled in the 2D modelling.
13) The springs relevant to semi-integral bridges have not been researched in this thesis.

14) The use of a pin type joints between the Abutment pilecap and the piles was not investigated.
15) The use of sleeved piles – although discussed in the Literature review, was not taken further in the modelling process.
16) The effect of angle of bridge skew was not investigated in this thesis.
17) Usually when designing an integral bridge, one would consider using two models for the same bridge – one with an upper bound and one with a lower bound set of soil properties, in order to examine the sensitivity of the results. This was only done in this research in the 2D Prokon models. The purpose of including the upper bound and lower bound properties in the 2D models was simply to give the reader an idea of how these properties can change results. If one was doing a design for a particular bridge, then it would always be recommended to use the upper bound/lower bound approach.
18) There are various vehicle loading models in existence from recognized codes of bridge design practice (eg. BS Codes, Eurocodes, AASHTO and TMH7). These loading models include point loads arranged in geometric axle layouts (eg. NB loading from TMH7) that simulate the loading effects of a (usually) generously loaded truck or extra-heavy vehicle moving over a bridge span. The live loading selected for use in the models in this thesis was a simple line load w (kN/m), which most codes also incorporate into their loading strategy in one way or another. The reason for doing this was mostly to ensure a simple understanding between the applied load and the DL + SDL, by relating this to a percentage basis for the live loading. One could in future conduct a similar set of model testing using specific codes of practice for the loading simulations.

4 CHAPTER 4 - Analysis results and discussion

The results of the analysis of the various spring models are fully detailed in Appendix C. Some typical reaction diagrams for various load cases are shown below for the 3D MIDAS models and the 2D Hambly type model.

Note that the results that are recorded in Appendix C are for the highest reaction value found in each load case. The tables also document the position of the start of the reactions (relative to the top of the abutment of pile, as the case may be), as well as the position of any points of contraflexure within the element (abutment or pile).

Finally, the magnitude of the maximum spring reaction is also compared with the total live load acting on an abutment face or a pile - as the case may be. This value is expressed as a percentage of the applied load in the table of results.

4.1 Typical Reactions diagrams (MIDAS and PROKON)

The diagrams below show the typical distribution of spring reactions that were noted in the analysis of the models that were setup. The spring results show how the spring reactions vary in their direction down the pile (and get smaller) as the pile has many points of reversed bending and contraflexure.

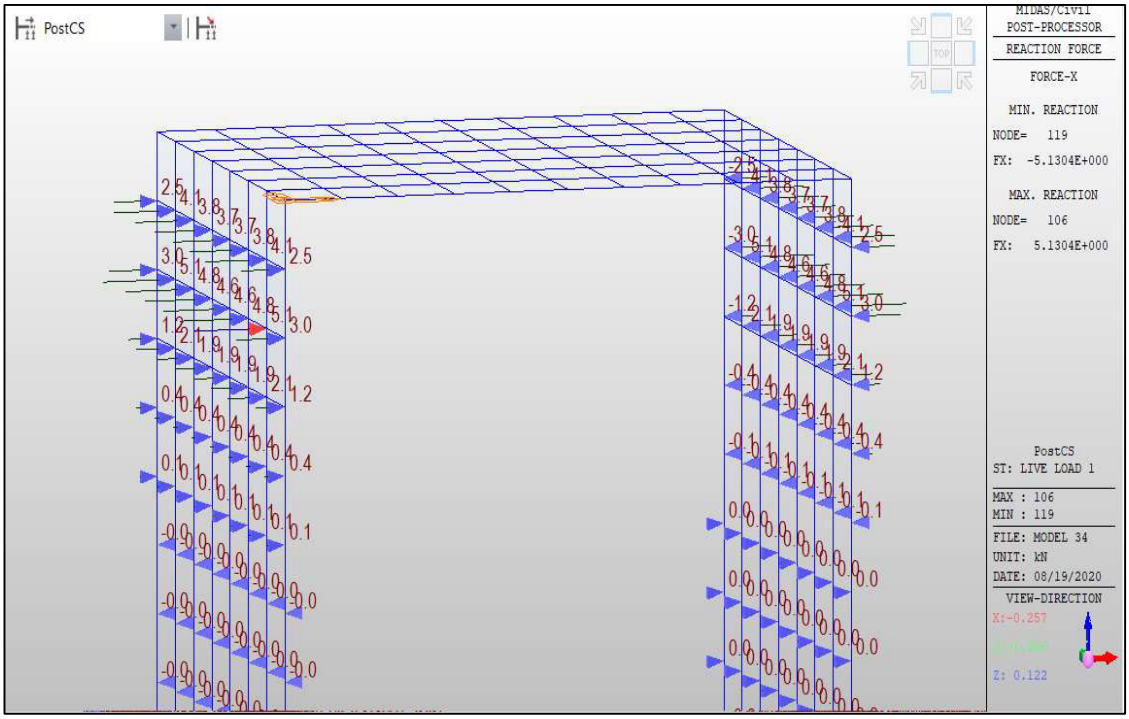

Figure *4.1*: Model 34 reactions (20% LL), 3m high abutment in stiff clay

The above diagram (**Figure *4.1***) shows how the spring reactions can vary considerably across the piles (as the pile experiences contraflexure down its shaft) as well as across the abutment face.

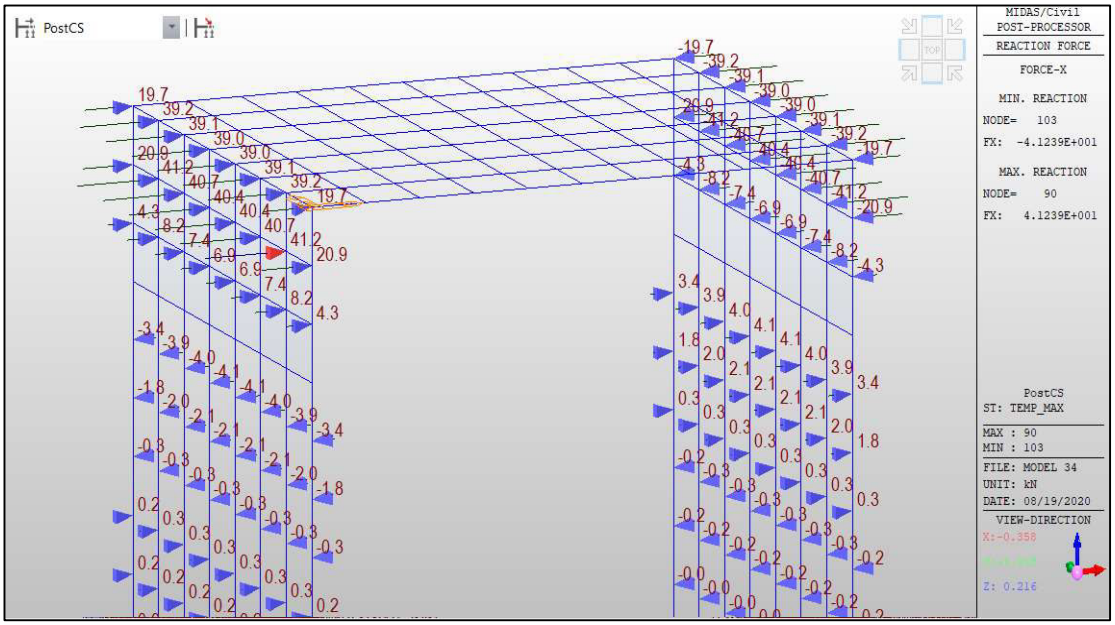

Figure *4.2*: Model 94 reactions (+15^{O}C Temp)

The above **Figure 4.2** shows how certain springs are activated across the abutment in accordance with the rotations developed in the structure. Reactions for a 2D Prokon type model are shown below in **Figure 4.3**, highlighting the simplicity in the 2D approach vs the 3D Grillage model approach.

Figure *4.3*: 2D Hambly type shallow strip foundation stiffness model reactions

4.2 Discussion of results

Below follows a discussion and presentation of the test results from the modelling that was undertaken. First, the results of the 2D models are examined and then the 3D models are discussed. Following this, the ratios of abutment to pile spring reactions are presented and then some correlation with pile and abutment bending moments and lateral deflections is presented and discussed. Lastly, some testing was done using shorter piles (6m in length), to understand what would the effects be on the spring reactions – these results are presented towards the end of the section.

The graphs below from **Figure 4.4** to **Figure 4.6** are for the Prokon models (bridge on footings), where Upper Bound and Lower bound values were used for each model (to test for sensitivity in results). These graphs essentially demonstrate a linear progression in the spring reactions.

The graph of spring reaction development with span is significant since it either indicates that the spring value is plateauing (to a fixed value), or it suggests that the spring value is still increasing with span (or load). The model test results have shown that different soil and geometric configurations will result in differing rates of increase for the spring reactions. The following points may be noted from the graphs that have been produced:

4.2.1 2D Model results – Foundation Stiffness (Hambly, 1991)

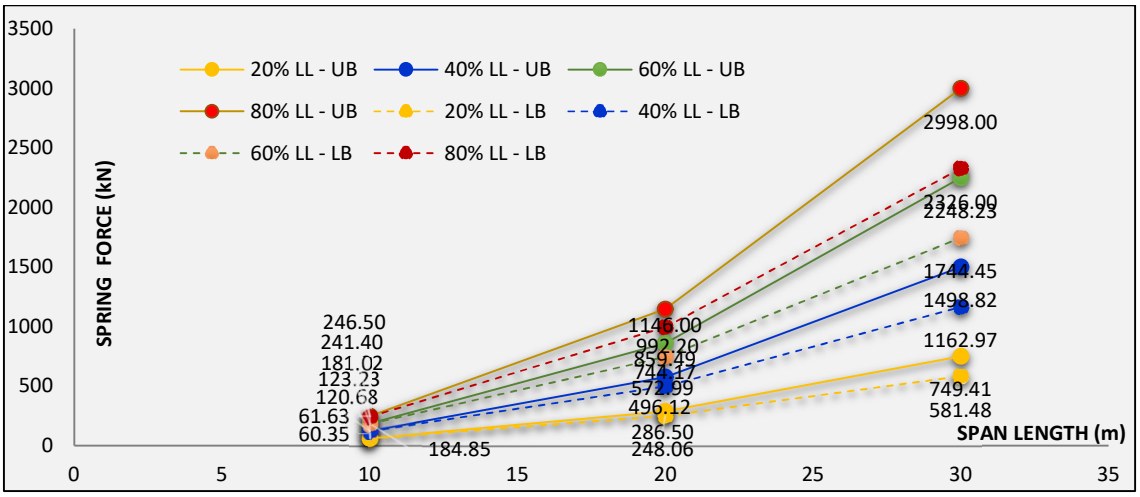

Figure *4.4*: Upper and Lower bound maximum horizontal spring reactions for Span vs Live load percentage in Very Stiff clay (2D Foundation Stiffness Model)

In regards to **Figure 4.4**, **Figure 4.5**, **Figure 4.6**, **Figure 4.11** and **Figure 4.12**, the results have shown an approximately linear progression of live load spring reaction as the deck live loading is increased. It is noticeable from the graphs for the 2D models that as the span length increases from 20m onwards, the increase in spring reaction forces are more pronounced as the span increases. The graphs also demonstrate that the rate of increase of the spring reaction grows larger with increased live load. This type of behaviour has similarly been demonstrated and verified in the 2D models (eg **Figure 4.4**) as well as the 3D model (eg. **Figure 4.12**) results. The implication for designers would be to be more

aware of the effects on the structural system of very-high live loading, which may produce the yielding of the soil springs, leading to non-linear behaviour and excessive backfill strains. Sustained super-heavy loads for example, could cause damage to the integral bridge backfill in such situations.

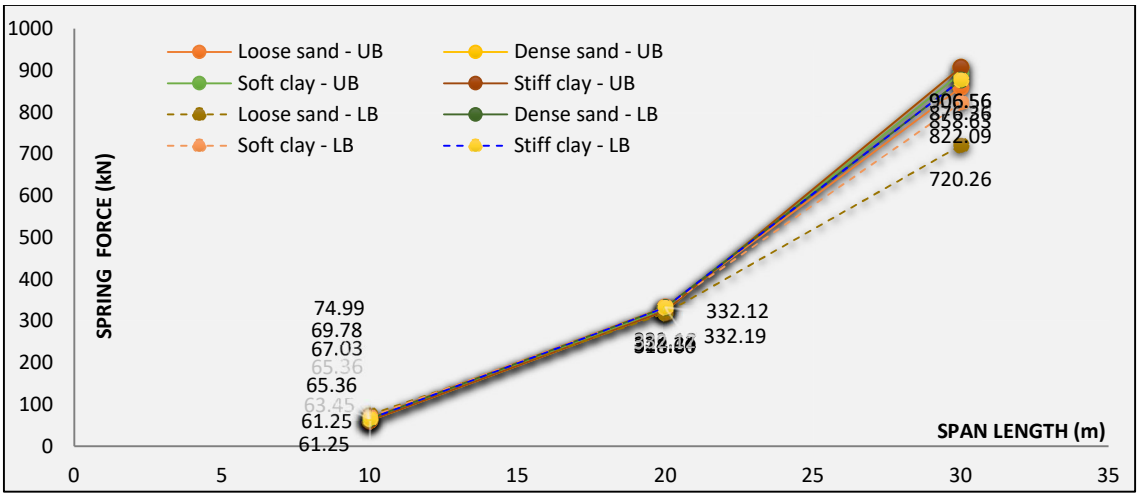

Figure *4.5*: Upper and Lower bound maximum horizontal spring reactions for Span vs Soil condition (40% Live loading, 2D Foundation Stiffness Model)

The graph above shows that the effect of soil type only begins to play a role after the 20m span has been exceeded, for the 2D Modelling using elastic spring supports.

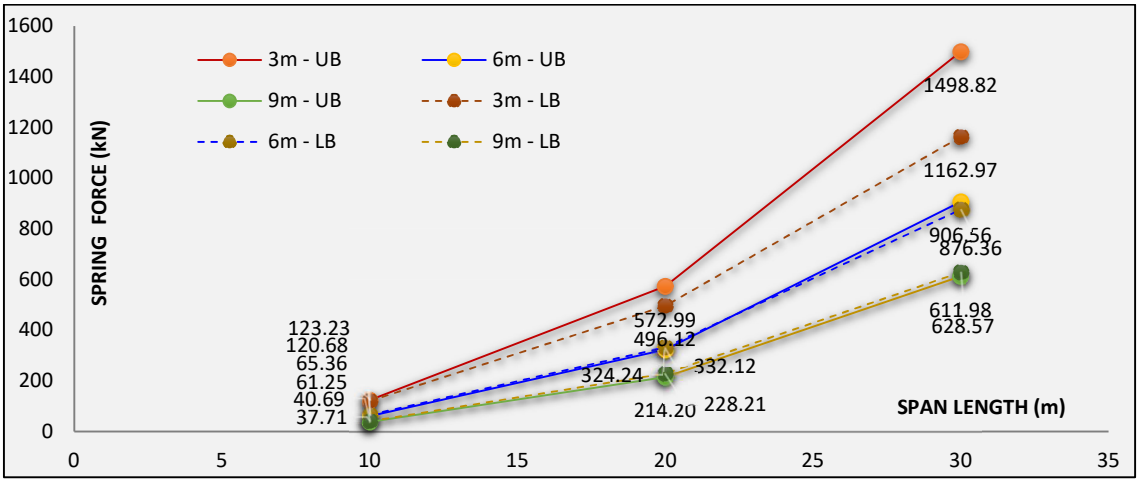

Figure *4.6*: Upper and Lower bound maximum horizontal spring reactions for Span vs Abutment height in Very Stiff clay (40% Live loading, 2D Foundation Stiffness Model)

4.2.2 2D Model results – Contraction on flexible supports (Dobry and Gazetas, 1986)

The graphs below from **Figure 4.7** to **Figure 4.9** are for the 2D Flexible Support Prokon models (bridge on footings).

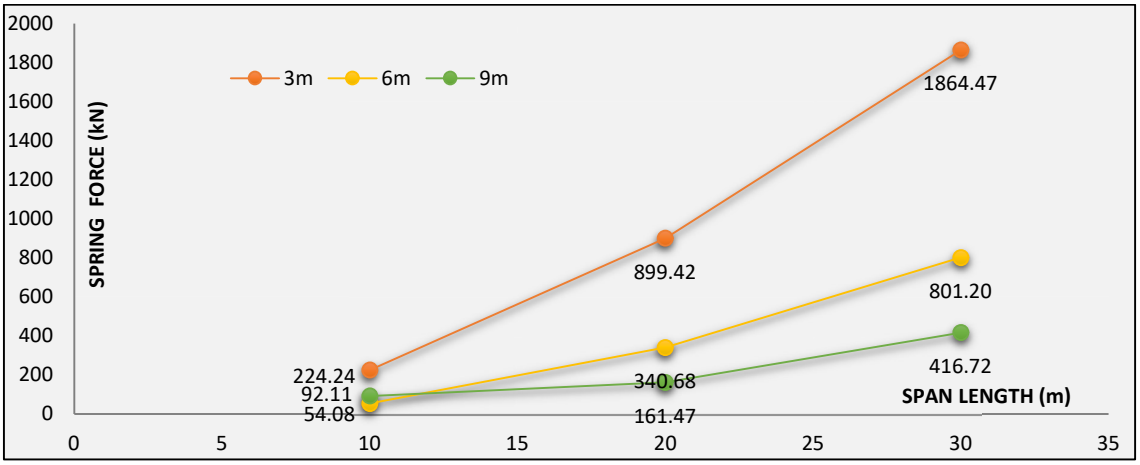

Figure *4.7*: Abutment Horizontal Spring reactions for Span vs Abutment Height with 30° contraction, 2D Model

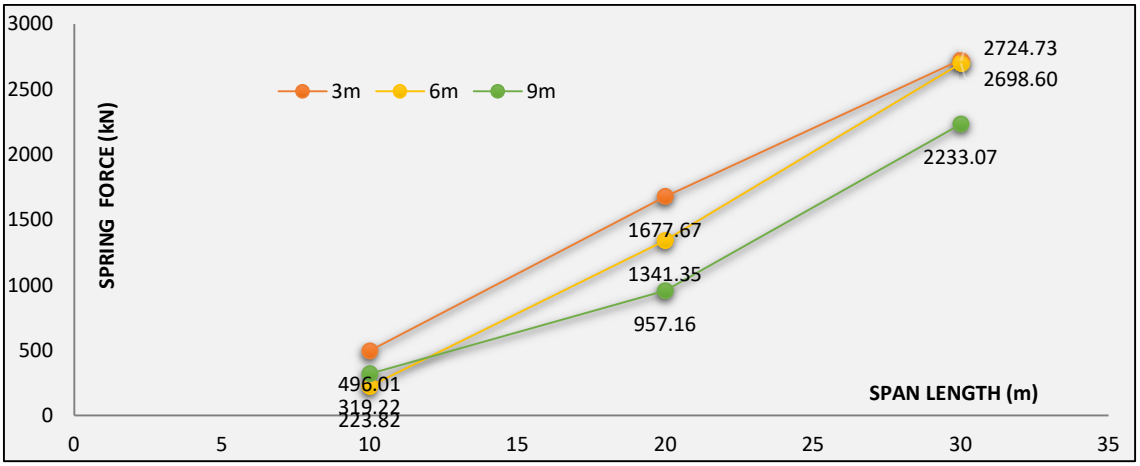

Figure *4.8*: Abutment Torsional Spring reactions for Span vs Abutment Height with 30° contraction, 2D Model

4.2.3 2D Model results – Deck expansion conventional spring model (O' Brien & Keogh, 1999)

In regards to the above plots in **Figure *4.7***, **Figure *4.8*** and **Figure *4.9***, these plots are for the 2D Flexible supports model, with a contraction and an expansion, and the plots show a mostly linear progression in

spring reaction force with increasing span. Only 10m to 30m spans were considered in this analysis section. The **Figure *4.9*** graph below shows that the 9m abutment initially has lower reactions – this would mostly be due to the increased flexibility of the higher abutment. Note also that **Table 3.8** shows a higher spring stiffness for the higher abutment, yet the spring reaction for the 9m abutment is not the highest for the smaller span of 10m. The spring stiffness has been calculated using the formulas shown in Equation 34. The net effect of spring stiffness and abutment flexibility is that the springs for the 9m high abutment do not initially (for smaller spans) attract as much force as the shorter abutments do.

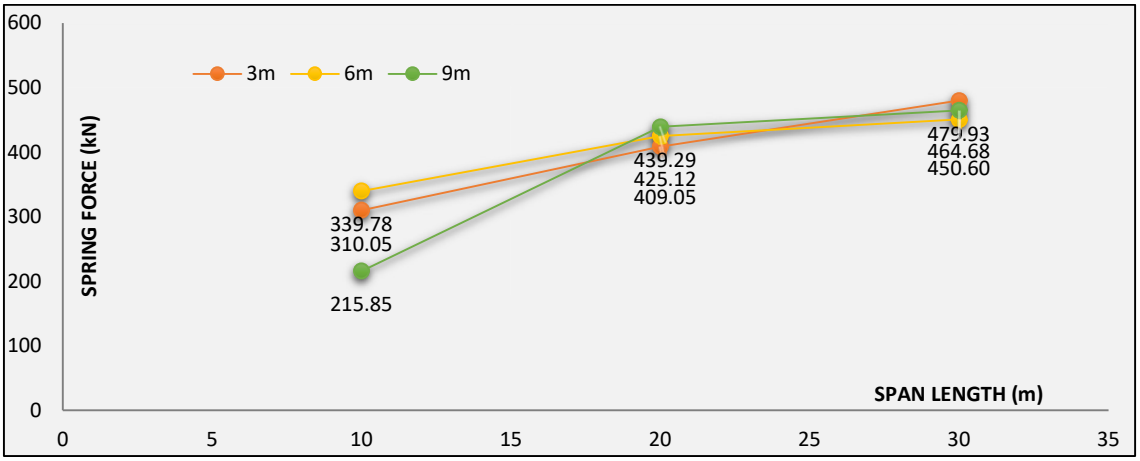

Figure *4.9*: Abutment Horizontal Spring reactions for Span vs Abutment Height with 30° expansion, 2D Model

4.2.4 2D Model results – Deck expansion equivalent spring at deck level model (Lehane, 1999)

The graph below for **Figure 4.10** is for the 2D Equivalent Spring Prokon models (bridge on footings). As can be seen from the graph, the progression of the spring reactions with increasing span is mostly linear in nature as the span increases.

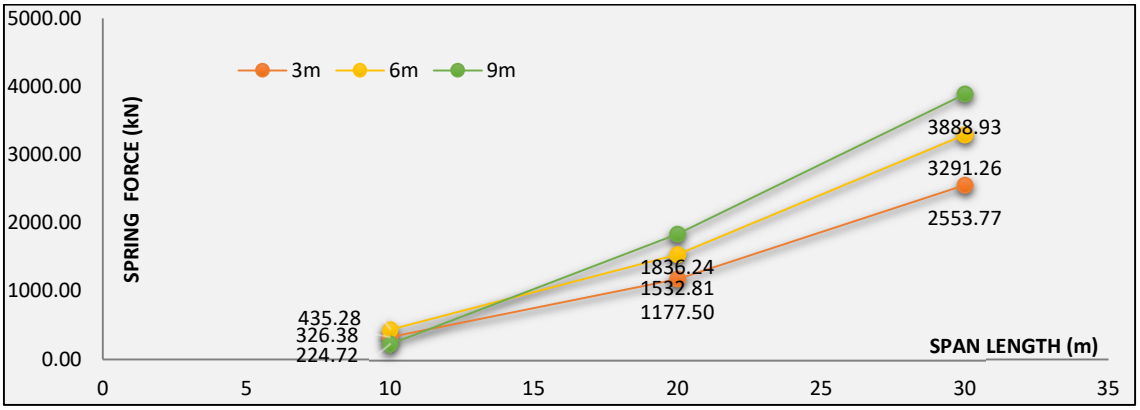

Figure *4.10*: Equivalent Horizontal Spring reactions for Span vs Abutment Height, 20% Live Load

4.2.5 3D Grillage Model results

Figure 4.11 and **Figure 4.12** show spring reaction plots for increases in live load vs span (and see also

Figure 4.25), for a constant abutment height of 3m, and in stiff clay. The two plots are very similar in nature and demonstrate a similar linear progression in spring reaction force. The implications of this are discussed below.

The graphs below from **Figure 4.11** to **Figure 4.16** are for the 3D MIDAS models (bridge on piles).

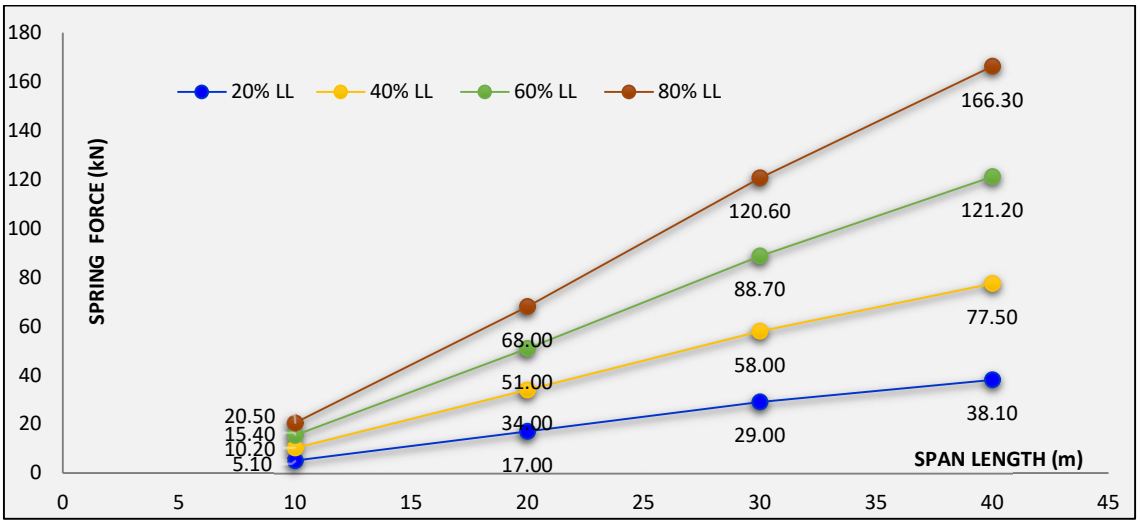

Figure *4.11*: Abutment spring maximum reactions for Span vs Live load percentage. 3m high abutments in Stiff clay founding conditions (3D Grillage model)

The graph shown in **Figure 4.13** (variable abutment height vs span length, in stiff clay) is of interest as it shows three very different reaction development plots. This graph shows that the 3m and the 6m curves tends to increase at (different rates), whilst the 9m curve appears that it has a parabolic type of shape ($y = kx^2$). Longer span lengths could be investigated to determine what the extent of the curve for the 9m high abutment looks like. Although the graph for the 6m high abutment shows an ever-increasing spring reaction with increases in span, it is more likely than not that the curve will plateau to a fixed value. This could be investigated further, by using larger span models.

The results shown in **Figure 4.14** again show how the pile spring reactions progress from a linear type of curve ($y = ax + b$) towards a more parabolic / asymptotic shaped, non-linear curve ($y = kx^2$) when going from the 3m high abutment to the 9m high abutment. This is explained by the fact that the piles will take progressively less load (with the abutments resisting more load), the higher the abutments are made, but also by the non-linear behaviour of the piles, under lateral loading (refer to Section 2.3.3, **Figure 2.14** and **Figure 2.15**). It is of course not common practice to routinely build 9m high abutments. The implications of **Figure 4.13**, **Figure 4.14** and **Figure 4.26** have already been discussed above.

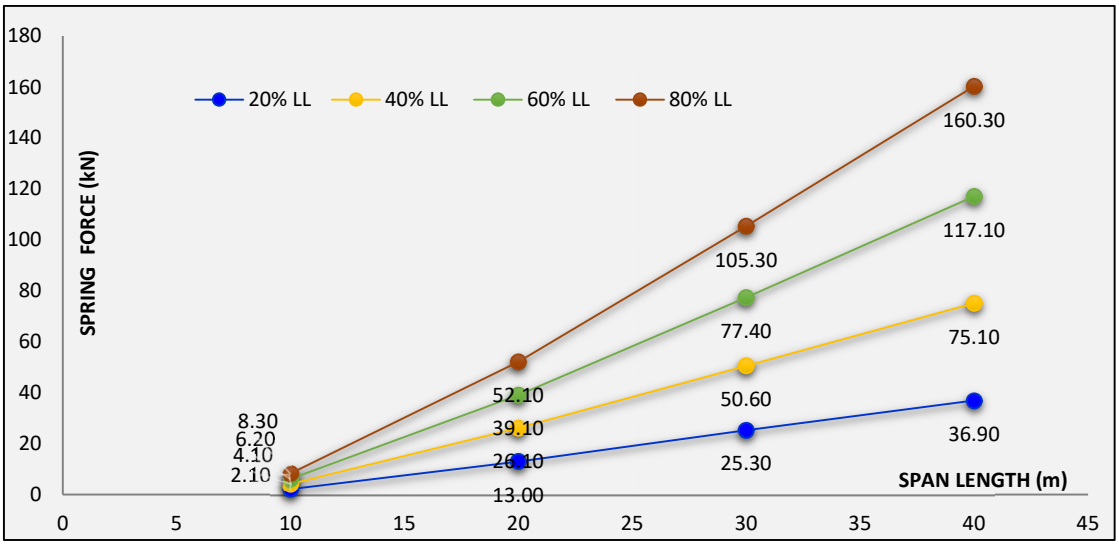

Figure *4.12*: Pile spring maximum reactions for Span vs Live load percentage, 3m high abutments in Stiff clay founding conditions (3D Grillage model)

Spring reaction plots that are shallow in their gradient (as an example, see the pile spring reactions for the 9m high abutments in **Figure 4.14**) do not reach yielding of the springs as 'quickly' as steep gradient line reaction plots such as the pile spring reactions for the 3m high abutment in **Figure 4.14**.

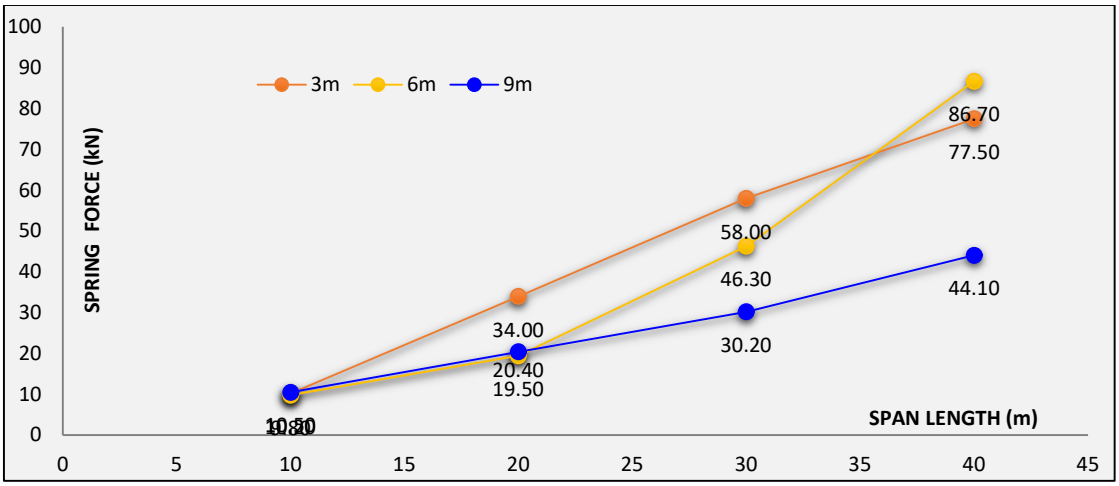

Figure *4.13*: Abutment Spring reactions for Span vs Abutment Height, stiff clay founding conditions (40% Live load, 3D Grillage model)

An important effect to be aware of in considering all the graphs that have been produced is that as the abutment height is increased, the distance between the centre of the deck and the centre of the backfill reaction force would tend to increase (refer to **Figure 2.49**). Since the two forces are in opposition to each other, a force couple (applied moment) is induced into the abutment/deck system. The effects of this are complex since it involves the interaction of the backfill friction with the abutment, additional bending on the abutment wall, as well as strain ratcheting effects and the spring reactions.

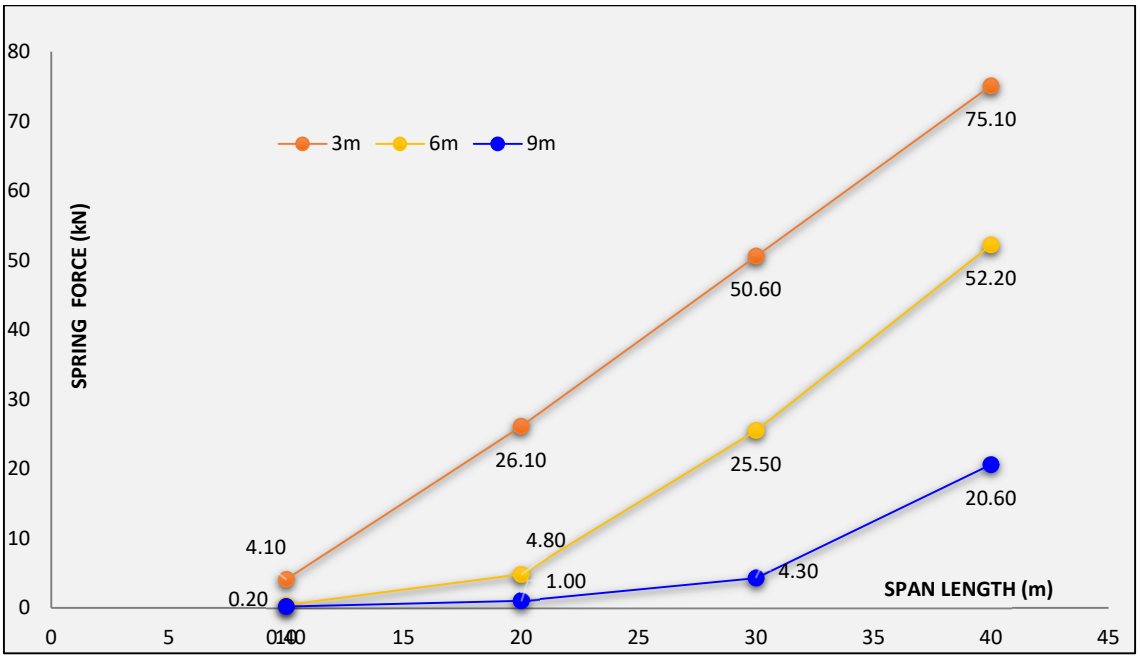

Figure *4.14*: Pile Spring reactions for Span vs Abutment Height, stiff clay founding conditions (40% Live load, 3D Grillage model)

From **Figure 4.5** it appears as though the soil type and stiffness does not have a major effect on the spring reaction progression (with constant live load), with differences only really appearing after the 20m span has been exceeded. Note that this is applicable to the case for the 2-D model with a footing. Interestingly, this behaviour is repeated (and confirmed) in **Figure 4.15**, which is for the 3-D MIDAS model.

The spring reaction graphs shown in **Figure 4.16** are of significant interest as they show that beyond a certain span length (20m), the pile spring reaction graphs differ in their behaviour and depend heavily thereafter on the environmental soil conditions that the piles are founded in. This behaviour is also seen in the 2D model graphs of **Figure 4.5**. The stiff clay springs exhibit a linear spring reaction progression with increasing span, whilst the soft clays undergo a softening (with little reaction development). The non-cohesive materials undergo significant spring reaction increase as the spans get longer – this could be attributed to their increased densification. The reason for the apparent randomness in **Figure 4.16** is due to the shifting in pile contraflexures down the length of the piles, causing the pile reaction forces to be switched in sign, magnitude and load sharing with the abutment. Note how the abutment forces make sense (progressive increase), yet the pile forces are more random. It is evident how the soil properties play a large role in generating these spring reactions in the piles, as they soften and/or densify.

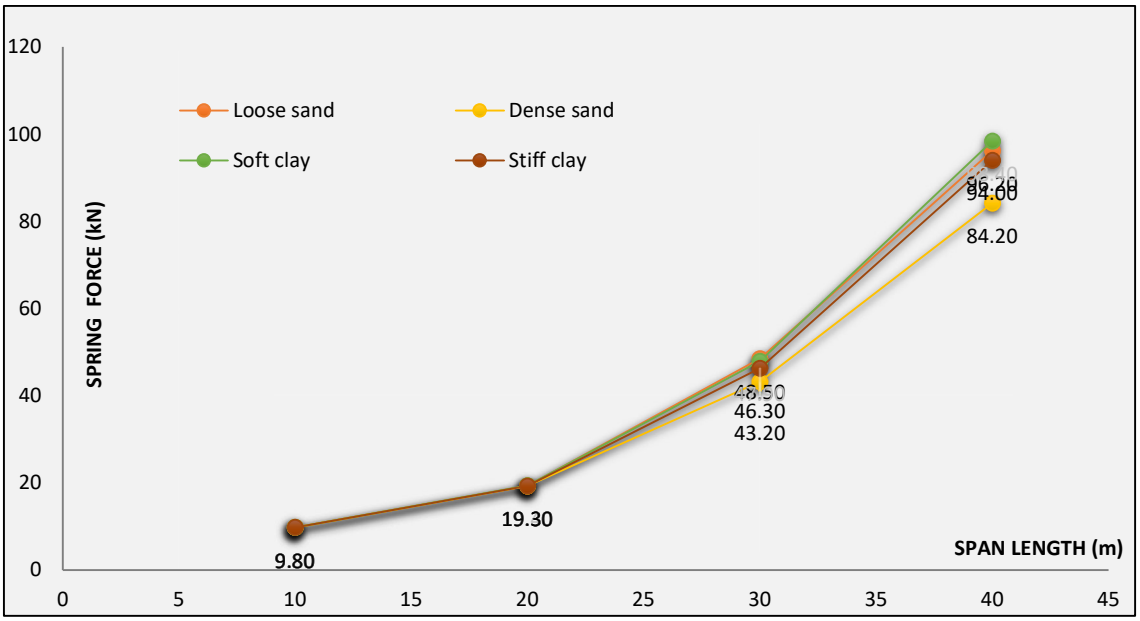

Figure *4.15*: Abutment Spring reactions for Span vs Soil condition, for 40% Live load, 6m high abutment (3D Grillage model)

In **Figure 4.15**, note how the pile soil type produces a relatively minimal change to the abutment spring reactions, which is not unexpected since the abutment backfill material always stays the same.

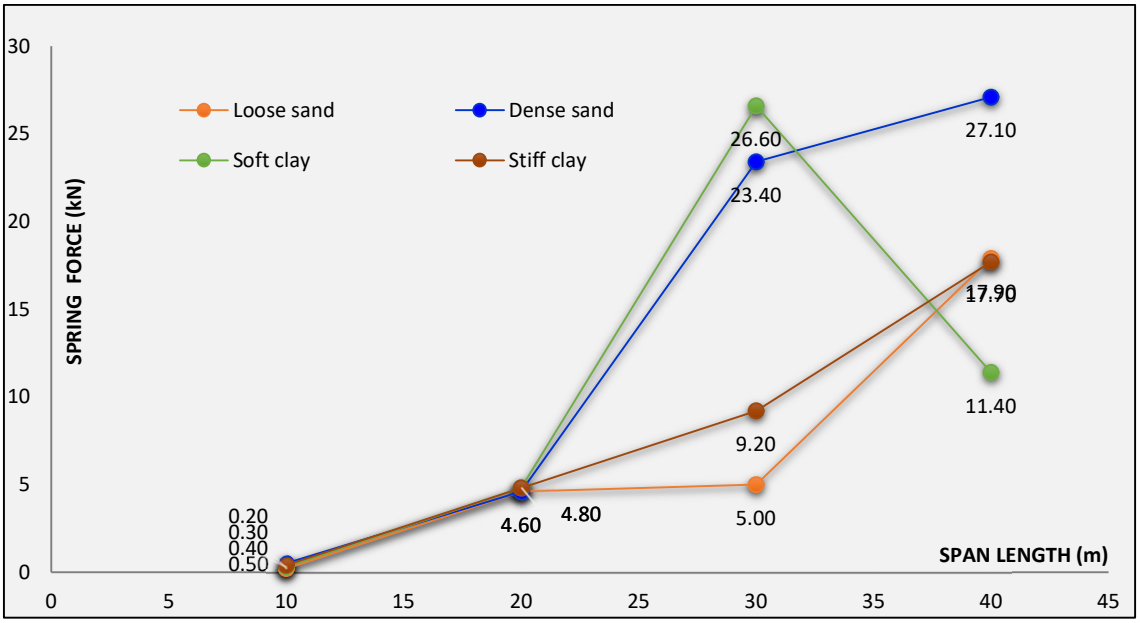

Figure 4.16: Pile Spring reactions for Span vs Soil condition (40% Live load, 3D Grillage model). Note that after 20m, the pile spring reactions are dramatically affected by the soil type

The graphs below from **Figure 4.17** to **Figure 4.20** are for the 3D MIDAS models (bridge on piles), which are subjected to temperature loading in the form of expansion and contraction.

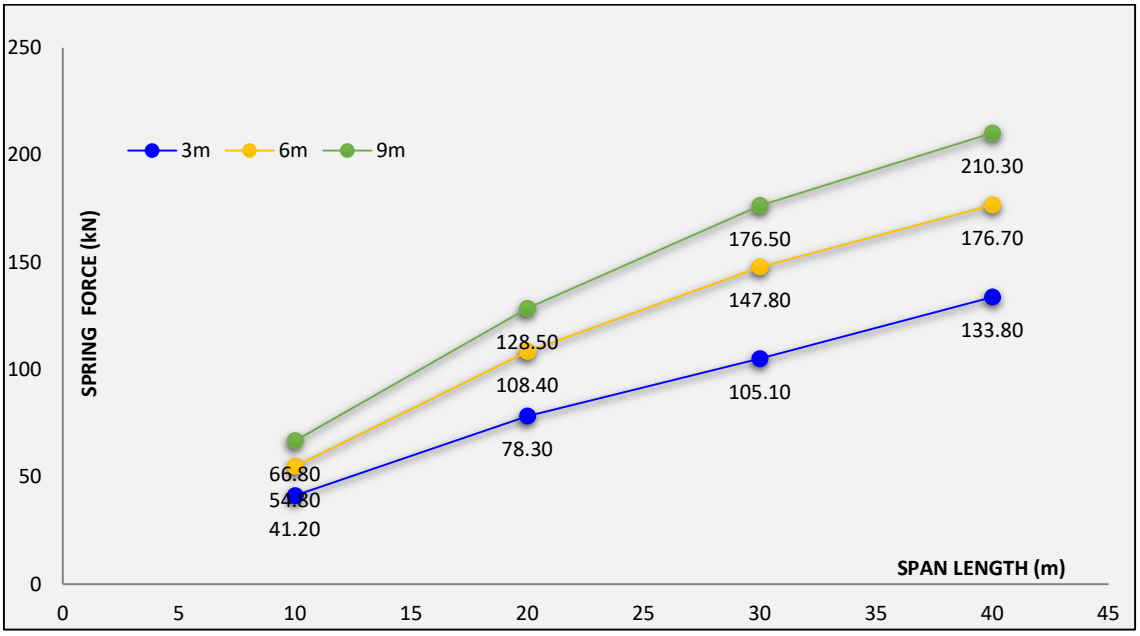

Figure *4.17*: Abutment Spring Reactions for Span length vs Abutment height (Temperature rise condition), stiff clay founding conditions (3D Grillage model)

Figure 4.28 shows results that are in relation to the temperature expansion load case and should be read in conjunction with **Figure 4.17** and **Figure 4.18**. Note that the equation below describes the linear movement of the deck to temperature changes, and note furthermore that this equation ignores the restraining effects of the abutment/pile system:

$$\Delta = \alpha . \Delta T . L_b \qquad \text{(Eqn. 65)}$$

Where:
Δ = bridge displacement (expansion or contraction)
α = coefficient of thermal expansion
ΔT = temperature difference between the effective bridge temperature and the original construction temperature
L_b = Length of bridge from the neutral point (normally the bridge centre point) to the deck end

The aspect to bear in mind here is that Eqn 65 is a linear equation, and yet it is clear from **Figure 4.28** above that the spring's response is non-linear in nature. This is due to the non-linear lateral load response, mostly from the pile behaviour – refer to Section 2.3.3, **Figure 2.14** and **Figure 2.15**.

It may noted again in **Figure 4.17** and **Figure 4.18** how the 3m high abutment has a significantly different behaviour to the 6m and 9m high abutment spring reaction graphs – this is due to the significantly larger bending effects that take place, the higher the abutment is made, with a corresponding reduction in pile spring force. See also **Figure 2.49** and earlier comment above **Figure *4.14***.

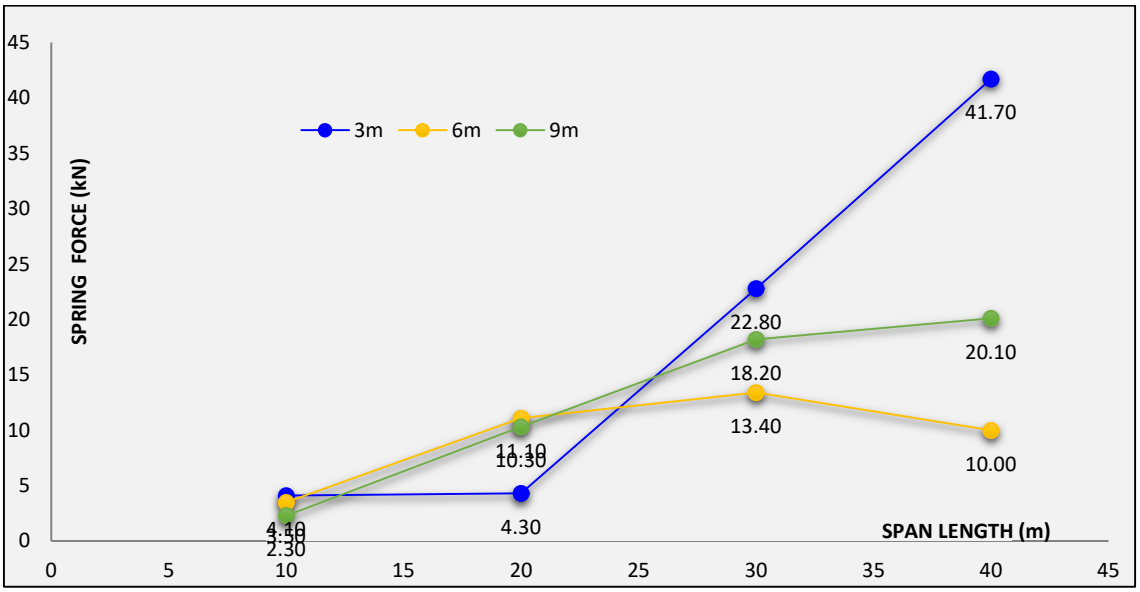

Figure *4.18*: Pile Spring Reactions for Span length vs Abutment height (Temperature rise condition), stiff clay founding conditions (3D Grillage model)

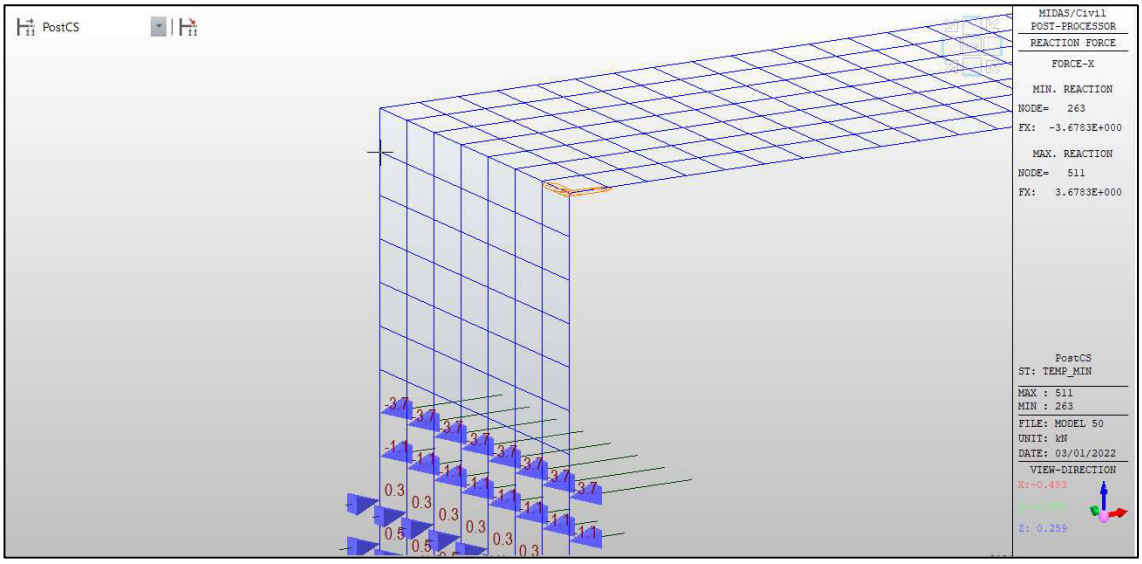

Figure *4.19*: Abutment Spring Reactions for Span length vs Abutment height (Temperature fall condition) stiff clay founding conditions (3D Grillage model). Note that the diagram shows that no reactions occurred in the abutments (typical for all the models analyzed)

Figure 4.19 is a sample of one of the many models that were tested for the Temperature Fall loading condition. Note that the reaction diagram shows that no abutment spring reactions were recorded in any of the 3D MIDAS models for the temperature contraction load case, with pile spring reactions only being found (as can be seen in this sample reaction diagram). In a typical realistic loading combination case however, where dead and superimposed dead loads are added to the temperature contraction loading case, it is unlikely that the end-result would be that the entire abutment does not have any spring reactions. In practice, it is quite normal for the top parts of the abutment to pull away from the backfill, leaving the bottom section of the abutment still in contact with some of the fill (and therefore still creating spring reactions).

When comparing **Figure 4.17** and **Figure 4.20** with each other, the figures show spring reaction graphs for temperature increase and temperature fall respectively that are essentially linear in nature, (ie. increase in span produces an increase in spring reactions) but opposite in the direction of their spring reaction progression.

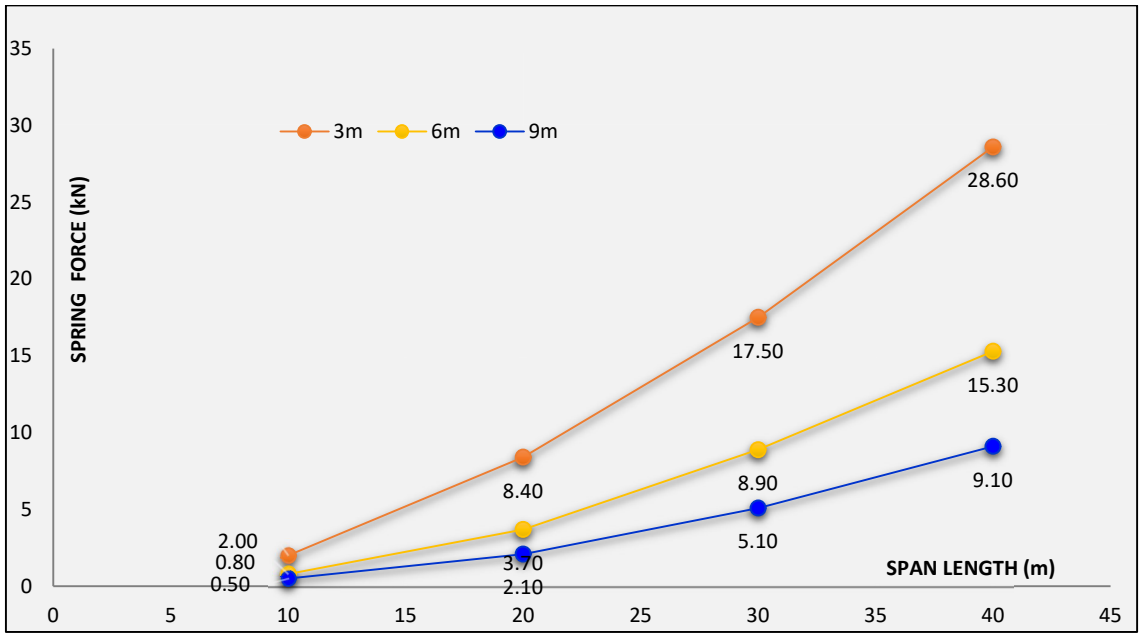

Figure *4.20*: Pile Spring Reactions for Span length vs Abutment height (Temperature fall condition), stiff clay founding conditions (3D Grillage model)

Figure 4.17 (for temperature increase) shows a plot that appears to be progressing towards a set of finite values, which makes sense since the backfill will tend to become 'harder' (and abutment springs will yield) in its resistance to the linear increase (see Equation 65) in the expansion load that is applied to the deck/abutment system.

Figure 4.20 shows a set of graphs of the parabolic form $y = kx^2$ that are increasing in pile spring reaction vs. span. For the temperature fall case, the active pressures behind the abutment would be mobilized (which are significantly less than the passive pressures), however in the piles, the effect that is demonstrated in **Figure 4.20** is that the pile system is entirely resisting the deck contraction that is

applied, and the more the contraction load, the more the pile resistance load. It is also notable that the 9m high abutment pile loading is less than the 3m high abutment loading, which is not unexpected since there is a greater lever arm created by the 9m high abutment piles, and therefore less load reaction is required.

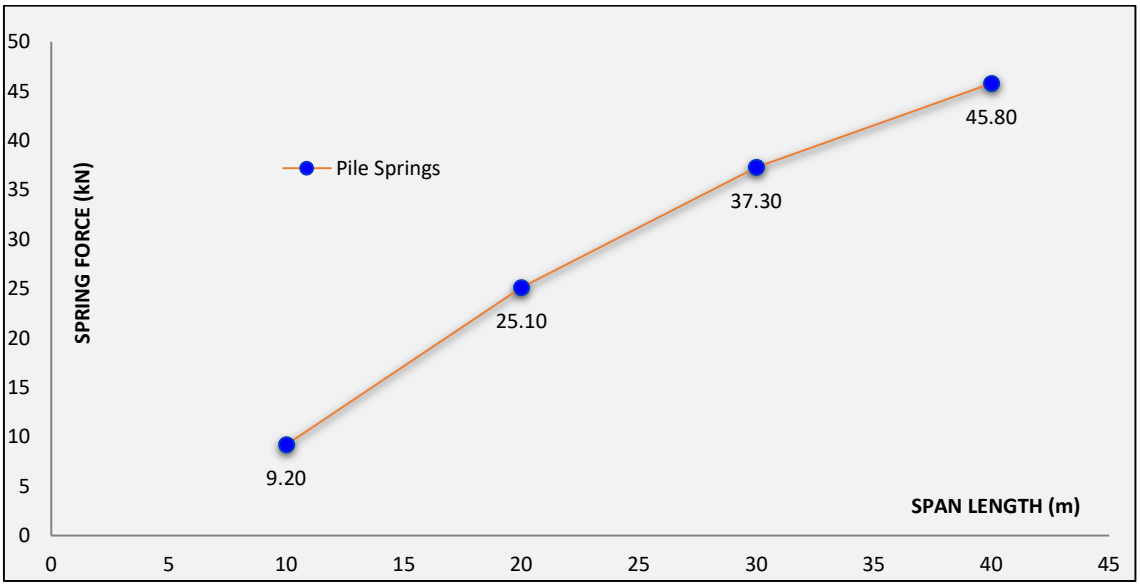

Figure *4.21*: Pile Spring Reactions vs Span length for a 3m high Abutment in Stiff clay (Positive Temperature gradient condition, (3D Grillage model)

In relation to **Figure *4.21*** note that the reason why only the pile spring force has been plotted is because there were no activated abutment reactions under this loadcase (positive temperature gradient). This is similar to **Figure 4.19**, which shows that there were no recorded abutment spring reactions. **Figure *4.21*** does however show a parabolic increase of spring reaction for a positive temperature gradient condition in the piles. The deflection diagram corresponding to the positive temperature gradient loadcase is shown below in **Figure *4.22*** whilst the diagram for the negative temperature gradient is shown in **Figure *4.24***. Note the reverse curvatures in the structure, between these two diagrams due to the different induced directions of the loading – these reversed curvatures are basically as expected, and these deflection diagrams correlate reasonably well with the information shown in **Figure *2.2*** earlier. Note that the deflections and rotations observed under the effects of this loadcase are quite small, hence this loadcase has not generated substantial reactions in either the piles or the abutment. The pile reactions diagram is nonetheless of interest as it demonstrates the non-linear (parabolic) behaviour that would be expected in the pile behaviour (see **Figure 2.15**). From the shape and direction that the reaction curve follows, one could infer that the pile spring reaction will ultimately taper off to a finite value (which would make sense in terms of the fact that pile springs ultimately have a finite value).

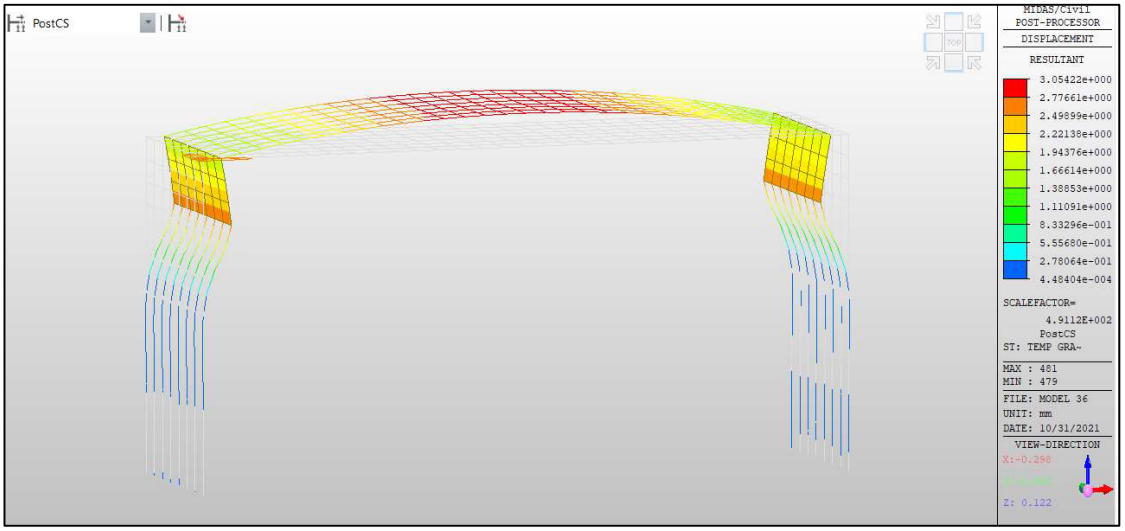

Figure *4.22*: Deflection diagram for a 3m high Abutment in Stiff clay (Positive Temperature gradient condition, 3D Grillage model), deck with upward deflection

The reaction diagram shown in **Figure *4.23*** shows a curve that is the inverse to that of **Figure *4.21***, and is for the temperature negative gradient loadcase. One can see from this curve that there is a progressively linear increase in the pile spring reactions for this loadcase, and that the magnitude of the reactions are smaller to those of **Figure *4.21*** – eg. compare for the 40m span result, 45.8 kN for the positive temperature gradient vs 29.3 kN for the negative temperature gradient. One would need to evaluate longer length spans to gain a better understanding of how the curve of **Figure *4.23*** ultimately progresses.

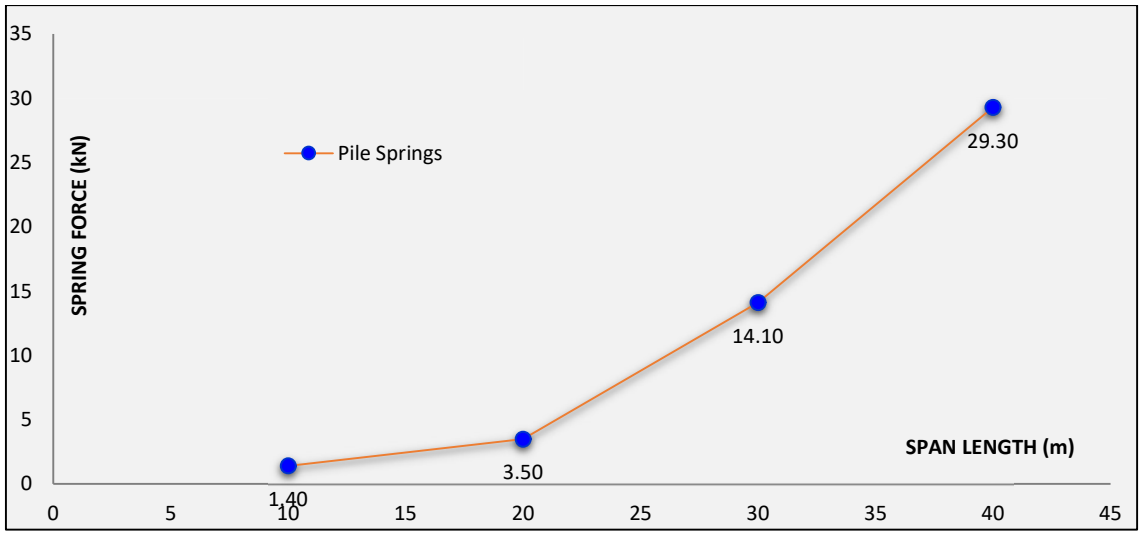

Figure *4.23*: Pile Spring Reactions vs Span length for a 3m high Abutment in Stiff clay (Negative Temperature gradient condition, 3D Grillage model)

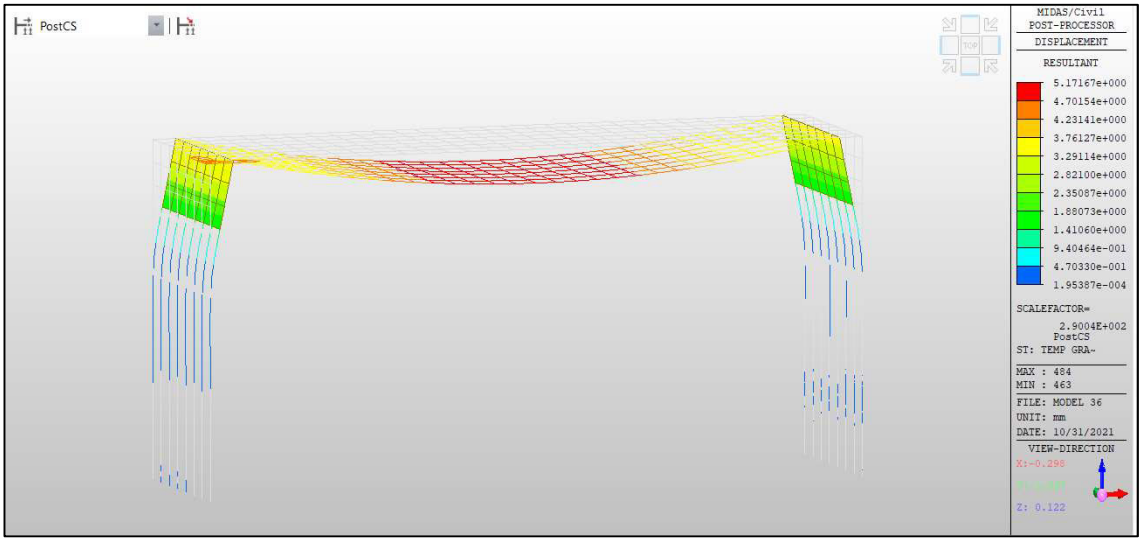

Figure *4.24*: Deflection diagram for a 3m high Abutment in Stiff clay (Negative Temperature gradient condition, 3D Grillage model), deck with downward deflection

4.2.6 3D Grillage Model reaction ratios

From a load equilibrium point of view, the maximum horizontal spring reactions to the applied loads tend to be split between the piles and the abutment. In some scenarios, the bulk of the spring reaction resistance force is found in the abutments, in other instances the bulk of the spring reaction is found in the piles. As the geometry changes, so changes occur in the load sharing between these two elements in the system.

The plots below illustrate how the ratio of the Abutment reaction to Pile reaction varies, for the 3D MIDAS models that were analysed. **Figure 4.25** shows how the ratio of maximum abutment/pile spring reaction tends towards a value of unity, with an increase in span (despite changes in the abutment height) – this is also seen in **Figure 4.26**. The design implication of the above result is that one would expect to find that similarly sized abutments and piles for the longer spans will be appropriate, whereas for the shorter spans, the elements may not be similarly matched in their sizing.

Of note is the distinct difference in the Abutment/Pile spring reaction ratio for the 9m high abutment vs the 3m high abutment in **Figure 4.26**. For a normal higher (9m) abutment (with no soil), one would expect less force due to the increased flexibility, however since there is an increased abutment soil-structure interaction, there is more area and more passive spring force, therefore the force is in fact increased, not reduced. The inference of these diagrams is that for short spans, the 9m high abutment generates significantly more reaction forces in the abutment, with significantly smaller forces and bending moments being generated in the piles. The further design implication of this is that for the shorter spans, designers should test for sensitivity in pile lengths to determine how much resistance is really required to the applied forces, as further optimization may be possible in this regard. The 3m high abutment is significantly less affected by variations in span length, in terms of the forces and reactions generated in the abutments/piles, therefore one can expect to see more equally sized elements for this abutment height.

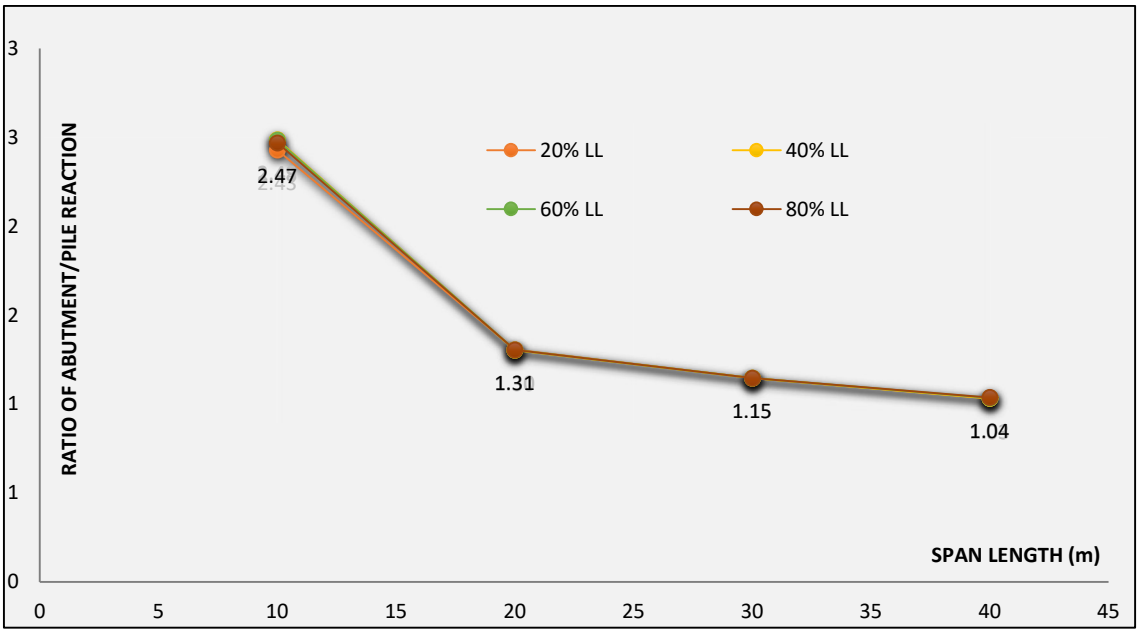

Figure 4.25: Maximum (Abutment / Pile) Spring Reaction ratios for variable live load vs Span length (3m high abutment, founding in stiff clay, 3D Grillage model)

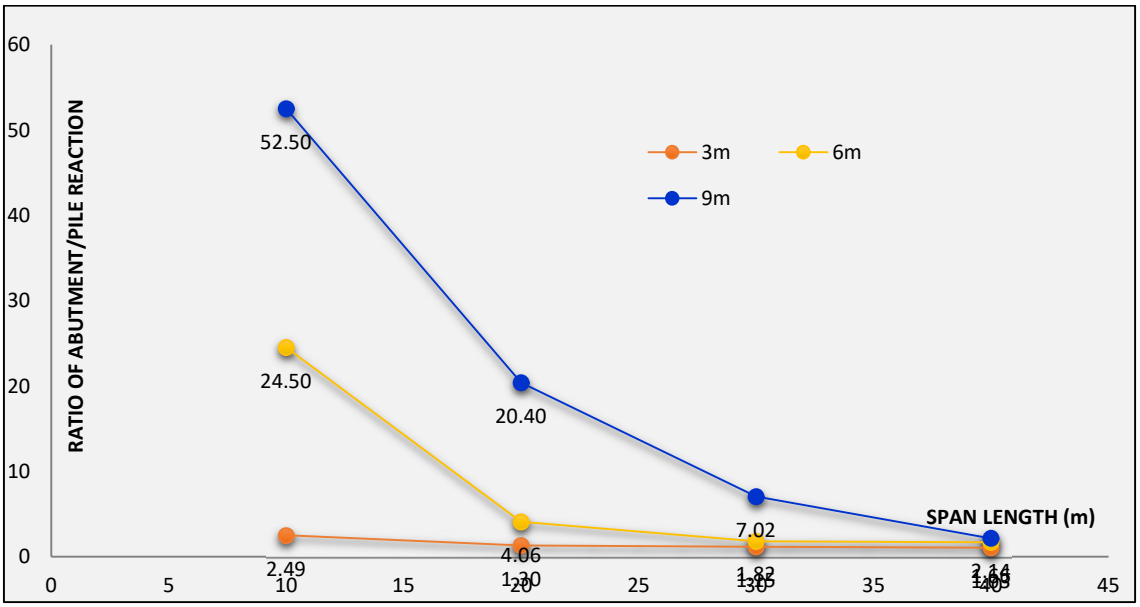

Figure 4.26: Maximum (Abutment / Pile) Spring Reaction ratios for variable abutment height vs Span length (founding in stiff clay, 40% Live load, 3D Grillage model)

In regard to the plots shown in **Figure 4.16** and **Figure 4.27** below, these plots demonstrate how the founding soil conditions profoundly affect the design forces that arise in the abutments and piles. For

shorter spans, the ratio of Abutment/Pile spring reaction varies from 49.0 (loose sand) to 19.6 (dense sand), simply due to the founding condition that the piles are installed in. This is of significance for the designer of the bridge structure, ie. to bear this in mind when assessing the expected forces on these elements in the design. Seismic forces would consequently also be an important consideration in this regard, as the designer may choose to select differing founding conditions (if the choice of site is available), based on the response characteristics that the springs will have under seismic loading.

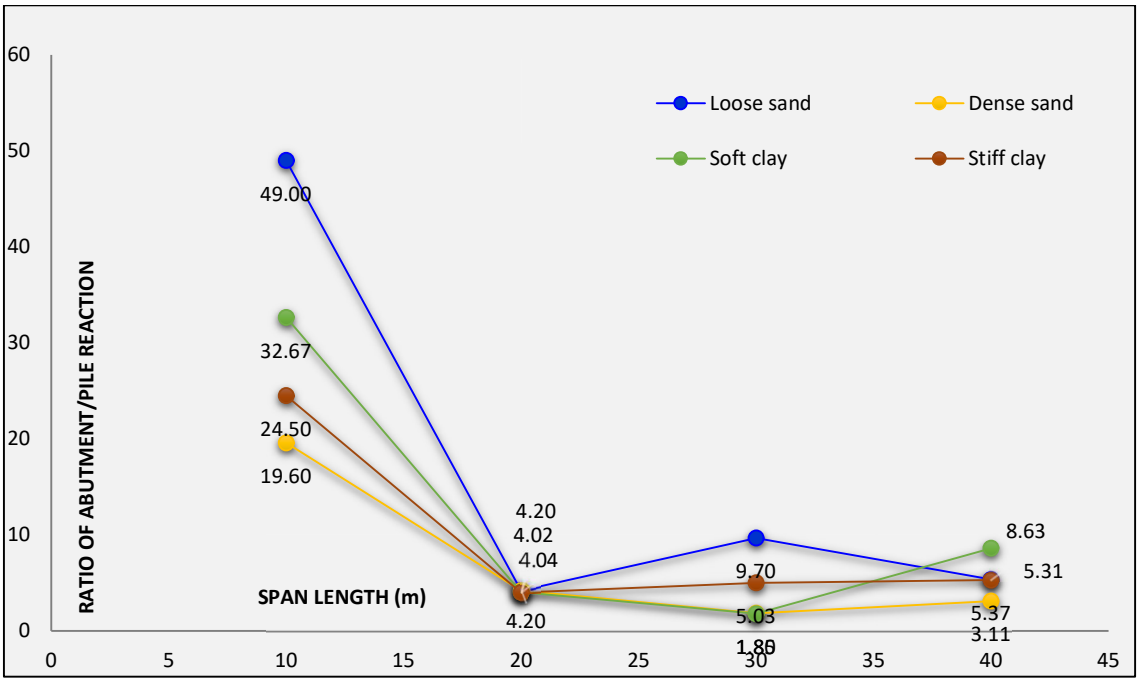

Figure 4.27: Maximum (Abutment / Pile) Spring Reaction ratios for variable soil conditions vs Span length (6m high abutments, 40% Live load, 3D Grillage model)

The other characteristic to take note of, is how the spring behaviour changes after the 20m span is exceeded – as can be seen in **Figure 4.27** above, this span represents a low point in the abutment/pile spring reaction ratio. The apparent randomness of this diagram can be understood better when considering the graphs shown above in **Figure 4.16** – the same comments made in relation to the non-linear behaviour of the pile reactions apply. It appears that this characteristic could also be a geometrical-force related phenomenon, in regards the abutment height to span relationship, since the 20m span is approximately (3x) the abutment height. This phenomenon requires further analysis in order to better understand the exact reason why the 20m span is significant to the structural system. It would be suggested that it could also be related to the Mohr circle principle stress jump that is described in **Figure 2.46**, or a function of the complex relationship between Height and Deck length that is evident in Equations 61, 62 and 64.

Appendix A contains the details of some of the models used in this thesis, as well as their loadings and the spring reactions that were noted in their analysis. Included are a further set of columns added to the set of results, entitled "% Avg Spring reaction load to total LL" and "% Spring load to total LL". Using

the following equations, the spring reactions have been related to the applied load on a strip of beam/tributary abutment/pile (as the case may be).

$$F_{sp\%} = \frac{F_{sp}}{\left(\frac{w.L}{2}\right)} \qquad \text{(Eqn. 66)}$$

This equation can be re-written as:

$$F_{sp} = F_{sp\%}.\left(\frac{w.L}{2}\right) \qquad \text{(Eqn. 67)}$$

Where:
F_{sp} = Maximum spring reaction (kN)
$F_{sp\%}$ = Coefficient from **Table 4.1** or **Table 4.2**, or other values from the columns for "spring load to total LL" in Appendix A
% = percentage of the dead load added to the superimposed dead load (%)
w = %(DL + SDL) = applied live load, as related to dead load (DL) + superimposed dead load (SDL)
L = bridge span (m)

It may be noted that the following tables may be drawn up, relating the spring reactions F_{sp} to the coefficient, $F_{sp\%}$. Note that these values are applicable to the 3D MIDAS models that were analysed.

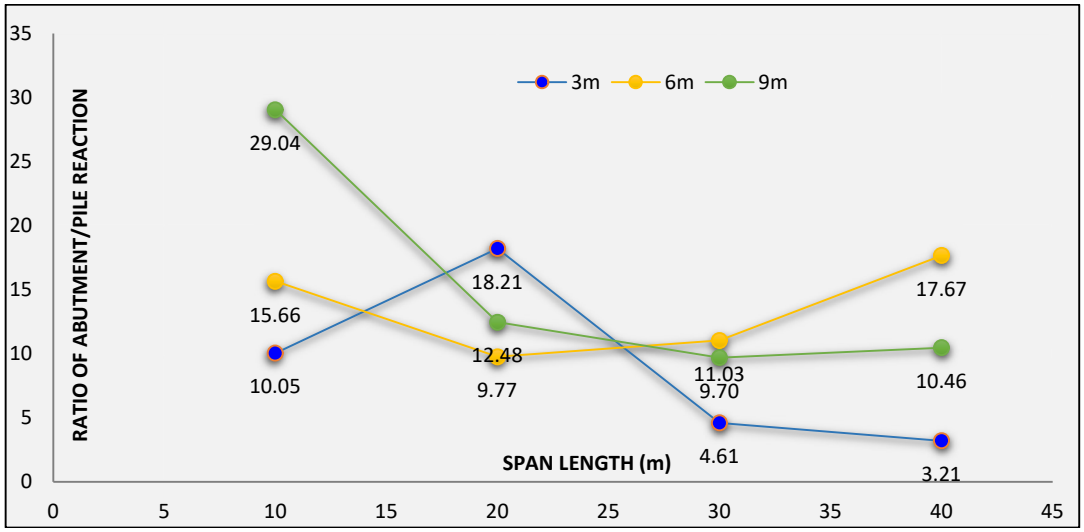

Figure 4.28: Maximum (Abutment / Pile) Spring Reaction ratios for variable abutment height vs Span length for temperature rise condition (Stiff clay founding condition, 3D Grillage model)

It is obvious from the results that the higher the abutment, the more significant is the passive resistance build up behind it, and that this is the beginning of various non-linear spring reaction effects. This effect has been observed previously by Xanthakos (1994) who noted that some additional axial and bending moments are induced in integral bridge decks as restraint and stiffness increases. It was also noted that the short stub type of abutment on piles is flexible enough to withstand these additional forces without serious structural distress.

Bridge Span	Fsp% - Abutment	Fsp% - Pile
m	%	%
10,000	39%	16%
20,000	45%	34%
30,000	39%	34%
40,000	31%	30%

Table 4.1: $F_{sp\%}$ = Coefficients for calculating maximum spring reactions, for various spans vs live load %'s. In this instance, similar coefficients as per this table were found for the range 20% to 80% (DL+SDL)

Bridge Span	Fsp% - Abutment	Fsp% - Pile
m	%	%
10,000	40%	1%
20,000	27%	1%
30,000	20%	3%
40,000	18%	8%

Table 4.2: $F_{sp\%}$ = Coefficients for calculating maximum spring reactions, for various spans and 9m high abutment

Many other tables may be produced from the analysis results, however one can refer to Appendix A for these $F_{sp\%}$ values.

The temperature related pile spring reactions for varying abutment height vs. span in stiff clay conditions are shown in **Figure 4.18**. What should be borne in mind when interpreting these results is that the absolute value of the spring reaction has been used to draw these plots (similarly with all other graphs shown in this thesis). Although the 3m high abutment graph appears suspect, there is in reality a switching over of the pile reaction signs, which is demonstrated below in **Figure 4.29**. In other words, the 3m abutment height pile reaction in reality shifts from -4.1kN to +4.3kN, when going from 10m to 20m spans respectively. If one considers the smaller 10m span in **Figure 4.28**, it is evident that the 3m abutment has the lowest abutment/pile spring reaction ratio, and that despite a stress reversal at 20m (see earlier comment in relation to **Figure 2.46**), the ratio still keeps on getting smaller (in other words the abutment keeps on 'losing' load to the piles as the spans increase). The 9m abutment starts at the 10m span with significantly more load in the abutment than in the piles (which again makes sense since there is more area to develop soil spring resistance load), and as the span (and applied deck force) is increased, the abutment sheds its maximum load to the piles. The 6m abutment follows a spring reaction ratio that at first (10m span) lies between the 3m and the 9m abutment, but then shows a progressive increase in load being shed to the abutment as opposed to the piles (40m span). One should bear in mind, with interpretation of the graphs that relate abutment height to span that Equation. 1 (taken from the PD6694-1:2011 Code) shows an inverse relationship with abutment height and pressure.

It may also be observed in **Figure 4.18** that the 6m and 9m high abutment pile reaction plots show a decreasing pile spring reaction as the span length is increased. This suggests that the springs begin to reach their capacity and yield for the longer span lengths, as well as shedding their load to the abutment springs. The graph again verifies the non-linear behaviour of piles under lateral loading (see Section 2.3.3).

It is noted that Thomson (1999) reports that the exact location of the resultant force on the abutment depends on the wing-wall geometry. As the angle between the wing-wall and the abutment changes from the parallel position to perpendicular position, the resultant force moves up the abutment. This phenomenon could not be verified in this series of tests since wing walls were not included in the modelling.

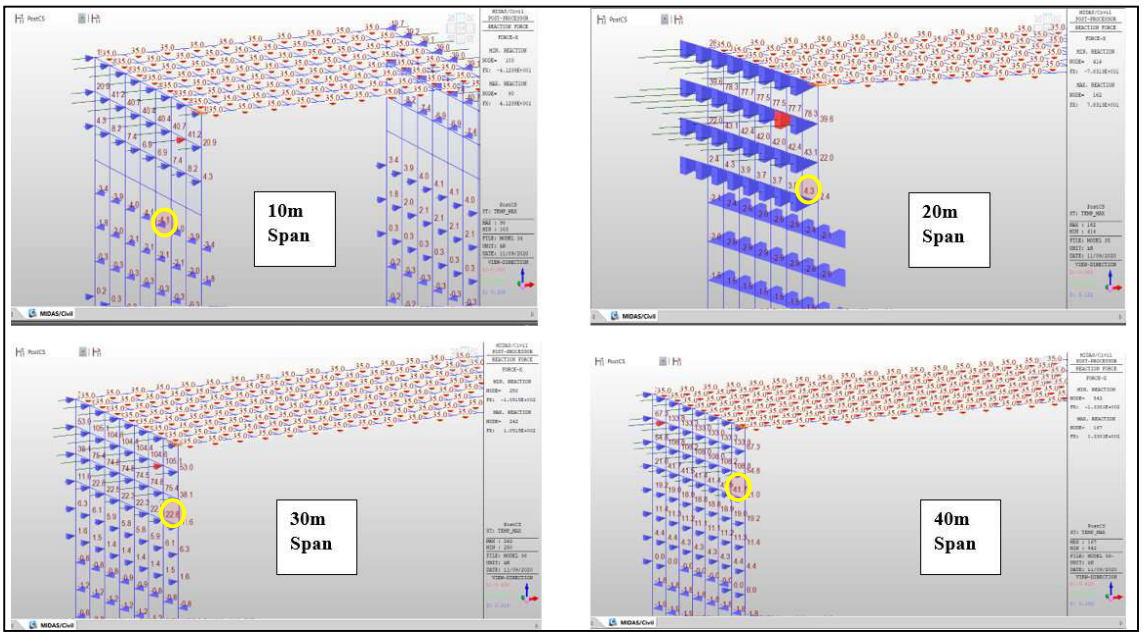

Figure 4.29: Spring reaction diagrams from which the 3m high abutment spring reaction line in **Figure 4.18** is taken, showing how the max pile reaction in fact changes in its direction between 20m and 30m

4.2.7 3D Grillage Model - Bending Moments and lateral deflections

In addition to the above examination of the spring values, the Bending Moments and the Deflections were also considered and the following plots were produced. The purpose of this exercise was in essence to verify the behaviour of the spring reaction plots that have already been produced. Maximum pile and abutment bending moments were considered, as well as maximum pile and abutment lateral deflections.

The positions reported on in the following figures for the maximum bending moment in the abutment and the piles are shown below in **Figure 4.30** (these are typical positions where the bending moment is maximum in the respective abutment and pile elements). The maximum hogging bending moment in the incoming beam (in kN.m) which joins into the top of the abutment is matched by the moment formed in the top of the abutment, this can be checked in the image at the bottom of **Figure 4.30**, which shows the abutment bending moments (in kN.m/m). As can be seen from the lower diagram, the same does not hold true for the piles, which are generally not as stiff as the abutments (this is only true in this particular set of model testing) and therefore are not generating the same magnitude of bending moment as per the abutment bending moments.

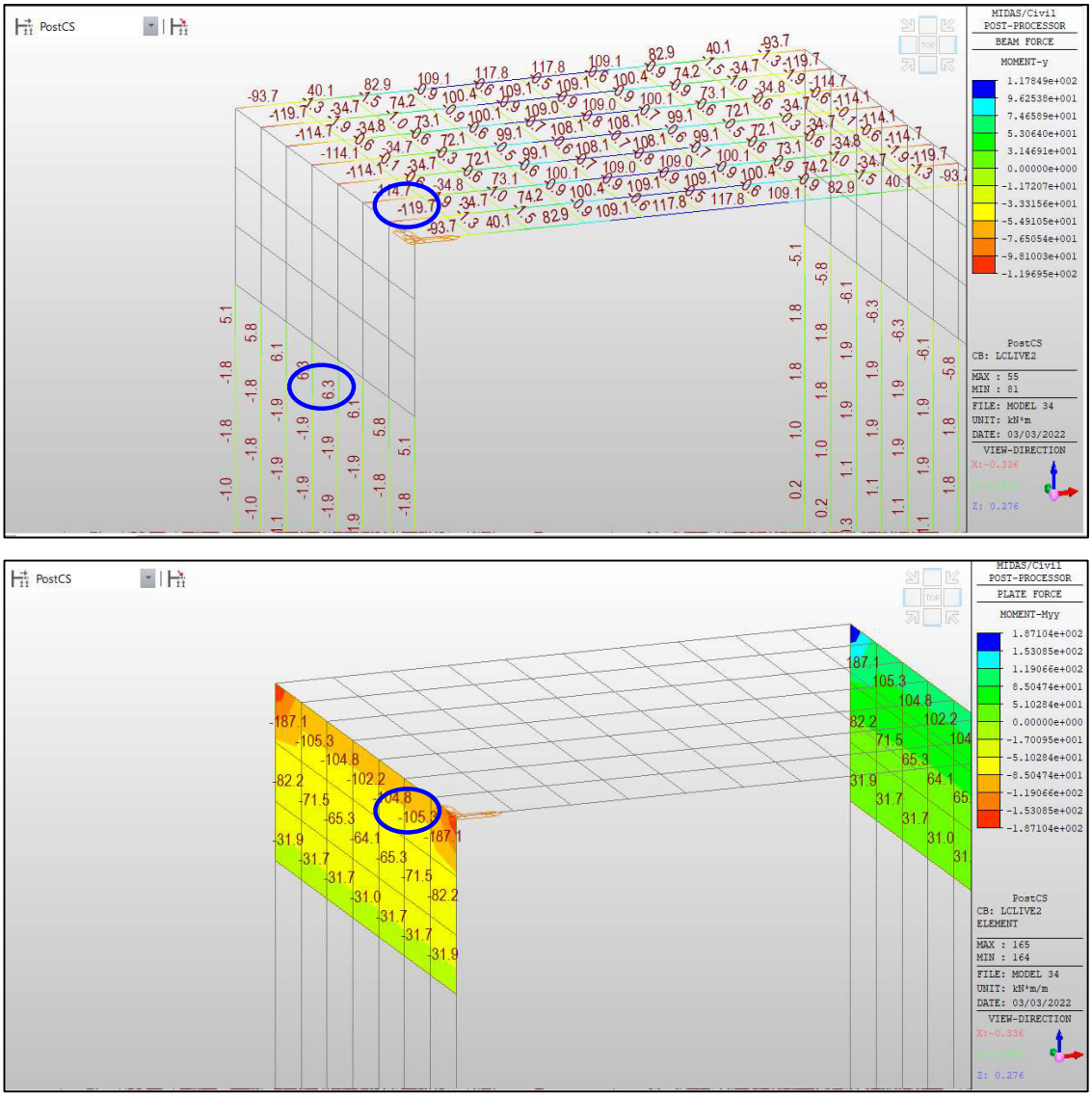

Figure 4.30: Abutment and Pile Bending moments (kN.m)

To capture the extreme live load cases, the 20% and the 80% applied Live loading cases were considered. The effects of effective bridge temperature increase and decrease were also included in the diagrams below.

The Bending moment and deflection diagrams in **Figure 4.31** and **Figure 4.32** are for the case of 20% live load applied to the deck, for 3m high abutments, in stiff clay founding conditions. The diagrams essentially demonstrate a 'shallow' parabolic behaviour that approximately matches the linear shaped spring reaction diagrams for 3m high abutments found in previous graphs (eg. **Figure 4.13** and **Figure 4.14**).

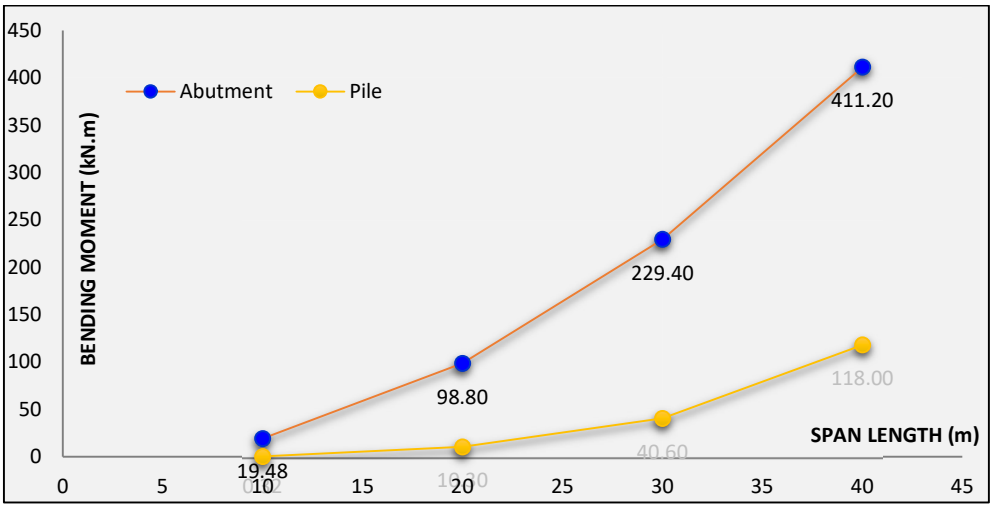

Figure *4.31*: Maximum bending moments for abutments and piles, 3m high abutments, 20% Live load, stiff clay founding conditions

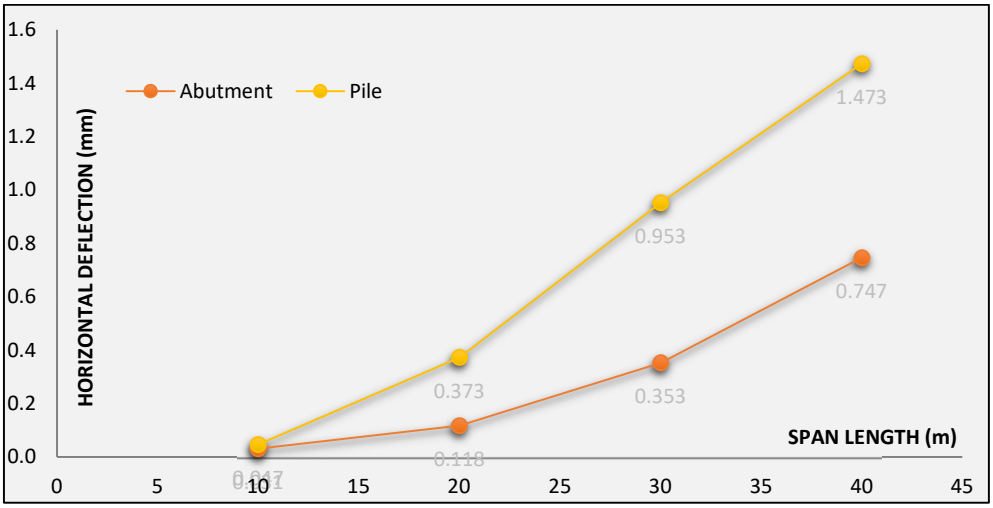

Figure *4.32*: Maximum lateral deflections for abutments and piles, 3m high abutments, 20% Live load, stiff clay founding conditions

Figure 4.33 and **Figure 4.34** are for the case of 80% live load applied to the deck, for 3m high abutments, in stiff clay founding conditions. Note that these diagrams have very similar characteristics and shapes as the previous two figures, despite the fact that the load has increased significantly – this would imply that the load magnitude has not changed the bending and deflection behaviour of the system. Also of note when observing the curvature of these graphs, is that the pile attracts bending moments at a much slower rate than the abutment (and hence the deck) since it is less stiff. This makes sense since the load is not being applied directly to the piles (they are stationed further away from the site of the application of the loading), as it is being applied directly to the deck.

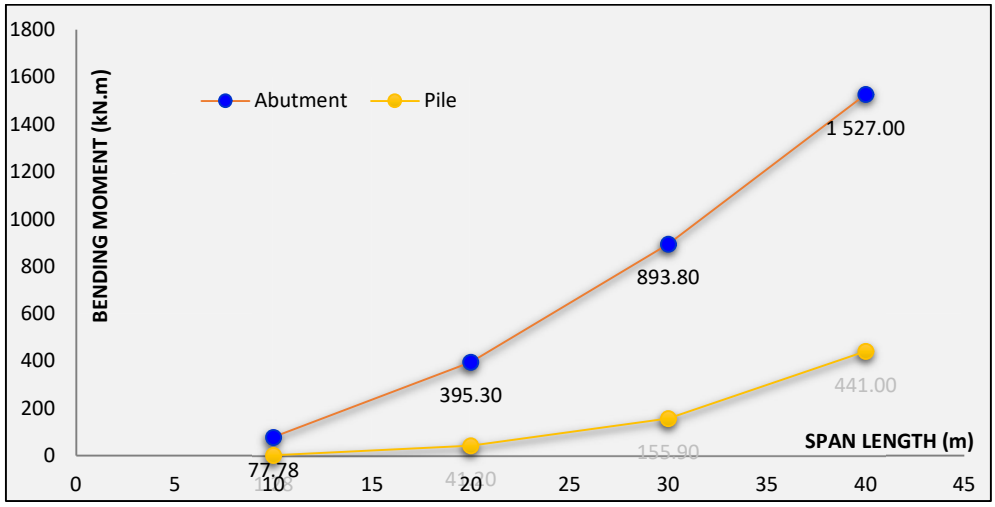

Figure *4.33*: Maximum bending moments for abutments and piles, 3m high abutments, 80% Live load, stiff clay founding conditions

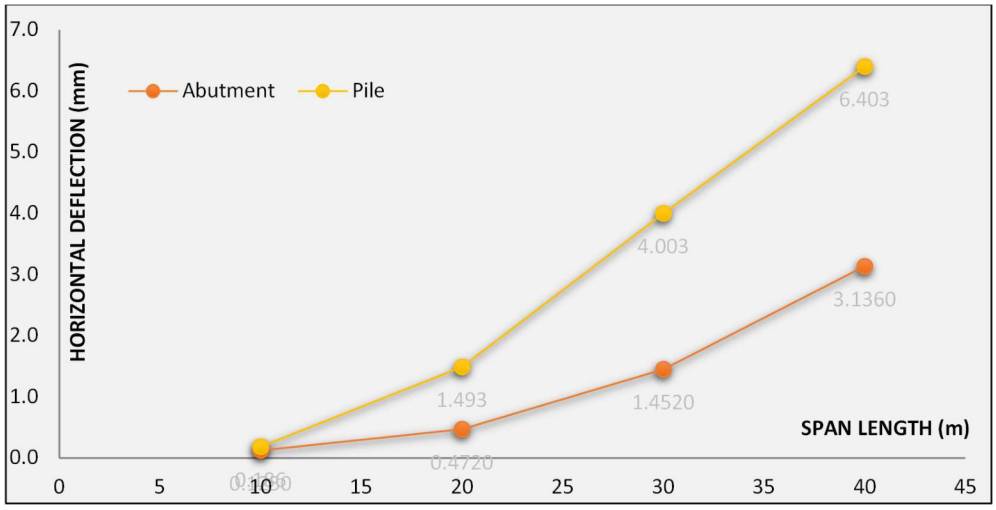

Figure *4.34*: Maximum lateral deflections for abutments and piles, 3m high abutments, 80% Live load, stiff clay founding conditions

Figure *4.32* shows however that the pile lateral deflections are greater in magnitude than the abutment lateral deflections – this would again be because the pile is not as stiff as the abutments. In summary, **Figure *4.31*** to **Figure *4.34*** confirm the spring behaviours observed in previous Figures.

The Bending moment and deflection diagrams **Figure 4.35** and **Figure 4.36** are for the case of a 15^{O}C temperature increase applied to the deck, for 3m high abutments, in stiff clay founding conditions. The diagrams are of interest as they show how the abutment bending moments develop in a linear manner, whilst the piles struggle to develop in the same manner as their load interaction (and including stiffness effects) is more complex (P-Y behaviour). This confirms the graphs shown in **Figure 4.17** and **Figure 4.18**, which show that some initial stress reversal occurs in the piles as the deck expands.

The complex interaction of active and passive abutment pressures (and the load sharing that occurs as a result of this) as well as the contraflexure of the piles is evident in these two figures as being possible reasons for the deflection reversal seen in **Figure *4.36***. Another fact to bear in mind in interpreting these figures is that the equations for the pile response (Equations 7 to 15) are highly non-linear in nature, and that the formula changes as the pile diameter changes.

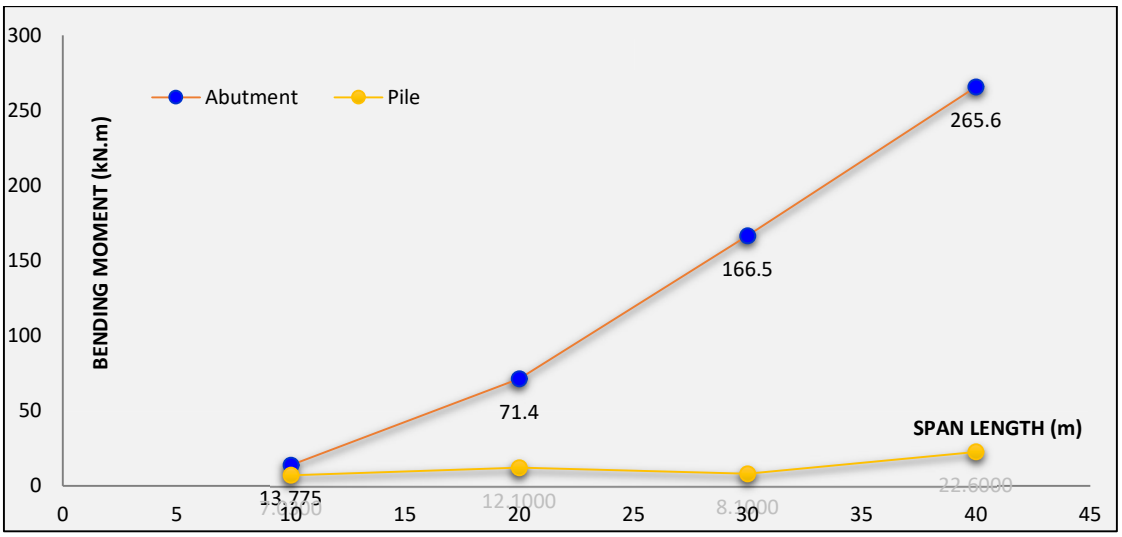

Figure *4.35*: Maximum bending moments for abutments and piles, 3m high abutments, 15^{O}C temperature increase, stiff clay founding conditions

A further point to note in the analysis of the above graphs is that the Live load bending moments in the abutments are significantly larger than the temperature rise induced bending moments. This is in contrast to the spring reactions shown further on in **Table 4.5**, which show that the maximum abutment spring reactions due to the temperature rise case are similar to the live load induced maximum spring reactions. The reason for this could simply be that the live load induced forces impact more of the abutment (and a complex deflected shape arises – see **Figure *4.39***), in comparison with the structure that is interacted with in the temperature rise loadcase.

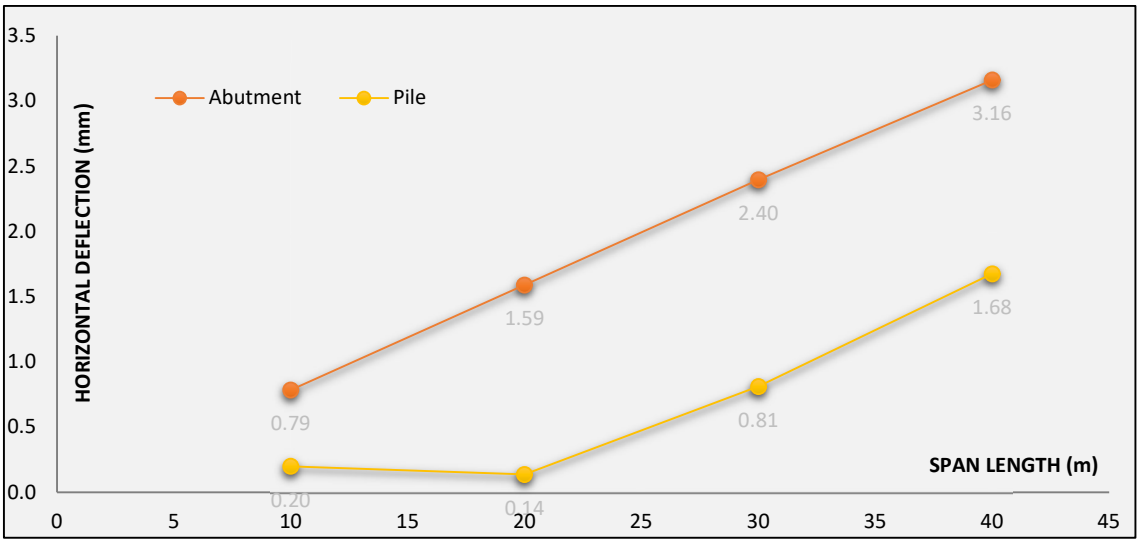

Figure *4.36*: Maximum lateral deflections for abutments and piles, 3m high abutments, 15^{O}C temperature increase, stiff clay founding conditions

The graphs **Figure 4.37** and **Figure 4.38** show progressively linear increases of both maximum bending moments and deflections for a temperature decrease scenario. This is again of interest since the shapes of these pile reaction curves are not similar to those found in the temperature increase scenario for the pile spring reactions. In the decreasing temperature condition, the active pressures will come more into play, whereas in the temperature increase scenario the interaction appears to be more complex.

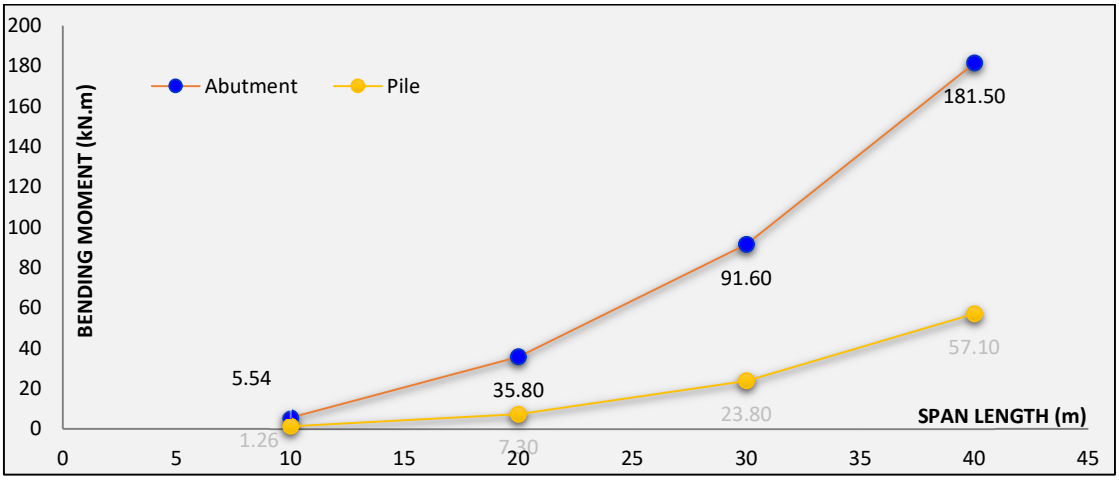

Figure *4.37*: Maximum bending moments for abutments and piles, 3m high abutments, 15^{O}C temperature decrease, stiff clay founding conditions

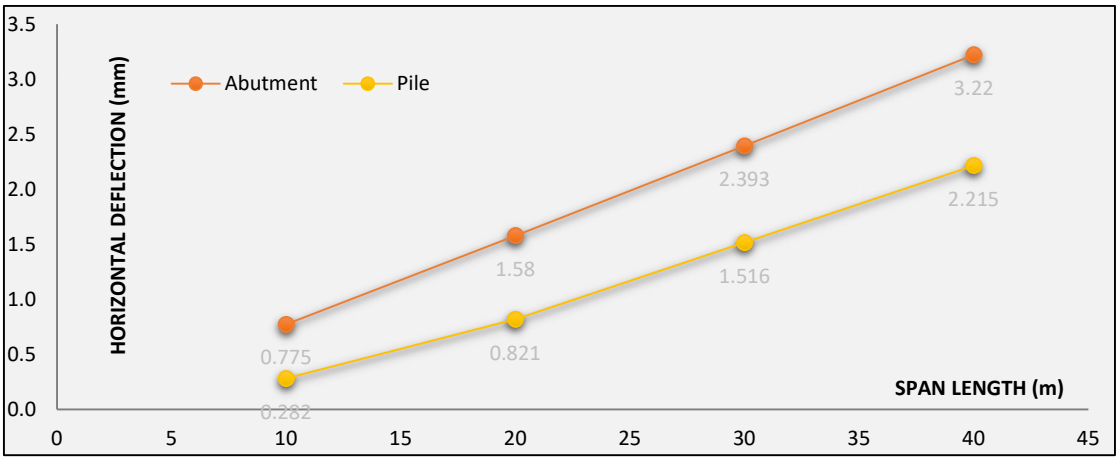

Figure *4.38*: Maximum lateral deflections for abutments and piles, 3m high abutments, 15^{O}C temperature decrease, stiff clay founding conditions

In the above **Figure *4.36*** and **Figure *4.38*** it can be noted how the abutment deflection is generally higher than the pile deflection for the temperature related loadcases (whether dealing with contraction or expansion). This is due to the fact that it is the deck which pushes (or pulls away from) the abutment, causing the spring reaction loads and deflections to develop in the area of direct load application (and area of related stiffness in the structural element). Since the piles are reasonably far away from where the load is being applied, the impact on them in terms of deflections, spring reactions and bending moments is smaller than the effects seen in the abutment. These effects can clearly be seen in **Figure *4.40*** below.

In **Figure *4.39*** below, the deflected shape diagram for 20% Live load is shown for the 3m high abutment in stiff clay. The two positions where the maximum deflections (that are shown in **Figure *4.32***) are taken from are highlighted in this diagram for the abutments and the piles. One can see from this diagram how the abutment and pile deflections are related to the abutment and pile curvature. Note how the maximum deflection in the abutment occurs at a position which is below the level of the top of the abutment (for live loading), whereas for the temperature related loading, the maximum abutment deflection occurs at the top of the abutment (see **Figure *4.40*** and **Figure *4.41***). The positions where the deflections that are recorded in **Figure *4.36*** and **Figure *4.38*** are taken from are highlighted (blue circles) in these diagrams. Note that the maximum pile deflection is generally always recorded as being at the top of the pile, since this is the region where the pile joins with the abutment.

The Table below (**Table 4.3**) shows an interesting comparison between the percentage increase in the development of the spring reactions as the span is increased vs. the percentage increase in maximum bending moments for the abutment and piles for a 3m high abutment founded in stiff clay, with 20% Live load applied.

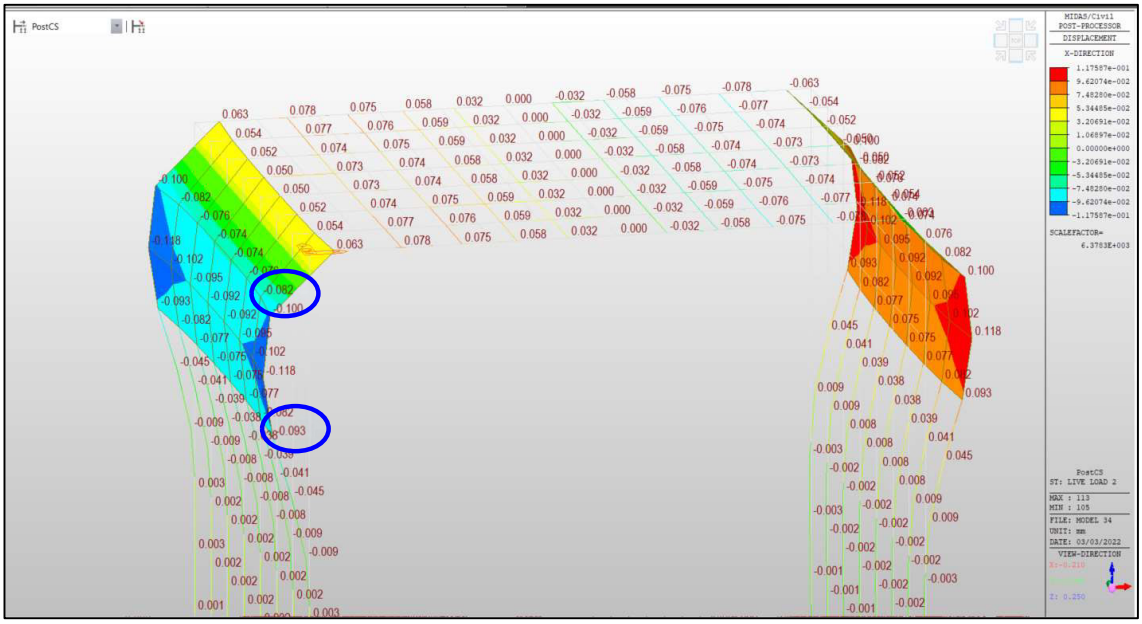

Figure *4.39*: Deflected shape diagram for 20% Live load applied to the structure

Clearly, the rate of increase in bending moments is not the same as the rate of increase in the spring force reactions (eg. Abutment Moments increase by 2010 %, whilst the spring reaction has only increased by 647%).

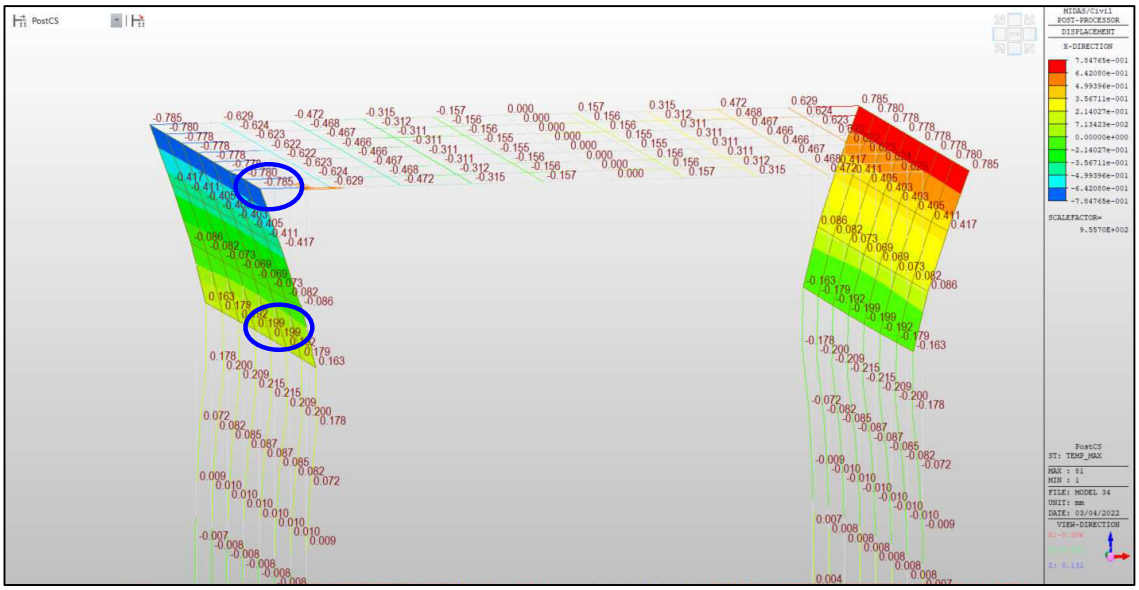

Figure *4.40*: Deflected shape diagram for a 15º temp increase applied to the deck

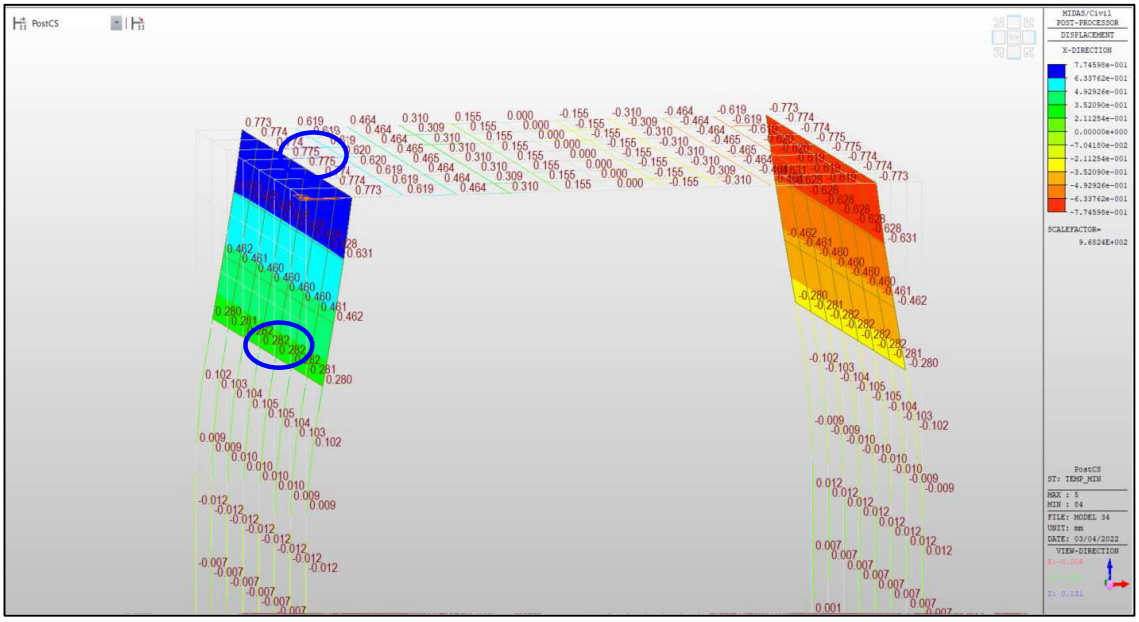

Figure *4.41*: Deflected shape diagram for a 15° temp decrease applied to the deck

There are various reasons why the rates of increase are not similar – the mathematics behind the spring reaction calculation and relationship to the deck is significantly more complex (with its non-linear response) and is completely different to the bending moment calculation which tends to be more linear in nature.

	3m Abutment, 20% Live load, Stiff Clay			
	Bending Moments		Spring reactions	
	Abutment	Pile	Abutment	Pile
SPAN	% increase	% increase	% increase	% increase
m				
10	0,00%	0,00%	0,00%	0,00%
20	407,16%	3128,84%	233,33%	519,05%
30	1077,56%	12627,27%	468,63%	1104,76%
40	2010,77%	36890,60%	647,06%	1657,14%

Table 4.3: Table showing the percentage increase in bending moment for abutment and piles vs the increase in spring reaction

4.2.8 3D Grillage Model – Spring Sensitivity study for shorter piles

Further to the above, a brief pile length sensitivity analysis, whereby the pile length was shortened to half its length (6m), was undertaken. The results of this analysis are shown below in the following Figures.

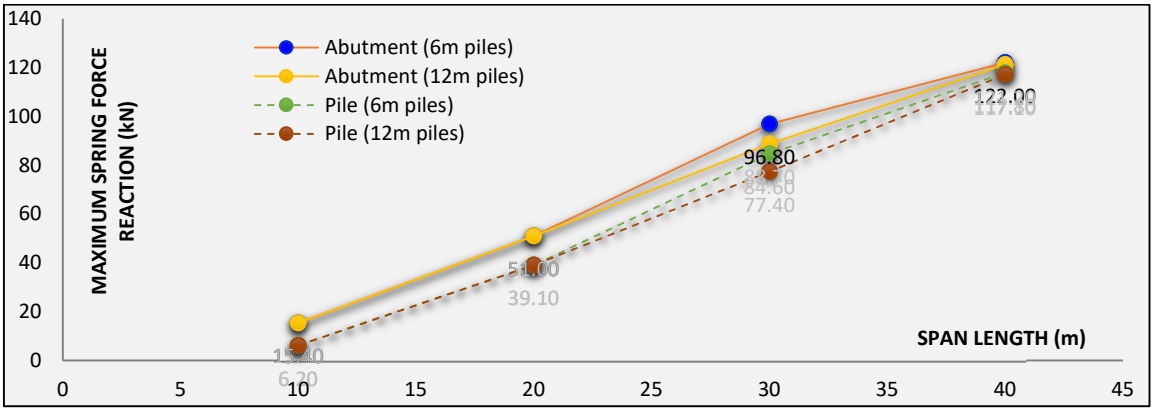

Figure *4.42*: Maximum spring reactions for piles and abutments – 3D Grillage model with 6m long piles and 12m long piles, founded in stiff clay, 3m high abutments, 60% Live load

As can be seen from **Figure 4.42** and **Figure 4.43**, the difference in the spring response is marginal when using the shorter length piles. In reality, the shorter the piles get, the stiffer and less flexible they become, thereby attracting more load. One can see that the 6m pile spring reaction is slightly larger than the 12m pile reaction for this very reason. Further testing with even shorter piles would be necessary to get a full picture of the pile length effect in relation to the spring reactions.

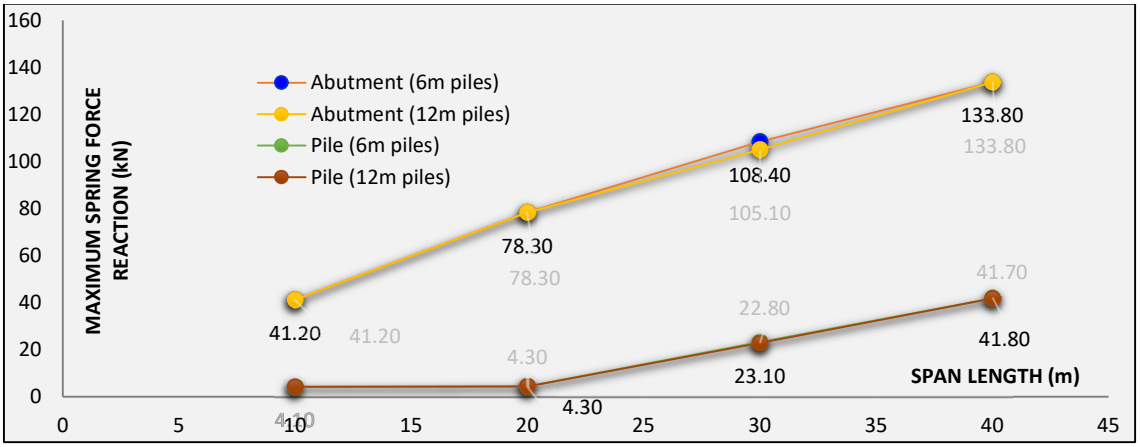

Figure *4.43*: Maximum spring reactions for piles and abutments – 3D Grillage model with 6m long piles and 12m long piles, founded in stiff clay, 3m high abutments, 15^{O}C temperature decrease.

Note that the pile spring forces for the 6m and the 12m long piles are almost exactly the same, hence they are practically indecipherable from each other in the above **Figure *4.43*** graph (similarly for the abutments).

4.3 Reactions tables

The results of the various analysis tables are shown in Appendix C.

4.4 Reflection

An overall reflection on the results obtained above shows that the founding conditions have quite a significant effect on the spring reactions, for deck spans increasing from 20m onwards (eg. **Figure *4.5***, **Figure *4.15*** and **Figure 4.16**), with a more pronounced effect being seen in the piles of the 3D Grillage model – most likely due to their slenderness and lack of stiffness in comparison to the abutments.

In other instances, the shorter abutment height (3m abutment) with corresponding increased stiffness has resulted in higher spring forces being generated than the taller abutment (9m abutment, which is more flexible) – examples of this are seen in **Figure *4.7***, **Figure *4.13*** and **Figure *4.20***.

Note that the maximum spring forces in the 2D models are higher than those in the 3D Grillage models because the 3D Grillage models have a maximum spring tributary area of 1m x 1.2m, whilst a typical 2D spring has a tributary area of 1m x 8.4m.

Also in relation to the 2D models, comparisons can be made between the magnitudes of the maximum spring reactions for live loading, contraction (Dobry and Gazetas model) and expansion (O' Brien & Keogh) loading – such a comparison is tabulated below in **Table 4.4**. Note that for the purposes of comparison, the Live load model results shown here are for the Upper Bound solution, and that the temperature variation loading applied to both the expansion and contraction models is a 30° temperature load. One can see that the 2D expansion model generates significantly smaller forces in comparison to the 2D contraction forces model.

Live load variability (for variable span lengths)					Spring model on flexible supports – Contraction (2D Model) Dobry & Gazetas	Spring model on flexible supports – Expansion (2D Model) O' Brien & Keogh
Span length (m)	Horizontal Reaction (kN) - Upper bound					
	% Live load applied					
	20% LL - UB	40% LL - UB	60% LL - UB	80% LL - UB		
10	61.63	123.23	184.85	246.50	224.24	310.05
20	286.50	572.99	859.49	1146.00	899.42	409.05
30	749.41	1498.82	2248.23	2998.00	1864.47	479.93

Table 4.4: Table of Abutment maximum spring reactions for Live load and temp rise/fall

The contraction spring forces are similar in magnitude to the 60% LL case. The reason why the contraction loadcase has higher reactions could be due to the fact that the model includes a rotational spring which attracts additional stiffness. The contraction model furthermore has a point spring for horizontal force resistance (see **Figure C.6**), whereas the conventional spring model that is described by O'Brien &Keogh has the springs spread out across the abutment face (which is more realistic, but results in smaller forces) – see **Figure B.11**.

In consideration of the deflection diagrams, it makes sense that the abutment deflection would be larger than the pile deflection for the temperature rise or temperature decrease loading case, since the deck is the element that increases or decreases in length (directly causing the abutment to translate into or away from the backfill), while the pile bends and follows its behaviour on (to a lesser degree) from the abutment translation (as can be seen in **Figure *4.40*** and **Figure *4.41***). This is not the same however in the case where live loading is applied, as can be seen in **Figure *4.32***, **Figure *4.34*** and **Figure *4.39***, where a different form of bending is clearly occurring in the deck/abutment system, causing the piles to have larger lateral deflections than the abutments.

In many instances, linear behaviour in the spring reactions was clearly seen with increases in deck span – this would most likely be seen in actual design practice and would not have been possible if the models had not been setup in such a linear fashion (with standardized increases in model spring and element dimensions) to start with. This increase in element dimensions with span would be expected in a real design case scenario, although not all sizes that were used would necessarily be the choice of the bridge designer in the final analysis. Examples of this linear behaviour are **Figure *4.11*** and **Figure *4.12***. Examples of non-linear behaviour are found in **Figure 4.16**, **Figure *4.18*** and **Figure 4.26** where the effects of the non-linear pile (P-Y) responses coupled with pile flexibility have clearly also had an impact on the spring reactions that were produced.

Certain results make intuitive sense, such as **Figure *4.14*** and **Figure 4.26** (the higher the abutment, the less pile spring force will be generated in the pile) or **Figure *4.11*** (the higher the applied load, the higher the spring reaction force). **Figure 4.25** shows that no matter what the live load is, the ratio between the abutment and pile force remains the same with increasing deck span – this is despite the increase in spring reaction with increasing span that is seen in **Figure *4.11*** and **Figure *4.12*** with increasing live load.

The tables below (**Table 4.5** and **Table 4.6**) show a comparison between the maximum spring reaction forces for the live loads vs the temperature rise and fall load cases in the abutments and the piles respectively for the 3D Grillage models, with 3m high abutments in stiff clay.

	Horizontal Spring Reaction (kN) - ABUTMENT					
Span length (m)	Live load variability				Temperature loading	
	% Live load applied				(15° RISE in Temp)	(15° FALL in Temp)
	20% LL	40% LL	60% LL	80% LL		
10	5.10	10.20	15.40	20.50	41.20	0.00
20	17.00	34.00	51.00	68.00	78.30	0.00
30	29.00	58.00	88.70	120.60	105.10	0.00
40	38.10	77.50	121.20	166.30	133.80	0.00

Table 4.5: Table of Abutment maximum spring reactions for Live load and temp rise/fall

The abutment temperature loading reactions (**Table 4.5**) are in general higher than the pile load reactions (**Table 4.6**), and the temperature rise case has generated reactions which are not too different from the 80% LL case. This can be attributed to the fact that the abutment is directly impacted by rising temperatures in the deck, and therefore generates significant reactions.

	Horizontal Spring Reaction (kN) - PILES					
Span length (m)	Live load variability					
	% Live load applied				(15° RISE in Temp)	(15° FALL in Temp)
	20% LL	40% LL	60% LL	80% LL		
10	2.10	4.10	6.20	8.30	4.10	2.00
20	13.00	26.10	39.10	52.10	4.30	8.40
30	25.30	50.60	77.40	105.30	22.80	17.50
40	36.90	75.10	117.10	160.30	41.70	28.60

Table 4.6: Table of Pile maximum spring reactions for Live load and temp rise/fall

The pile reactions that are shown in **Table 4.6** show that the temperature fall case in general has smaller reactions in comparison with the temperature rise case, and that the 20% LL case has created similar reactions to the 15° C Temp rise case reactions.

The study of the maximum abutment/pile spring reaction ratio under live loading has been useful as it has shown the surprising result that the spring reaction ratio tends towards unity as the span is increased (**Figure 4.26**). This is especially curious since the equations that define the stiffness calculations for the abutments and the piles are quite different from each other. This result is possibly due to the 'homogenization' of the abutment/pile system as the span increases in terms of its response to loading. Also note that the formula in Equation 61 shows a reduction in lateral spring stiffness with increasing span for the abutments – this is most likely why the spring reaction in the abutment gets smaller with increasing span. The diagrams and analysis of the spring reactions has shown some interesting results and has shown intriguing relationships between the calculated spring stiffnesses and the spring reactions generated (eg. **Figure *4.9***). The results have shown that while one needs to appreciate the variables that go into the formulas used to calculate spring stiffnesses, these appear to not always be the only defining characteristic in the determination of the final spring reactions (flexibility and element stiffness also play a role).

The limitations in the models that were setup are discussed in Section 3.10 and future study possibilities are discussed at the end of the Conclusions Chapter. The lessons learnt in the interpretation of the diagrams found in the above section can be applied to the initial element sizing of an integral bridge since the larger the spring reactions, the larger the element will tend to be.

5 CHAPTER 5 - Conclusion and Recommendations

General

This work has studied the soil-structure analysis of integral bridges and the characteristics of the spring reactions that pertain to the analysis of the single span integral type bridge. Usually, when one is designing an integral bridge structure, there is an iterative effort required in order to calculate the longitudinal displacement and corresponding abutment backfill pressure – this is as described in the PD6694-1:2011 code. In terms of the iterative analysis recommended by this Code, this thesis has focussed on the first iteration that one would undertake in the soil-structure interaction analysis.

The spring reaction forces (from the abutments and the piles) vary from season to season and from day to night. These forces determine the integral bridge behaviour in the modelling that is undertaken for the integral bridge structure (Arup, 2011). The significance therefore of comparing and examining the properties of these spring reactions is invaluable to understanding the likely outcomes of the analysis, as well as the sizing of the elements.

The study has essentially confirmed the basic hypothesis that 3D models using realistic spring properties are required in order to capture the true behaviour of the integral bridge springs (and the soil-structure interaction). In addition, the simplified 2D models have provided insight and some basic understanding of the spring behaviour and characteristics.

Traditionally, the bending moments and shear forces in the abutments and the integral bridge deck have been examined by various authors, with live loading factors being considered (eg. Dicleli and Erhan, 2009), the optimization of pile shapes, the backfill pressure characteristics induced by temperature and shrinkage (Skorpen, 2018), investigations into the ultimate integral bridge length attainable (Lan, 2012), performance under seismic loads, etc. In the model testing used in this thesis however, the spring reactions alone were considered with the view to understanding what their characteristics might be, under various parametric loading, founding and geometric variances. It should be noted that the theory used for calculating abutment spring reactions (Lehane, 1999) vs. the theory used for calculating pile spring reactions (Elson, 1984) are quite different from each other and depend on different factors, as described under Section 2.3.3 and 2.5. This made for a challenging literature review since different authors refer to different computational methods for these spring value calculations.

One of the other challenges in this thesis was that despite the fact that there are numerous studies on integral bridge behaviour, there is a lack of studies and understanding in the consideration of the spring reactions on the abutments and the piles themselves. The springs are a point of interest due to their non-linear behaviour in real-world bridge behaviour. Furthermore, there is a plethora of confusing terms for the soil's lateral subgrade reaction and Young's Modulus, with various authors - Bowles (1997), Craig (1997), Elson (1984) producing not just independent values, but also independent terminology for the various soil types and parameters. A further challenge that was encountered was the problem of how to ensure that each model related to the other models in a particular series (eg. 3m high abutments, with 10m, 20m and 30m spans) in a similar way, so that analysis results would be meaningful. This challenge was overcome by ensuring that beam span-to-depth ratios were relatively consistent and kept within a narrow margin of tolerance. Similar thinking was applied to the sizing of the abutments and piles (maintaining a 1:1 ratio for inertia of the deck to inertia of the abutment), which ensured that a consistent approach was applied to the sizing of elements in the creation of each model. In practice and in the normal course of a bridge design, these limits may not necessarily be used exactly as they have been used here in this thesis.

In order to study the changes to the spring reactions in various scenarios, a set of 2D Prokon line models (representing bridges on footings) as well as a series of 3D MIDAS Civil grillage beam and slab models (for bridges on piles) were setup and analysed for their maximum abutment and pile spring reactions. The 2D Prokon models are simple representations of an integral bridge, using different elastic support theories that are described in publications by Hambly (1991) and O'Brien and Keogh (1999), where the soil resistance is modelled as either a single spring (located at the top of the abutment), or as a series of springs. The 3D models provide a more accurate assessment of the parametrically varied structures, and this includes a more advanced representation of the springs (including non-linear effects as well as the ability to be made redundant when in tension) as well as the entire bridge deck/abutment structure. In the model loading, live load was applied as a series of line loads to the models, based on varying percentages of load that are related to the dead (DL) + superimposed dead (SDL) loading of the bridge deck. Temperature expansion and contraction loads as well as temperature gradients were also examined in this study. The parameters of span length, abutment height, soil condition and loading were investigated in the modelling and their effects on maximum abutment and pile spring reactions was studied through the series of analysis models and subsequent graphical/tabular interpretation of the results. Spring reaction rate of increase vs bending moment (B.M) rate of increase was also compared for the abutments and the piles in a limited study, and while some correlation is evident (although rates of increase are very different), this aspect could be studied in detail, in further studies.

A short study on the sensitivity of the pile length was also included which showed that for the lengths studied there was very little effect on the spring reactions. Note that in regard to the parametric variation in soil conditions, the abutments were always provided with a granular backfill, and that the variation in founding conditions was applicable to the piles only for the 3D MIDAS modelling. Conversely, in the 2D Prokon models, the variation in soil founding condition was applied to the abutment/footing springs. Note also that only the 3D models allow for creep and shrinkage effects in the material whilst the 2D models do not allow for these effects. Concrete cracking effects were also not included as the analysis assumed a degree of linearity in the material behaviour.

Verifications

Some basic verification studies were undertaken, and the results of these studies are shown in Appendix D. Some reasonable agreement was found between the two 3D Grillage models that were setup, and the free expansion analysis (temperature loading) proved to be a useful tool in estimating the pile moments, although this was found to be very dependent on the assumed pile length. Certain 2D frames were used to compare results with each other, and these provided for order of magnitude checks only.

Conclusions

As mentioned above, the spring reaction results were plotted graphically for maximum spring reaction vs span. Further analysis of results was done using the ratio of maximum abutment spring/maximum pile spring, as well as the total load per pile vs the spring reaction. From these results, it may be concluded that the spring reactions and spring stiffnesses clearly depend on the soil conditions, the bridge geometry and the applied loads. The main conclusions that may be drawn from the model testing are as follows:

- In regard to the case where live loading only is increased in the models (with no other geometric changes being made), the spring reaction graph shows lines with gradients that tend to increase (the spring reaction vs span graphs get steeper) as the live loading is increased. This implies that the rate of spring reaction tends to increase, the larger the live load that is applied. The implication for design is that one would expect larger responses, larger forces and bending moments in the bridge elements (piles, deck and abutments) as the applied loading increases.

This should be borne in mind by bridge designers when assessing integral bridges for super-heavy loads as significant abutment backfill strain may occur.

- For the span range 10m - 20m, the effects of foundation soil type (whether clay or sand) made very little difference to the abutment spring reactions (see **Figure 4.5** and **Figure 4.15**). After the 20m span is exceeded, the effects of the foundation soil type made more of a difference in the spring reaction results.
- With reference to **Figure 4.16**, after the 20m span is exceeded, the pile springs in stiff clay founding conditions exhibit a linear spring reaction progression with increasing span, whilst the soft clays undergo a softening (with little spring reaction development). The non-cohesive materials undergo significant pile spring reaction increase as the spans get longer – this could be attributed to their increased densification. Clearly therefore, the founding soil type can play a significant role in pile member sizing for spans exceeding 20m.
- The temperature contraction load case modelling showed that the 'temperature resistance' of the bridge structural system was mostly generated by the bridge piles, with no reactions arising in the abutments. The recommendation therefore would be for designers to be aware of this phenomenon, by ensuring that the load case is correctly included in the analysis, and to appropriately size the piles for such temperature contraction resistance effects. Similar effects were found for the temperature gradient loadcases, with a lack of reaction being generated in the abutments. Needless to say, in practice one would combine these reactions with dead and live loading, which would mean that there would most likely be abutment reactions created as a result of the load combination effect. Certain conclusions in relation to raw loading may not hold when the combination of loads is taken into consideration – eg. temperature contraction loading, when combined with dead load will most likely activate the abutment springs.
- The temperature expansion loadcase modelling has shown that significant spring reactions can be created towards the top of the abutment, and this can create forces which are similar in magnitude to highly loaded live loading scenarios (eg – see results shown in **Table 4.5**). Further analysis has shown however that this does not necessarily translate into higher bending moments in the abutment (see comments made in the text, in relation to bending moments after **Figure *4.35***).
- Of significance in the understanding of the load resistance sharing between the piles and the abutment, is the bending and force effects from the lever arm that develops between the deck and the abutment as the abutment is made higher (as seen in **Figure 2.49**). This is demonstrated by the non-linear load sharing when comparing the graphs of **Figure 4.13** and **Figure 4.14** (for example). The model testing showed that for the smaller spans, the higher abutment heights generated significantly more spring reaction than in the piles (see **Figure 4.26**) – this would imply that the abutments could possibly be made larger in dimension than the piles in this scenario, but also that the designer should be careful before using higher abutments as they tend to attract significant forces in them due to the SSI effects.
- The non-linear response of piles under lateral loading was demonstrated in graphs such as those found in **Figure 4.14**, **Figure 4.16** and **Figure 4.18**.
- An unexpected result was that the model testing showed that as the span lengths increase, the abutment and pile spring maximum loads tend to converge and become the same, ie. they match each other in magnitude. The inference of this is that one should expect to see that pile and abutment elements are similarly sized, the longer the span length used in the design. This effect is demonstrated by the graph found in **Figure 4.26**.
- One can see in comparing the behaviour of the springs for the footings vs. the springs for the piled structures:- the springs for the footings generally behaved linearly, whilst the springs for the piled structures in general behaved non-linearly. This difference could be attributed to the non-linear behaviour of the piles themselves under the lateral loading, as well as the spring properties assigned to the models.

- What has become apparent in the model results and testing is that it is important to understand the effect of changing the variables for the equations that underly the calculation of the spring stiffness values (eg. Equations 22-24, 29-31, 34 and 41). Values such as pile diameter, deck span, abutment height and soil type have either a proportional or an inversely proportional effect in the spring stiffness calculation – the results of these calculations are documented in **Table 3.5** to **Table 3.9**, and the corresponding soil spring reaction has in general not been completely aligned with the spring stiffness calculation. This effect is specifically evident when observing the results in the 2D frames, where the combination of diminishing spring stiffness has not always resulted in decreased spring reaction, for reasons that are most likely related to the element stiffness and flexibility.

South Africa has many examples of jointed bridges which over the years of service have tended to develop leaks in their joints, with consequent staining of the reinforced concrete and general lack of aesthetic. Examples of integral bridges are few and far between in South Africa. The integral bridge is a more robust solution which does not have these particular durability issues, and it would be hoped that designers would use the lessons learnt from this thesis to improve their understanding of how these bridges behave, with an accompanying increase in them being specified for use around the country.

Recommendations

The following recommendations may be made from inferences regarding the test results:

- Bridge designers should take greater cognisance of the effects of soil founding conditions for spans greater than 20m. This may especially be applicable to design scenarios where seismic forces are prevalent. From the author's previous design experience with bridges in seismic regions, the effects of soil founding conditions can have a profound effect on the bridge response (hence the differing response spectrum curves that the various codes of Practice specify; eg. AASHTO LRFD).
- The bridge designer should check and be cognisant of the effects of deck temperature expansion and contraction on the integral bridge design, especially in regard to the pile design for deck contraction, and to the abutment design in regard to temperature expansion. Although this is normally done in the course of design, the results have highlighted the effects that one needs to be aware of.
- The designer should verify the sizing ratio of bridge elements, bearing in mind the abutment height to span ratio.
- The designer should be aware of the influence of the parameters of deck length and pile diameter on the calculation of spring stiffness for the abutments and piles. Despite the influence of spring stiffness however, the element stiffness and flexibility may play a larger role in determining the spring reaction. A lack of good correlation has been shown in this thesis between the magnitude of the spring stiffness vs the magnitude of the spring reaction as evidenced in certain graphs that have been produced (in other words, if the formula for the calculation of spring stiffness shows that the spring stiffness is diminishing in magnitude with increasing span, this does not necessarily always imply that the spring reaction will also diminish with increasing span).
- The effects of super heavy loading on integral bridges should be carefully considered, and the strain effects on the abutment backfill should be checked.

Further research opportunities

The approach of studying the spring reactions is a relatively new one and it may be applied again in a parametric type study in further research opportunities. The analysis work covered in this thesis is therefore the foundation for an approach that could be applied to various other topics. As an example, one could examine the effects of seismic loading on the integral bridge spring reactions, or one could consider the impact of rail-structure interaction (RSI) on the spring reactions.

Looking forward, there are significantly more testing and model regimes that could be considered, that will add to the general knowledge of integral bridge type behaviour in regard to the spring reactions. These have already mostly been highlighted in the section above entitled "Limitations of the modelling simulations", however, to re-iterate:

- Further simulations using longer spans, multi spans and with different degrees of skew could be considered in order to understand the spring reaction characteristics of these bridges and the effects that the intermediate piers would have on the load sharing characteristics of the abutment and pile springs.
- More intermediate points (intermediate spans) could be added to the graphs that have been produced thus far.
- Rates of increase for BM and Shear force vs rates of increase for spring reaction could be studied in further detail, with more load types being considered.
- The use of composite steel bridges could also be considered.
- The use of different abutment backfill material could be investigated, from a spring reaction point of view, as well as with the view to understanding any changes that may occur in relation to the centre of the backfill reaction force vs the deck centre.
- Wing walls could be added to the models, to improve the overall accuracy and realism of the modelling.
- The effects of including an approach slab could be studied. The use of an approach slab adds frictional resistance to the deck's expansion and contraction and its effects on spring reactions are unknown at this point in time.
- The effects of pile sizing and further studies relating to the pile length, on the spring reactions could be studied and included.
- Various vehicle loads from different respected international codes could be included in the modelling process.
- Further variations in the bridge temperatures and gradients could be considered (only 3m high abutments were tested for temperature gradient loads).
- Since there is a wide variation in where the maximum spring reaction occurs across the abutments and piles, a variance in overall deck width could be studied.
- The 3D grillage modelling study could be extended to include the normal pad footing foundation solution.
- Spring reactions for semi-integral bridges could be included in the research.
- Effects of the inclusion of pin type joints between the Abutment pilecap and the piles could be included in the modelling.
- Sleeved piles could be used in the modelling process.
- Additional studies could be undertaken where the energy of the system is considered – this could easily be done, by considering the bridge deflections, and translating this into spring energy equations.
- Studies considering the lateral loading from behind the abutment (vehicle travelling over the bridge) could be undertaken.

REFERENCES

1) AASHTO. (2012) *AASHTO LRFD Bridge Design Specifications, SI Units, 4th Edition*. American Association of State Highway and Transportation Officials, Washington.

2) Andersen, K.H., Pool, J.H., Brown, S.F. & Rosenbrand, W.F. (1980). *Cyclic and static laboratory tests on Drammen clay*. ASCE, J. of Geotech. Eng., 106, (5): 499–529.

3) American Society of Agricultural and Biological Engineers (ASABE). (2012) *ANSI/ASAE EP486.2. Shallow post and pier foundation design*. St. Joseph, Mich.: ASABE.

4) Al-Ani M, Murashev A, Palermo A et al. (2018) *Criteria and guidance for the design of integral bridges.* Proceedings of the Institution of Civil Engineers – Bridge Engineering 171(3): 143-154.

5) Arockiasamy, M., Butrieng, N., and Sivakumar, M. (2004) *State-of-the-art of integral abutment bridges: Design and practice*. Journal of Bridge Engineering, 9(5), 497-506.

6) Arsoy, S., Duncan, J.M. and Barker, R.M. (1999) *The Behaviour of Integral Abutment bridges*. Virginia transportation research council, Charlottesville, Virginia.

7) Arthur, J. R. F, Dunstan, T. and Chua, K. S. (1977) *Induced anisotropy in sand*. Geotechnique 27, 13-30.

8) Arthur, J. R. F, Dunstan, T., Chua, K. S. and del Rodriquez, C. (1980) *Principal stress rotation: a missing parameter*. Proceedings of the ASCE 106 (GT4) 419-433.

9) Arthur, J. R. F, Dunstan, T., Dalili, A and Wong, R.K.S. (1991) *The initiation of flow in granular materials*. Powder technology 65, 89-101.

10) Ashford, S. (2005) *Effect of the pile diameter on the modulus of subgrade reaction*. Publication number SSRP–2001/22, University of California, San Diego. 322 p. + 32 app. p. ISBN 952-15-1620-8.

11) ASTRA. (2011) *Swiss directive on bridges building details "Chapter 3 – Bridges abutments"* (Directive "Détails de construction des ponts. Chapitre 3, extrémités de ponts" in french).

12) Banks KR and Bloodworth AG. (2018) *Lateral stress profiles on integral bridge abutments.* Proceedings of the Institution of Civil Engineers – Bridge Engineering 171(3): 155-168.

13) Bohnhoff, D. (2014) *Modelling soil behaviour with Simple Springs, Part 1 – Spring placement and properties*. Frame Building News.

14) Bohnhoff, D. (2014) *Modelling soil behaviour with Simple Springs, Part 2 – Determining the Ultimate Lateral Capacity of a Post/Pier Foundation*. Frame Building News.

15) Bowles, J. (1997) *Foundation Analysis and Design – 5th Edition*. McGraw-Hill, Singapore.

16) Bozorgzadeh A. (2007) *Effect of structure backfill on stiffness and capacity of bridge abutmetns, Thesis: PhD.* University of California, San Diego, California, USA.

17) Briseghella, B., Lavorato, D., Bergami, A. V., Rago, C., Ma, H. B., Nuti, C., Vanzi, I., Zhou, W. D. (2017) *Seismic behaviour of isolated RC bridges subjected to asynchronous seismic*

input. 6th *International Conference on Computational Methods in Structural Dynamics and Earthquake Engineering Methods in Structural Dynamics and Earthquake Engineering*, Rhodes, June 2017.

18) Broms, B. (1964a) *Lateral resistance of pile in cohesive soil*. Journal of Soil Mechanics Foundation Division, ASCE, 90(SM3):27–56.

19) Broms, B. (1964b) *Lateral resistance of pile in cohesionless soil*. Journal of Soil Mechanics Foundation Division, ASCE, 90(SM3): 123–156.

20) Broms, B. (1971) *Lateral Earth Pressures due to Compaction of Cohesionless Soils.* Proceedings of 4th Budapest Conference. Soil Mechanics, Sect. 2, 373 - 384 Budapest.

21) Burdet, OL. (2010) *Thermal effects in the long-term monitoring of bridges. Report presented at 34th IABSE Symposium on Large Structures and Infrastructures for Environmentally Constrained and Urbanised Areas*. Vol A-755, Venice, 2010. 7pp.

22) Burke, Jr., M.P. (1987) *Bridge Approach Pavements, Integral Bridges and Cycle Control Joints*. Transportation Research Record 1113, TRB, National Research Council, Washington, D.C., 1987.

23) Burke, Jr., M.P. (1996) *The genesis of integral bridges in Ohio*. Concrete International, Vol. 18, July, pp. 48-51.

24) Burke, Jr., M.P. (2009) *Integral and semi-integral bridges*. Chichester (Royaume-Uni), Wiley-Blackwell. http://www.dawsonera.com/depp/reader/protected/external/AbstractView/S9781444316377/S52.6

25) British Highways Agency. (1996) BA 42/96 - 3.5.3 *The Design of Integral Bridges [Incorporating Amendment No. 1 dated May 2003] Highways Agency*, HMSO, London, UK.

26) Briaud, Jean-Louis; James, R. W.; and Hoffman, S. B. (1997) *Settlement of bridge approaches (The bump at the end of the bridge)*. National Academy Press, Washington, D.C., pp. 75.

27) Byrne, G., Chang, N., Raju V. (2019) A Guide to Practical Geotechnical Engineering in Africa – Fifth Edition. Franki – Keller.

28) Card G. B., Carder D. R. (1993) *A Literature review of the Geotechnical aspects of the design of Integral bridge abutments – Project Report 52*. Transport Research Laboratory, Berkshire.

29) Caristo A, Barnes J and Mitoulis SA. (2018) *Numerical modelling of integral abutment bridges under seasonal thermal cycles*. Proceedings of the Institution of Civil Engineers – Bridge Engineering 171(3): 179-190.

30) Clayton, C. R. I., Xu, M., and Bloodworth, A. (2007) *A laboratory study of the development of earth pressure behind integral abutments*. Géotechnique, 56(8), 561–571.

31) Committee of State Road Authorities. (1981) *TMH7 Parts 1 and 2: Code of Practice for the Design of Highway Bridges and Culverts in South Africa*.

32) Concrete Society, The. (2010) *Integral Concrete bridges to Eurocode 2*. Surry: CCIP Publications.

33) Connal, J. (2004) *Integral Abutment Bridges - Australian and US Practice.* Hobart: Austroads.

34) Craig, R.F. (1997) *Soil Mechanics – Sixth Edition*. E & FN Spon, New York.

35) Davies, L., Bull, J. and Kucki, T., (2014) *Lightweight backfill materials in integral bridge construction*. In Proceedings of the Institution of Civil Engineers-Bridge Engineering (Vol. 167, No. 1, pp. 3-16). Thomas Telford Ltd.

36) Danish Geotechnical Institute. (1978) *Code of Practice for Foundation Engineering*. Danish Geotechnical Institute, Bulletin No. 32, p 52.

37) Dicleli, M. (2000) *A rational design approach for prestressed-concrete girder integral bridges*. Engineering Structures, 22(3), 230-245.

38) Dicleli, M and Erhan, S. (2009) *Effect of superstructure-abutment continuity on live load distribution in integral abutment bridge girders*. Structural Engineering and Mechanics, Vol. 34, No. 5 (2010) 000-000.

39) Dobry, R. and Gazetas, G. (1986) *Dynamic response of arbitrarily shaped foundations*, ASCE J. Geotech. Eng., 112(2), 109–35.

40) Dreier, D., Burdet, O., & Muttoni, A. (2011) *Transition Slabs of Integral Abutment Bridges*. Structural Engineering International, 21, 144 - 150.

41) Dunstan, T. Arthur J. R. F.,Dalili A. Ogunbeken, O. O and Wong, R. K. K. (1988) *Limiting mechanisms of slow dilatant plastic shear deformation of granular media*. Nature 336, 52 – 54.

42) Elson W.K., (1984) *CIRIA Report 103 - Design of laterally-loaded piles*. Construction Industry Research & Information Association (CIRIA).

43) England, G.L, (1994) *The performance and behaviour of biological filter walls as affected by cyclic temperature changes. Serviceability of earth retaining structures*. ASCE Geotechnical Special Publication 42, 57-76.

44) England, G.L., Tsang, N.C.M and Bush, D.I. (2000) *Integral Bridges: A fundamental approach to the time-temperature loading problem.* Thomas Telford, London.

45) Emerson, M. (1973) *The Calculation of the Distribution of Temperature in Bridges*. Transport and Road Research Laboratory (TRRL) Report 561.

46) Emerson, M. (1976) *Bridge temperatures estimated from the shade temperature*. TRRL Report 696.

47) Emerson, M. (1977) *Temperature Differences: Basis of Design Requirements*. TRRL Report 765.

48) Faraji, S., Ting, J.M. and D.S. Crovo. (2001) *Nonlinear Analysis of Integral Bridges: Finite Element Model,* Journal of Geotechnical and GeoEnvironmental Engineering: 454-461.

49) Fib, (2010) *Fib Model Code for Concrete Structures 2010*, Ernst & Sohn GmbH & Co. KG.

50) Flener, E.B. (2004) *Soil-Structure Interaction for Integral Bridges and Culverts*, Licentiate Thesis, Royal Institute of Technology, Stockholm.

51) Frank, R., Bauduin, C., Driscoll, R., Kavvadas, M., Krebs Ovesen, N., Orr, T. and Schuppener, B. (2004) *Designers' Guide to EN 1997-1, Eurocode 7: Geotechnical design - General rules*. Thomas Telford Ltd, London, UK.

52) Frosch, R., Lovell, M. (2011) *Long-Term Behaviour of Integral Abutment Bridges*. Purdue University, West Lafayette.

53) Frosch, R.J., Kreger, M.E. and Talbott, A.M. (2009) *Earthquake Resistance of Integral Bridges*. Joint Transportation Research Program, p.324.

54) Gaba, A.R, Simpson. B, Powrie, W., Beadman D. R. (2003) *CIRIA 580 – Embedded retaining walls – Guidance for economic design*. 6 Storey's Gate, Westminster, London SW1P 3AU.

55) Gergess, A. (2019) A*nalysis of Bonded Link Slabs In Precast, Prestressed Concrete Girder Bridges.* Pci Journal. 64. 47-65. 10.15554/pcij64.3-03.

56) Gerolymos, N., Escoffier, S., Gazetas, G., and Garnier, J. (2009) *Numerical Modelling of Centrifuge Cyclic Lateral Pile Load Experiments*. Earthquake Engineering and Engineering Vibration 8 (1): 61–76.

57) Griemann, L.F., Abendroth, R.E., Johnson, D.E et al. (1987) *Pile design and tests for integral abutment bridges*. IOWA DOT Project HR-273. Iowa State University, Ames.

58) Hambly, E.C. (1991) *Bridge deck behaviour – Second Edition*. Taylor & Francis, Bath.

59) Haynes J. (2014) *Bridge Engineering Module Handbook Level 7 2014-15*. Salford University.

60) Highways Agency / Arup. (2011) *Guidance on Integral Bridge design and Construction – Commentary on PD 6694-1 (2011) Clause 9 Integral Bridges*. Scotstoun House, South Queensferry, West Lothian, England.

61) Hoppe, E. J. and Gomez, J. P. (1996) *Field study of an integral backwall bridge*, Virginia Transportation Research Council, VTRC 97-R7, October 1996, 47 p.

62) Hoppe, E.J. (2005) *Field Study of Integral Backwall with Elastic Inclusion*. Virginia Transportation Research Council, Charlottesville, pp. 36.

63) Horvath, John. (2000) *Integral-Abutment Bridges: Problems and Innovative Solutions Using EPS Geofoam and Other Geosynthetics*. 10.13140/RG.2.2.30823.09128.

64) Horvath, John. (2005) *Integral-Abutment Bridges: A Complex Soil-Structure Interaction Challenge.* Geotechnical Special Publication. 10.1061/40744(154)31.

65) Iles, D C. (2005) *SCI Publication P340 – Integral Steel bridges: A summary of current practice in design and construction.* The Steel Construction Institute.

66) Iles, D C. (2014) *SCI Publication P356 – Composite Highway Bridge Design in accordance with Eurocodes and the UK National Annexes (Including Corrigendum, March 2014).* The Steel Construction Institute.

67) INTAB. (2010) *INTAB Design Guide - Economic and Durable Design of Composite Bridges with Integral Abutments.* RWTH Aachen University, Germany.

68) Ishihara K. (1982) *Evaluation of soil properties for use in earthquake response.* Proc Int Symp. On Numerical Models in Geomechanics, Zurich, pages 237-259.

69) Jaky J. (1948) *Pressure in silos*. Proc. 2nd International Conference on Soil Mechanics and Foundation Engineering, Rotterdam, Netherlands, vol. 1: 103-107.

70) Javier R & Francisco M & Marti, Joaquin. (2011) *Integral Bridge for High-Speed Railway*. Structural Engineering International. 21. 297-303. 10.2749/101686611X13049248219881.

71) Jin, X. and Shao, X. (2004) *New technologies in China's first jointless integral-abutment bridge*, IABSE Reports, 88, 172-173.

72) Kim, W. et al. (2016) *Comparative study of integral abutment bridge structural analysis methods*. NRC Research Press, 389(43) pg. 378-389.

73) Kaufmann, W. (2009) *Integral bridges: State of practice in Switzerland. fib Symposium,Concrete: 21st century superhero: Building a sustainable future*, June 2009. Zagreb:Structural Engineering Conferences.

74) Kerokoski, O. (2006) *Soil-Structure Interaction of Long Jointless Bridges with Integral Abutments, PhD thesis*, Tampere University of Technology, Finland.

75) Krauthammer, T.; Kennelly, J.; and Abdelkarim, L. (1994) *Bridge superstructure research: Integral abutment bridges and their pile design*, Research Project 90-11, Commonwealth of Pennsylvania, Department ofTransportation, University Park, PA, August 1994, pp. 91.

76) Krier D. (2009) *Modelling of Integral Abutment Bridges Considering Soil-Structure Interaction Effects,* Thesis: Ph.D., The University of Oklahmoa.

77) Kumar, A. (1998) *Deck slab continuity for composite bridges*. *The Structural Engineer*. Vol 76, Nos. 23 & 24, December 1998, pp 447 to 458.

78) Kunin, J., and Alampalli, S. (1999) *Integral Abutment Bridges: Current Practice in the United States and Canada. Special Report 132*, Transportation Research and Development Bureau, New York State Department of Transportation.

79) Laaksonen, A. (2011) *Structural Behaviour of Long Concrete Integral Bridges*. (Tampere University of Technology. Publication; Vol. 978). Tampere University of Technology.

80) Lan, C. (2012) *On the performance of Super-Long Integral Abutment Bridges – Parametric analyses and design optimization*. University of Trento.

81) Lehane, B. (1999) *Predicting the restraint to integral bridge deck expansion*, in Proceedings of 12th European Conference on Soil Mechanics and Geotechnical Engineering, Amsterdam, Balkema, Rotterdam.

82) Liikenneviraston ohjeita (Finnish Transport Agency Guidelines). (2012) *Sillan geotekninen suunnittelu - Sillat ja muut taitorakenteet*, Liikennevirasto. Helsinki.

83) Maruri R., Petro S. (2005) *Integral Abutments and Jointless Bridges (IAJB) 2004 Survey Summary.* Federal Highway Administration (FHWA)/Constructed Facilities Center (CFC) at West Virginia University.

84) Marx, S & Seidl, G. (2011) *Integral Railway Bridges in Germany*. Structural Engineering International. 21. 332-340. 10.2749/101686611X12994961034534.

85) Mayne, P.W., and Kulhawy, F.H. (1982) *Ko-OCR Relationships in Soil*. Journal of the Geotechnical Engineering Division, ASCE, Vol 108, No. GT6, June, pp. 851-872.

86) Mattsson, H.A. and Sundquist, H. (2007) *The Real Service Life of Road Bridges*, Bridge Engineering, 160, 173-179.

87) Mitoulis S, Palaiochorinou A, Georgiadis I, Argyroudis S. (2016) *Extending the application of integral frame abutment bridges in earthquake-prone areas by using novel isolators of recycled materials*. Earthq Eng Struct Dyn. doi:10.1002/eqe.2760.

88) Nicholson, B.A. (1998) *Integral Abutments for Prestressed Beam Bridges*, Prestressed Concrete Association, Leicester, UK.

89) Nikravan, N. (2013) *Structural Design Issues for Integral Abutment Bridges*. Toronto: Digital Commons @ Ryerson.

90) Oesterle, Ralph & Tabatabai, Habib. (2014) *Design Considerations for Integral Abutment/Jointless Bridges in the USA*. Proceedings of the 1st International Workshop on Integral Abutment/Jointless Bridges, Fuzhou University, China, March 2014, pp. 71-101.

91) Oesterle, R. G.; Tabatabai, H.; Lawson, T. J.; Refai, T.M.; Volz, J. S.; and Scanlon, A. (1998) *Jointless and integral abutment bridges summary report*. CTL of Skokie, IL, to be published, under review by FHWA.

92) O'Brien, E., Keogh, D. (1999) *Bridge Deck Analysis*. New York: E & FN Spon.

93) PD 6694-1:2011. (2011) *Recommendations for the design of structures subject to traffic loading to BS EN 1997-1:2004*. BSi

94) Panday, A. (2015) *Recent trend to enhance bridge features. fib Symposium, Concrete – Innovation and Design*, May 2015. Technical University of Denmark.

95) Pétursson, H. (2015) *Design of Steel Piles for Integral Abutment Bridges*. Luleå University of Technology SE-971 87 Luleå.

96) Place, D., Farooq, I., and Tang, V. (2006) *Integral Bridges with Frame Abutments*, Proceedings of the 1st International Conference on Advances in Bridge Engineering. London, June 26-28.

97) Reese, L.C. and Matlock, H. (1956) *Non-dimensional solutions for laterally-loaded piles with soil modulus assumed proportional to depth*. Proceedings of the 8th Texas Conference on Soil Mechanics and Foundation Engineering, Austin, Texas, pp. 1–41.

98) Reese, L.C and Van Impe, W. (2011) *Single piles and pile groups under lateral loading, 2nd Edition*. CRC Press, Taylor and Francis Group. London, UK.

99) Rhodes, S. (2014) *Integral Bridges and the Modelling of Soil-Structure Interaction*. LUSAS.

100) Rombach, G.A. (2011) *Finite-element Design of Concrete Structures: Practical Problems and their Solutions (Second Edition)*, ICE Publishing, London, 2011.

101) Skorpen, S., Kearsley, E., Kruger, E. (2018) *Measured temperature and shrinkage effects on a 90m long integral bridge in South Africa.* Department of Civil Engineering, University of Pretoria.

102) Shah, B.R (2007) *3D Finite Element Analysis of Integral Abutment Bridges Subjected to Thermal Loading*, Kansas State University, Kansas.

103) Shah B.R., Peric D. and Esmaeily A. (2008) *Effects of Ambient Temperature Changes on Integral Bridges, K-TRAN: KSU-06-2*, Kansas State University, Manhattan, Kansas.

104) Springman S M, Norrish A. R. M. and C. W. W. Ng. (1996) *TRL146 - Cyclic loading of sand behind integral bridge abutments*. Transport Research Laboratory, Crowthorne.

105) Soltani, A. A. and Kukreti, A. R. (1992) *Performance Evaluation of Integral Abutment Bridges*, Transportation Research Record 1371; Committee on General Structures; 17-25.

106) Tatsuoka, Fumio & Tateyama, Masaru & Koda, Masayuki & Kojima, Ken-ichi & Yonezawa, Toyoji & Shindo, Yoshinori & Tamai, Shin-ichi. (2016) *Recent research and practice of GRS integral bridges for railways in Japan*. Japanese Geotechnical Society Special Publication. 2. 2307-2312. 10.3208/jgssp.IGS-03.

107) Terzaghi K., Peck R.B. (1967) *Soil Mechanics in Engineering Practice*. Wiley International Edition. University of Michigan.

108) Thomson T. A. (1999) *Passive earth pressures behind integral bridge abutments – PhD thesis*. University of Massachusetts, Amherst, Massachusetts, USA.

109) Tomlinson, M.J. (1994) *Pile Design and Construction Practice, 6th Ed*. E & FN Spon, London.

110) Wassermann, E. P., Walker, J. H. (1996) *Integral Abutments for continuous steel bridges*. Workshop on Integral abutment bridges, November 13-15, 1996, Pittsburgh, PA, 31 p.

111) White, H. (2007) *Integral Abutment Bridges: Comparison of Current practice between European countries and the United States of America*. Transportation Research and Development Bureau, New York.

112) White, H. (2008) *Wingwall Type Selection for Integral Abutment Bridges: Survey of Current Practice in the United States of America, Special Report 154,* Transportation Research and Development Bureau, New York State Department of Transportation.

113) Wolde-Tinsae, A. M., and Klinger, J. (1987) *Integral Bridge Design and Construction*. FHWA/MD-87/04. Maryland Department of Transportation, Hanover.

114) Wolde-Tinsae, A. M., Greimann L. and Yang P. S., (1988), *End-Bearing Piles In Jointless Bridges, Journal of Structural Engineering*, Vol. 114, No. 8, pp. 1870-1884.

115) Wood J, Murashev A, Palermo A (2015) *Criteria and Guidance for the Design of Integral Bridges in New Zealand.* New Zealand Transport Agency, Wellington, New Zealand, Research Report 577.

116) Xanthakos, P. (1994) *Theory and Design of bridges*. John Wiley and Sons Inc. USA.

117) Xu M., Bloodworth A.G.and Clayton C.R.I. (2007) *Behaviour of a stiff clay behind embedded integral abutments*. J. Geotech and Geoenvir. Engrg., 133, 6, 721-730.

118) Yang, Pe-Shen., Wolde-Tinsae, A.M., and Greimann, L.F. (1985) *Effects of predrilling and layered soils on piles*. Journal of Geotechnical Engineering, ASCE, Vol. 111, No.1, January, pp. 18-31.

119) Zordan, T., Briseghella, B., Lan, C., (2011) *Parametric and pushover analyses on integral abutment bridge*. Engineering Structures 33 (2), 502-515.

120) Zordan, T., Briseghella, B., Lan, C., (2010) *Optimized Design for Soil-Pile Interaction and Abutment Size of Integral Abutment Bridges.* ABSE Symposium Report. 34th International Symposium on Bridge and Structural Engineering, Venice, 2010.

A Appendix A – Spreadsheets used for model development

| MODEL IE RE NO | Analysis Model Summary | | |

| MODEL REFERENCE | Analysis Model Summary | | |

B Appendix B - Typical MIDAS and Prokon models

Prokon 2D models:

i) Shallow strip foundations (2D Model, using Hambly type model)

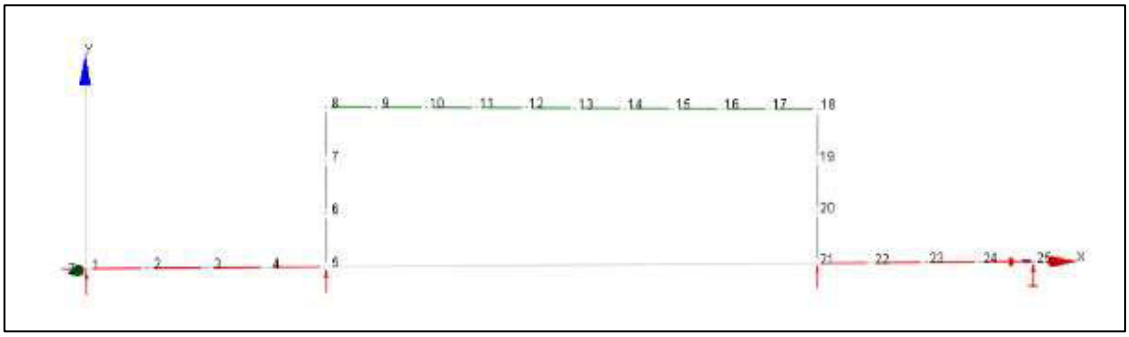

Figure B.1: Analysis model for 10m spans, 3m High Abutments

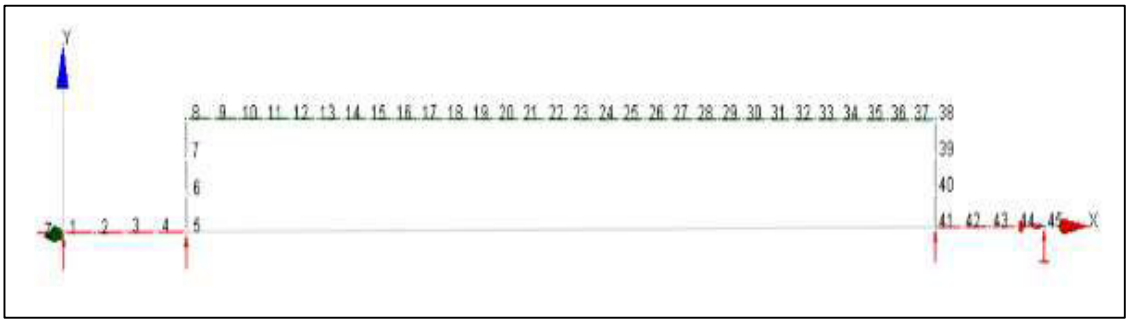

Figure B.2: Analysis model for 30m spans, 3m High Abutments

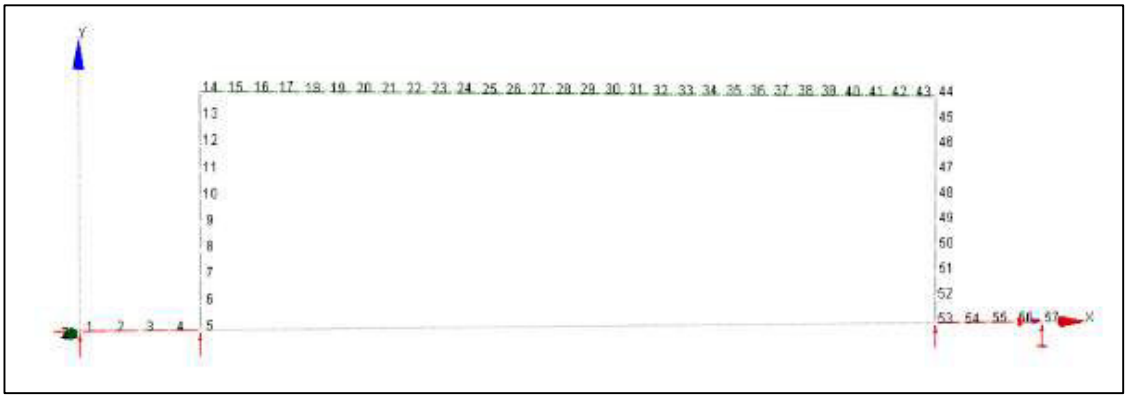

Figure B.3: Analysis model for 30m spans, 9m High Abutments

ii) Full 3D MIDAS spring models

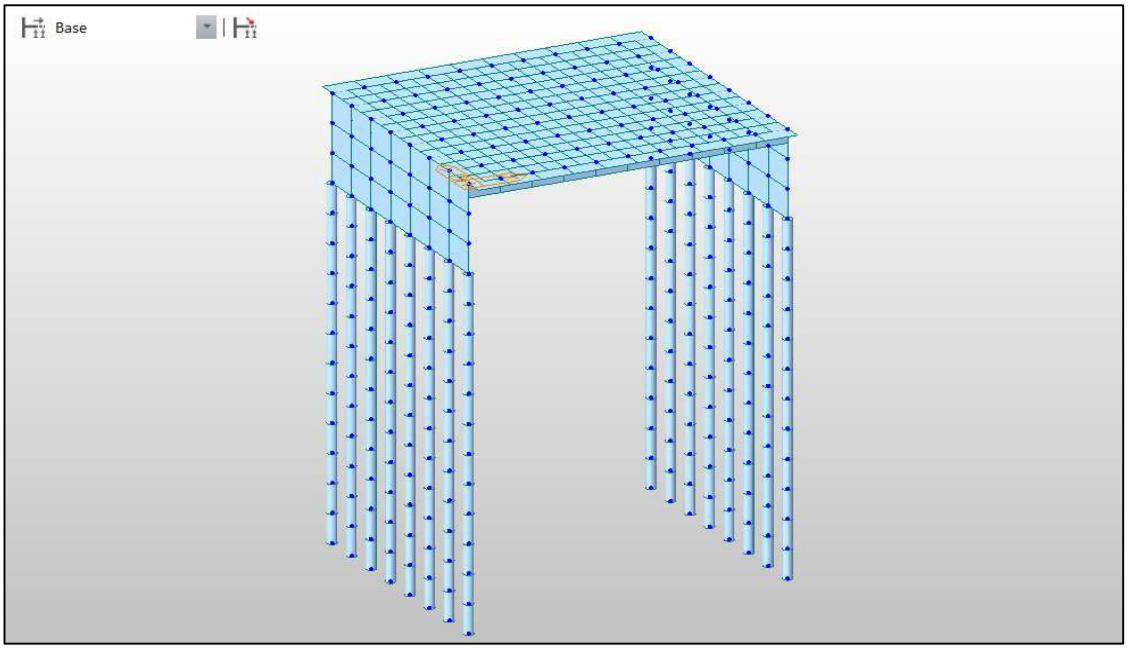

Figure B.4: 10m span 3D MIDAS Model with 3m deep abutments, 12m deep piles

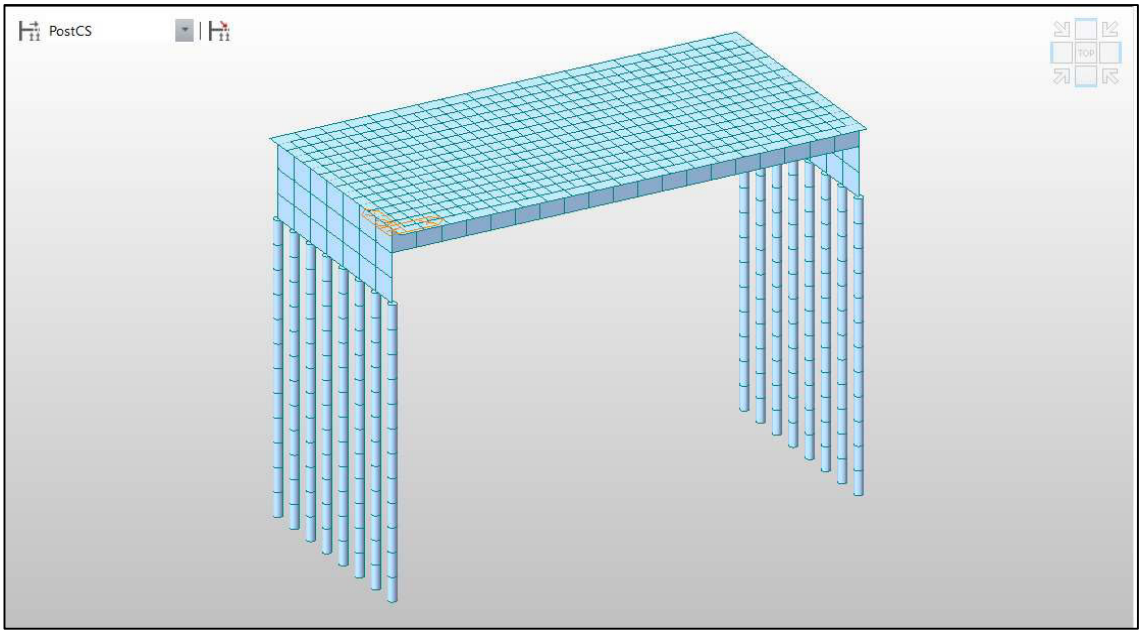

Figure B.5: 20m span 3D MIDAS Model with 3m deep abutments, 12m deep piles

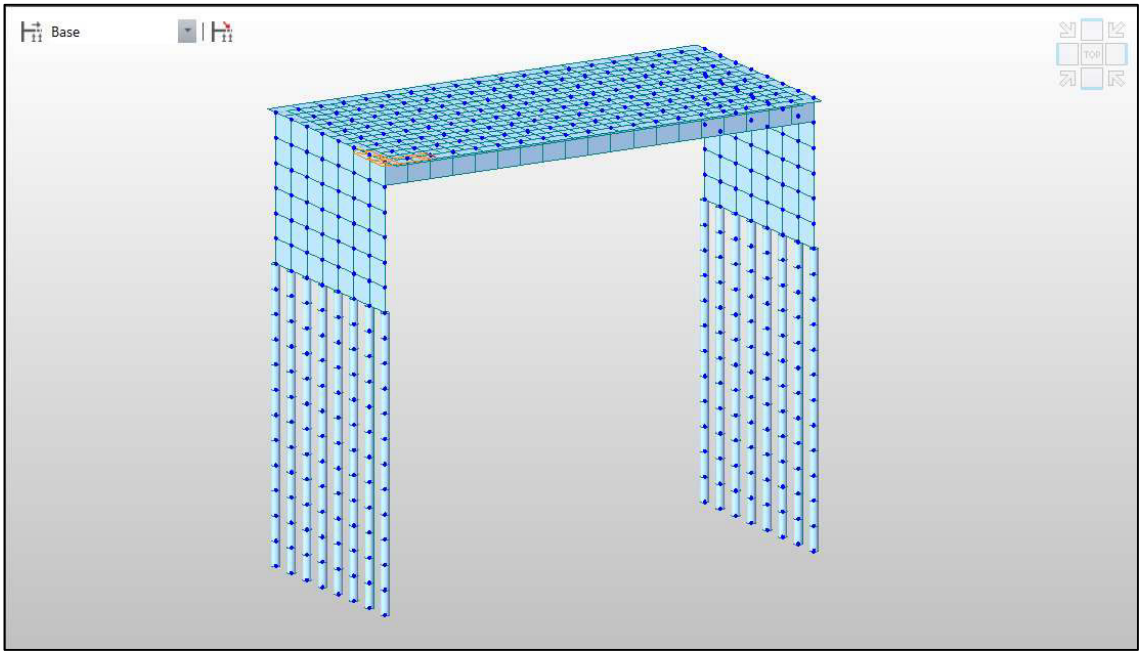

Figure B.6: 20m span 3D MIDAS Model with 6m deep abutments, 12m deep piles

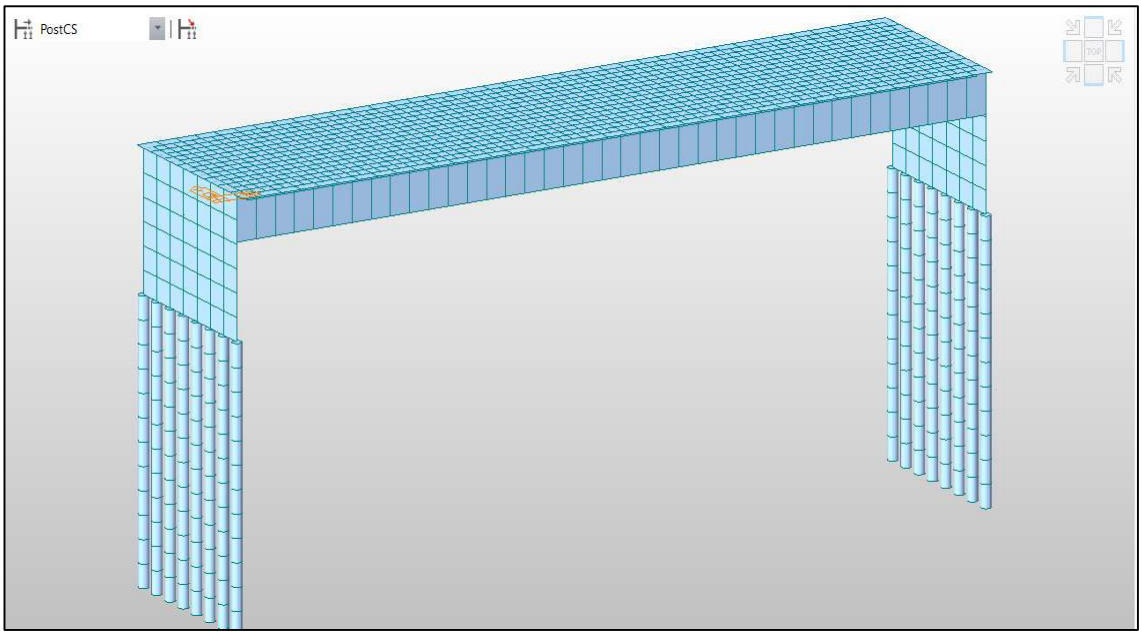

Figure B.7: 40m span 3D MIDAS Model with 6m deep abutments, 12m deep piles

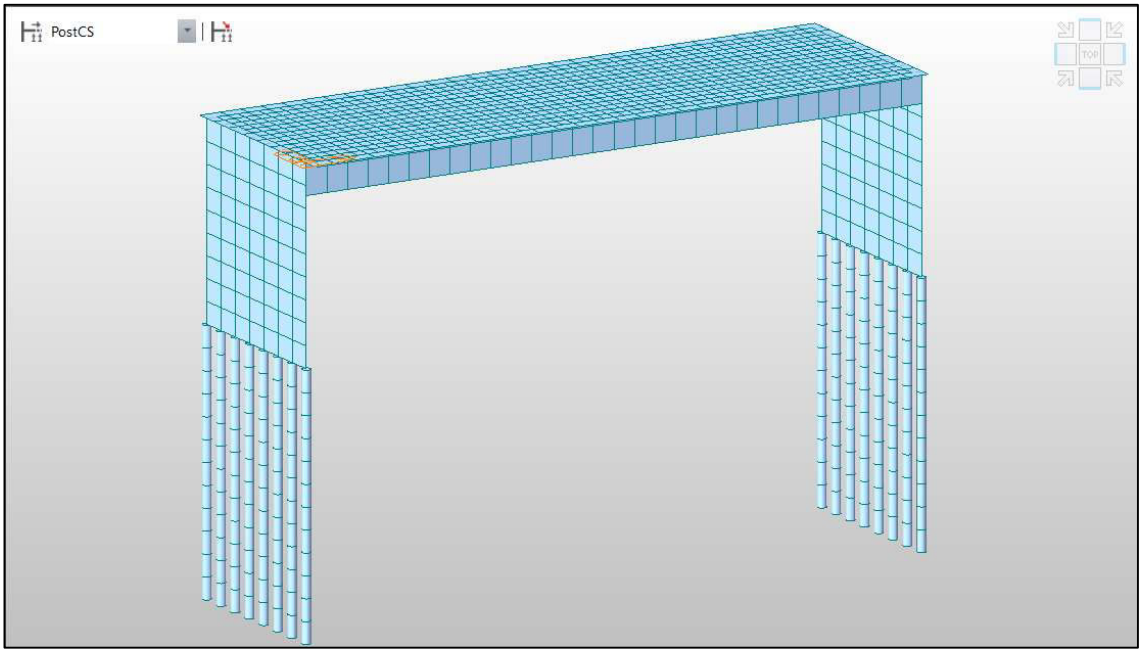

Figure B.8: 30m span 3D MIDAS Model with 9m deep abutments, 12m deep piles

iii) Spring model on flexible supports – Contraction (2D Model)

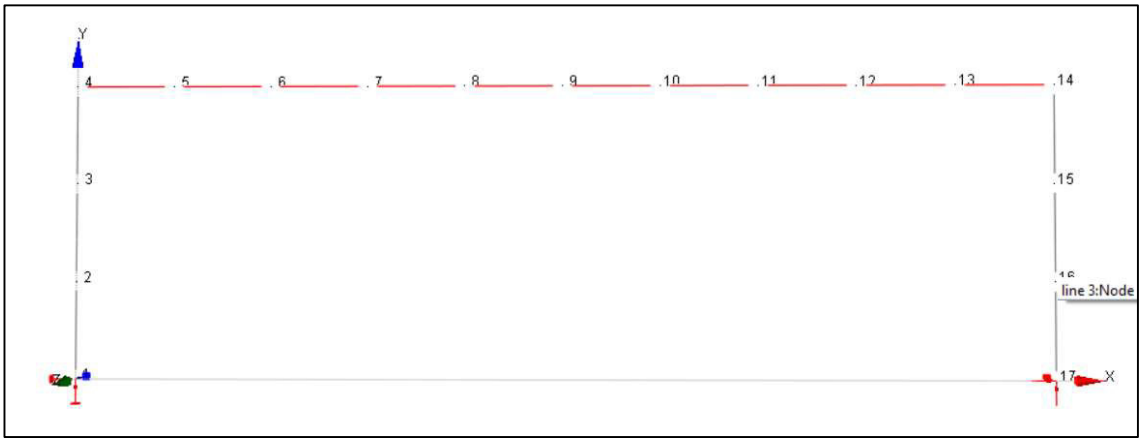

Figure B.9: Analysis model for 10m span, 30º Contraction, 3m High Abutments

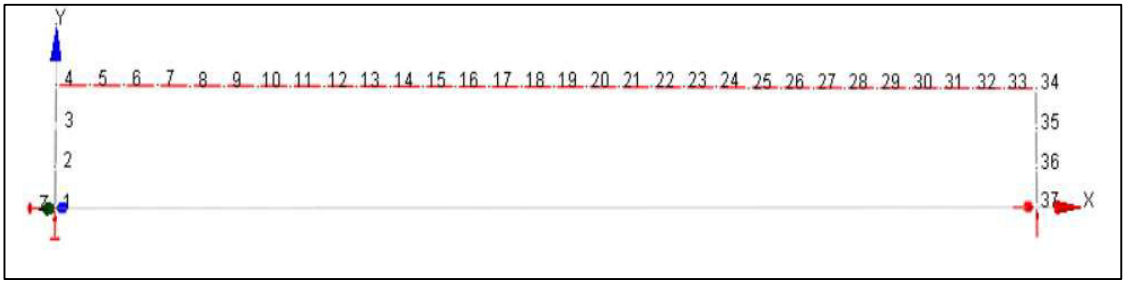

Figure B.10: Analysis model for 30m span, 30º Contraction, 3m High Abutments

iv) Spring model on flexible supports – Expansion (2D Model)

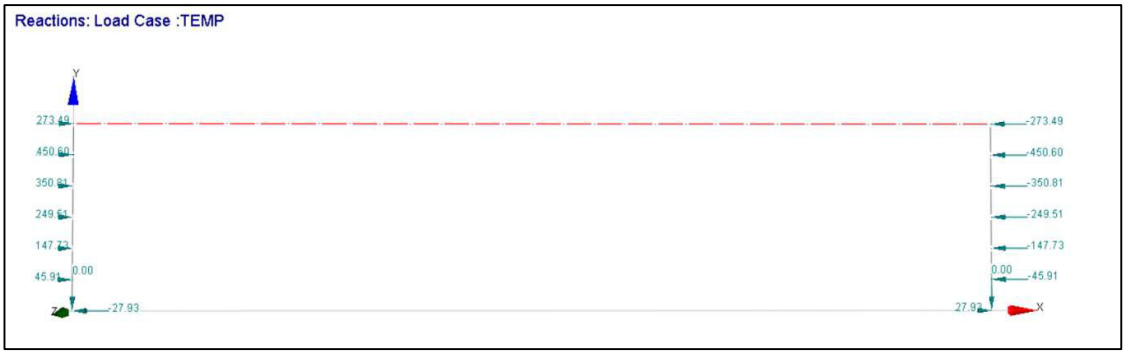

Figure B.11: Analysis model for 30m span, 30º Expansion, 6m High Abutments

v) Equivalent spring at deck level model – Expansion (2D Model)

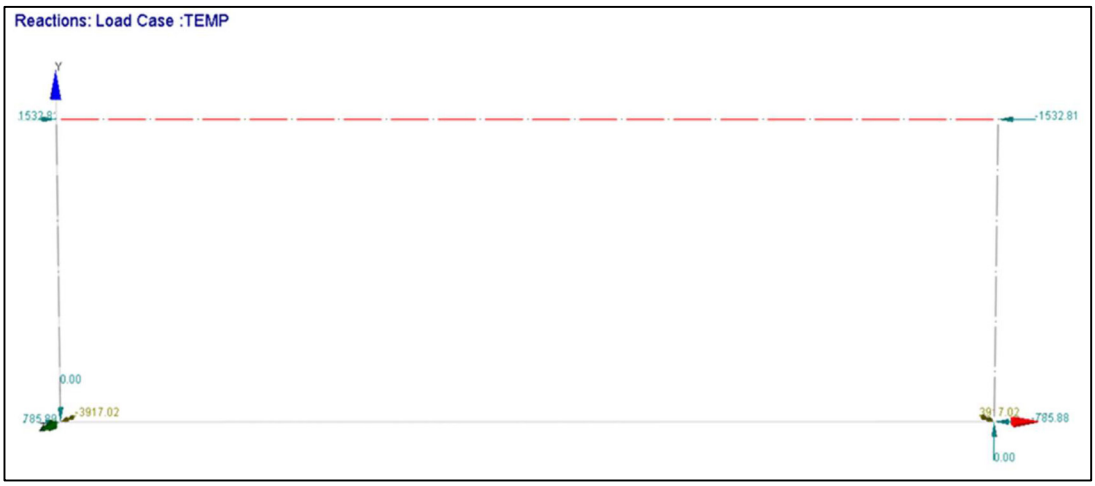

Figure B.12: Analysis model for 30m span, 30º Expansion, 6m High Abutments

C Appendix C – Model tables and Results

C.1 Model numbers and descriptions

The Tables below provide a Summary of the Model numbers for the above parametric studies:

i) Shallow strip foundations (2D PROKON Model).

Live load variability (for variable span lengths)				
Span length (m)	**Model Number**			
	% Live load applied			
	20% LL	**40% LL**	**60% LL**	**80% LL**
10	1	4	7	10
20	2	5	8	11
30	3	6	9	12

Table C.1: Summary of live load variability vs span variability - for shallow strip foundations (2D Model). Note that the Abutment height = 3.0m, Footing Size = 3.0m x 0.5m. Soil condition = Stiff clay

Abutment depth variability (for variable span lengths)			
Span length (m)	**Model Number**		
	Abutment height (m)		
	3	**6**	**9**
10	13	16	19
20	14	17	20
30	15	18	21

Table C.2: Summary of abutment height variability vs constant span variability for shallow strip foundations (2D Model). Note that the % Live load applied = 40%, Footing Size = 3.0m x 0.5m. Soil condition = Stiff clay

Soil variability (for variable span lengths)				
Span length (m)	**Model Number**			
	Soil type			
	Loose sand	**Dense sand**	**Soft clay**	**Stiff clay**
10	22	25	28	31
20	23	26	29	32
30	24	27	30	33

Table C.3: Summary of Ground condition variability vs constant span variability for shallow strip foundations (2D Model). Note that the % Live load applied = 40%. Footing Size = 3.0m x 0.5m. Note that the Abutment height = 6.0m.

ii) Full 3D spring modelling (3D MIDAS Model), pile depth = 12m.

Live load variability (for variable span lengths)				
Span length (m)	**Model Number**			
	% Live load applied			
	20% LL	**40% LL**	**60% LL**	**80% LL**
10	34	37	40	43
20	35	38	41	44
30	36	39	42	45
40	36a	39a	42a	45a

Table C.4: Summary of live load variability vs span variability - for piled foundations (3D Model). Note that the Abutment height = 3.0m, Pile depth = 12m, Pile diameter = 0.3m to 0.5m. Soil condition = Stiff clay

Abutment depth variability (for variable span lengths)			
Span length (m)	**Model Number**		
	Abutment height (m)		
	3	**6**	**9**
10	46	49	52
20	47	50	53
30	48	51	54
40	48a	51a	54a

Table C.5: Summary of abutment height variability vs constant span variability for piled foundations (3D Model). Note that the % Live load applied = 40%. Soil condition = Stiff clay

Soil variability (for variable span lengths)				
Span length (m)	**Model Number**			
	Soil type			
	Loose sand	**Dense sand**	**Soft clay**	**Stiff clay**
10	55	58	61	64
20	56	59	62	65
30	57	60	63	66

Table C.6: Summary of Ground condition variability vs constant span variability for piled foundations (3D Model). Note that the % Live load applied = 40%, and that the Abutment height = 6.0m.

iii) Spring model on flexible supports – Contraction (2D Model)

Abutment depth variability (for variable span lengths)			
Span length (m)	**Model Number**		
	Abutment height (m)		
	3	**6**	**9**
10	67	70	73
20	68	71	74
30	69	72	75

Table C.7: Summary of Abutment variability vs span variability - for shallow strip foundations (2D Model). Note that the change in temperature = 30ºC, Footing Size = 3.0m x 0.5m. Soil condition = Abutment backfill

iv) Spring model on flexible supports – Expansion (2D Model)

Abutment depth variability (for variable span lengths)			
Span length (m)	**Model Number**		
	Abutment height (m)		
	3	**6**	**9**
10	76	79	82
20	77	80	83
30	78	81	84

Table C.8: Summary of Abutment variability vs span variability - for shallow strip foundations (2D Model). Note that the change in temperature = 30ºC, Footing Size = 3.0m x 0.5m. Soil condition = Abutment backfill

v) Equivalent spring at deck level model – Expansion (2D Model)

Abutment depth variability (for variable span lengths)			
Span length (m)	**Model Number**		
	Abutment height (m)		
	3	**6**	**9**
10	85	88	91
20	86	89	92
30	87	90	93

Table C.9: Summary of Abutment variability vs span variability - for shallow strip foundations (2D Model). Note that the change in temperature = 30ºC, Footing Size = 3.0m x 0.5m. Soil condition = abutment backfill

vi) 3D MIDAS model for temperature expansion (+15°C) as well as temperature contraction (-15°c), pile depth = 12m

Abutment depth variability (for variable span lengths)			
Span length (m)	**Model Number**		
	Abutment height (m)		
	3	**6**	**9**
10	94	97	100
20	95	98	101
30	96	99	102
40	96a	99a	102a

Table C.10: Summary of span variability vs abutment height variability - for piled foundations (3D Model). Pile depth = 12m, Pile diameter = 0.3m to 0.5m. Soil condition = Stiff clay

C.2 Result Tables

1) The tables below are for the 2-D Hambly elastic support model results.

Live load variability (for variable span lengths)				
Span length (m)	**Horizontal Reaction (kN) - Upper bound**			
	% Live load applied			
	20% LL - UB	**40% LL - UB**	**60% LL - UB**	**80% LL - UB**
10	61,63	123,23	184,85	246,50
20	286,50	572,99	859,49	1146,00
30	749,41	1498,82	2248,23	2998,00

Table C.11: Horizontal Reactions for Span length vs percentage Live load (Upper Bound)

Live load variability (for variable span lengths)				
Span length (m)	**Horizontal Reaction (kN) - Lower bound**			
	% Live load applied			
	20% LL - LB	**40% LL - LB**	**60% LL - LB**	**80% LL - LB**
10	60,35	120,68	181,02	241,40
20	248,06	496,12	744,17	992,20
30	581,48	1162,97	1744,45	2326,00

Table C.12: Horizontal Reactions for Span length vs percentage Live load (Lower Bound)

Abutment depth variability (for variable span lengths)			
Span length (m)	Horizontal Reaction (kN) - Upper bound		
	Abutment height (m)		
	3 - UB	6 - UB	9 - UB
10	123,23	61,25	37,71
20	572,99	324,24	214,20
30	1498,82	906,56	611,98

Table C.13: Horizontal Reactions for Span length vs Abutment height (Upper Bound)

Abutment depth variability (for variable span lengths)			
Span length (m)	Horizontal Reaction (kN) - Lower bound		
	Abutment height (m)		
	3 - LB	6 - LB	9 - LB
10	120,68	65,36	40,69
20	496,12	332,12	228,21
30	1162,97	876,36	628,57

Table C.14: Horizontal Reactions for Span length vs Abutment height (Lower Bound)

Soil variability (for variable span lengths)				
Span length (m)	Horizontal Reaction (kN) - Upper bound			
	Soil type			
	Loose sand - UB	Dense sand - UB	Soft clay - UB	Stiff clay - UB
10	67,03	61,25	63,45	61,25
20	333,18	324,24	329,41	324,24
30	858,63	906,56	892,80	906,56

Table C.15: Horizontal Reactions for Span length vs Soil type (Upper Bound)

Soil variability (for variable span lengths)				
Span length (m)	Horizontal Reaction (kN) - Lower bound			
	Soil type			
	Loose sand - LB	Dense sand - LB	Soft clay - LB	Stiff clay - LB
10	74,99	65,36	69,78	65,36
20	318,60	332,12	332,19	332,12
30	720,26	876,36	822,09	876,36

Table C.16: Horizontal Reactions for Span length vs Soil type (Lower Bound)

2) The tables below are for the 3-D MIDAS model results.

Live load variability (for variable span lengths)				
Span length (m)	Horizontal Spring Reaction (kN) - Abutment			
	% Live load applied			
	20% LL	40% LL	60% LL	80% LL
10	5,10	10,20	15,40	20,50
20	17,00	34,00	51,00	68,00
30	29,00	58,00	88,70	120,60
40	38,10	77,50	121,20	166,30

Table C.17: Horizontal Abutment Spring Reactions for Span length vs percentage Live load

Live load variability (for variable span lengths)				
Span length (m)	Horizontal Spring Reaction (kN) - Piles			
	% Live load applied			
	20% LL	40% LL	60% LL	80% LL
10	2,10	4,10	6,20	8,30
20	13,00	26,10	39,10	52,10
30	25,30	50,60	77,40	105,30
40	36,90	75,10	117,10	160,30

Table C.18: Horizontal Pile Spring Reactions for Span length vs percentage Live load

Abutment depth variability (for variable span lengths)			
Span length (m)	Horizontal Spring Reaction (kN) - Abutment (40% Live load applied)		
	Abutment height (m)		
	3m	6m	9m
10	10,20	9,80	10,50
20	34,00	19,50	20,40
30	58,00	46,30	30,20
40	77,50	86,70	44,10

Table C.19: Horizontal Abutment spring Reactions for Span length vs Abutment Height

Abutment depth variability (for variable span lengths)			
Span length (m)	Horizontal Spring Reaction (kN) - Piles (40% Live load applied)		
	Abutment height (m)		
	3m	6m	9m
10	4,10	0,40	0,20
20	26,10	4,80	1,00
30	50,60	25,50	4,30
40	75,10	52,20	20,60

Table C.20: Horizontal Pile spring Reactions for Span length vs Abutment Height

Soil variability (for variable span lengths)				
Span length (m)	Horizontal Spring Reaction (kN) - Abutment			
	40% Live load, 6m Abutment height			
	Soil type			
	Loose sand	Dense sand	Soft clay	Stiff clay
10	9,80	9,80	9,80	9,80
20	19,30	19,30	19,40	19,30
30	48,50	43,20	47,90	46,30

Table C.21: Horizontal Abutment Spring Reactions for Span length vs Soil type

Soil variability (for variable span lengths)				
Span length (m)	Horizontal Spring Reaction (kN) - Piles			
	40% Live load, 6m Abutment height			
	Soil type			
	Loose sand	Dense sand	Soft clay	Stiff clay
10	0,20	0,50	0,30	0,40
20	4,60	4,60	4,80	4,80
30	5,00	23,40	26,60	9,20

Table C.22: Horizontal Pile Spring Reactions for Span length vs Soil type

3) The tables below are the results for the 2-D flexible support model with a 30º contraction applied.

Abutment depth variability (for variable span lengths)			
Span length (m)	Horizontal Spring Reaction (kN) - Abutment (30º Contraction applied)		
	Abutment height (m)		
	3m	6m	9m
10	224,24	54,08	92,11
20	899,42	340,68	161,47
30	1864,47	801,20	416,72

Table C.23: Horizontal Reactions for Span length vs Abutment height

Abutment depth variability (for variable span lengths)			
Span length (m)	Torsional Spring Reaction (kN.m) - Abutment (30º Contraction applied)		
	Abutment height (m)		
	3m	6m	9m
10	496,01	223,82	319,22
20	1677,67	1341,35	957,16
30	2724,73	2698,60	2233,07

Table C.24: Torsional Reactions for Span length vs Abutment height

4) The tables below are the results for the 2-D flexible support model with expansion applied.

Abutment depth variability (for variable span lengths)			
Span length (m)	Horizontal Spring Reaction (kN) - Abutment (30° Expansion applied)		
	Abutment height (m)		
	3m	6m	9m
10	310,05	339,78	215,85
20	409,05	425,12	439,29
30	479,93	450,60	464,68

Table C.25: Horizontal Reactions for Span length vs Abutment height

5) The tables below are the results for the 2-D Equivalent Horizontal Spring model with expansion applied. In this scenario, an equivalent spring is applied at the deck level of the bridge, behind the abutment.

Abutment depth variability (for variable span lengths)			
Span length (m)	Equivalent Horizontal Spring Reaction (kN) - (30° Expansion applied)		
	Abutment height (m)		
	3m	6m	9m
10	326,38	435,28	224,72
20	1177,50	1532,81	1836,24
30	2553,77	3291,26	3888,93

Table C.26: Equivalent Horizontal Spring reactions for Span vs Abutment Height

6) The tables below are the results for the 3-D MIDAS Spring model with temperature expansion and contraction applied.

Abutment depth variability (for variable span lengths)			
Span length (m)	Horizontal Spring Reaction (kN) - Abutment (15° RISE in Temp)		
	Abutment height (m)		
	3m	6m	9m
10	41,20	54,80	66,80
20	78,30	108,40	128,50
30	105,10	147,80	176,50
40	133,80	176,70	210,30

Table C.27: Horizontal Abutment Spring Reactions for Span length vs Abutment height (Temperature rise condition)

Abutment depth variability (for variable span lengths)			
Span length (m)	Horizontal Spring Reaction (kN) - Piles (15º RISE in Temp)		
	Abutment height (m)		
	3m	6m	9m
10	4,10	3,50	2,30
20	4,30	11,10	10,30
30	22,80	13,40	18,20
40	41,70	10,00	20,10

Table C.28: Horizontal Pile Spring Reactions for Span length vs Abutment height (Temperature rise condition)

Abutment depth variability (for variable span lengths)			
Span length (m)	Horizontal Spring Reaction (kN) - Abutment (15º FALL in Temp)		
	Abutment height (m)		
	3m	6m	9m
10	0,00	0,00	0,00
20	0,00	0,00	0,00
30	0,00	0,00	0,00
40	0,00	0,00	0,00

Table C.29: Horizontal Abutment Spring Reactions for Span length vs Abutment height (Temperature fall condition)

Abutment depth variability (for variable span lengths)			
Span length (m)	Horizontal Spring Reaction (kN) - Piles (15º FALL in Temp)		
	Abutment height (m)		
	3m	6m	9m
10	2,00	0,80	0,50
20	8,40	3,70	2,10
30	17,50	8,90	5,10
40	28,60	15,30	9,10

Table C.30: Horizontal Pile Spring Reactions for Span length vs Abutment height (Temperature fall condition)

C.3 Typical Model Result Diagrams

The following diagrams show screenshots taken from some of the model analysis results, which demonstrate to the reader the variability in the spring reactions across the abutment and the piles.

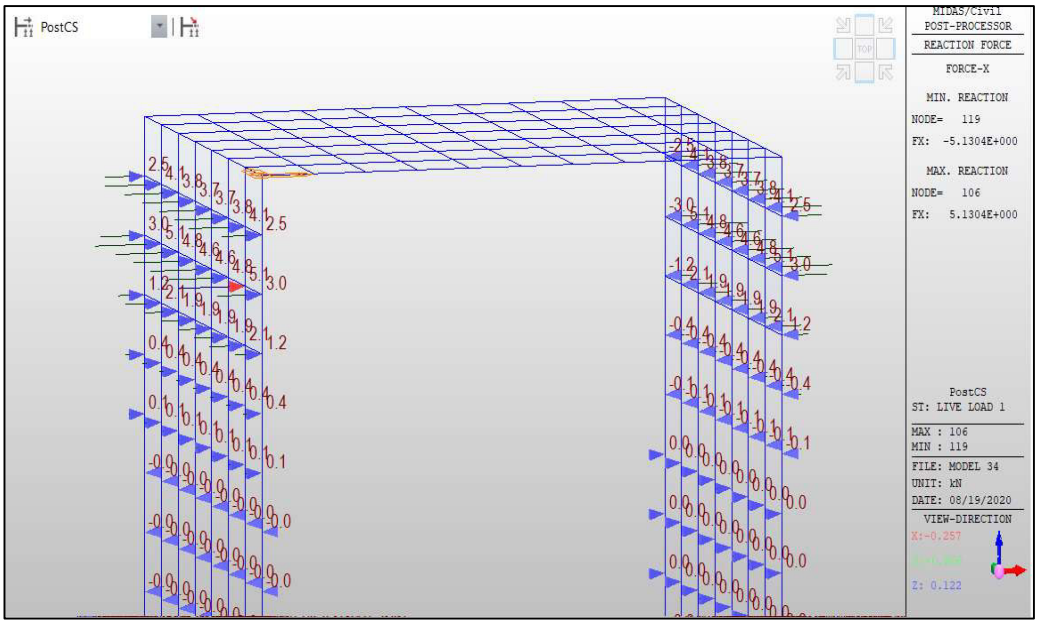

Figure C.1: Model 34 reactions (20% LL)

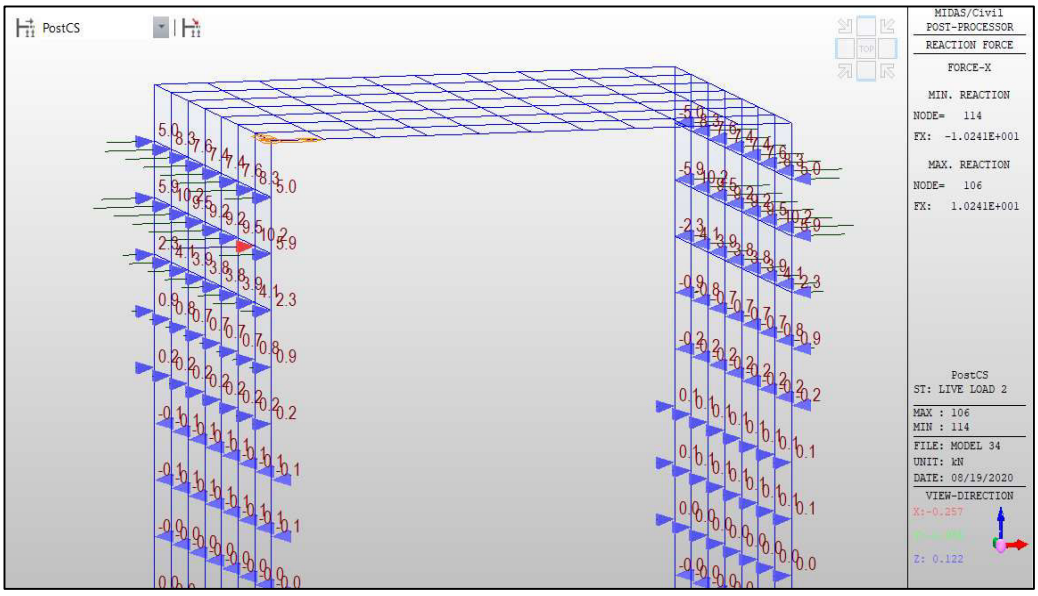

Figure C.2: Model 37 reactions (40% LL)

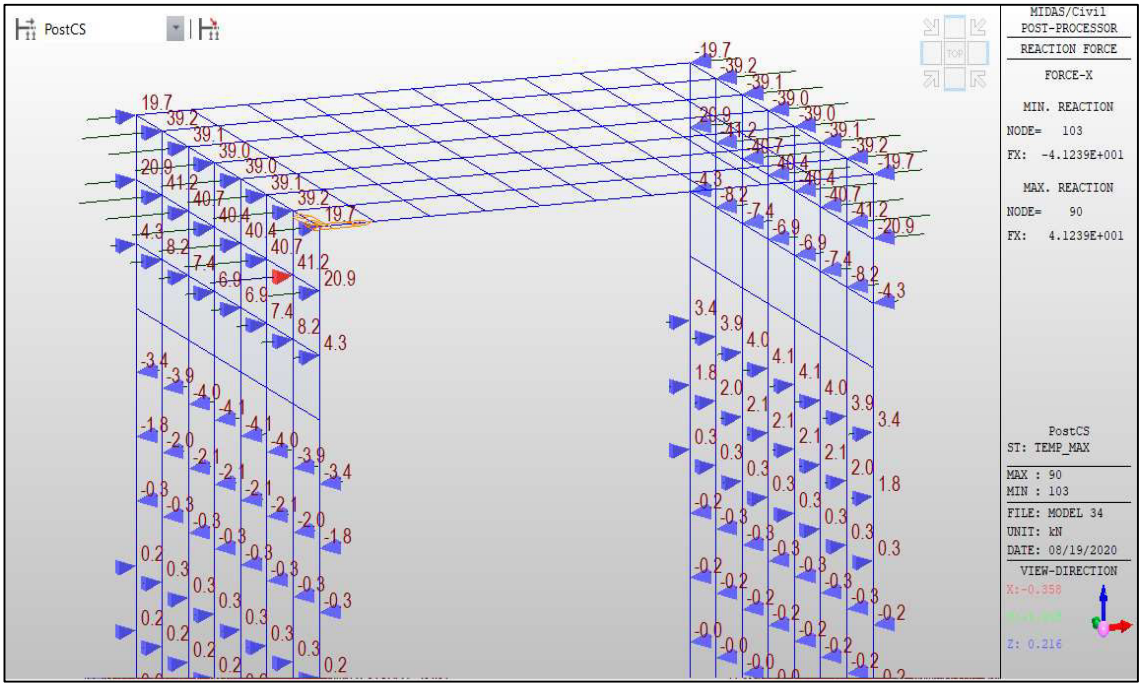

Figure C.3 : Model 94 reactions (+15^{O}C Temp)

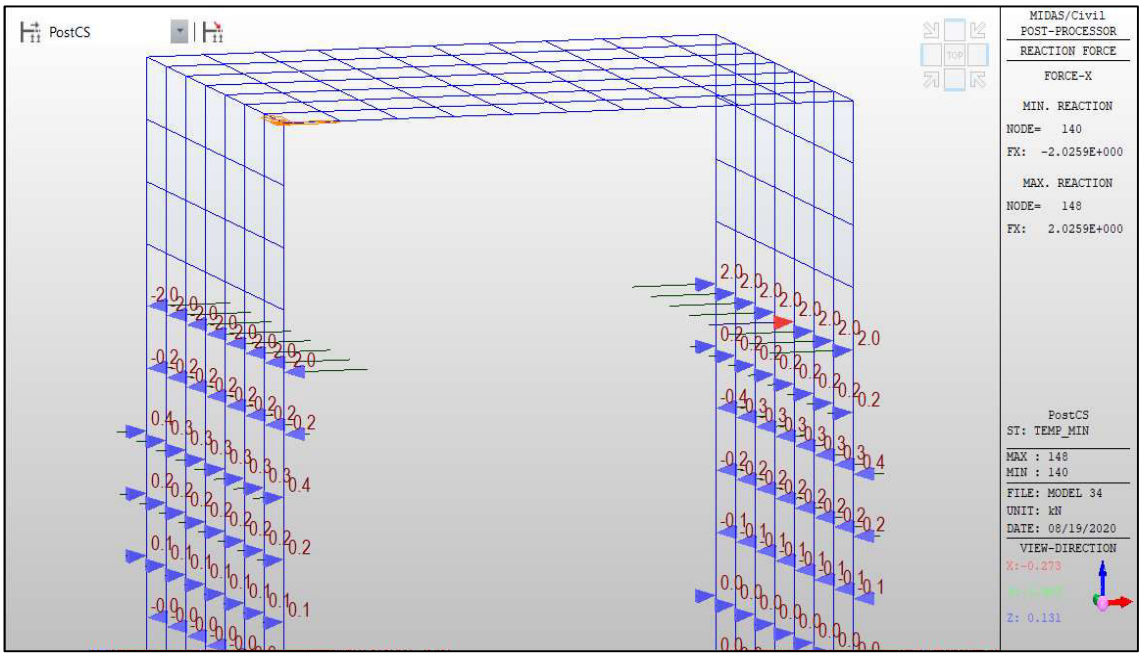

Figure C.4: Model 94 reactions (-15^{O}C Temp)

Reactions for some of the 2D Prokon type models are shown below in the diagrams that follow:

Figure C.5: 2D Hambly type shallow strip foundation elastic model reactions

Figure C.6: 2D Flexible supports - contraction type model reactions

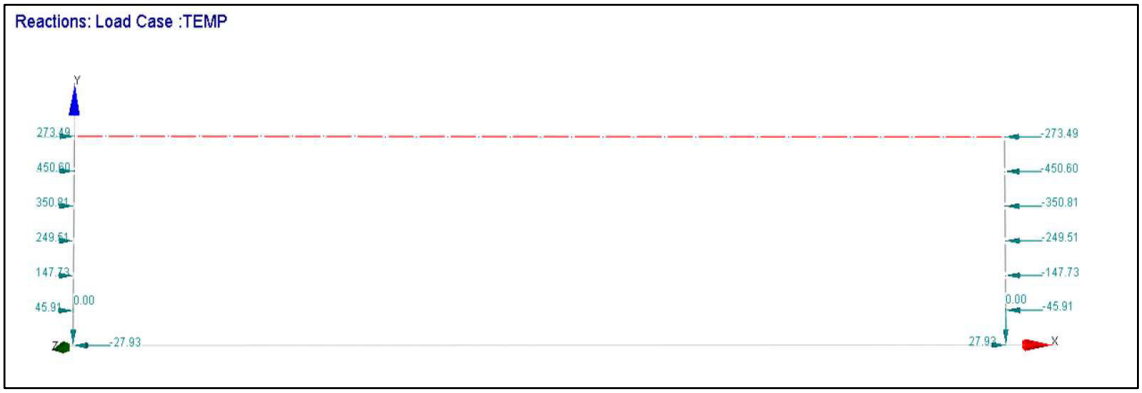

Figure C.7: 2D Flexible supports – expansion type model reactions

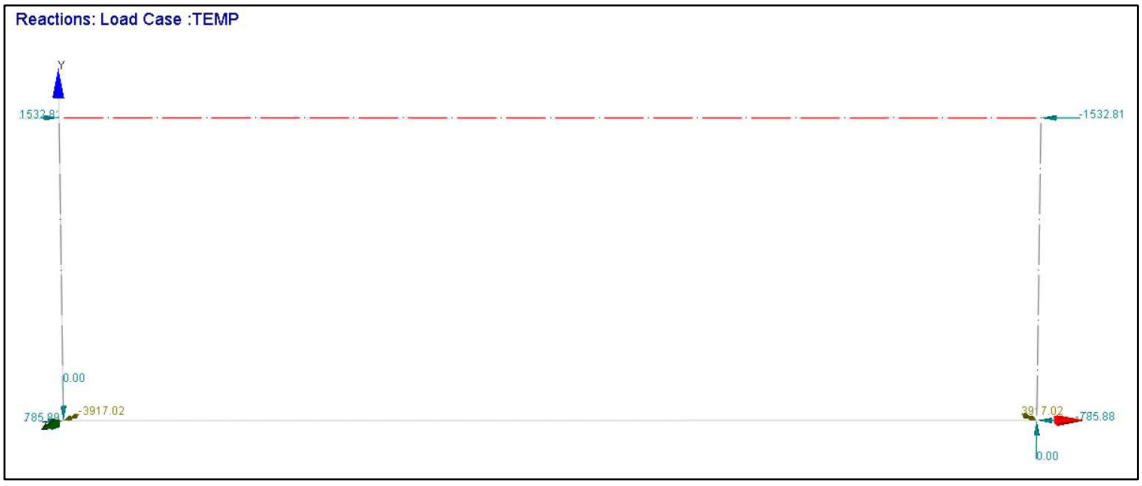

Figure C.8: 2D equivalent spring type model reactions

D Appendix D – Verification calculations

It is important to be able to verify the results obtained from the various models that have been described in this thesis by using an alternative method of analysis or using hand calculations. Due to the large number of results obtained from this parametric study, it is not possible to verify every single result, however, some order of magnitude checks have been undertaken as follows:

1) In order to provide a verification check on the live loading results obtained from the 3D MIDAS models, a Prokon finite element grillage analysis model (**Figure D.1**) was setup in order to compare the results for the live loading. The diagram below shows the model that was created for this purpose (created in a very similar manner as the MIDAS model).

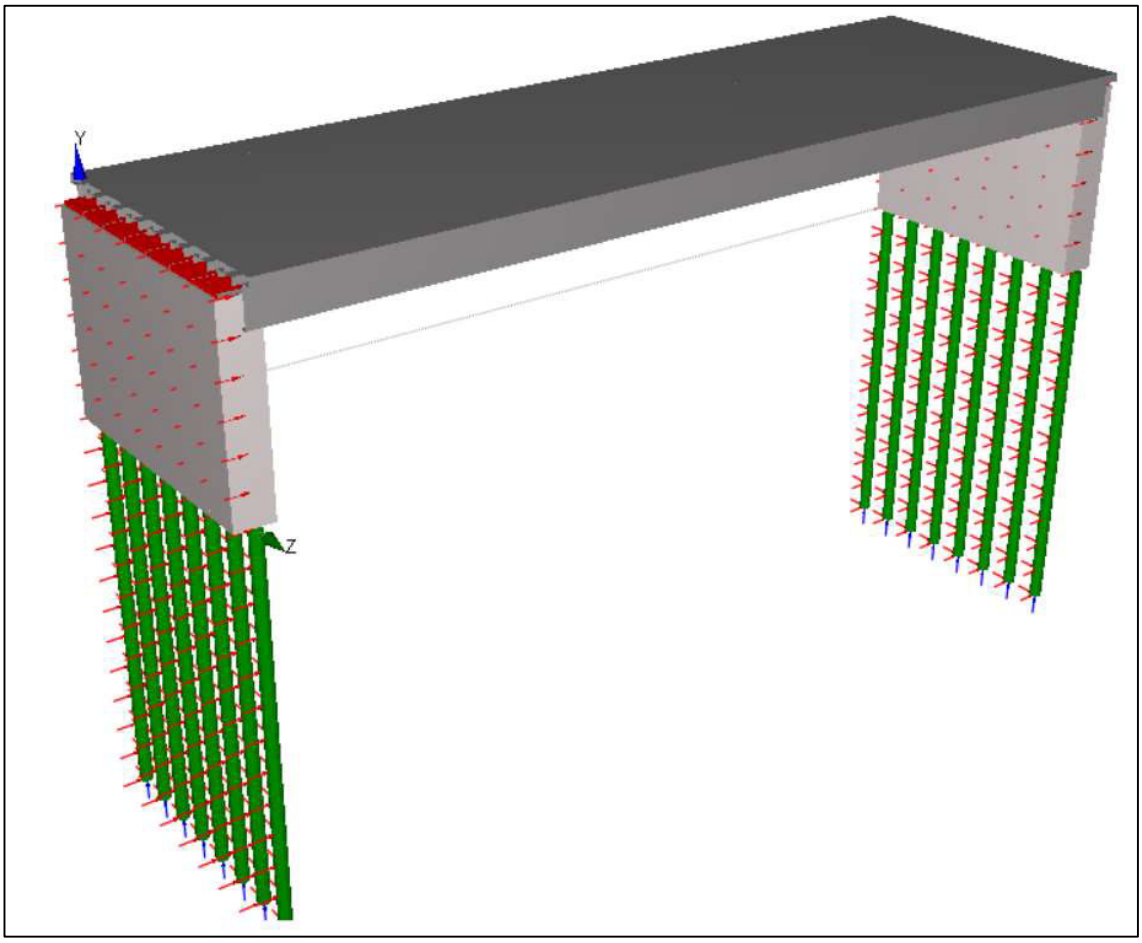

Figure D.1: 3D Prokon model check (30m span, 12m long piles, 6m high abutments)

Note that the Prokon model shown above is different to the MIDAS model in that it does not have non-linear springs for the piles and the abutment, in other words, the springs can keep on generating an increasing reaction, as the load increases. As noted previously, this is not realistic (soil has a finite spring value, as discussed in Section 2.5.7. The model nevertheless gives a useful order of magnitude check of the reactions that were found in the 3D MIDAS modelling that was undertaken.

The basic soil spring parameters used in the Prokon model were taken from the CIRIA 103 (1984) reference. A differential temperature of 30^{O}C was assumed (similar to the value used in the MIDAS modelling for the abutment springs). The two tables below (**Table D.1** and **Table D.2**) show the calculations leading up to the spring stiffness values that were assigned to the Prokon model.

Abutment calculations for Youngs Modulus (Lehane 1999)														
Span, L	Void ratio (e)	p'	p_{atm}	Differential Deck Temp. ΔT	H	α coefficient of expansion	δ	Υ = 2δ/(3H)	E_s	Trans spacing	Vert spacing	K_H *= 2.0tE_s	1/2K_H *= 1.0tE_s	1/4K_H *= 0.5tE_s
m	m	kPa	kPa	m	m		m		kPa (kN/m^2)	m	m	kN/m	kN/m	kN/m
20,00	0,38	50,00	100,00	30,00	6,00	1,20E-05	3,60E-03	4,00E-04	141 442,3	1,20	1,00	282 884,6	141 442,3	70 721,1
30,00	0,38	50,00	100,00	30,00	6,00	1,20E-05	5,40E-03	6,00E-04	120 266,0	1,20	1,00	240 531,9	120 266,0	60 133,0
40,00	0,38	50,00	100,00	30,00	6,00	1,20E-05	7,20E-03	8,00E-04	107 193,2	1,20	1,00	214 386,4	107 193,2	53 596,6
* ANSI/ASAE EP486.2														
See also CIRIA 103, 4.2.2, which says that K = 0.8 to 1.8E (approx)														

Table D.1: Abutment spring value calculations and assumptions

Pile calculations for pile springs (CIRIA 103)				
Span, L	Soil type	Coefficient of Subgrade Reaction (Kh) (Terzaghi - CIRIA 103)	Pile dia.	Pile Spring value
m		kN/m^3	m	kN/m
10,000	Stiff Clay	30 000,0	300	9000,00
20,000	Stiff Clay	30 000,0	350	10500,00
30,000	Stiff Clay	30 000,0	400	12000,00
40,000	Stiff Clay	30 000,0	500	15000,00

Table D.2: Horizontal Pile Spring value determination

The following graphs (**Figure D.2** to **Figure D.5**) show the direct comparisons that can be made between the spring reactions found in the MIDAS models and the Prokon models. As can be seen from the Figures below there is some good congruence in certain regions of the two sets of results, in terms of the values of the spring reactions and in terms of the shape of the spring development curve with increasing span.

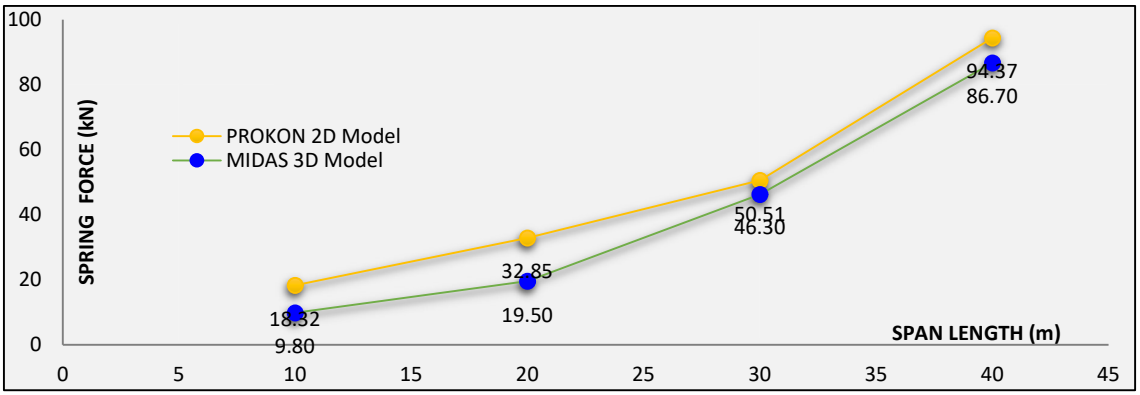

Figure D.2: Abutment spring reactions vs span for 6m high abutments in stiff clay – comparison between Prokon 3D model and MIDAS 3D model

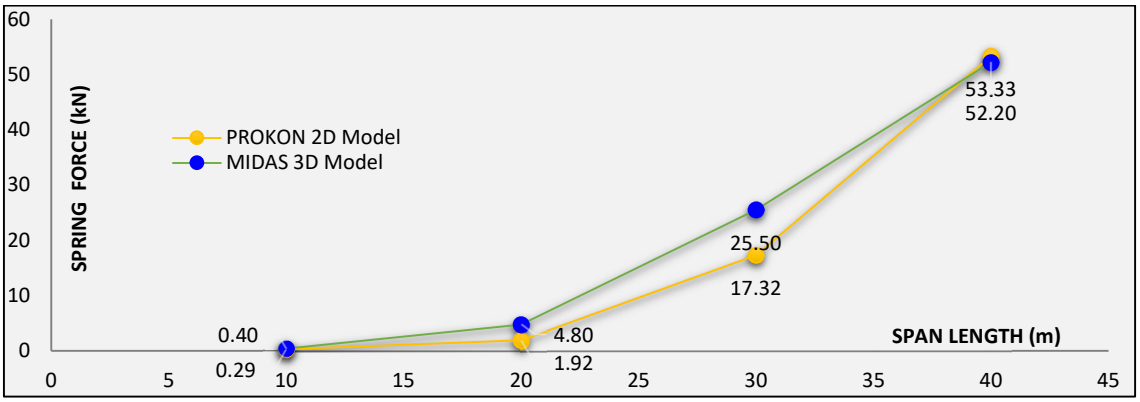

Figure D.3: Pile spring reactions vs span for 6m high abutments in stiff clay – comparison between Prokon 3D model and MIDAS 3D model

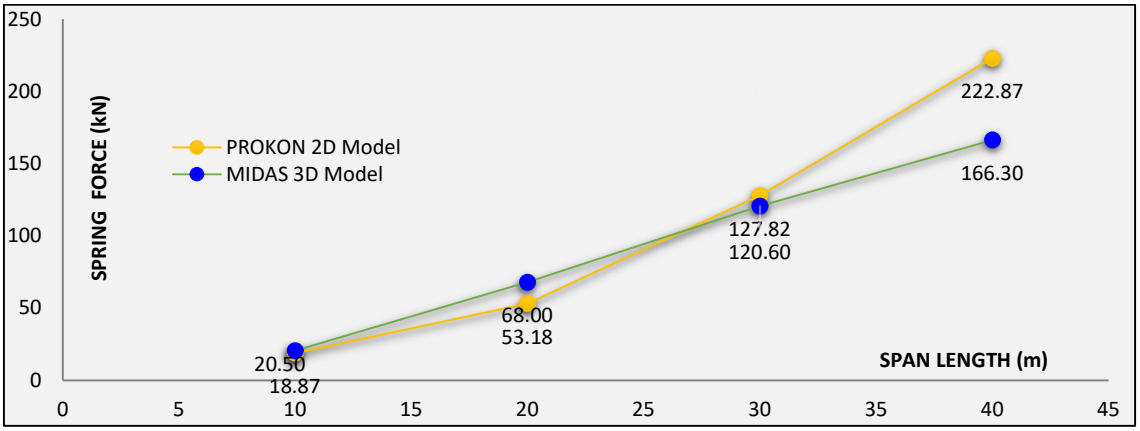

Figure D.4: Abutment spring reactions vs span for 3m high abutments in stiff clay – comparison between Prokon 3D model and MIDAS 3D model

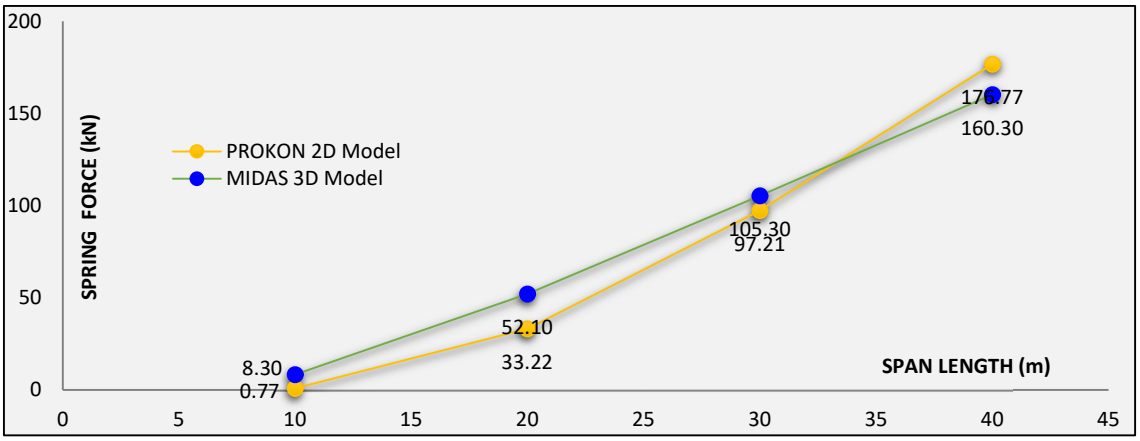

Figure D.5: Pile spring reactions vs span for 3m high abutments in stiff clay – comparison between Prokon 3D model and MIDAS 3D model

2) The results of the 2D contraction models can be compared with each other (the model by Lehane and the model by O'Brien and Keogh) for interest. It is not expected that the two models will give very similar results since the conventional spring model has springs that are spread across the abutment, whilst the Lehane model has a single equivalent spring located at deck level, and therefore should not be very accurate in regards to its estimate of spring force. The sum of the reactions from the conventional spring model are nevertheless compared below with the equivalent spring force reactions and show that although the two models give quite differing results, they both increase in a linear fashion, with some agreement occurring at the 10m and 20m span positions.

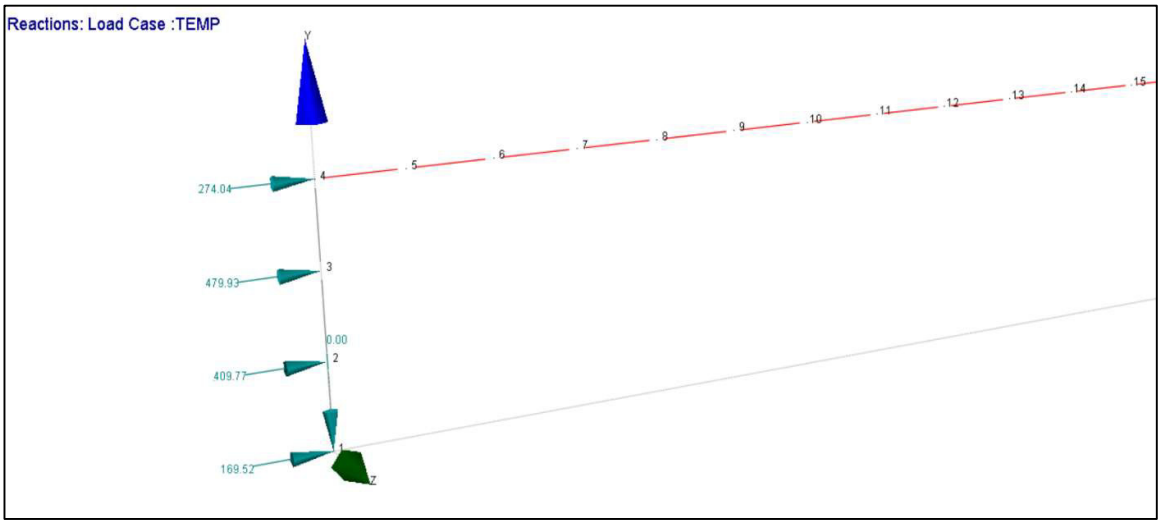

Figure D.6: Abutment spring reactions for 30m span model. The reactions are summed together and compared with the result of the single equivalent deck spring used in the Lehane model

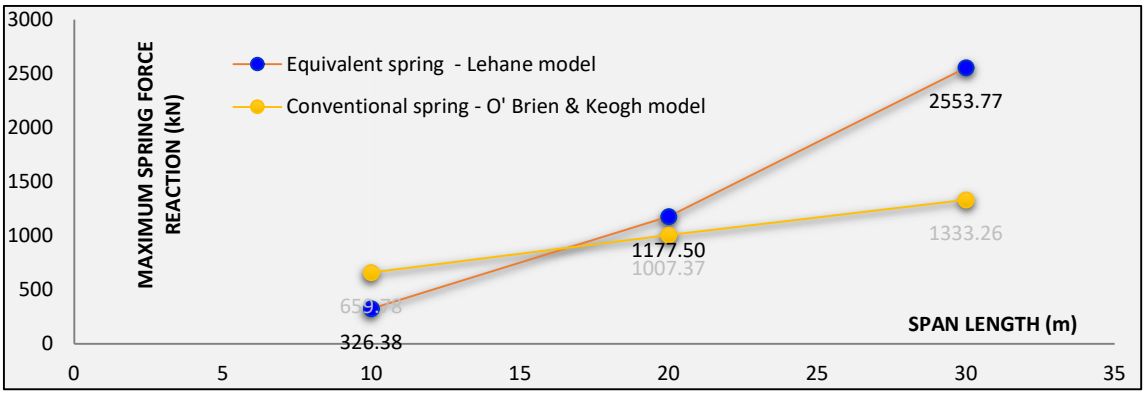

Figure D.7: Abutment spring reactions for 3m high Abutment, using equivalent spring model and conventional spring model for deck expansion

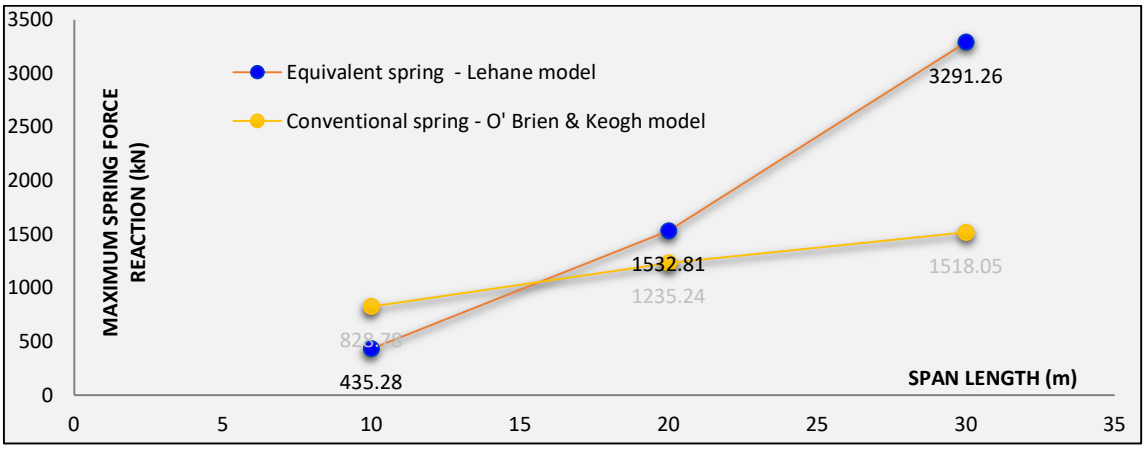

Figure D.8: Abutment spring reactions for 3m high Abutment, using equivalent spring model and conventional spring model for deck expansion

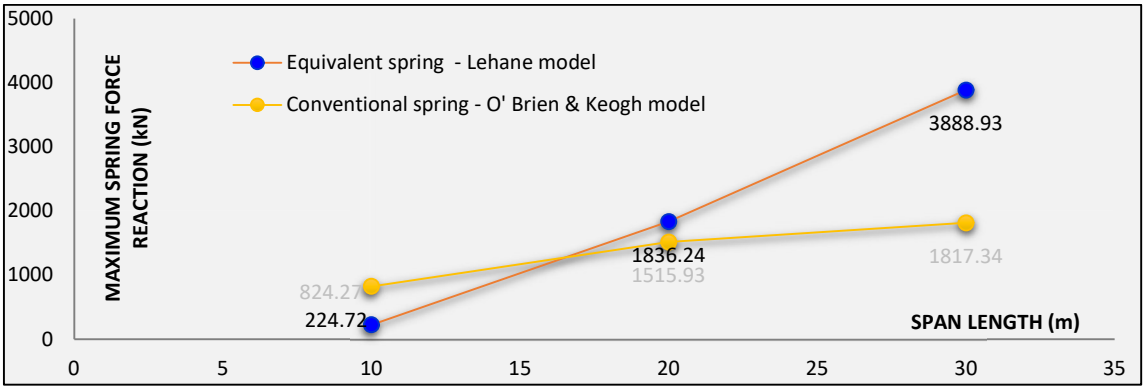

Figure D.9: Abutment spring reactions for 3m high Abutment, using equivalent spring model and conventional spring model for deck expansion

3) Lastly, formulas from a free expansion analysis (see **Figure D.10**) may be compared with the results obtained from the 3D MIDAS Grillage.

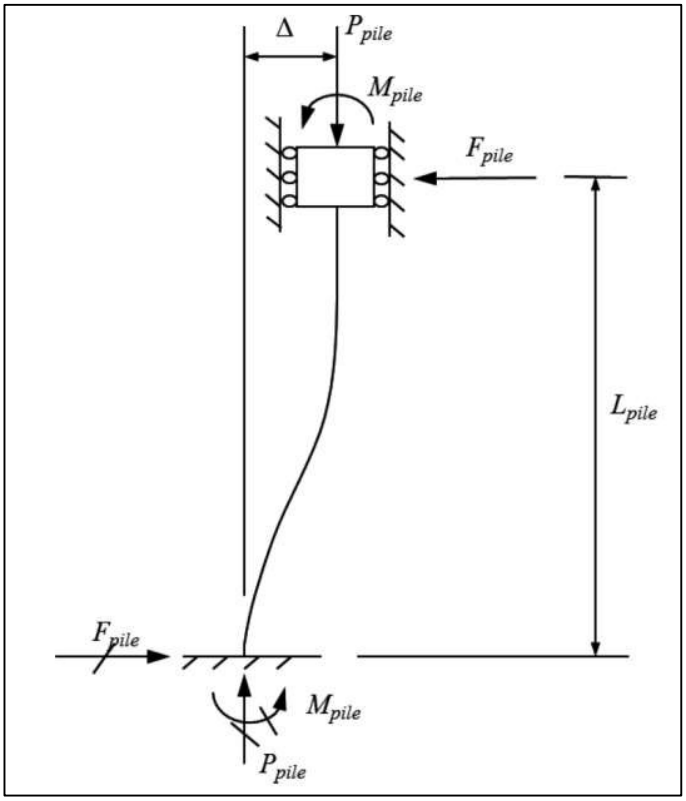

Figure D.10: Free expansion analysis of a pile with lateral load induced by temperature variation (Kim, W. et al, 2016)

There are numerous MIDAS Grillage models that could be compared with the free expansion analysis results. The best agreement was found in the 3m high abutments, founded in stiff clay with +15ºC temperature expansion. A comparison of the two sets of information is shown below in **Figure D.11**, and provides a reasonable degree of agreement between the results, however this is heavily dependent on the length of pile assumed in the analysis.

After some testing, it was found that a reasonable pile length to assume in this calculation is 5500mm (see **Table D.3**). Note that the pile length assumed in the calculation relates to the position of the maximum bending moment that is being calculated, therefore the length of pile used in the calculation relates to the point in the soil where the pile effectively 'cantilevers' from.

12m Piles, 15 degree temp					
			ΔTemp	15,00	^{o}C
			α conc	1,20E-05	
			E conc	31,00	GPa
Span	10 000	20 000	30 000	40 000	mm
δ pile	0,90	1,80	2,70	3,60	mm
Pile diam	300	350	400	500	mm
Lpile	5 500	5 500	5 500	5 500	mm
Ipile	397 607 820	736 617 574	1 256 637 061	3 067 961 576	mm^4
Fpile	0,800	2,965	7,586	24,695	kN
Mpile	2,200	8,153	20,862	67,911	kN.m

Table D.3: Free expansion analysis calculations table

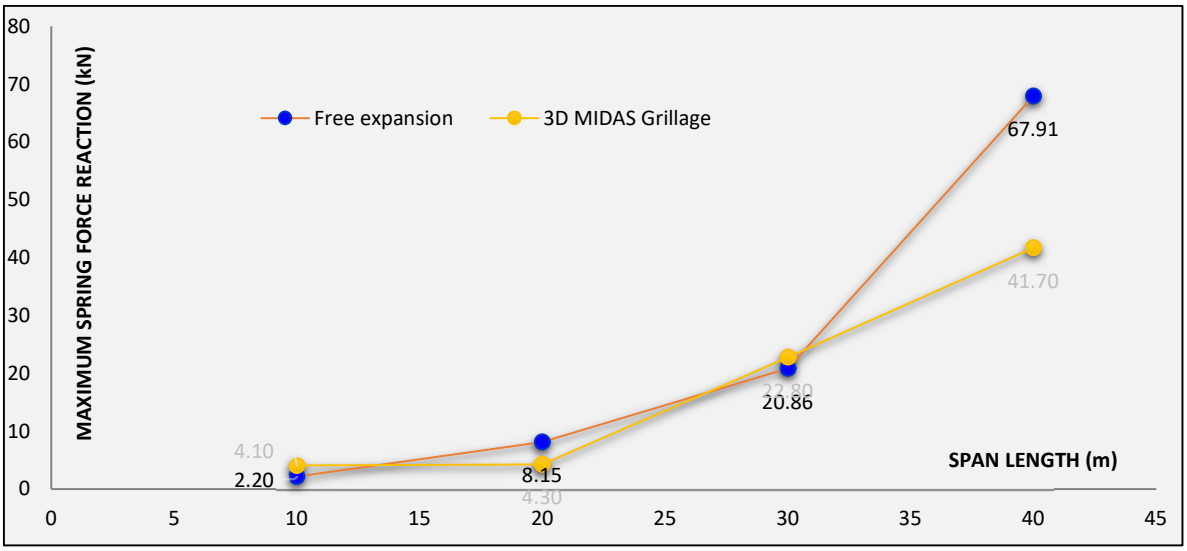

Figure D.11: Free expansion analysis vs results obtained in 3D Grillage (3m abutment height, founded in stiff clay, with +15ºC temperature expansion loadcase)